1-1-2013

Polymeric Nanocarriers And Their Oral Inhalation Formulations For The Regional Delivery Of Nucleic Acids To The Lungs

Denise Santos Conti
Wayne State University,

POLYMERIC NANOCARRIERS AND THEIR ORAL INHALATION FORMULATIONS FOR THE REGIONAL DELIVERY OF NUCLEIC ACIDS TO THE LUNGS

by

DENISE SANTOS CONTI

DISSERTATION

Submitted to the Graduate School

of Wayne State University,

Detroit, Michigan

in partial fulfillment of the requirements

for the degree of

DOCTOR OF PHILOSOPHY

2013

MAJOR: CHEMICAL ENGINEERING

Approved by:

_____

Advisor Date

_____

_____

_____

_____

ACKNOWLEDGEMENTS

Looking back five years ago, I am very impressed in realizing how fast time has passed by, how many amazing people I have met, and how many close friends I have made. All these people helped me to reach the current stage at which I am now. First of all, I would like to thank my parents, my sister, and my close friends in Brazil who supported me in my decision to pursue my Ph.D. degree outside our country. I would like to express my warmest gratitude to my husband for his love, care, comprehension, patience, and motivation, which have lead me to pursue my goals each day. Without my husband, I would never have reached this final stage.

I would like to thank my Ph.D. advisor Dr. Sandro da Rocha for accepting me in his research group and providing me guidance and supervision during my tenure as a graduate student. A special thanks to Dr. Mao, Dr. Matthew, and Dr. Merkel for agreeing to be part of my dissertation committee and providing constructive advice to my research. I also would like to thank all the professors in the Department of Chemical Engineering for the times that they were my instructors in classes, and a special thanks to Dr. Manke, Dr. Potoff, and Dr. da Rocha for giving me the opportunity to work with them as a teaching assistant.

My research would never have been completed without the friendship and help of my former lab mates – Libo, Balaji, Sowmya, Daniel, Jordan, Sumanth, and Fernando Cassio – and my current lab mates – Lin, Qian, Elizabeth, Anant, and Radovan. Special thanks to all exchange students who shared some time with me in the lab – Ligia, Willyan, Juliana Carneiro, Alexsandra, Vania, Juliana De Conto, and Gustavo

Borges. Thank you all for the wonderful company which ensured that our presence in the lab was not confined to research only.

I would like to thank all people from outside the Department of Chemical Engineering who somehow helped me to conduct my research – Dr. Pile (Biological Sciences), Dr. Zhi Mei "Mike" and Dr. Liu (SEM/TEM), Dr. Shay (MALDI), Dr. Ksebati (NMR), Dr. Chow, Dr. Brock, and Dr. Verani (Chemistry), Dr. Oupický, Dr. Reineke, and Dr. Merkel (Department of Pharmaceutical Sciences), Dr. Hüttemann (School of Medicine), Dr. Back, Mr. Van Buren, and Mary Olive (MICR).

Last, I would like to express my gratitude to Dr. da Rocha, the Department of Chemical Engineering, and the Graduate School at Wayne State University for their financial support during my tenure as a graduate student. Thank you to all my family and friends for their support which has helped me to reach this happy moment in my personal and professional life.

TABLE OF CONTENTS

Acknowledgements ..... **ii**

List of Tables ..... **x**

List of Figures ..... **xi**

List of Abbreviations ..... **xvi**

List of Original Publications ..... **xxii**

Chapter 1 – Introduction **1**

1.1 Overview and Objectives 1

1.2 Relevance and Innovation 13

1.3 References 13

Chapter 2 – Literature Review **26**

2.1 Carriers for Pulmonary Gene Delivery 26

2.2 siRNA Conjugates 31

2.3 Extra and Intracellular Barriers to Pulmonary Delivery of Nucleic Acids 33

2.3.1 Lung physiology, mucus layer, and lung surfactant 33

2.3.2 Cellular internalization 36

2.3.3 Endolysosomal escape 38

2.3.4 Degradation by nucleases in the cytoplasm 39

2.3.5 Nucleic acid release from the carrier 40

2.4 PEGylation as Alternative to Overcome Extracellular Barriers in Gene Therapy to the Lungs 40

2.5 pMDIs for the Delivery of Nucleic Acids via OI Administration 41

2.6 References 44

Chapter 3 – Solvation in Hydrofluoroalkanes: How can Ethanol Help? 57

3.1 Introduction 57

3.2 Experimental Section 59

3.2.1 Materials 59

3.2.2 Pretreatment of substrates and atomic force microscopy (AFM) tips 60

3.2.3 Surface chemical modification of substrates and Si3N4 tips by solution deposition 61

3.2.4 Chemical force microscopy (CFM) 62

3.2.5 Modeling the adhesion force and molecular simulation 63

3.3 Results and Discussion 67

3.3.1 Solvation in HFAs without the presence of ethanol 68

3.3.2 Solvation in HFAs in the presence of ethanol 69

3.3.3 F_{ad}/R in presence of ethanol – analysis from CFM measurements and JKR theory 72

3.4 Conclusions 75

3.5 Declarations 76

3.6 References 76

Chapter 4 – Propellant-based Inhalers for the Non-invasive Delivery of Genes via Oral Inhalation 82

4.1 Introduction 82

4.2 Experimental Section 85

4.2.1 Materials 85

4.2.2 Depolymerization and characterization of chitosan (CS) for CS-DNA nanoparticles 86
4.2.3 Preparation and characterization of CS-DNA nanoparticles (NPs) 88
4.2.3.1 Preparation of polyplexes. 88
4.2.3.2 Size and morphology 89
4.2.3.3 DNA encapsulation efficiency 90
4.2.4 Synthesis and characterization of oligo(lactide)-*grafted*-CS (OLA-*g*-CS) co-oligomer 90
4.2.5 Preparation and characterization of CS-DNA core-shell particles 90
4.2.5.1 Preparation of core-shell particles 90
4.2.5.2 Size and morphology 91
4.2.5.3 DNA loading in core-shell particles 92
4.2.6 Preparation of pMDI formulations and evaluation of their physical stability 92
4.2.7 Aerosol characteristics 93
4.2.8 *In vitro* transfection 94
4.2.9 *In vitro* cytotoxicity 96
4.2.10 Stability of CS-DNA polyplexes and integrity of gWIz GFP pDNA 97
4.3 Results and Discussion 98
4.3.1 Depolymerization and characterization of CS for preparation of CS-DNA NPs 98
4.3.2 Preparation and characterization of CS-DNA NPs 100
4.3.2.1 Preliminary screening 100
4.3.2.2 CS-DNA NPs selected for further studies 102

4.3.3 Preparation and characterization of core-shell particles loaded with CS-DNA NPs 105
4.3.4 Physical stability of the CS-DNA core-shell particles in propellant HFA 107
4.3.5 Aerosol characteristics 109
4.3.6 *In vitro* transfection 113
4.3.7 *In vitro* cytotoxicity 115
4.3.8 Stability of CS-DNA polyplexes and integrity of gWIz GFP pDNA 116
4.4 Conclusions 119
4.5 Acknowledgements 120
4.6 References 121
Chapter 5 – Dendrimer Nanocarriers and their Aerosol Formulations for siRNA Delivery to the Lung Epithelium 129
5.1 Introduction 129
5.2 Experimental Section 131
5.2.1 Materials 131
5.2.2 Preparation and characterization of siRNA-G4NH2 dendriplexes 134
5.2.3 Gel retardation assay 136
5.2.4 RNase protection assay 136
5.2.5 *In vitro* release 137
5.2.6 *In vitro* cytotoxicity 137
5.2.7 *In vitro* gene knockdown 139
5.2.8 Preparation of CSLA microparticles loaded with dendriplexes 141
5.2.9 Preparation of mannitol microparticles loaded with dendriplexes 142

5.2.10 Characterization of CSLA and mannitol microparticles loaded with dendriplexes 142
5.2.11 Preparation of the pMDI formulations and evaluation of their physical stability 144
5.2.12 Aerosol characterization of the pMDI formulations 144
5.2.13 Statistical analysis 146
5.3 Results and Discussion 146
5.3.1 Preparation and characterization of siRNA-G4NH2 dendriplexes 146
5.3.2 Gel retardation assay of G4NH2 to siRNA 148
5.3.3 Protection of siRNA by G4NH2 against RNase degradation 149
5.3.4 *In vitro* release of siRNA from G4NH2 151
5.3.5 *In vitro* cytotoxicity of G4NH2 and siRNA-G4NH2 dendriplexes 154
5.3.6 *In vitro* gene knockdown of siRNA-G4NH2 dendriplexes 156
5.3.7 *In vitro* gene knockdown of siRNA-G4NH2 dendriplexes exposed to propellant HFA 159
5.3.8 Preparation and characterization of microparticles loaded with dendriplexes 160
5.3.9 Physical stability of microparticles loaded with dendriplexes in propellant HFA 163
5.3.10 Aerosol performance of the pMDI formulations with the engineered microparticles 164
5.4 Conclusions 168
5.5 Acknowledgments 169
5.6 References 170

Chapter 6 – siRNA-Dendrimer Conjugates for the Lung Epithelium: Synthesis, Characterization, and Gene Silencing 178

6.1 Introduction 178

6.2 Experimental Section 181

6.2.1 Materials 181

6.2.2 Synthesis and characterization of G4NH2-PDP conjugates 184

6.2.3 Synthesis and characterization of G4NH2-siRNA conjugates 186

6.2.4 *In vitro* gene knockdown 189

6.3 Results and Discussion 190

6.3.1 Synthesis and characterization of G4NH2-PDP conjugates 190

6.3.2 Synthesis and characterization of G4NH2-siRNA conjugates 194

6.3.3 *In vitro* gene knockdown 198

6.4 Conclusions 202

6.5 Acknowledgments 203

6.6 References 204

Chapter 7 – Conclusions and Future Directions 214

Appendix A – Supporting Information for Chapter 4 222

Appendix B – Supporting Information for Chapter 5 234

Appendix C – Publication 1 245

Appendix D – Publication 2 246

Abstract 247

Autobiographical Statement 249

LIST OF TABLES

Table 3.1. Molar volume, solubility parameters, and surface free energies for the chemistries used in this work. These values were used in the calculation of F_{ad}/R with the JRK theory. 66

Table 4.1. DNA and CS encapsulation efficiency (EE), particle size, and zeta potential of the CS-DNA NPs selected for further studies. The characteristics of the CS (Mw and DDA), nominal and actual N/P ratio are also shown. 102

Table 4.2. Aerodynamic characteristics of the CS-DNA NPs alone and engineered as core-shell particles. Polyplexes prepared with CS (31 kDa, 80% DDA), and pMDI formulations in HFA-227 at 298 K and saturation pressure of the propellant. CS-DNA core-shell particles at 2 $mg.mL^{-1}$ of propellant. DNA concentration ca. 4 $\mu g.mL^{-1}$ (Calf Thymus) and ca. 6 $\mu g.mL^{-1}$ (gWIz-GFP) for all formulations. Results in µg DNA ± s.d. (s.d. = standard deviation) for n = 3 (three independent runs) and twenty actuations each. 110

Table 5.1. Size of siRNA-G4NH2 dendriplexes determined by LS and SEM as a function of the N/P ratio. Zeta potential (ζ) and siRNA complexation efficiency (CE) are also shown. LS was performed with dendriplexes at 80 nM siRNA, and in 10 mM Tris-HCl pH 7.4 (for size) and pure water (for ζ). Image J was used to estimate the size of the dendriplexes from the SEM images: histograms of the measured diameters (> 400 particles) were fitted to Gaussian distributions, from which the average size and standard deviation was obtained 146

Table 5.2. Aerosol performance of pMDI formulations prepared with mannitol and CSLA microparticles loaded with siRNA-G4NH2 dendriplexes at N/P 10. All formulations at 2 mg particles per 1 mL of HFA-227 at 25°C and saturation pressure of the propellant. siRNA concentration of 290 - 550 $ng.mL^{-1}$ in formulations prepared with dendriplexes-loaded into mannitol, and 420 - 505 $ng.mL^{-1}$ in those prepared with CSLA. Results in ng siRNA ± deviation for n = 2 (two independent canisters) and 50 - 65 actuations each, from AC to Filter 165

LIST OF FIGURES

Figure 2.1. Mechanism of RNAi in mammalian cells 27

Figure 2.2. Polyplexes are formed by electrostatic interactions between cationic polymer and negatively charged DNA/siRNA 29

Figure 2.3. **(a)** Sites for conjugation onto siRNA (dashed circles), while the 5'-end of the antisense strand (solid circle line) is suggested to be free in order to keep the efficiency of the RNAi. **(b)** Disulfide bond (S-S) between the siRNA and the conjugated molecule (R) is reduced (2 HS-) due to the redox molecules (e.g. glutathione) present in the cytoplasm 33

Figure 2.4. Bifurcations of the lungs from trachea to alveolar sacs 34

Figure 2.5. Physical and immune barriers to successful lung nucleic acid transfer 34

Figure 2.6. **(a)** The mucus layer, a mixture of carbohydrates, glycoproteins and polysaccharides, resides on the surface of the airways epithelium and forms a barrier for nanocarriers. **(b)** Pulmonary surfactant, alveolar fluid and macrophages as barriers in the alveolus. 35

Figure 2.7. Most common mechanisms of internalization and intracellular trafficking found in mammalian cells 37

Figure 2.8. Proton-sponge hypothesis. Protonation of the amine-based cationic polymer causes influx of protons and counter-ions into endocytic vesicles, increasing the osmotic pressure, and leading the vesicle to swell and rupture 39

Figure 2.9. Schematic diagram of a typical pMDI 43

Figure 3.1. Effect of the volume fraction of ethanol on the Fad/R of **(a)** alkyl (C8)-; **(b)** ether (COC)-; **(c)** ester (COOC)-based moieties. (•) CFM measurements were at 298 K and in HPFP/ethanol mixtures; (—) F_{ad}/R calculated using the JKR theory, considering γ_d = 18.8, γ_p = 2.6, and γ_t = 21.4 mN.m^{-1} for ethanol; and (- - -) F_{ad}/R calculated using the JKR theory, considering for ethanol: γ_d = 18.8, γ_p = 0.0, and γ_t = 18.8 mN.m^{-1}. *Insets:* Molecular structures of **(a)** C8TS; **(b)** COCTS; and **(c)** COOCTS. The moieties of interest are shown in brackets..... 70

Figure 4.1. **(a)** Plot for the determination of intrinsic viscosity [η] of non-depolymerized CS (310 kDa, 80% DDA) based on inherent and reduced viscosities; **(b)** Exponential reduction in the Mw of CS (80% DDA) according to the depolymerization time. 99

Figure 4.2. Histograms and Gaussian fits to the particle size distributions obtained from the SEM images of the CS-DNA NPs prepared with CS (31 kDa, 80% DDA) and **(a)** Calf Thymus DNA at nominal N/P ratio of 6; or **(b)** gWIz-GFP DNA at nominal N/P ratio of 7. *Insets*: SEM and AFM images of the CS-DNA NPs. 104

Figure 4.3. Histograms and Gaussian fits to the particle size distributions obtained from the SEM images of the core-shell particles loaded with CS-DNA NPs prepared with CS (31 kDa, 80% DDA) and **(a)** Calf Thymus DNA at nominal N/P ratio of 6; or **(b)** gWIz-GFP DNA at nominal N/P ratio of 7. *Insets*: SEM and TEM images of the CS-DNA core-shell particles. .. 107

Figure 4.4. Aerodynamic characteristics of the CS-DNA NPs alone and engineered as core-shell particles. Polyplexes prepared with CS (31 kDa, 80% DDA) and **(a)** gWIz-GFP DNA at nominal N/P ratio of 7; or **(b)** Calf Thymus DNA at nominal N/P ratio of 6. pMDI formulations in HFA-227 at 298 K, and saturation pressure of the propellant. CS-DNA core-shell particles at 2 $mg.mL^{-1}$ of propellant, and DNA concentration ca. 4 $\mu g.mL^{-1}$ (Calf Thymus) and ca. 6 $\mu g.mL^{-1}$ (gWIz-GFP) for all formulations. AC, IP and F refer to actuator, induction port and filter, respectively. *Insets*: Core-shell particles loaded with CS-DNA polyplexes – dispersion stability of freshly prepared pMDI formulations (*right*), and SEM of particles actuated from pMDIs after one year of storage (*left*). 108

Figure 4.5. Fluorescence microscope images of A549 cells transfected in vitro with **(a)** free DNA (negative control); **(b)** CS-DNA NPs; **(c)** Core-shell particles loaded with CS-DNA NPs; **(d)** TransFast™ Transfection Reagent (positive control); **(e)** CS-DNA core-shell particles and **(f)** CS-DNA NPs after 6 weeks of storage in HFA-227 at 298 K and saturation pressure of the propellant. CS-DNA polyplexes prepared with CS (80% DDA, 31 kDa) and gWIz-GFP DNA at nominal N/P ratio of 7. Dosage of 0.25 µg DNA per well. All images at 10x magnification. 113

Figure 4.6. Cytotoxicity of **(a)** CS-DNA NPs **(b)** OLA-*g*-CS co-oligomer; and **(c)** core-shell particles loaded with CS-DNA NPs. Polyplexes prepared with CS (31kDa, 80% DDA) and gWIz-GFP DNA at nominal N/P ratio of 7. All experiments carried out in A549 cell line. 115

Figure 4.7. **(a)** Gel electrophoresis for evaluation of the stability of complexed gWIz-GFP pDNA after exposure of the CS-DNA NPs to DNase I: free

pDNA (control, *lane 1*); CS-DNA NPs freshly prepared before (*lane 2*) and after (*lane 3*) incubation with chitosanase/lysozyme; CS-DNA NPs + DNase I (1 μU *lane 4*, 50 μU *lane 5*, 0.5 U *lane 6*, 1 U *lane 7*, and 2 U *lane 8*) + chitosanase/lysozyme. U means units DNase I per 1μg pDNA. **(b)** Gel electrophoresis for monitoring the integrity of gWIz-GFP pDNA after particle preparation and exposure to propellant HFA: free pDNA (control, *lane 1*); CS-DNA polyplexes freshly prepared before (*lane 2*) and after (*lane 3*) incubation with chitosanase/lysozyme; CS-DNA core-shell particles freshly prepared before (*lane 4*) and after (*lane 5*) incubation with chitosanase/lysozyme; CS-DNA core-shell particles stored in HFA-227 at 298K and saturation pressure of the propellant for 12 days before (*lane 6*) and after (*lane 7*) incubation with chitosanase/lysozyme. All CS-DNA polyplexes at N/P ratio of 7 – same as those used in all other studies. 117

Figure 5.1. Size and morphology of siRNA-G4NH2 dendriplexes at N/P 20 as determined by LS (*main distribution in the center*), SEM (*upper left inset*), and AFM (*lower left inset*). Histogram and Gaussian fit to the diameter distribution obtained from SEM images (> 400 particles) of the dendriplexes is also shown (*upper right inset*) 147

Figure 5.2. siRNA complexation efficiency as a function of the N/P ratio, as quantified by PicoGreen® Assay of residual free siRNA in the dispersion after preparation of the dendriplexes. *Inset:* Non-denaturating agarose gel electrophoresis of the corresponding dendriplexes: N/P 0.2 (*lane 2*), 0.5 (*lane 3*), 0.8 (*lane 4*), 1 (*lane 5*), 2 (*lane 6*), 3 (*lane 7*), 5 (*lane 8*), 10 (*lane 9*), 20 (*lane 10*), 30 (*lane 11*). Untreated siRNA control (300 ng) is shown in *lane 1* 148

Figure 5.3. RNase protection assay (non-denaturing agarose gel electrophoresis) of the siRNA-G4NH2 dendriplexes as a function of the N/P ratio. Dendriplexes incubated in the absence (-) or presence (+) of the treatments: RNase A (0.162 μg per 1 μg siRNA) for 6 h at 37 °C, followed by 1μL (40 U) RiboLock® RNase inhibitor for 30 min at 37°C to block RNase activity, and heparin (455 U per 1 μg siRNA) for 30 min at 37°C to dissociate the siRNA from the dendrimer. Aqueous medium: TE buffer 1X pH 8. Untreated siRNA control (300 ng) before (*lane 1*) and after (*lane 2*) incubation with RNase A..... 150

Figure 5.4. RNase protection assay (non-denaturing agarose gel electrophoresis) of the siRNA-G4NH2 dendriplexes (N/P 5) as a function of the RNase A concentration. Dendriplexes incubated in presence (+) or absence (-) of the treatments: RNase A (0.35, 0.7, 1.0, 1.5, and 3.5 μg per 1 μg siRNA, in *lanes 4-7*, *8-11*, *12-15*, *16-19*, *20-23*, respectively) for 6 h at 37°C, followed by 1μL (40 U) RiboLock® RNase inhibitor for 30 min at 37°C to block RNase activity, and heparin (455 U per 1 μg siRNA) for

30 min at 37 °C to dissociate the siRNA from the dendrimer. Aqueous medium: TE buffer 1X pH 8. Untreated siRNA control (250 ng) in *lane 1*, after incubation with heparin (*lane 2*) and 0.35 μg RNase A per 1 μg siRNA (*lane 3*)..... 151

Figure 5.5. *In vitro* release of siRNA from dendriplexes in 0.1 M citrate/phosphate buffer (pH 5 and 7.4, mimicking intracellular endosomes/lysosomes and cytosol, respectively) at 37°C. siRNA-G4NH2 dendriplexes differ by N/P ratio: N/P 10 **(a)**, N/P 20 **(b)**, and N/P 30 **(c)** 153

Figure 5.6. *In vitro* cytotoxicity of G4NH2 alone **(a)** and siRNA-G4NH2 dendriplexes at N/P 30 **(b)** in increased concentrations in A549 cell line. ∗ = statistically different compared to untreated cells control; n.s.d. = no statistical difference among them (*p* value < 0.05, One-Way ANOVA) 154

Figure 5.7. *In vitro* knockdown of eGFP expression in A549 cells stably expressing eGFP. siRNA-G4NH2 dendriplexes at N/P 5, 10, 20, and 30, were prepared with **(a)** siRNA as received from the supplier and **(b)** at N/P 20 with lyophilized siRNA stored in HFA-227 (HFA, at 25°C and saturation pressure of the propellant) and in freezer at -20°C (FRE, at 253 K) for 2 months. Specificity of the knockdown (positive siRNA sequence, anti-eGFP) is maintained by comparison to effects with the negative siRNA sequence (scramble). Lipofectamine® 2000 (LF) and TransFast™ (TF) were the commercial transfection reagents used as controls, and bare siRNA was negative control. G4NH2 concentration at N/P 30 corresponds to 1.95 μM, and siRNA concentration in all systems was 80 nM. ∗∗ = statistically different compared to untreated eGFP A549 cells control; ∗ = statistically different compared to eGFP A549 cells treated with bare siRNA; n.s.d. = no statistical difference among them (*p* value < 0.05, One-Way ANOVA)..... 157

Figure 5.8. Size and morphology of mannitol **(a)** and CSLA **(b)** microparticles loaded with siRNA-G4NH2 dendriplexes at N/P 10 as determined by LS (*main distribution on right*) and SEM (*lower left inset*). Particles were dispersed in HPFP (2 $mg.mL^{-1}$) to perform LS, and after that, the HPFP was evaporated and 1 mL DI-water was added to dissolve the mannitol or CSLA shell, and LS was performed again, but at this time, the size of the dendriplexes released from the mannitol (or CSLA) was measured by LS (*upper left inset*). Non-denaturing agarose gel electrophoresis (*upper right inset*) show the integrity of the siRNA after its release from mannitol (or CSLA) shell and G4NH2 dendrimer by incubation in aqueous heparin solution (455 U per 1 μg siRNA) for 30 min at 37°C. Untreated siRNA (250 ng) as positive control in *lane 1*; mixture of G4NH2, mannitol (or CSLA) and heparin (but no siRNA) as negative control in *lane 2*; siRNA-G4NH2 dendriplexes at N/P 10

loaded into mannitol (or CSLA) microparticles after incubation with aqueous heparin in *lane 3* 161

Figure 5.9. Aerosol properties of the pMDI formulations prepared with siRNA-G4NH2 dendriplexes at N/P 10 loaded into **(a)** mannitol and **(b)** CSLA microparticles. All formulations at 2 mg particles per 1 mL of HFA-227 at 25°C, and saturation pressure of the propellant. siRNA concentration of 290 - 550 $ng.mL^{-1}$ for pMDI formulations prepared with mannitol loaded with dendriplexes, and 420 - 505 $ng.mL^{-1}$ for those prepared CSLA loaded with dendriplexes. AC, IP, and F refer to actuator, induction port and filter, respectively. *Insets:* Physical stability of freshly prepared pMDI formulations 167

Figure 6.1. Schematic illustrating the two-step preparation of G4NH2-siRNA conjugate. **(a)** Synthesis of the G4NH2-PDP ***(3)*** via reaction between G4NH2 ***(1)*** and SPDP ***(2)*** crosslinker. **(b)** Synthesis of G4NH2-siRNA conjugate ***(5)*** via reaction between G4NH2-PDP ***(3)*** prepared in the first step and siRNA-SH immediately after thiol deprotection ***(4)***..... 184

Figure 6.2. ^{1}H NMR characterization of **(a)** G4NH2, **(b)** G4NH2-PDP, **(c)** G4NH2-FITC, and **(d)** G4NH2-FITC-PDP conjugates. *Insets:* molecular structures (*upper left*) and MALDI-TOF spectra (*upper right*)..... 192

Figure 6.3. Non-denaturating agarose gel electrophoresis of ds-siRNA-SH kept under reaction conditions (but no presence of PDP-modified G4NH2) for 6 h (*lane 3*), 1 day (*lane 4*), 4 days (*lane 5*), 5 days (*lane 6*), 7 days (*lane 7*), 8 days (*lane 8*), 12 days (*lane 9*), 13 days (*lane 10*), and 14 days (*lane 11*). Untreated ds-siRNA before (*lane 1*) and immediately after (*lane 2*) thiol deprotection were used as controls. All lanes were loaded with ca. 300 ng siRNA..... 194

Figure 6.4. Non-denaturating agarose gel electrophoresis of G4NH2-siRNA conjugate without (*lane 2*) and with (*lane 3*) DTT treatment. Free and untreated siRNA control (300 ng) is shown in *lane 1* 196

Figure 6.5. *In vitro* knockdown of eGFP expression in A549 cells stably expressing eGFP. G4NH2-siRNA conjugates were equivalent to 80, 160, and 320 nM siRNA, as indicated in the plot. Lipofectamine® 2000 (LF), TransFast™ (TF), and free siRNA were used as controls at 80 nM siRNA concentration. Knockdown with positive siRNA sequence (anti-eGFP) is compared with the irrelevant siRNA sequence (negative). G4NH2 concentration in the conjugate equivalent to 320 nM siRNA was 0.06 μM. ∗∗ = statistically different compared to untreated eGFP A549 cells control; ∗ = statistically different compared to eGFP A549 cells treated with free siRNA; *p* value < 0.05, One-Way ANOVA..... 199

LIST OF ABBREVIATIONS

^{1}H-NMR	Proton Nuclear Magnetic Resonance Spectroscopy
AB	Antibiotics (Penicillin-Streptomycin liquid)
AC	Actuator
ACI	Andersen Cascade Impactor
AFM	Atomic Force Microscopy
AON	Antisense Oligonucleotide
ARDS	Acute Respiratory Distress Syndrome
ATCC	American Type Culture Collection
BAL	Bronchoalveolar Lavage
BALF	Bronchoalveolar Lavage Fluid
bp	base pairs
C8TS	n-Octyltrichlorosilane
CE	Complexation Efficiency
CF	Cystic Fibrosis
CFCs	Chlorofluorocarbons
CFM	Chemical Force Microscopy
CME	Clathrin-mediated Endocytosis
COCTS	3-Methoxypropyltrimethoxysilane
COOCTS	Acetoxypropyltrimethoxysilane
COPD	Chronic Obstructive Pulmonary Disease
CS	Chitosan

CSLA	Oligo(lactide)-*grafted*-Chitosan
CvME	Caveolae-mediated Endocytosis
D_2O	Deuterium Oxide
DAB	Diaminobutane
DDA	Degree of Deacetylation
DEPC	Diethylpyricarbonate
DHB	2,5-Dihydroxybenzoic Acid
DI-water	Deionized water
DLS	Dynamic Light Scattering
DMEM	Dulbecco's Modified Eagle Medium
DMSO	Dimethyl Sulfoxide
DMSO-d6	Deuterated Dimethyl Sulfoxide
DNA	Deoxyribonucleic Acid
DOTAP	1,2-dioleoyl-3-trimethylammonium-propane
DP	Degrees of Polymerization
DPIs	Dry Powder Inhalers
ds-DNA	Double-stranded DNA
ds-DS-siRNA	Double-stranded Dicer Substrate siRNA
ds-RNA	Double-stranded RNA
ds-siRNA	Double-stranded siRNA
DTT	Dithiothreitol
EDTA	Ethylenediaminetetraacetic Acid
EE	Encapsulation Efficiency

eGFP	enhanced Green Fluorescent Protein
FA	Folic Acid
FACS	Fluorescence-activated Cell Sorting
F_{ad}	Adhesion Force
FBS	Fetal Bovine Serum
FDA	Food and Drug Administration
FITC	Fluorescein Isothiocyanate
FPF	Fine Particle Fraction
FR	Folate Receptors
FTIR	Fourier Transform Infrared Spectroscopy
G4NH2	Generation-four amine-terminated PAMAM Dendrimer
GFP	Green Fluorescent Protein
GRAS	Generally Recognized As Safe
GSD	Geometric Standard Deviation
GSH	Glutathione
GWP	Global Warming Potential
HA	Hyaluronic Acid
HBSS	Hank's Balanced Salt Solution
HFA-134a	1,1,1,2-tetrafluoroethane
HFA-227	1,1,1,2,3,3,3-heptafluoropropane
HFAs	Hydrofluoroalkanes
HFOs	Hydrofluoroolefins
HPFP	2H,3H-perfluoropentane

i.v.	Intravenous
ILD	Interstitial Lung Disease
IP	Induction Port
IPF	Idiopathic Pulmonary Fibrosis
JKR	Johnson-Kendall-Roberts theory
LA	Lactide
LS	Light Scattering
MALDI-TOF	Matrix-assisted Laser Desorption Ionization Time-of-Flight mass spectrometry
MFI	Median Fluorescence Intensity
MMAD	Mass Median Aerodynamic Diameter
mRNA	messenger RNA
MTS	[(3-(4,5-dimethylthiazole-2-yl)-5-(3-carboxymethoxyphenyl)-2-(4-sulfophenyl)-2H-tetrazolium, inner salt]
Mw	Molecular Weight
MWCO	Molecular Weight Cut-off
N/P	Nitrogen/Phosphate ratio
NPs	Nanoparticles
OI	Oral Inhalation
OLA-*g*-CS	Oligo(lactide)-*grafted*-Chitosan
ON	Oligonucleotide
PAMAM	Poly(amidoamine)
PAP	Pulmonary Alveolar Proteinosis

PBS	Phosphate Buffered Saline
pDNA	plasmid DNA
PEG	Poly(ethylene glycol)
PEI	Polyethylenimine
PGA	Poly(glycolic acid)
PLA	Poly(lactic acid)
PLGA	Poly(D,L-lactic-*co*-glycolic acid)
PLL	Polylysine
PLO	Poly-L-ornithine
PLR	Poly-L-arginine
pMDIs	Pressurized Metered Dose Inhalers
PMS	Phenazine Methosulfate
PNCs	Polymeric Nanocarriers
PPI	Polypropyleneimine
PRINT	Particle Replication in Non-wetting Templates
p-TSA	p-Toluenesulfonic Acid monohydrate
QD	Quantum Dots
RADS	Reactive Airways Dysfunction Syndrome
RI	Tris-EDTA buffer
RISC	RNA-Induced Silencing Complex
RNAi	RNA interference
RNase A	Ribonuclease A
RSV	Respiratory Syncytial Virus

SARS	Severe Acute Respiratory Syndrome
SEM	Scanning Electronic Microscopy
Si_3N_4	Silicon Nitride
siRNA	Small Interfering Ribonucleic Acid
siRNA-SH	siRNA after thiol deprotection
$SnOct_2$	Stannous Octoate
SPDP	*N*-succinimidyl 3-(2-pyridyldithio) propionate
TAE	Tris Base, Acetic Acid and EDTA buffer
TCEP	Tris (2-carboxyethyl) phosphine hydrochloride
TE	Tris-EDTA buffer
TEM	Transmission Electronic Microscopy
USP	United States Pharmacopeia
UV-Vis	Ultraviolet-Visible Absorption Spectroscopy

LIST OF ORIGINAL PUBLICATIONS

This dissertation is based on the following publications:

1. **Conti, D. S.**;[1] Bharatwaj, B.;[1,2] Brewer, D.;[1,3] da Rocha, S. R. P.[1] Propellant-based inhalers for the non-invasive delivery of genes via oral inhalation. *Journal of Controlled Release* **2012**, 157, (3), 406-417.
2. **Conti, D. S.**;[1] Grashik, J.;[1] Yang, L.;[1] Wu, L.;[1,4] da Rocha, S. R. P.[1] Solvation in hydrofluoroalkanes: How can ethanol help? *Journal of Pharmacy and Pharmacology* **2011**, 64, (9), 1236-1244.
3. **Conti, D. S.**;[1] Brewer, D.;[1,3] Grashik, J.;[1] Avasarala, S.;[1] da Rocha, S. R. P.[1] Dendrimer Nanocarriers and their Aerosol Formulations for siRNA Delivery to the Lung Epithelium. *To be submitted to Molecular Pharmaceutics*, **2013**.
4. **Conti, D. S.**;[1] Zhong, Q.;[1] Patel, A. M.;[1] da Rocha, S. R. P.[1] siRNA-Dendrimer Conjugates for the Lung Epithelium: Synthesis, Characterization, and Gene Silencing. *To be submitted to Journal of the American Chemical Society*, **2013**.

[1] Department of Chemical Engineering and Materials Science, College of Engineering, Wayne State University, Detroit, MI, USA.

Present addresses:

[2] Merck & Co., Summit, NJ, USA.

[3] BASF Co., Wyandotte, MI, USA.

[4] Teva Respiratory LLC, USA.

CHAPTER 1

Introduction

1.1 Overview and Objectives

Oral inhalation (OI) is a promising route for the administration of therapeutics including small molecules and biomacromolecules, such as nucleotides, peptides, and proteins, *to* (regionally) and *through* (systemically) the lungs.[1, 2] The large surface area of the lungs, good epithelial permeability, and small aqueous volume at the absorptive surface are some advantages of systemic delivery via the pulmonary route.[1] OI is especially attractive for the delivery of nucleic acids (deoxyribonucleic acid – DNA, and small interfering ribonucleic acid – siRNA, for example) as it provides for a direct and non-invasive means of targeting different regions of the lungs. Fewer side effects are expected compared to intravenous (i.v.) administration, which is an indirect way of targeting the lungs, as lower dosages may be required due to enhanced local bioavailability.[2]

However, despite all potential advantages, the use of OI to deliver nucleic acids for the treatment of medically relevant pulmonary diseases such as lung cancer, cystic fibrosis, and asthma, still remains relatively unexploited.[3] The progress of OI formulations for the delivery of nucleic acids to the lungs has been hampered largely by the lack of efficient carriers capable of overcoming the lung architecture, the extra and intracellular barriers present in the lung tissue,[4, 5] and formulation challenges.[6, 7] We attempt to address some of these challenges in this work.

Polymeric nanocarriers (PNCs) have great potential when combined with OI therapies for the delivery of nucleic acids. PNCs can be applied to condense, encapsulate or conjugate nucleic acids, so as to enhance their cellular internalization. Moreover, PNCs can protect nucleic acids from degradation, promote sustainable release, and offer versatility in terms of cellular internalization and targeting through conjugation of ligands.[8] Ligand conjugation to PNCs have been shown to improve cellular uptake and specificity in cell binding.[9] Reductive, pH-, and thermo-responsive polymers can be used as a strategy for escaping lysosomal degradation, and improving the release of the therapeutics.[9, 10] Therefore, PNCs may offer unique opportunities to overcome extra and intracellular barriers to improve the delivery of therapeutics (including nucleic acids) *to* and *through* the lungs.

Inhaled delivery systems can be divided in three categories: nebulizers, pressurized metered dose inhalers (pMDIs), and dry powder inhalers (DPIs).[11] Nebulizers are used mostly in hospitals and usually are not preferred by patients with pulmonary diseases because they are large, inconvenient,[12] and have low delivery efficiency.[13] pMDIs and DPIs are the two most commonly used OI devices for treatment of lung diseases,[13] accounting for approximately 67% of the total sales in the respiratory market in 2007 – US, France, Germany, Italy, Spain, and UK.[14] pMDIs are the most widely used OI devices because they are compact, portable, inexpensive, provide multiple and reproducible doses, and the environment is sealed – no degradation of the therapeutic.[15, 16] DPIs also offer advantages – e.g. portability, compact, breath actuation, and no hand-mouth co-ordination is required – but humidity may cause powder aggregation and capsules to soften, and the respirable dose depends on the

inspiratory flow rate.[15] On the other hand, pMDIs also can be used by patients with diseased lungs, because it is propellant-based and not respiratory driven,[16, 17] and thus, they may be more suitable for children and elderly. pMDIs are thus very strong candidates for the delivery of nucleic acids *to* and *through* the lungs.[18]

Formulation Challenges. In order to efficiently deliver DNA and siRNA *to* the lungs using pMDIs, several formulation challenges need to be overcome. The *first* one is related to the aerodynamic particle size distribution, which needs to be between 1 and 5 μm for optimal lung deposition,[1, 19, 20] although some published works have mentioned the range of 0.5 - 5 μm.[13, 21] The rationale is that particles having aerodynamic size > 5 μm trend to be deposited in the oropharynx and large conducting airways due to inertial impaction, those between 1 and 5 μm are subject to gravitational sedimentation that occurs in the respiratory bronchioles and smaller airways, and those ≤ 0.5 μm are deposited by diffusion (Brownian motion).[22] *Secondly*, the particles need also to be well dispersed in the propellant to provide good aerosol performance,[23, 24] that is, they must have a surface chemistry able to be well-solvated by the propellant to prevent particle aggregation.[24-26] *Finally*, the effect of ethanol – the most used co-solvent in pMDIs to enhance solubility of therapeutics and excipients in propellant hydrofluoroalkanes (HFAs)[27, 28] – on solvation of surfactant tail groups in HFAs needs to be better understood, since good solvation is pre-requisite for particle stabilization upon surfactant adsorption.[26, 27, 29]

Nucleic Acid Delivery. While traditional routes for the delivery of nucleic acids (i.v.,[30-36] oral,[36-40] and intranasal[41-44]) have been extensively discussed in literature, much less attention has been given to OI. Nebulization is the most prominent OI

strategy that has been proposed so far for the delivery of nucleic acids to the lungs.[6, 45-53] However, current approaches (jet, ultrasonic, and mesh nebulizers)[45] are still inefficient due to shearing forces causing degradation/denaturation of the nucleic acid,[11] adhesion to the device components,[11] large residual dead volume, and evaporation.[6, 54-56] On DNA formulated in DPIs, some studies have demonstrated the potential of DNA-based lipoplexes dry powders,[57-59] and DNA-based polyplexes dry powders prepared by supercritical CO_2 using chitosan (CS) as cationic PNC.[60, 61] Literature on the formulation of DNA in pMDIs has been fairly limited.[54, 62] A single work discussing delivery of DNA applying HFA-based pMDI has been found up-to-date,[54] and it consists in the use of surfactant-coated DNA particles prepared by reverse microemulsion. On siRNA delivered to the lungs via DPIs, there are few reports describing preparation of siRNA-based dry powders using supercritical CO_2 and sugars,[63] particle replication in non-wetting templates (PRINT),[64] spray drying of siRNA encapsulated in poly(D,L-lactic-*co*-glycolic acid) nanoparticles (PLGA NPs)[65] and in cationic lipid-modified PLGA NPs.[66] To the best of our knowledge, no work has been reported about siRNA delivered to the lungs via pMDIs to date, and most of the *in vivo* studies use either intratracheal or intranasal routes.[41, 67, 68]

Within this context, the ***objectives*** of this dissertation are:

Objective # 01: Design PNCs capable of efficiently delivering nucleic acids to the lung epithelium. Gene therapy is a promising approach for the treatment of genetic and chronic diseases, and its application to treat pulmonary disorders that affect both the alveoli and airways is of great relevance.[69] In spite of the tremendous potential in

targeting DNA and siRNA to the lungs,[70, 71] there several barriers that need to overcome. Extracellular barriers include:[4, 72-74] lung architecture, mucociliary and cough clearance processes, macrophages, neutrophils, mucus layer and lung surfactant. Intracellular barriers include:[75-78] internalization, endolysosomal escape, nuclease degradation, release from the carrier, nuclear import and assembly into the RNA-induced silencing complex (RISC) – these latter two for DNA and siRNA, respectively. Since administration of free DNA and siRNA does not lead to the desired therapeutic effect,[76, 79] current research has focused on natural or synthetic carriers (viruses, lipids, peptides, and polymers) engineered to pack, protect, and deliver the nucleic acid to target cells.[79, 80] In this work, cationic polymers were chosen as PNCs for DNA and siRNA because they provide an attractive alternative to viruses and lipids – the complexes formed between cationic polymers and nucleic acids are more stable and less toxic.[36] Cationic polymers condense large genes into nanoparticles (NPs), protect them during cellular uptake and traffic, and provide flexibility since their physicochemical properties can be modulated by varying the polymer composition, molecular weight, architecture (linear, branched, dendrimer, block and graft copolymer), and chemistry (introduction of side chains and target-specific ligands).[81] In addition, their biological responses can be regulated by their size, surface charge, polymer degradation rate, and the mechanism of nucleic acid release, all characteristics that can be modulated.[81] We studied complexes formed between chitosan (CS) and DNA (*CS-DNA polyplexes*), and generation-four amine-terminated poly(amidoamine) dendrimer (PAMAM G4NH2) and siRNA (*siRNA-G4NH2 dendriplexes*). The studies were initiated with DNA, but switched to siRNA because DNA-based therapies have a key disadvantage – in order to

be properly expressed, the DNA must enter into the nucleus of the target cell. However, since such nuclear entry is a very inefficient process, this step has been faced as the biggest barrier to the success of DNA delivery.[67] The delivery of double-stranded RNA (small interfering RNA – siRNA – typically consisting of 20-27 base pairs in length)[82] which targets the RISC located in the cell cytoplasm is a very promising approach with great therapeutic potential to treat many diseases.[67] Moreover, there are also disadvantages associated with polyplexes and dendriplexes – *(i)* the sizes vary widely from as low as 50 nm to ca. 750 nm, with high polydispersity and variable shapes[83-85] which can affect the cellular uptake;[86] *(ii)* the highly positive charges can be cytotoxic due to non-specific interactions with the cellular components,[81, 87] and *(iii)* cause aggregation in negatively charged fluids (e.g. serum, bronchoalveolar lavage, mucus and lung surfactant);[81, 83, 87] in addition, *(iv)* polyplexes and dendriplexes can be entrapped by the negatively charged mucus layer and lung surfactant components, and have reduced transport and cellular uptake.[72] However, it has been demonstrated that charge is necessary, but not sufficient enough for cellular uptake.[88] Direct conjugation of molecules to siRNA is an alternative that has demonstrated to increase the delivery efficiency to the target tissue, while maintaining the gene silencing activity.[89] Therefore, in order to address these issues and have a PNC capable to overcome extra and intracellular barriers involved in pulmonary gene delivery, we designed and tested siRNA-PNC conjugates. We used PAMAM G4NH2 as PNC, synthesized *G4NH2-siRNA conjugates*, and tested their ability to deliver siRNA *to* the lung epithelium as a gene silencing strategy. Details about the design and studies involving the *CS-DNA*

polyplexes, *siRNA-G4NH2 dendriplexes*, and *G4NH2-siRNA conjugates* will be further described in the following chapters.

Objective # 02: Develop oral inhalation formulations of PNCs containing DNA and siRNA in propellant-based metered-dose inhalers. As discussed earlier, the direct targeting of DNA and siRNA *to* the lungs via OI administration has tremendous potential.[70, 71] However, the use of pMDIs in pulmonary delivery of nucleic acids is still relatively unexploited, mainly due to challenges related to formulation – particles in suitable aerodynamic size for deep lung deposition,[1, 13, 19] and containing an appropriate surface chemistry for solvation in propellant HFAs.[24-26] In order to address these issues, we first developed a general platform for the delivery of nucleic acids *to* the lungs via pMDIs based on the *engineering of core-shell particles*. Micron-sized core-shell particles (polyplexes or dendriplexes as core, and a biodegradable water soluble co-oligomer as shell) were prepared by emulsification diffusion, which allows particle size modulation by changing the parameters.[24] The shell was made from oligo(lactide)-*grafted*-CS (OLA-*g*-CS) co-oligomer which is designed to be HFA-philic, and thus provides the appropriate surface chemistry for colloidal stability to the pMDI formulation.[24] We tested this general platform to deliver two different types of DNA (CS-DNA polyplexes) and siRNA (siRNA-G4NH2 dendriplexes) *to* the lung epithelium via pMDIs. We also engineered *mannitol spray-dried micron-sized particles* to aid in the delivery of siRNA via OI pMDIs. Mannitol is a sugar alcohol that is FDA approved for OI,[15] it is clinically used for airway hydration,[90] it has high aqueous solubility, and is generally recognized as safe (GRAS) excipient widely used as bulking agent and non-

active carrier in DPIs.[91, 92] It has been shown that micron-sized mannitol particles demonstrated less adhesion/cohesion in propellant HFA-134a, slower sedimentation rate, and superior aerosol performance than lactose ones.[93] Moreover, since solvation is a pre-requisite for particle stabilization upon surfactant adsorption in suspension-based pMDI formulations,[26, 27, 29] *the effect of ethanol as cosolvent in solvation* is an important factor to be considered during the development of the pMDI formulation. Thus, in order to address this issue, we performed a study to evaluate the ability of ethanol mixed with propellant HFA to improve solvation of moieties of relevance to pMDIs. We applied chemical force microscopy (CFM) to measure the adhesion force (F_{ad}) between various moieties in 2H,3H-perfluoropentane (HPFP) mixed with ethanol. HPFP is a liquid at ambient conditions that mimics propellant HFAs.[94] The F_{ad} results were thus a measure of solvation in HFAs. Johnson-Kendall-Roberts (JKR) theory was used to model the experimental results. Details about the design and studies involving *the engineering of core-shell particles*, *the use of mannitol spray-dried particles*, and *the effect of ethanol in solvation* will be further described in the following chapters.

In Chapter 2 we present the literature review about carriers for pulmonary gene delivery, siRNA conjugates, extra and intracellular barriers to pulmonary delivery of nucleic acids, and pMDIs for the delivery of nucleic acids via OI administration.

In Chapter 3 we discuss *the effect of ethanol cosolvent in solvation forces in hydrofluoroalkanes*. The goal of this work was to evaluate the ability of ethanol added to propellant HFA to improve solvation of moieties of relevance in pMDIs. Chemical force microscopy (CFM) was used to measure the adhesion force (F_{ad}) between alkyl-,

ether- and ester-based moieties (C8/C8, COC/COC and COOC/COOC interactions) in liquid mixtures of HPFP and ethanol. The C8 moiety was selected as baseline, as it represents the tail groups of surfactants currently used in commercial pMDI formulations, e.g. oleic acid and sorbitan trioleate,[27, 95] which have very low solubility in HFAs,[95] and are poorly solvated by HFAs alone, being unable to stabilize drug suspensions in HFAs.[26, 27, 96] The COC and COOC moieties contain more polar groups, which provide possible sites to form strong polar interactions with the HFAs.[28] The substrates and AFM cantilevers were surface-modified via solution deposition, and the CFM measurements were performed in a liquid cell. Since there is no propellant HFA which is liquid at ambient conditions, HPFP was used because it is very well known to mimic HFAs.[94] The F_{ad} values were thus a measure of solvation in HFAs, and the Johnson-Kendall-Roberts (JKR) theory was used to model the experimental results. This chapter is based on the published manuscript: **Conti, D. S.**; Grashik, J.; Yang, L.; Wu, L.; da Rocha, S. R. P. Solvation in hydrofluoroalkanes: How can ethanol help? *Journal of Pharmacy and Pharmacology* **2011**, 64, (9), 1236-1244.

In Chapter 4 we discuss *the use of CS as PNC for DNA delivery (CS-DNA polyplexes) to the lung epithelium, and their formulation in pMDIs using engineered core-shell particles*. CS was selected as cationic PNC because it is biodegradable, biocompatible, and has shown low cytotoxicity in relevant epithelial models.[36, 97] CS with molecular weight (Mw) varying between 10 and 100 kDa,[98] when considered in combination with other relevant parameters such as degree of deacetylation (DDA), nitrogen/phosphate (N/P) ratio, pH and serum content of the culture medium, and cell type,[36] seems to optimize the *in vitro* gene expression of the DNA. Thus, large Mw CS

(100 - 300 kDa and 80% DDA) was depolymerized,[99] and the Mw was characterized by viscometry.[100] Calf Thymus DNA (18,940 bp) and a plasmid DNA (pDNA, 5,757 bp) encoding for green fluorescent protein (GFP) were chosen as models of nucleic acid. The use of two different DNAs (plasmid *vs.* linear) is relevant to demonstrate the applicability of the proposed approach for the delivery of a broad range of nucleic acids to the lungs. CS-DNA polyplexes were characterized according to size, morphology, surface charge, complexation efficiency, and DNA protection against nuclease degradation. Oligo(lactide)-*grafted*-CS (OLA-*g*-CS, the co-oligomer shell) was synthesized according to a modified method from literature,[24, 101] and characterized by ^{1}H-NMR, FTIR and MALDI-TOF. Emulsification diffusion was used to prepare the core-shell particles (CS-DNA polyplexes as core and OLA-*g*-CS as shell) and the resulting micron-sized particles were characterized according to size, morphology, and DNA loading efficiency. These microparticles were then formulated in propellant HFA-227, and the suspension-based pMDIs were evaluated according to their physical stability and aerosol performance using Andersen Cascade Impactor (ACI). The biological functionality and integrity of the pDNA were demonstrated via *in vitro* gene transfection in A549 cell line (human lung adenocarcinoma cell line, an *in vitro* model of Type II alveolar epithelium)[102] and gel electrophoresis, respectively. *In vitro* cytotoxicity studies of CS and OLA-*g*-CS were performed in A549 cell line as well. This chapter is based on the published manuscript: **Conti, D. S.**; Bharatwaj, B.; Brewer, D.; da Rocha, S. R. P. Propellant-based inhalers for the non-invasive delivery of genes via oral inhalation. *Journal of Controlled Release* **2012**, 157, (3), 406-417.

In Chapter 5 we discuss *the use of PAMAM G4NH2 as PNC to deliver siRNA (siRNA-G4NH2 dendriplexes) to the lung epithelium, and their formulation in pMDIs using mannitol spray-dried micron-sized and core-shell particles*. PAMAM dendrimers are highly branched polymers with low polydispersity, high functionality, and provide an ideal structure for construction of effective drug carriers, gene transfer vehicles, and imaging of biological systems.[103, 104] There has been a growing interest in the use of PAMAM with low generation (≤ G4) due to their low cytotoxicity at relevant concentrations.[105] Dendriplexes were prepared and fully characterized according to size, morphology, surface charge, and siRNA complexation efficiency. Their ability to protect the siRNA against nuclease degradation, and to release the siRNA at pH-dependent *in vitro* conditions was evaluated according to different N/P ratios. The *in vitro* gene knockdown of eGFP (enhanced green fluorescent protein) in A549 cell line (stably expressing eGFP) was demonstrated using siRNA before and after a long-term exposure in propellant HFA-227. *In vitro* cytotoxicity studies of G4NH2 (pure and as dendriplexes) were performed in A549 cell line as well. The siRNA-G4NH2 dendriplexes were formulated in pMDIs using two strategies – *mannitol spray-dried* and *core-shell particles*. The microparticles containing dendriplexes were characterized according to size, morphology, siRNA loading efficiency and integrity, and the suspension-based pMDIs were evaluated according to their physical stability and aerosol characteristics using ACI. This chapter is based on the manuscript: **Conti, D. S.**; Brewer, D.; Grashik, J.; Avasarala, S.; da Rocha, S. R. P. Dendrimer Nanocarriers and their Aerosol Formulations for siRNA Delivery to the Lung Epithelium. *To be submitted to Molecular Pharmaceutics*, **2013**.

In Chapter 6 we discuss *synthesis, characterization, and gene knockdown efficiency of G4NH2-siRNA conjugates*. As discussed earlier, free siRNA being delivered to lung cells is very susceptible to degradation, and it has poor cellular internalization.[76] Current strategies (polyplexes, dendriplexes, and polyesteres NPs) for delivering siRNA have demonstrated limitations, and thus, a PNC with conjugated siRNA may offer unique opportunities to overcome extra and intracellular barriers encountered in the pulmonary epithelia. In terms of conjugation, PAMAM dendrimers are very attractive as PNCs due to their very small size (c.a. 4.5 nm), molecular uniformity, and abundance of functional groups, which allows for chemical modification and linkage of different compounds, including imaging agents and ligands along with the therapeutic molecules.[106] PAMAM G4NH2 and siRNA were conjugated via *N*-succinimidyl 3-(2-pyridyldithio) propionate (SPDP) crosslinker, which allows a reducible disulfide bond between the dendrimer and siRNA, and it is expected to be cleaved preferentially in the reductive space of the cytosol, thus releasing the siRNA in its target site.[89] G4NH2 was firstly reacted with SPDP crosslinker, and this intermediate conjugate was characterized using ^{1}H-NMR, MALDI-TOF, UV-Vis Spectroscopy, and DLS. Next, the G4NH2-PDP was reacted with siRNA, and the final G4NH2-siRNA conjugate was characterized via DLS, UV-Vis Spectroscopy, and non-denaturing agarose gel electrophoresis. The ability of G4NH2-siRNA conjugates to deliver siRNA to the lung epithelium was tested using *in vitro* gene knockdown experiments in A549 cells stably expressing eGFP. This chapter is based on the manuscript: **Conti, D. S.**; Zhong, Q.; Patel, A. M.; da Rocha, S. R. P. siRNA-Dendrimer Conjugates for the Lung

Epithelium: Synthesis, Characterization, and Gene Silencing. *To be submitted to Journal of the American Chemical Society*, **2013**.

In Chapter 7 we discuss conclusions and future directions.

1.2 Relevance and Innovation

This research is *innovative* in several aspects. Since gene knockdown or expression is relevant in the treatment of many lung diseases, the use of DNA and siRNA as therapeutics is very attractive.[107] This is the first time that DNA and siRNA as polyplexes and dendriplexes are formulated and tested in pMDIs. In addition, several reports describe the conjugation of siRNA with other compounds, e.g. hyaluronic acid (HA),[108] PLGA,[109] poly(ethylene glycol) (PEG),[110-117] polylysine(PLL)-PEG-peptide,[118] gold[119, 120] and magnetic NPs,[121] quantum dots (QD),[122, 123] α-tocopherol,[124] poly(PEG acrylate),[125] amphipathic poly(vinyl ether),[126] and cell penetrating peptides.[127-129] However, there is no literature reporting siRNA-dendrimer conjugates. This research is also *relevant* as pMDIs are commonly used as OI devices for treatment of pulmonary diseases.[13, 14] Therefore, this work contributes to the development of new gene-based therapies that may be employed in the treatment of medically relevant pulmonary diseases such as cystic fibrosis, lung cancer, tuberculosis, and asthma, among others, and aid in their further formulation in such inexpensive OI devices.

1.3 References

1. Patton, J. S.; Byron, P. R. Inhaling medicines: Delivering drugs to the body through the lungs. *Nat. Rev. Drug Discovery* **2007,** *6*, (1), 67-74.

2. Laube, B. L. The expanding role of aerosols in systemic drug delivery, gene therapy, and vaccination. *Respir. Care* **2005,** *50*, (9), 1161-1176.

3. Merkel, O. M.; Zheng, M.; Debus, H.; Kissel, T. Pulmonary gene delivery using polymeric nonviral vectors. *Bioconjugate Chem.* **2011**.

4. Gill, D. R.; Davies, L. A.; Pringle, I. A.; Hyde, S. C. The development of gene therapy for diseases of the lung. *CMLS, Cell. Mol. Life Sci.* **2004,** *61*, (3), 355-368.

5. Densmore, C. L. Advances in noninvasive pulmonary gene therapy. *Curr. Drug Delivery* **2006,** *3*, 55-63.

6. Birchall, J. Pulmonary delivery of nucleic acids. *Expert Opin. Drug Delivery* **2007,** *4*, (6), 575-578.

7. Shoyele, S. A.; Cawthorne, S. Particle engineering techniques for inhaled biopharmaceuticals. *Adv. Drug Delivery Rev.* **2006,** *58*, (9-10), 1009-1029.

8. Gary, D. J.; Puri, N.; Won, Y.-Y. Polymer-based siRNA delivery: Perspectives on the fundamental and phenomenological distinctions from polymer-based DNA delivery. *J. Controlled Release* **2007,** *121*, (1-2), 64-73.

9. Brewer, E.; Coleman, J.; Lowman, A. Emerging technologies of polymeric nanoparticles in cancer drug delivery. *J. Nanomater.* **2011,** *2011*, 1-10.

10. Engler, A. C.; Bonner, D. K.; Buss, H. G.; Cheung, E. Y.; Hammond, P. T. The synthetic tuning of clickable pH responsive cationic polypeptides and block copolypeptides. *Soft Matter* **2011,** *7*, (12), 5627-5637.

11. Dolovich, M. B.; Dhand, R. Aerosol drug delivery: Developments in device design and clinical use. *The Lancet* **2011,** *377*, (9770), 1032-1045.

12. Telko, M. J.; Hickey, A. J. Dry powder inhaler formulation. *Respir. Care* **2005,** *50*, (9), 1209-1227.

13. Goel, A.; Sahni, J.; Ali, J.; Baboota, S. Exploring targeted pulmonary delivery for treatment of lung cancer. *Int. J. Pharm. Invest.* **2013,** *3*, (1), 8-14.

14. Oversteegen, L. Inhaled medicines: Product differentiation by device. *Innovations Pharm. Technol.* **2008,** *26*, 62-65.

15. Labiris, N. R.; Dolovich, M. B. Pulmonary drug delivery. Part II: The role of inhalant delivery devices and drug formulations in therapeutic effectiveness of aerosolized medications. *Br. J. Clin. Pharmacol.* **2003,** *56*, (6), 600-612.

16. Zhang, J.; Wu, L.; Chan, H.-K.; Watanabe, W. Formation, characterization, and fate of inhaled drug nanoparticles. *Adv. Drug Delivery Rev.* **2011,** *63*, (6), 441-455.

17. Marijani, R.; Shaik, M. S.; Chatterjee, A.; Singh, M. Evaluation of metered dose inhaler (MDI) formulations of ciclosporin. *J. Pharm. Pharmacol.* **2007,** *59*, (1), 15-21.

18. Bell, J.; Newman, S. The rejuvenated pressurised metered dose inhaler. *Expert Opin. Drug Delivery* **2007,** *4*, (3), 215-234.

19. U.S. Department of Health and Human Services, Guidance for industry - metered dose inhaler (MDI) and dry powder inhaler (DPI) drug products - chemistry, manufacturing, and controls documentation. Food and Drug Administration (FDA), Center for Drug Evaluation and Research (CDER): 1998; p 62.

20. O'Donnell, K. P.; III, R. O. W. Pulmonary dispersion formulations: The impact of dispersed powder properties on pressurized metered dose inhaler stability. *Drug Dev. Ind. Pharm.* **2013,** *39*, (3), 413-424.

21. Fink, J. B.; Colice, G. L.; Hodder, R. Inhaler devices for patients with COPD. *J. Chronic Obstruct. Pulm. Dis.* **2013**, 130508125222007.

22. Yang, W.; Peters, J. I.; Williams III, R. O. Inhaled nanoparticles - A current review. *Int. J. Pharm.* **2008,** *356*, (1–2), 239-247.

23. Peguin, R. P. S.; Wu, L.; da Rocha, S. R. P. The ester group: How hydrofluoroalkane-philic is it? *Langmuir* **2007,** *23*, (16), 8291-8294.

24. Wu, L.; Bharatwaj, B.; Panyam, J.; da Rocha, S. Core-shell particles for the dispersion of small polar drugs and biomolecules in hydrofluoroalkane propellants. *Pharm. Res.* **2008,** *25*, (2), 289-301.

25. Bharatwaj, B.; Wu, L.; Whittum-Hudson, J. A.; Rocha, S. R. P. d. The potential for the noninvasive delivery of polymeric nanocarriers using propellant-based inhalers in the treatment of Chlamydial respiratory infections. *Biomaterials* **2010,** *31*, 7376-7385.

26. Wu, L.; Peguin, R. P. S.; da Rocha, S. R. P. Understanding solvation in hydrofluoroalkanes: *Ab Initio* calculations and chemical force microscopy. *J. Phys. Chem. B* **2007,** *111*, (28), 8096-8104.

27. da Rocha, S. R. P.; Bharatwaj, B.; Saiprasad, S., Science and Technology of Pressurized Metered-Dose Inhalers. In *Controlled Pulmonary Drug Delivery* Smyth, H. D. C.; Hickey, A. J., Eds. Springer New York: 2011; pp 165-201.

28. Wu, L.; da Rocha, S. R. P. Applications of the atomic force microscope in the development of propellant-based inhalation formulations. *KONA Powder and Particle Journal* **2008,** *26*, 106-128.

29. Peguin, R. P. S.; da Rocha, S. R. P. Solvent-solute interactions in hydrofluoroalkane propellants. *J. Phys. Chem. B* **2008,** *112*, (27), 8084-8094.

30. Sato, A.; Takagi, M.; Shimamoto, A.; Kawakami, S.; Hashida, M. Small interfering RNA delivery to the liver by intravenous administration of galactosylated cationic liposomes in mice. *Biomaterials* **2007,** *28*, (7), 1434-1442.

31. de Wolf, H. K.; Snel, C. J.; Verbaan, F. J.; Schiffelers, R. M.; Hennink, W. E.; Storm, G. Effect of cationic carriers on the pharmacokinetics and tumor localization of nucleic acids after intravenous administration. *Int. J. Pharm.* **2007,** *331*, (2), 167-175.

32. Verbaan, F. J.; Oussoren, C.; van Dam, I. M.; Takakura, Y.; Hashida, M.; Crommelin, D. J. A.; Hennink, W. E.; Storm, G. The fate of poly(2-dimethyl amino ethyl)methacrylate-based polyplexes after intravenous administration. *Int. J. Pharm.* **2001,** *214*, (1-2), 99-101.

33. Howard, K. A. Delivery of RNA interference therapeutics using polycation-based nanoparticles. *Adv. Drug Delivery Rev.* **2009,** *61*, (9), 710-720.

34. Ge, Q.; Evans, D.; Xu, J. J.; Yang, H. H.; Lu, P. Y., Pulmonary delivery of small interfering RNA for novel therapeutics. In *Delivery Technologies for Biopharmaceuticals: Peptides, Proteins, Nucleic Acids and Vaccines* John Wiley & Sons, Ltd: 2009; pp 269-289.

35. Merdan, T.; Kunath, K.; Petersen, H.; Bakowsky, U.; Voigt, K. H.; Kopecek, J.; Kissel, T. PEGylation of poly(ethylene imine) affects stability of complexes with plasmid DNA under *in vivo* conditions in a dose-dependent manner after intravenous injection into mice. *Bioconjugate Chem.* **2005,** *16*, (4), 785-792.

36. Kim, T.-H.; Jiang, H.-L.; Jere, D.; Park, I.-K.; Cho, M.-H.; Nah, J.-W.; Choi, Y.-J.; Akaike, T.; Cho, C.-S. Chemical modification of chitosan as a gene carrier *in vitro* and *in vivo*. *Prog. Polym. Sci.* **2007,** *32*, (7), 726-753.

37. Li, G.; Liu, Z.; Liao, B.; Zhong, N. Induction of Th1-type immune response by chitosan nanoparticles containing plasmid DNA encoding house dust mite allergen der p 2 for oral vaccination in mice. *Cell. Mol. Immunol.* **2009,** *6*, (1), 45-50.

38. Chen, J.; Yang, W.-L.; Li, G.; Qian, J.; Xue, J.-L.; Fu, S.-K.; Lu, D.-R. Transfection of mEpo gene to intestinal epithelium *in vivo* mediated by oral delivery of chitosan-DNA nanoparticles. *World J. Gastroenterol.* **2004,** *10*, (1), 112-116.

39. Roy, K.; Mao, H.-Q.; Huang, S.-K.; Leong, K. W. Oral gene delivery with chitosan-DNA nanoparticles generates immunologic protection in a murine model of peanut allergy. *Nat. Med.* **1999,** *5*, (4), 387-391.

40. Guliyeva, Ü.; Öner, F.; Özsoy, S.; Haziroglu, R. Chitosan microparticles containing plasmid DNA as potential oral gene delivery system. *Eur. J. Pharm. Biopharm.* **2006,** *62*, (1), 17-25.

41. Bitko, V.; Barik, S., Nasal delivery of siRNA. In *Methods in Molecular Biology*, Humana Press: Totowa, NJ, 2008; Vol. 442 - RNAi: Design and application, pp 75-82.

42. Konstan, M. W.; Davis, P. B.; Wagener, J. S.; Hilliard, K. A.; Stern, R. C.; Milgram, L. J. H.; Kowalczyk, T. H.; Hyatt, S. L.; Fink, T. L.; Gedeon, C. R.; Oette, S. M.; Payne, J. M.; Muhammad, O.; Ziady, A. G.; Moen, R. C.; Cooper, M. J. Compacted DNA nanoparticles administered to the nasal mucosa of cystic fibrosis subjects are safe and demonstrate partial to complete cystic fibrosis transmembrane regulator reconstitution. *Hum. Gene Ther.* **2004,** *15*, (12), 1255-1269.

43. Yang, X.; Yuan, X.; Cai, D.; Wang, S.; Zong, L. Low molecular weight chitosan in DNA vaccine delivery via mucosa. *Int. J. Pharm.* **2009,** *375*, (1-2), 123-132.

44. Han, I.-K.; Kim, M.; Byun, H.-M.; Hwang, T.; Kim, J.; Hwang, K.; Park, T.; Jung, W.-W.; Chun, T.; Jeong, G.-J.; Oh, Y.-K. Enhanced brain targeting efficiency of intranasally administered plasmid DNA: An alternative route for brain gene therapy. *J. Mol. Med.* **2007,** *85*, (1), 75-83.

45. Arulmuthu, E. R.; Williams, D. J.; Baldascini, H.; Versteeg, H. K.; Hoare, M. Studies on aerosol delivery of plasmid DNA using a mesh nebulizer. *Biotechnol. Bioeng.* **2007,** *98*, (5), 939-955.

46. Dailey, L. A.; Kleemann, E.; Merdan, T.; Petersen, H.; Schmehl, T.; Gessler, T.; Hänze, J.; Seeger, W.; Kissel, T. Modified polyethylenimines as non viral gene delivery systems for aerosol therapy: Effects of nebulization on cellular uptake and transfection efficiency. *J. Control. Release* **2004,** *100*, (3), 425-436.

47. Rudolph, C.; Müller, R. H.; Rosenecker, J. Jet nebulization of PEI/DNA polyplexes: physical stability and *in vitro* gene delivery efficiency. *J. Gene Med.* **2002,** *4*, (1), 66-74.

48. Nielsen, E.; Nielsen, J.; Becker, D.; Karlas, A.; Prakash, H.; Glud, S.; Merrison, J.; Besenbacher, F.; Meyer, T.; Kjems, J.; Howard, K. Pulmonary gene silencing in transgenic EGFP mice using aerosolised chitosan/siRNA nanoparticles. *Pharm. Res.* **2010,** *27*, (12), 2520-2527.

49. Zamora-Avila, D. E.; Zapata-Benavides, P.; Franco-Molina, M. A.; Saavedra-Alonso, S.; Trejo-Avila, L. M.; Resendez-Perez, D.; Mendez-Vazquez, J. L.; Isaias-Badillo, J.; Rodriguez-Padilla, C. WT1 gene silencing by aerosol delivery of PEI-RNAi complexes inhibits B16-F10 lung metastases growth. *Cancer Gene Ther.* **2009,** *16*, (12), 892-899.

50. Xu, C.-X.; Jere, D.; Jin, H.; Chang, S.-H.; Chung, Y.-S.; Shin, J.-Y.; Kim, J.-E.; Park, S.-J.; Lee, Y.-H.; Chae, C.-H.; Lee, K. H.; Beck, G. R., Jr.; Cho, C.-S.; Cho, M.-H. Poly(ester amine)-mediated, aerosol-delivered Akt1 small interfering RNA suppresses lung tumorigenesis. *Am. J. Respir. Crit. Care Med.* **2008,** *178*, (1), 60-73.

51. Taratula, O.; Kuzmov, A.; Shah, M.; Garbuzenko, O. B.; Minko, T. Nanostructured lipid carriers as multifunctional nanomedicine platform for pulmonary co-delivery of anticancer drugs and siRNA. *J. Controlled Release* **2013,** *In Press, Accepted Manuscript. 10.1016/j.jconrel.2013.04.018*.

52. Mohammadi, Z.; Dorkoosh, F. A.; Hosseinkhani, S.; Gilani, K.; Amini, T.; Najafabadi, A. R.; Tehrani, M. R. *In vivo* transfection study of chitosan-DNA-FAP-B nanoparticles as a new non viral vector for gene delivery to the lung. *Int. J. Pharm.* **2011,** *421*, (1), 183-188.

53. Densmore, C. L.; Orson, F. M.; Xu, B.; Kinsey, B. M.; Waldrep, J. C.; Hua, P.; Bhogal, B.; Knight, V. Aerosol delivery of robust polyethyleneimine-DNA complexes for gene therapy and genetic immunization. *Mol. Ther.* **2000,** *1*, (2), 180-188.

54. Bains, B. K.; Birchall, J. C.; Toon, R.; Taylor, G. *In vitro* reporter gene transfection via plasmid DNA delivered by metered dose inhaler. *J. Pharm. Sci.* **2010,** *99*, (7), 3089-3099.

55. Li, H. Y.; Seville, P. C.; Williamson, I. J.; Birchall, J. C. The use of amino acids to enhance the aerosolisation of spray-dried powders for pulmonary gene therapy. *J. Gene Med.* **2005,** *7*, (3), 343-353.

56. Beck-Broichsitter, M.; Knuedeler, M.-C.; Schmehl, T.; Seeger, W. Following the concentration of polymeric nanoparticles during nebulization. *Pharm. Res.* **2013,** *30*, (1), 16-24.

57. Seville, P. C.; Kellaway, I. W.; Birchall, J. C. Preparation of dry powder dispersions for non-viral gene delivery by freeze-drying and spray-drying. *J. Gene Med.* **2002,** *4*, (4), 428-437.

58. Jinturkar, K. A.; Anish, C.; Kumar, M. K.; Bagchi, T.; Panda, A. K.; Misra, A. R. Liposomal formulations of Etoposide and Docetaxel for p53 mediated enhanced cytotoxicity in lung cancer cell lines. *Biomaterials* **2012,** *33*, (8), 2492-2507.

59. Li, H.-Y.; Birchall, J. Chitosan-modified dry powder formulations for pulmonary gene delivery. *Pharm. Res.* **2006,** *23*, (5), 941-950.

60. Mizuno, T.; Mohri, K.; Nasu, S.; Danjo, K.; Okamoto, H. Dual imaging of pulmonary delivery and gene expression of dry powder inhalant by fluorescence and bioluminescence. *J. Control. Release* **2009,** *134*, (2), 149-154.

61. Okamoto, H.; Sakakura, Y.; Shiraki, K.; Oka, K.; Nishida, S.; Todo, H.; Iida, K.; Danjo, K. Stability of chitosan-pDNA complex powder prepared by supercritical carbon dioxide process. *Int. J. Pharm.* **2005,** *290*, (1-2), 73-81.

62. Brown, A. R.; Chowdhury, S. I. Propellant-driven aerosols of DNA plasmids for gene expression in the respiratory tract. *J. Aerosol Med.* **1997,** *10*, (2), 129-146.

63. Pathak, P.; Quinn, B.; Rebits, L.; Sievers, R., Supercritical fluid technology for pulmonary delivery of siRNA oligonucleotides. In *20th Rocky Mountain Regional Meeting of the American Chemical Society* Denver, CO, United States, 2007 'Vol.' 175.

64. Garcia, A.; Mack, P.; Williams, S.; Fromen, C.; Shen, T.; Tully, J.; Pillai, J.; Kuehl, P.; Napier, M.; DeSimone, J. M. Microfabricated engineered particle systems for respiratory drug delivery and other pharmaceutical applications. *J. Drug Delivery* **2012,** *2012*, 1-10.

65. Jensen, D. M. K.; Cun, D.; Maltesen, M. J.; Frokjaer, S.; Nielsen, H. M.; Foged, C. Spray drying of siRNA-containing PLGA nanoparticles intended for inhalation. *J. Controlled Release* **2010,** *142*, (1), 138-145.

66. Jensen, D. K.; Jensen, L. B.; Koocheki, S.; Bengtson, L.; Cun, D.; Nielsen, H. M.; Foged, C. Design of an inhalable dry powder formulation of DOTAP-modified PLGA nanoparticles loaded with siRNA. *J. Controlled Release* **2012,** *157*, (1), 141-148.

67. Lam, J. K.-W.; Liang, W.; Chan, H.-K. Pulmonary delivery of therapeutic siRNA. *Adv. Drug Delivery Rev.* **2012,** *64*, (1), 1-15.

68. Bitko, V.; Musiyenko, A.; Shulyayeva, O.; Barik, S. Inhibition of respiratory viruses by nasally administered siRNA. *Nat. Med.* **2004,** *11*, (1), 50-55.

69. Park, T. G.; Jeong, J. H.; Kim, S. W. Current status of polymeric gene delivery systems. *Adv. Drug Delivery Rev.* **2006,** *58*, (4), 467-486.

70. Roy, I.; Vij, N. Nanodelivery in airway diseases: Challenges and therapeutic applications. *Nanomedicine* **2010,** *6*, (2), 237-244.

71. Harada-Shiba, M.; Takamisawa, I.; Miyata, K.; Ishii, T.; Nishiyama, N.; Itaka, K.; Kangawa, K.; Yoshihara, F.; Asada, Y.; Hatakeyama, K.; Nagaya, N.; Kataoka, K. Intratracheal gene transfer of adrenomedullin using polyplex nanomicelles attenuates monocrotaline-induced pulmonary hypertension in rats. *Mol. Ther.* **2009,** *17*, (7), 1180-1186.

72. Sanders, N.; Rudolph, C.; Braeckmans, K.; De Smedt, S. C.; Demeester, J. Extracellular barriers in respiratory gene therapy. *Adv. Drug Delivery Rev.* **2009,** *61*, (2), 115-127.

73. Merkel, O. M.; Kissel, T. Nonviral pulmonary delivery of siRNA. *Acc. Chem. Res.* **2011,** *45(7)*, (7), 961-970.

74. Rytting, E.; Nguyen, J.; Wang, X.; Kissel, T. Biodegradable polymeric nanocarriers for pulmonary drug delivery. *Expert Opin. Drug Delivery* **2008,** *5*, (6), 629-639.

75. Gottfried, L. F.; Dean, D. A., Extracellular and intracellular barriers to non-viral gene transfer. In *Novel Gene Therapy Approaches*, Licensee InTech: 2013; pp 75-88.

76. Wang, J.; Lu, Z.; Wientjes, M.; Au, J. Delivery of siRNA therapeutics: Barriers and carriers. *AAPS J.* **2010,** *12*, (4), 492-503.

77. Dominska, M.; Dykxhoorn, D. M. Breaking down the barriers: siRNA delivery and endosome escape. *J. Cell Sci.* **2010,** *123*, (8), 1183-1189.

78. Whitehead, K. A.; Langer, R.; Anderson, D. G. Knocking down barriers: Advances in siRNA delivery. *Nat. Rev. Drug Discovery* **2009,** *8*, (2), 129-138.

79. Grigsby, C. L.; Leong, K. W. Balancing protection and release of DNA: Tools to address a bottleneck of non-viral gene delivery. *J. R. Soc. Interface* **2010,** *7*, (Suppl 1), S67-S82.

80. Gao, X.; Kim, K.-S.; Liu, D. Nonviral gene delivery: What we know and what is next. *AAPS J.* **2007,** *9*, (1), E92-E104.

81. Sun, X.; Zhang, N. Cationic polymer optimization for efficient gene delivery. *Mini-Rev. Med. Chem.* **2010,** *10*, 108-125.

82. Arima, H.; Yoshimatsu, A.; Ikeda, H.; Ohyama, A.; Motoyama, K.; Higashi, T.; Tsuchiya, A.; Niidome, T.; Katayama, Y.; Hattori, K.; Takeuchi, T. Folate-PEG-appended dendrimer conjugate with α-cyclodextrin as a novel cancer cell-selective siRNA delivery carrier. *Mol. Pharmaceutics* **2012,** *9*, (9), 2591-2604.

83. Beyerle, A.; Braun, A.; Merkel, O.; Koch, F.; Kissel, T.; Stoeger, T. Comparative *in vivo* study of poly(ethylene imine)/siRNA complexes for pulmonary delivery in mice. *J. Controlled Release* **2011,** *151*, (1), 51-56.

84. Chou, L. Y. T.; Ming, K.; Chan, W. C. W. Strategies for the intracellular delivery of nanoparticles. *Chem. Soc. Rev.* **2011,** *40*, (1), 233-245.

85. Nafee, N.; Taetz, S.; Schneider, M.; Schaefer, U. F.; Lehr, C.-M. Chitosan-coated PLGA nanoparticles for DNA/RNA delivery: Effect of the formulation parameters on complexation and transfection of antisense oligonucleotides. *Nanomedicine* **2007,** *3*, (3), 173-183.

86. Rejman, J.; Oberle, V.; Zuhorn, I. S.; Hoekstra, D. Size-dependent internalization of particles via the pathways of clathrin- and caveolae-mediated endocytosis. *Biochem. J.* **2004,** *377*, (1), 159-169.

87. Remaut, K.; Sanders, N. N.; De Geest, B. G.; Braeckmans, K.; Demeester, J.; De Smedt, S. C. Nucleic acid delivery: Where material sciences and bio-sciences meet. *Mater. Sci. Eng., R* **2007,** *58*, (3-5), 117-161.

88. Patil, M. L.; Zhang, M.; Betigeri, S.; Taratula, O.; He, H.; Minko, T. Surface-modified and internally cationic polyamidoamine dendrimers for efficient siRNA delivery. *Bioconjugate Chem.* **2008,** *19*, (7), 1396-1403.

89. Jeong, J. H.; Mok, H.; Oh, Y.-K.; Park, T. G. siRNA conjugate delivery systems. *Bioconjugate Chem.* **2009,** *20*, (1), 5-14.

90. Ibrahim, B. M.; Park, S.; Han, B.; Yeo, Y. A strategy to deliver genes to cystic fibrosis lungs: A battle with environment. *J. Controlled Release* **2011,** *155*, (2), 289-295.

91. Kho, K.; Hadinoto, K. Effects of excipient formulation on the morphology and aqueous re-dispersibility of dry-powder silica nano-aggregates. *Colloids Surf. A, Physicochem. Eng. Asp.* **2010,** *359*, (1–3), 71-81.

92. Steckel, H.; Bolzen, N. Alternative sugars as potential carriers for dry powder inhalations. *Int. J. Pharm.* **2004,** *270*, (1-2), 297-306.

93. Young, P. M.; Adi, H.; Patel, T.; Law, K.; Rogueda, P.; Traini, D. The influence of micronised particulates on the aerosolisation properties of pressurised metered dose inhalers. *J. Aerosol Sci.* **2009,** *40*, (4), 324-337.

94. Rogueda, P. G. A. HPFP, a model propellant for pMDIs. *Drug Dev. Ind. Pharm.* **2003,** *29*, (1), 39-49.

95. Vervaet, C.; Byron, P. R. Drug-surfactant-propellant interactions in HFA-formulations. *Int. J. Pharm.* **1999,** *186*, (1), 13-30.

96. Rogueda, P. Novel hydrofluoroalkane suspension formulations for respiratory drug delivery. *Expert Opin. Drug Delivery* **2005,** *2*, (4), 625-638.

97. MacLaughlin, F. C.; Mumper, R. J.; Wang, J.; Tagliaferri, J. M.; Gill, I.; Hinchcliffe, M.; Rolland, A. P. Chitosan and depolymerized chitosan oligomers as condensing carriers for *in vivo* plasmid delivery. *J. Controlled Release* **1998,** *56*, (1-3), 259-272.

98. Strand, S. P.; Lelu, S.; Reitan, N. K.; de Lange Davies, C.; Artursson, P.; Vårum, K. M. Molecular design of chitosan gene delivery systems with an optimized balance between polyplex stability and polyplex unpacking. *Biomaterials* **2010,** *31*, (5), 975-987.

99. Tian, F.; Liu, Y.; Hu, K.; Zhao, B. Study of the depolymerization behavior of chitosan by hydrogen peroxide. *Carbohydr. Polym.* **2004,** *57*, (1), 31-37.

100. Kasaai, M. R. Calculation of Mark-Houwink-Sakurada (MHS) equation viscometric constants for chitosan in any solvent-temperature system using experimental reported viscometric constants data. *Carbohydr. Polym.* **2007,** *68*, (3), 477-488.

101. Conti, D. S.; Bharatwaj, B.; Brewer, D.; da Rocha, S. R. P. Propellant-based inhalers for the non-invasive delivery of genes via oral inhalation. *J. Controlled Release* **2012,** *157*, (3), 406-417.

102. Foster, K. A.; Oster, C. G.; Mayer, M. M.; Avery, M. L.; Audus, K. L. Characterization of the A549 cell line as a type II pulmonary epithelial cell model for drug metabolism. *Exp. Cell Res.* **1998,** *243*, (2), 359-366.

103. Heiden, T. C. K.; Dengler, E.; Kao, W. J.; Heideman, W.; Peterson, R. E. Developmental toxicity of low generation PAMAM dendrimers in zebrafish. *Toxicol. Appl. Pharmacol.* **2007,** *225*, (1), 70-79.

104. Ouyang, D.; Zhang, H.; Parekh, H. S.; Smith, S. C. The effect of pH on PAMAM dendrimer-siRNA complexation - Endosomal considerations as determined by molecular dynamics simulation. *Biophys. Chem.* **2011,** *158*, (2-3), 126-133.

105. Arima, H.; Motoyama, K.; Higashi, T. Potential use of polyamidoamine dendrimer conjugates with cyclodextrins as novel carriers for siRNA. *Pharmaceuticals* **2012,** *5*, (1), 61-78.

106. Singha, K.; Namgung, R.; Kim, W. J. Polymers in small-interfering RNA delivery. *Nucleic Acid Ther.* **2011,** *21*, (3), 133-147.

107. Durcan, N.; Murphy, C.; Cryan, S.-A. Inhalable siRNA: Potential as a therapeutic agent in the lungs. *Mol. Pharmaceutics* **2008,** *5*, (4), 559-566.

108. Park, K.; Yang, J.-A.; Lee, M.-Y.; Lee, H.; Hahn, S. K. Reducible hyaluronic acid-siRNA conjugates for target specific gene silencing. *Bioconjugate Chem.* **2013,** *24*, (7), 1201-1209.

109. Lee, S. H.; Mok, H.; Lee, Y.; Park, T. G. Self-assembled siRNA-PLGA conjugate micelles for gene silencing. *J. Controlled Release* **2011,** *152*, (1), 152-158.

110. Jung, S.; Lee, S. H.; Mok, H.; Chung, H. J.; Park, T. G. Gene silencing efficiency of siRNA-PEG conjugates: Effect of PEGylation site and PEG molecular weight. *J. Controlled Release* **2010,** *144*, (3), 306-313.

111. Choi, S. W.; Lee, S. H.; Mok, H.; Park, T. G. Multifunctional siRNA delivery system: Polyelectrolyte complex micelles of six-arm PEG conjugate of siRNA and cell penetrating peptide with crosslinked fusogenic peptide. *Biotechnol. Prog.* **2009,** *26*, (1), 57-63.

112. Kim, S. H.; Jeong, J. H.; Lee, S. H.; Kim, S. W.; Park, T. G. Local and systemic delivery of VEGF siRNA using polyelectrolyte complex micelles for effective treatment of cancer. *J. Controlled Release* **2008,** *129*, (2), 107-116.

113. Kim, S. H.; Jeong, J. H.; Lee, S. H.; Kim, S. W.; Park, T. G. LHRH receptor-mediated delivery of siRNA using polyelectrolyte complex micelles self-assembled from siRNA-PEG-LHRH conjugate and PEI. *Bioconjugate Chem.* **2008,** *19*, (11), 2156-2162.

114. Lee, S. H.; Kim, S. H.; Park, T. G. Intracellular siRNA delivery system using polyelectrolyte complex micelles prepared from VEGF siRNA-PEG conjugate and cationic fusogenic peptide. *Biochem. Biophys. Res. Commun.* **2007,** *357*, (2), 511-516.

115. Kim, S. H.; Jeong, J. H.; Lee, S. H.; Kim, S. W.; Park, T. G. PEG conjugated VEGF siRNA for anti-angiogenic gene therapy. *J. Controlled Release* **2006,** *116*, (2), 123-129.

116. Oishi, M.; Nagasaki, Y.; Itaka, K.; Nishiyama, N.; Kataoka, K. Lactosylated poly(ethylene glycol)-siRNA conjugate through acid-labile β-thiopropionate linkage to construct pH-sensitive polyion complex micelles achieving enhanced gene silencing in hepatoma cells. *J. Am. Chem. Soc.* **2005,** *127*, (6), 1624-1625.

117. Oishi, M.; Sasaki, S.; Nagasaki, Y.; Kataoka, K. pH-responsive oligodeoxynucleotide (ODN)-poly(ethylene glycol) conjugate through acid-labile β-thiopropionate linkage: Preparation and polyion complex micelle formation. *Biomacromolecules* **2003,** *4*, (5), 1426-1432.

118. Meyer, M.; Dohmen, C.; Philipp, A.; Kiener, D.; Maiwald, G.; Scheu, C.; Ogris, M.; Wagner, E. Synthesis and biological evaluation of a bioresponsive and endosomolytic siRNA-polymer conjugate. *Mol. Pharmaceutics* **2009,** *6*, (3), 752-762.

119. Lee, J.-S.; Green, J. J.; Love, K. T.; Sunshine, J.; Langer, R.; Anderson, D. G. Gold, poly(β-amino ester) nanoparticles for small interfering RNA delivery. *Nano Lett.* **2009,** *9*, (6), 2402-2406.

120. Giljohann, D. A.; Seferos, D. S.; Prigodich, A. E.; Patel, P. C.; Mirkin, C. A. Gene regulation with polyvalent siRNA-nanoparticle conjugates. *J. Am. Chem. Soc.* **2009,** *131*, (6), 2072-2073.

121. Medarova, Z.; Pham, W.; Farrar, C.; Petkova, V.; Moore, A. *In vivo* imaging of siRNA delivery and silencing in tumors. *Nat. Med.* **2007,** *13*, (3), 372-377.

122. Singh, N.; Agrawal, A.; Leung, A. K. L.; Sharp, P. A.; Bhatia, S. N. Effect of nanoparticle conjugation on gene silencing by RNA interference. *J. Am. Chem. Soc.* **2010,** *132*, (24), 8241-8243.

123. Derfus, A. M.; Chen, A. A.; Min, D.-H.; Ruoslahti, E.; Bhatia, S. N. Targeted quantum dot conjugates for siRNA delivery. *Bioconjugate Chem.* **2007,** *18*, (5), 1391-1396.

124. Nishina, K.; Unno, T.; Uno, Y.; Kubodera, T.; Kanouchi, T.; Mizusawa, H.; Yokota, T. Efficient *in vivo* delivery of siRNA to the liver by conjugation of α-tocopherol. *Mol. Ther.* **2008,** *16*, (4), 734-740.

125. Heredia, K. L.; Nguyen, T. H.; Chang, C.-W.; Bulmus, V.; Davis, T. P.; Maynard, H. D. Reversible siRNA-polymer conjugates by RAFT polymerization. *Chem. Commun.* **2008**, (28), 3245-3247.

126. Rozema, D. B.; Lewis, D. L.; Wakefield, D. H.; Wong, S. C.; Klein, J. J.; Roesch, P. L.; Bertin, S. L.; Reppen, T. W.; Chu, Q.; Blokhin, A. V.; Hagstrom, J. E.; Wolff, J. A. Dynamic polyconjugates for targeted *in vivo* delivery of siRNA to hepatocytes. *Proc. Natl. Acad. Sci. U.S.A.* **2007,** *104*, (32), 12982-12987.

127. Moschos, S. A.; Jones, S. W.; Perry, M. M.; Williams, A. E.; Erjefalt, J. S.; Turner, J. J.; Barnes, P. J.; Sproat, B. S.; Gait, M. J.; Lindsay, M. A. Lung delivery studies using siRNA conjugated to TAT(48−60) and penetratin reveal peptide induced reduction in gene expression and induction of innate immunity. *Bioconjugate Chem.* **2007,** *18*, (5), 1450-1459.

128. Juliano, R. L. Intracellular delivery of oligonucleotide conjugates and dendrimer complexes. *Ann. N. Y. Acad. Sci.* **2006,** *1082*, (1), 18-26.

129. Muratovska, A.; Eccles, M. R. Conjugate for efficient delivery of short interfering RNA (siRNA) into mammalian cells. *FEBS Lett.* **2004,** *558*, (1-3), 63-68.

CHAPTER 2

Literature Review

2.1 Carriers for Pulmonary Gene Delivery

Gene therapy is a broad term that involves any approach to treat diseases using intracellular transfer of nucleic acids (e.g. DNA and siRNA) to modulate cellular functions by expressing proteins, or inhibiting induction of specific genes.[1, 2] Gene therapy has attracted attention in the fields of medicine, pharmacy, and bionanotechnology due to its potential for treating a large number of relevant diseases.[3]

Exogenous gene transfer to the lungs provides an important strategy for the treatment of several heritable and acquired lung diseases. Treatment of airway diseases, such as cystic fibrosis (CF), asthma, reactive airways dysfunction syndrome (RADS), primary pulmonary hypertension, bronchitis, and bronchiectasis, requires delivery of relevant genes to the airway epithelium.[4-7] In contrast, the alveolar region is the target for diseases such as α1-antitrypsin deficiency, emphysema, chronic pulmonary microlithiasis, idiopathic pulmonary fibrosis (IPF), pulmonary alveolar proteinosis (PAP), acute respiratory distress syndrome (ARDS), interstitial lung disease (ILD), and respiratory syncytial virus (RSV) infection.[4, 8-11] Chronic obstructive pulmonary disease (COPD) refers to two lung diseases, chronic bronchitis and emphysema, and it requires gene delivery to airways and alveoli.[12] In addition, most types of lung cancer arise from the small bronchi/bronchioles and alveoli.[13] While the promise in gene delivery to treat lung diseases is great, there are many challenges to overcome for the development of effective gene therapies to the lung tissue.

Due to the structural similarity between DNA and siRNA,[14] the barriers to their delivery are somewhat similar. Both nucleic acids must overcome the extracellular barriers present in the airways and alveolar epithelia, be internalized by the cell, and escape from lysosomal degradation. However, while DNA needs to enter into the nucleus for initiation of transcription of the encoded gene, siRNA functions in the cytoplasm – this is a determinant advantage of siRNA over DNA[15] especially for non-mitotic cells, where nuclear internalization is significantly challenging.[15, 16] RNA interference (RNAi, Figure 2.1) is a natural gene silencing pathway in eukaryotic cells by which sequence-specific siRNA is able to target and cleave complementary messenger RNA (mRNA).[17] However, the lack of safe and effective siRNA and DNA carriers and effective portable OI formulations have hindered the clinical progress of lung gene therapy.[18]

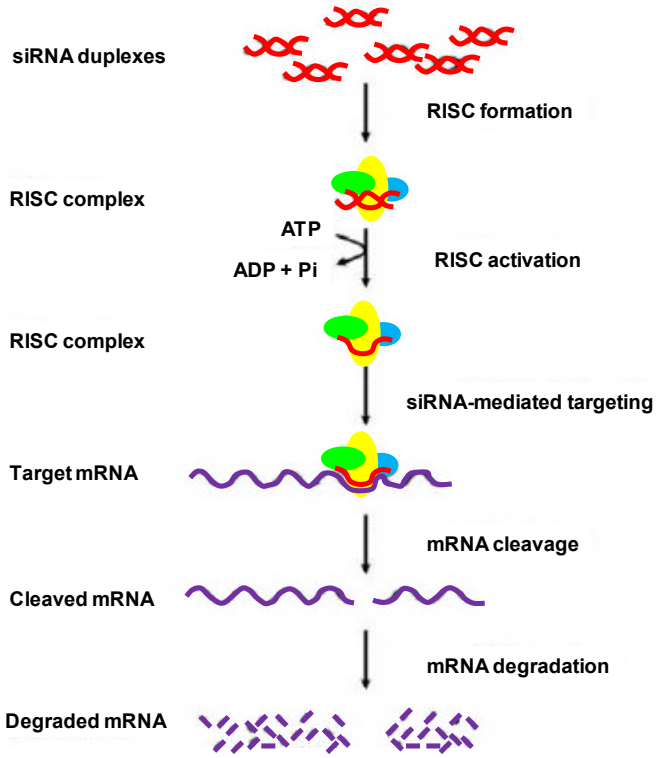

Figure 2.1. Mechanism of RNAi in mammalian cells.[19]

Administration of free DNA, in most cases, results in insufficient quantities of intact coding sequences reaching the nucleus of the target cell.[18] Similarly, free siRNA is readily degraded by nucleases, and does not cross the cell membrane through passive diffusion due to its large molecular weight (Mw ~ 13 kDa) and negative charge. Thus, administration of free siRNA usually fails to produce therapeutic effects as well.[16] Current research has focused on the use natural or synthetic carriers (viruses, lipids, peptides, and polymers) engineered to pack, protect, and deliver DNA and siRNA to target cells.[18, 20]

Cationic polymers provide an attractive alternative to viruses and lipids, since they are able to form ionic complexes with DNA and siRNA, which are more stable and less toxic.[21] Cationic polymers condense large genes into nanoparticles (NPs) and protect the nucleic acid during cellular uptake. The use of cationic polymers provides flexibility since the chemical and physical properties of polyplexes (Figure 2.2) can be modulated by varying the polymer composition, Mw, architecture (linear, branched, dendrimer, block and graft copolymer) and chemistry (conjugation of side chains and target-specific ligands).[22, 23] In addition, the biological response of the polyplexes can be regulated by their size, surface charge and polymer degradation rate. The mechanism of DNA/siRNA release can be modulated as well.[22] Several cationic polymers have been studied as carriers for DNA to the lungs, *in vitro* and *in vivo*, such as poly-L-lysine (PLL), poly-L-arginine (PLR), poly-L-ornithine (PLO), polyethylenimine (PEI), chitosan (CS) and poly(amidoamine) (PAMAM) dendrimers.[24-33] Similarly, CS/siRNA, PEI/siRNA, folate-CS-*g*-PEI/siRNA, CS-*g*-PEI/siRNA, and PEG-PEI/siRNA polyplexes have shown gene knockdown in lung cells *in vitro*[34-36] and *in vivo*.[34, 35, 37-40]

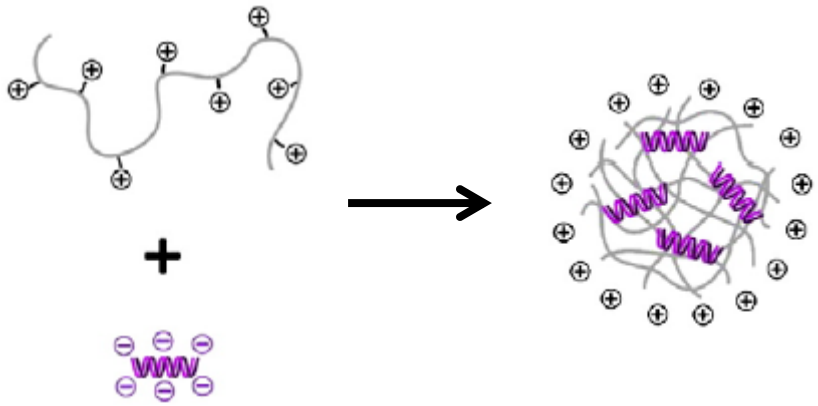

Figure 2.2. Polyplexes are formed by electrostatic interactions between cationic polymer and negatively charged DNA/siRNA.[23]

However, the delivery of nucleic acids using polyplexes has some disadvantages. Since the complexation process is electrostatic and entropically driven,[41] attaining reproducible particles is extremely cumbersome,[22] and the sizes vary widely from as low as ca. 50 to 500 nm, with high polydispersity and variable shapes[42, 43] which could affect the cellular uptake.[44] Nevertheless, the size of DNA-based NPs needs to be maintained between 25 and 30 nm to facilitate nuclear transport.[45, 46] Moreover, siRNA is a stiffer molecule than DNA, and thus, a 21 bp siRNA is not likely to further condense.[14] Disorderly interactions between siRNA and cationic polymers may result in low complexation efficiency and large NPs.[14] siRNA-based polyplexes are also expected to be less stable due to the lower number of negative charges compared to DNA.[47]

The highly positively charged polyplexes can also be cytotoxic due to non-specific interactions with the cellular components.[22, 48] Moreover, polyplexes may aggregate in negatively charged fluids (e.g. serum, BALF, mucus and lung surfactant).[22, 40, 48] This aggregation reduces the number of positive charges or causes

charge reversal, increasing the size of the polyplexes[49] which may have reduced cellular uptake and transfection efficiency.[44] Moreover, positively charged polyplexes can be entrapped by the negative charged mucus layer and lung surfactant components, and thus have reduced transport and cellular uptake.[50] Thus, the design of polyplexes with balanced cationicity level seems to be a plausible alternative to overcome the aforementioned hindrances.

Another alternative for delivering genes to cells and tissues is the encapsulation of the nucleic acid within a biodegradable polymer matrix, usually polyesters such as poly(lactic acid) (PLA), poly(glycolic acid) (PGA), and poly(D,L-lactic-*co*-glycolic acid) (PLGA).[51, 52] Using this approach, the gene can be protected from degradation in a physiological environment, and such particles have enhanced cellular uptake compared to free nucleic acids.[52] DNA/PLGA and siRNA/PLGA NPs have shown *in vitro* controlled-release ability over an extended period of time (> 30 days)[43, 52, 53] and prolonged gene expression *in vivo*.[29]

However, there are also disadvantages associated with gene delivery from biodegradable polymeric matrices: degradation of the nucleic acid during encapsulation,[49, 54, 55] poor gene loading,[48, 49] and reproducibility in size.[51] Hydrolysis of PLA, PGA, and PLGA releases acidic moieties and produces low pH environment, which potentially can result in DNA/siRNA degradation.[55, 56] Size and shape of the NPs are influenced by stabilizer and solvents used during their preparation.[51] Most stabilizers lead to negatively charged NPs, and thus, the nucleic acid encapsulation is achieved by double emulsion technique, which results in low gene loading.[48] The involvement of the nucleic acid with organic solvents can also impact its stability and

biological activity.[48, 51, 54] The negative surface charges of PLA, PGA, and PLGA NPs may limit their interaction with the cell membrane, leading to poor internalization.[43, 51] Thus, surface modification of the polyester NPs with different chemistries, such as cationic polymers (e.g. PLA and PLGA NPs coated with cationic surfactant[55] and chitosan[43, 51]) and PEG (e.g. PLA-PEG copolymer[57]) have been proposed as an alternative. Different strategies for particle preparation also have been proposed (solvent diffusion,[58] double- and single-emulsion, and spray-drying[112,114,115,119,122]).

The development of therapies for gene regulation in the lungs requires the efficient delivery of the nucleic acid to the target site of action.[59] siRNA has tremendous potential for the treatment of several pulmonary disorders, and clinical trials are already ongoing[15, 60-62] – aerosolization (phase IIa) and nasal spray (phases I and II) of siRNA to treat RVS,[63] inhalation to treat asthma (phase II),[64] and intravenous (i.v.) for metastatic lung cancer (phase I).[65] However, the delivery of stable and active siRNA to the lungs at high enough concentrations involves challenges in every step of the process.[66] The biggest hindrance to siRNA therapy is its effective delivery to the intracellular milieu within region of interest.[67] Viruses, complexation, and encapsulation in biodegradable polyesters NPs have been exploited *in vitro* and *in vivo*,[19, 60] but still present disadvantages. Thus, siRNA conjugated directly to the PNCs may be an interesting approach to overcome those limitations towards the success of the siRNA delivery.

2.2 siRNA Conjugates

Direct conjugation of molecules (e.g., antibodies, peptides and polymers) to siRNA is a potential alternative which can improve *in vivo* pharmacokinetic behavior of

the siRNA, enhance its biological half-life, increase its delivery efficiency to the targeted cell population, while maintaining the gene silencing activity,[68] and hence is a viable strategy to overcome the extra and intracellular barriers present in the lungs. Several reports have described the conjugation of siRNA with different compounds, e.g. hyaluronic acid (HA),[69] PLGA,[70] PEG,[71-78] PLL-PEG-peptide,[47] gold[79, 80] and magnetic NPs,[81] quantum dots (QD),[82, 83] α-tocopherol,[84] poly(PEG acrylate),[85] amphipathic poly(vinyl ether),[86] and cell penetrating peptides.[87-89] Thus, siRNA has a great versatility to be conjugated to several different molecules.

Since siRNA is a hybridized molecule of two complementary strands (sense and antisense) there are four terminal ends as potential conjugation sites. It has been observed that the integrity of the 5'-end of the antisense strand is important for the initiation of the RNAi mechanism.[90] Therefore, the 3'- and 5'-ends of the sense strand, and the 3'-end of the antisense strand (Figure 2.3a), are considered potential sites for conjugation with minimal influence on RNAi activity. In addition, most conjugates use cleavable linkages between siRNA and the conjugated molecule to facilitate the release of siRNA in the cell cytosol, such as acid-labile or reducible bonds (Figure 2.3b).[68] Disulfide bonds (S-S) are relatively stable in oxidizing environment, but can be easily cleaved by a reducing agent, forming two thiols (SH). In a polymeric backbone, the S-S bonds are readily reduced in the intracellular environment by small redox molecules, such as glutathione (GSH) and thioredoxin, either alone or with the aid of a enzymatic machinery.[91] GSH is very abundant in the cell cytoplasm, which functions as natural oxidant and the major reducing agent.[92] The intracellular concentration of GSH ranges from 0.5 to 20 mM, which makes the cell cytosol more reductive than the extracellular

environment[72] – e.g. 2 μM GSH in plasma.[92] Thus, the strategy of using disulfide bonds between the siRNA and the conjugated molecule provides a great opportunity for intracellular delivery of the siRNA as therapeutic.[92]

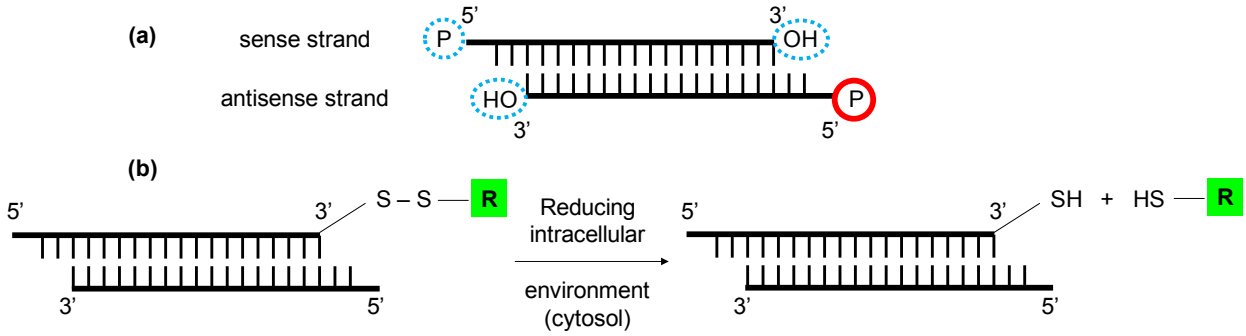

Figure 2.3. **(a)** Sites for conjugation onto siRNA (dashed circles), while the 5'-end of the antisense strand (solid circle line) is suggested to be free in order to keep the efficiency of the RNAi.[68] **(b)** Disulfide bond (S-S) between the siRNA and the conjugated molecule (R) is reduced (2 HS-) due to the redox molecules (e.g. glutathione) present in the cytoplasm.[91]

Independent on the gene carrier, the critical issue in delivering siRNA to the lungs via OI administration is the modulation of the interaction of formulation/nanocarrier with the biological extra and intracellular barriers,[93] which will be discussed next.

2.3 Extra and Intracellular Barriers to Pulmonary Delivery of Nucleic Acids

2.3.1 Lung physiology, mucus layer, and lung surfactant

Some of the extracellular barriers present in the lungs (Figures 2.4 and 2.5) include the branched pulmonary architecture, clearance processes (mucociliary and cough) and immune responses mediated by macrophages and neutrophils.[61, 94] In addition, mucus in the upper airways and surfactant in the lower airways represent the major barriers to cellular delivery of DNA and siRNA by entrapping the gene carriers and slowing down their diffusion.[61]

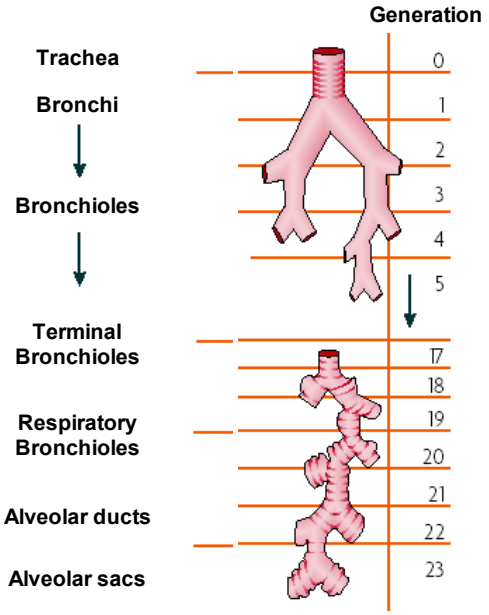

Figure 2.4. Bifurcations of the lungs from trachea to alveolar sacs.[95]

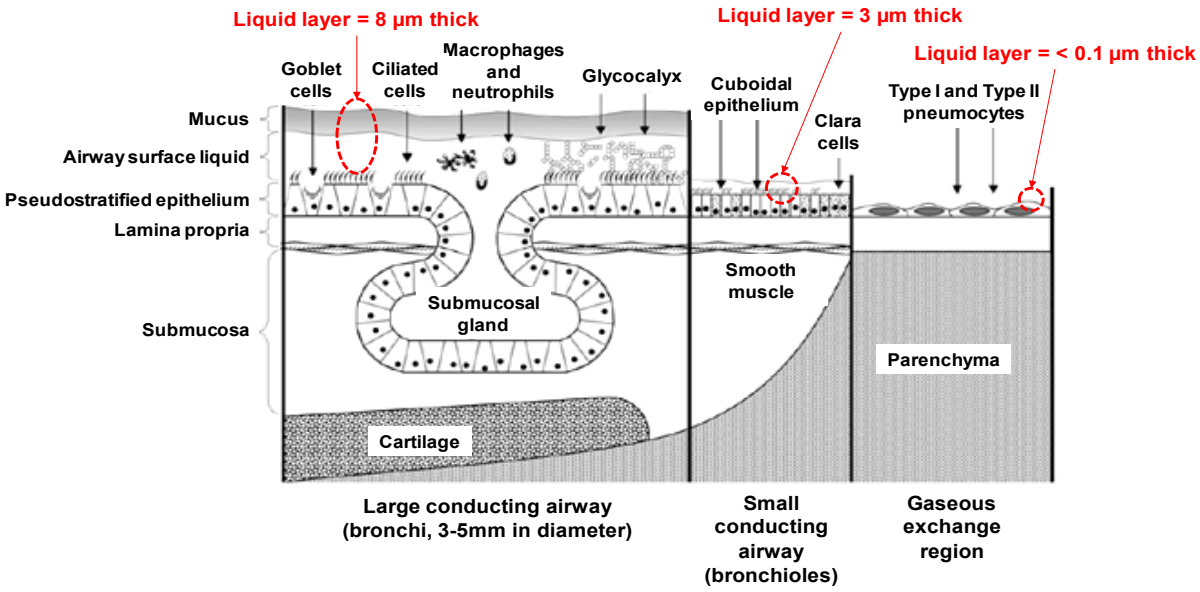

Figure 2.5. Physical and immune barriers to successful lung nucleic acid transfer.[95, 96]

The respiratory mucus lines the epithelium from the nose to the terminal bronchioles, and is mainly composed of a 3D network of cross-linked mucin chains (Figure 2.6a) which gives its viscoelastic properties.[97] Inhaled materials are entrapped

by the mucus and continuously transported by the cilia to the esophagus (mucociliary escalator). The location in the airways and the presence of pathologic conditions determine the thickness of the mucus layer (Figure 2.5). In non-pathological conditions, the mucus thickness is between 10 - 30 μm in the trachea, and between 2 - 5 μm in the bronchi, but some reports suggest that its thickness can vary from 5 to 260 μm.[50] However, under pathological condition, such as CF, the thickness of the mucus layer can be even higher,[50] and the viscosity and the composition of the mucus can also vary as well.[50]

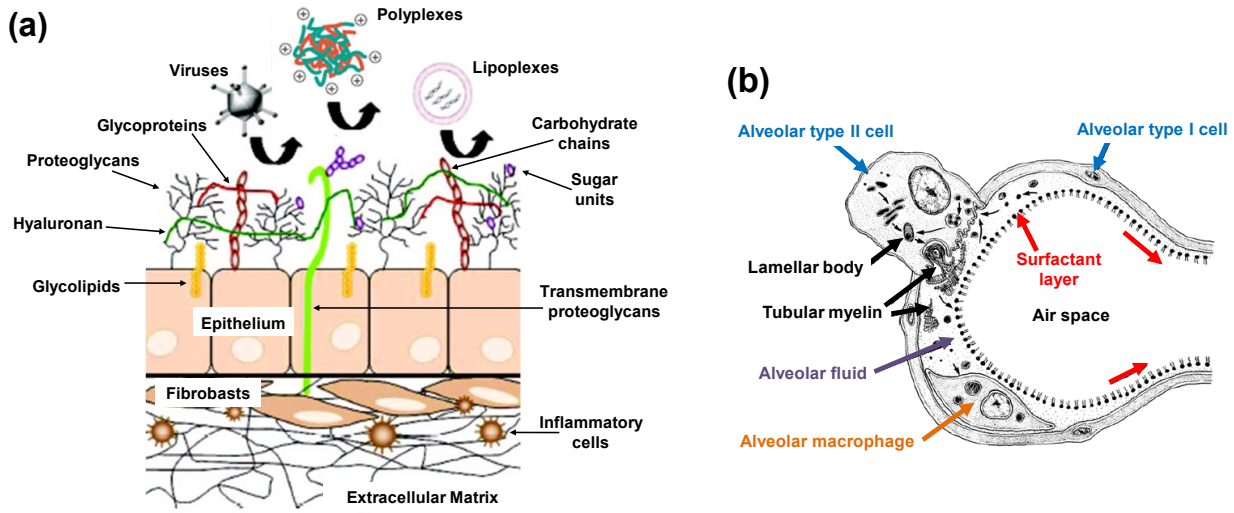

Figure 2.6. **(a)** The mucus layer, a mixture of carbohydrates, glycoproteins and polysaccharides, resides on the surface of the airways epithelium and forms a barrier for nanocarriers.[97] **(b)** Pulmonary surfactant, alveolar fluid and macrophages as barriers in the alveolus.[98]

Nanocarriers trying to cross the mucus layer will face three barriers: *(i)* the biopolymer network may block the diffusion of NPs by steric obstruction or by binding to the nanocarriers (function of the size and surface characteristics); *(ii)* macromolecules may also bind to the surface of the NPs, leading to aggregation; *(iii)* the removal of the mucus via mucociliary transport.[50] Thus, nanocarriers would be ideally small (100 nm in diameter or smaller) so as to allow free and fast passive diffusion through the mucus

network. In addition, the cationic surface of the NPs should be shielded by neutral and hydrophilic molecules to prevent strong interactions with the negatively charged biomolecules present in mucus.[50]

Lung surfactant (composed by phospholipids and specific surfactant-associated proteins) covers the alveolar epithelium (Figure 2.6b)[50, 98] and it is only ca. 50 - 80 nm thick.[94] The major function of the lung surfactant is to diminish the surface tension at the air-water interface of the terminal airways.[50, 98] Lung surfactant does represent a critical barrier to lipoplexes,[99] but polyplexes (e.g. DNA-PEI and DNA-PAMAM) have been demonstrated to be more resistant *in vitro*[100] and *in vivo*.[101] However, the effect of the lung surfactant on the properties of the gene carriers and transfection efficiency has received little attention.[99, 100, 102]

2.3.2 Cellular internalization

Once inside the cell, the nucleic acid has to be carried across several other barriers in order to reach the desired target and exert its therapeutic effect.[103] Even before that, however, the nanocarrier must first cross the cellular membrane which is composed of lipid bilayer, proteins (glycoproteins, proteoglycans and glycerolphosphates) and has a negative surface charge (Figure 2.7). Phagocytosis, macropinocytosis, and endocytosis are the main internalization pathways in mammalian cells.[104] Phagocytosis is performed by specialized cells (e.g. macrophages and neutrophils) on particles ca. 500 nm.[104] In macropinocytosis, the large endocytic vesicles (1 - 5 μm) acidify and shrink (Figure 2.7a).[104] Clathrin-mediated endocytosis (CME) is the predominant endocytic mechanism in most of the cells – it can be

receptor-dependent (endocytic vesicles ca. 100 - 120 nm) or receptor-independent (fluid-phase endocytosis).[104] CME leads to formation of early and late endosomes, and finally the lysosomes (the acidic and enzyme-rich environment ready for degradation of the NPs – Figure 2.7b).[104] Caveolae-mediated endocytosis (CvME) is slower than CME, and gives rise to caveolar vesicles (ca. 50 - 100 nm) that can be delivered to caveosomes, avoiding the degradative acidic enzyme-rich environment from lysosomes (Figure 2.7c).[104]

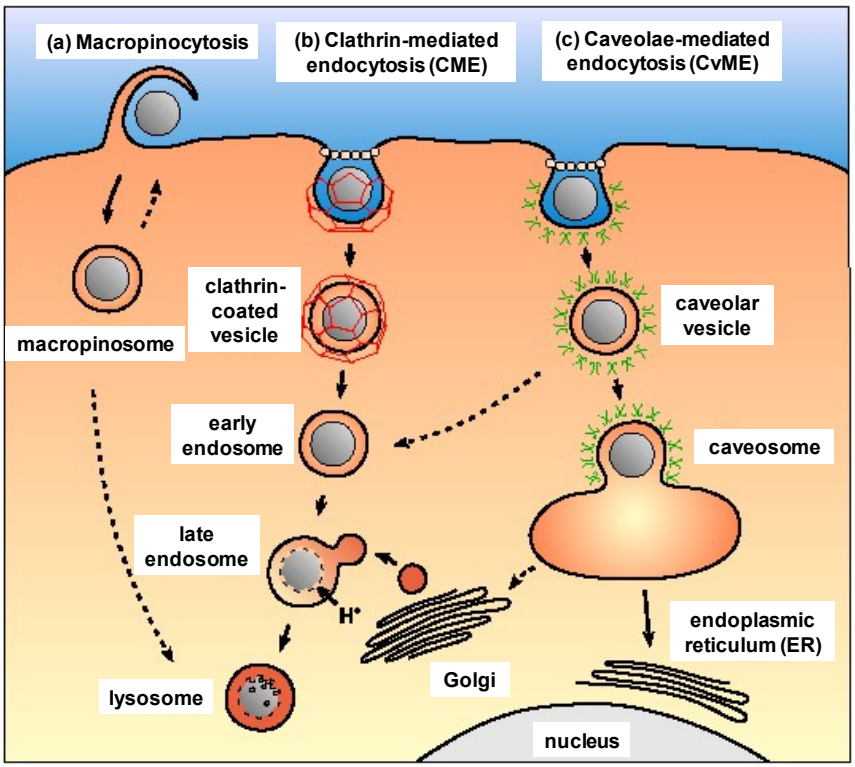

Figure 2.7. Most common mechanisms of internalization and intracellular trafficking found in mammalian cells.[104]

PNCs possess certain traits that can influence internalization and intracellular trafficking. Size is important, but its impact may vary according to the cell type, surface charge, and presence of ligands.[104] It has been observed that NPs < 200 nm are preferentially internalized by CME, while increasing the size (up to ca. 500 nm) alters

the mechanism to CvME.[104] The surface charge of the NPs impacts the interaction with the cell membrane, endosomes, lysosomes, mucus and lung surfactant, and usually positively charged NPs display better association and internalization rates,[104] but can stick in negatively charged components.[50] PEGylation is a strategy to shield the surface charges of NPs, but can prevent endosomal/lysosomal escape[50] and decrease cellular uptake.[105] Ligands (e.g. cholesterol, folic acid, and lauroyl) onto NPs can promote delivery to a specific cell population and/or control the endocytosis pathway and intracellular trafficking.[104] Folic acid (FA) is usually used as target ligand, since it has high affinity and specificity for folate receptors (FR)[106] which are over expressed in several types of epithelial cells.[107] FA is a ligand known to be internalized by CvME.[104] After FA receptor-mediated endocytosis, the FA-based conjugate is released into the cytosol for further metabolic processes, avoiding endolysosomal degradation.[108] On the other hand, PAMAM G3NH2-lauroyl conjugates have been shown to be internalized at a higher rate by CME in HT-29 human colon adenocarcinoma cell line compared to G3NH2 alone, which was internalized by CvME.[109] Therefore, understanding the mechanism of uptake and intracellular trafficking is of great relevance as both are influenced by the properties of the PNCs.[104]

2.3.3 Endolysosomal escape

Another obstacle to be addressed is the release of PNCs (and their cargo) from the endosomes (pH ca. 5.5 - 6) and lysosomes (pH ca. 4.5 - 5) into the cytoplasm.[110] The proton sponge effect (Figure 2.8)[103] is thought to be the predominant mechanism utilized by synthetic cationic polymers to help the cargo to escape endolysosomal degradation. Based on this hypothesis, the secondary and tertiary amines can exhibit

high buffering capacity in the pH range of 5 - 7, leading to the increase of protons and chloride ion influx during the endosome acidification, and thus, increase the osmotic pressure in the vesicle. As consequence, the passive diffusion of water also increases, resulting in the swelling and rupture of the endosome, releasing the gene-based complexes to the cytoplasm.[111]

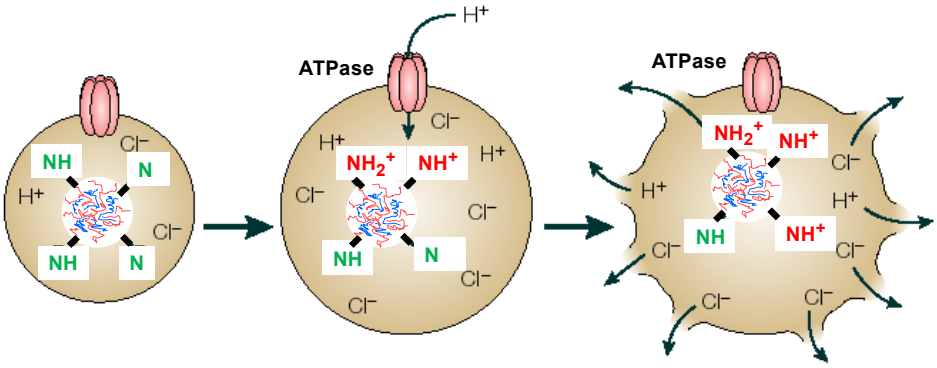

Figure 2.8. Proton-sponge hypothesis. Protonation of the amine-based cationic polymer causes influx of protons and counter-ions into endocytic vesicles, increasing the osmotic pressure, and leading the vesicle to swell and rupture.[103]

2.3.4 Degradation by nucleases in the cytoplasm

The cell cytoplasm is a critical region to the stability of DNA and siRNA, which needs to be protected from degradation. The majority of DNA enters into the nucleus during cell division, and thus, it must remain stable until the next disassembly of the nuclear envelope.[111] Another factor that plays an important role in the nucleic acid transit through the cytoplasm is its rate of mobility.[111] Large molecules such as free DNA have extremely low mobility in the cytoplasm, and thus, the formation of small and spherical NPs via complexation helps to increase the cytosolic mobility.[111] On the order hand, siRNA is more prone to degradation than DNA due to the extra hydroxyl group in the siRNA backbone, which makes it more susceptible to hydrolysis by serum nucleases.[14] Chemical modifications on the sugar-phosphate backbone of the siRNA

(e.g. 2'-fluoro and 2'-O-methyl)[112] increases its stability, while complexation, encapsulation, and/or shielding provide additional protection.[14]

2.3.5 Nucleic acid release from the carrier

The process of nucleic acid dissociation from complexes is attributed to anionic molecules present in the cytoplasm which replace the anionic DNA or siRNA.[111] However, the DNA dissociation can also take place in the nucleus,[111] the final intracellular barrier for DNA transfection. Since the nuclear membrane disassembles during mitosis, even large DNA-based complexes can gain access to the nucleus. However, during interphase, the sole pathway to enter into the nucleus is through the nuclear membrane, and just very small molecules (ca. 50 kDa, ca. 10 nm) or ions are able to diffuse passively through the nuclear pores. Since the upper size limit for this pathway of entry is ca. 25 - 30 nm,[45, 46] it is extremely important to have DNA-based complexes as small as possible.[111] In the case of siRNA delivery, the final intracellular barrier is its release into the cytoplasm followed by its assembly into the RISC.[67] Most siRNA-based conjugates use cleavable linkages between the siRNA and the conjugated molecule, such as acid-labile (to be cleaved in the endosomes) or reducible bonds (to be cleaved in the cytosol) to facilitate the release of siRNA from the carrier.[68]

2.4 PEGylation as Alternative to Overcome Extracellular Barriers in Gene Therapy to the Lungs

One strategy to avoid interaction of NPs containing nucleic acids with mucus and lung surfactant is to modify them with biocompatible, hydrophilic, and biologically inert polymers, such as PEG[50], so as to shield them from the external milieu. This approach

may also reduce clearance by alveolar macrophages.[50] The incorporation of PEG to complexes increases their aqueous solubility, reduces their serum protein coating, and prevents their aggregation.[113] PEG may be covalently coupled to cationic polymers used to prepare polyplexes, and during the complexation process, the cationic polymer and the nucleic acid interact with each other, creating a hydrophobic core that is surrounded by a shield of hydrophilic molecules. PEG can be also linked to the nucleic acid, e.g. siRNA-PEG conjugates,[71-74, 76] and those can be used to prepare lipoplexes[71, 72] and polyplexes,[72-74, 76] and the final NPs are surrounding by PEG molecules. It has been demonstrated that PEGylated lipoplexes and polyplexes are able to achieve efficient nucleic acid delivery even in presence of CF mucus components at concentrations similar to the ones observed *in vivo*.[50] PEGylation of PEI-DNA[76,104] and PEI-siRNA[110] polyplexes not only prevent aggregation of the NPs, but also provide shielding against charged anions, keeping their size stable and constant.[50] In addition, PEG-PEI-siRNA polyplexes have showed better lung transfection *in vivo*.[39] However, PEG chains at the surface of the nanocarriers can prevent endolysosomal escape.[50] PEGylated nanocarriers are also known to be less efficiently taken up by the cells.[105] Therefore, a balance between the positive charges from the cationic polymer, the size of PEG chains, and the PEG density on the complexes surface must be determined in order to achieve maximum gene delivery efficiency, or alternative strategies must be combined to overcome the PEGylation issues.

2.5 pMDIs for the Delivery of Nucleic Acids via OI Administration

Current routes for the regional delivery of nucleic acids to airway and alveolar epithelia include intranasal, intratracheal and oral inhalation (OI).[45] OI of aerosolized

formulations is a non-invasive approach that may result in increased nucleic acid distribution to distal airways and alveoli. pMDIs and DPIs are the OI devices commonly used for treatment of lung diseases,[114] accounting for approximately 67% of the total sales in the respiratory market in 2007 – US, France, Germany, Italy, Spain, and UK.[115] pMDIs are of great relevance, as they are widely used because they are compact, portable, inexpensive, provide multiple and reproducible doses, and the environment is sealed – no degradation of the therapeutic.[116, 117] pMDIs also can be used by patients with diseased lungs, because it is propellant-based and not respiratory driven,[117, 118] and thus, they may be more suitable for children and elderly. Therefore, pMDIs may be preferred over DPIs,[119] and become very strong candidates for the delivery of nucleic acids *to* and *through* the lungs.[120]

A typical pMDI is composed by a canister sealed with a metering valve, positioned upside down in an actuator (Figure 2.9). The compressed liquid propellant (> 98% of the formulation) is housed in the canister and in equilibrium with its vapor phase under saturation pressure.[121] pMDIs can be formulated as solution (therapeutics dissolved in the propellant, usually with the aid of a co-solvent) or suspension (therapeutics dispersed in the propellant with or without excipients). By pressing the actuator, the propellant and the ingredients are exposed to atmospheric pressure, forming an aerosol cloud containing the active therapeutic (with potentially other excipients) which is inhaled by the patient.[121, 122]

In order to overcome solubility limitations, the industry has resorted to a large extent to the use of cosolvents, especially ethanol,[123] not only as a solubility enhancer for drugs in solution formulations, but also as solubility enhancer for other excipients

(e.g. surfactants) in both solution and suspension formulations.[121, 123] However, there are also many issues associated with the use of ethanol.[118, 121, 123-125]

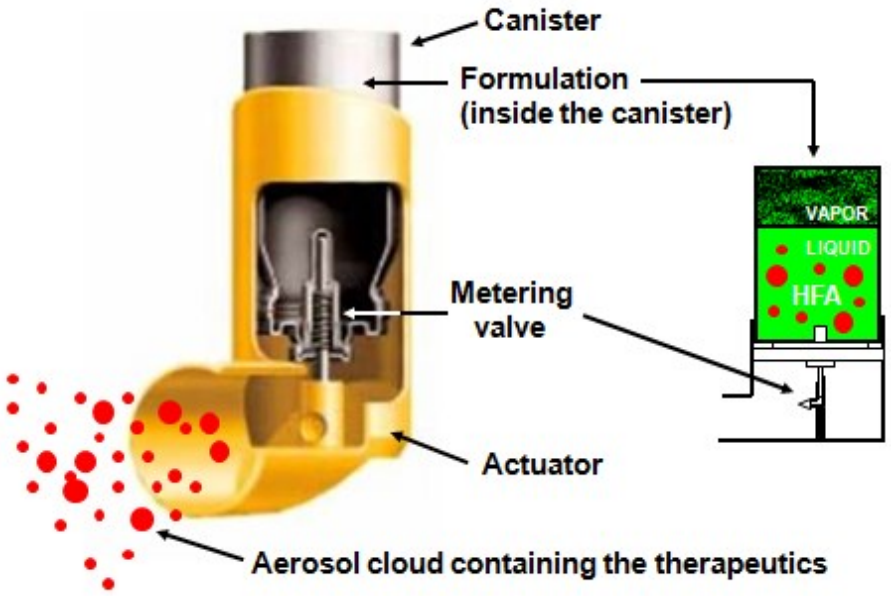

Figure 2.9. Schematic diagram of a typical pMDI (adapted from 3M Pharmaceuticals).

In solution-based formulations, ethanol may reduce the chemical stability, and depending on its concentration, it can adversely impact the aerosol performance.[123, 126, 127] In suspension-based formulations, ethanol may also affect the colloidal stability and aerosol characteristics.[118, 128] While the enhancement of the solubility of surfactants in propellant HFAs upon the addition of ethanol is understood and well described in literature,[120, 128, 129] the ability of ethanol to enhance the solvation of surfactant tail groups in HFAs, a pre-requisite for particle stabilization upon surfactant adsorption,[123, 130, 131] is less clear.

Formulation of nucleic acids in pMDIs has received very little attention. Only one work[132] has reported the formulation of surfactant-coated DNA particles in pMDIs using

propellant HFA, which is approved by FDA.[123] In that study, excipients and liposomes were used for improvement of colloidal stability, and *in vitro* transfection efficiency, respectively – however, addition of transfecting agent separately from the gene does not seem such a feasible strategy for commercial applications. With respect to siRNA-based propellant formulations, to the best of our knowledge, no work has been reported on pMDIs, and most *in vivo* studies have used either intratracheal or intranasal routes.[67]

2.6 References

1. Jeong, J. H.; Kim, S. W.; Park, T. G. Molecular design of functional polymers for gene therapy. *Prog. Polym. Sci.* **2007,** *32*, (11), 1239-1274.
2. Thomas, M.; Klibanov, A. M. Non-viral gene therapy: Polycation-mediated DNA delivery. *Appl. Microbiol. Biotechnol.* **2003,** *62*, (1), 27-34.
3. Park, T. G.; Jeong, J. H.; Kim, S. W. Current status of polymeric gene delivery systems. *Adv. Drug Delivery Rev.* **2006,** *58*, (4), 467-486.
4. Saito, H.; Nakamura, H.; Kato, S.; Inoue, S.; Inage, M.; Ito, M.; Tomoike, H. Percutaneous *in vivo* gene transfer to the peripheral lungs using plasmid-liposome complexes. *Am. J. Physiol. Lung Cell Mol. Physiol.* **2000,** *279*, L651-L657.
5. Bergeron, C.; Boulet, L.-P. Structural changes in airway diseases: Characteristics, mechanisms, consequences, and pharmacologic modulation. *Chest* **2006,** *129*, 1068-1087.
6. Barnes, P. J. Transcription factors in airway diseases. *Lab. Invest.* **2006,** *86*, 867-872.
7. Pilewski, J. M. Gene therapy for airway diseases: Continued progress toward identifying and overcoming barriers to efficiency. *Am. J. Respir. Cell Mol. Biol.* **2002,** *27*, 117-121.
8. Whitsett, J. A.; E.Wert, S.; E.Weaver, T. Alveolar surfactant homeostasis and the pathogenesis of pulmonary disease. *Annu. Rev. Med.* **2010,** *61*, 105-119.
9. Davies, L. A.; McLachlan, G.; Sumner-Jones, S. G.; Ferguson, D.; Baker, A.; Tennant, P.; Gordon, C.; Vrettou, C.; Baker, E.; Zhu, J.; Alton, E. W. F. W.; Collie, D. D. S.; Porteous, D. J.;

Hyde, S. C.; Gill, D. R. Enhanced lung gene expression after aerosol delivery of concentrated pDNA/PEI complexes. *Mol. Ther.* **2008,** *16*, (7), 1283-1290.

10. Zhang, W.; Yang, H.; Kong, X.; Mohapatra, S.; Juan-Vergara, H. S.; Hellermann, G.; Behera, S.; Singam, R.; Lockey, R. F.; Mohapatra, S. S. Inhibition of respiratory syncytial virus infection with intranasal siRNA nanoparticles targeting the viral NS1 gene. *Nat. Med.* **2005,** *11*, (1), 56-62.
11. Crystal, R. G. a1-Antitrypsin deficiency, emphysema, and liver disease: Genetic basis and strategies for therapy. *J. Clin. Invest.* **1990,** *85*, 1343-1352.
12. American Lung Association *State of lung disease in diverse communities*; Washington DC, 2010; pp 1-106. http://www.LungUSA.org.
13. Tang, X.; Shigematsu, H.; Bekele, B. N.; Roth, J. A.; Minna, J. D.; Hong, W. K.; Gazdar, A. F.; Wistuba, I. I. EGFR tyrosine kinase domain mutations are detected in histologically normal respiratory epithelium in lung cancer patients. *Cancer Res.* **2005,** *65*, 7568-7572.
14. Gary, D. J.; Puri, N.; Won, Y.-Y. Polymer-based siRNA delivery: Perspectives on the fundamental and phenomenological distinctions from polymer-based DNA delivery. *J. Controlled Release* **2007,** *121*, (1-2), 64-73.
15. Thomas, M.; Lu, J. J.; Chen, J.; Klibanov, A. M. Non-viral siRNA delivery to the lung. *Adv. Drug Delivery Rev.* **2007,** *59*, (2-3), 124-133.
16. Wang, J.; Lu, Z.; Wientjes, M.; Au, J. Delivery of siRNA therapeutics: Barriers and carriers. *AAPS J.* **2010,** *12*, (4), 492-503.
17. Fire, A.; Xu, S.; Montgomery, M. K.; Kostas, S. A.; Driver, S. E.; Mello, C. C. Potent and specific genetic interference by double-stranded RNA in Caenorhabditis elegans. *Nature* **1998,** *391*, (6669), 806-811.
18. Grigsby, C. L.; Leong, K. W. Balancing protection and release of DNA: Tools to address a bottleneck of non-viral gene delivery. *J. R. Soc. Interface* **2010,** *7*, (Suppl 1), S67-S82.
19. Durcan, N.; Murphy, C.; Cryan, S.-A. Inhalable siRNA: Potential as a therapeutic agent in the lungs. *Mol. Pharmaceutics* **2008,** *5*, (4), 559-566.
20. Gao, X.; Kim, K.-S.; Liu, D. Nonviral gene delivery: What we know and what is next. *AAPS J.* **2007,** *9*, (1), E92-E104.

21. Kim, T.-H.; Jiang, H.-L.; Jere, D.; Park, I.-K.; Cho, M.-H.; Nah, J.-W.; Choi, Y.-J.; Akaike, T.; Cho, C.-S. Chemical modification of chitosan as a gene carrier *in vitro* and *in vivo*. *Prog. Polym. Sci.* **2007,** *32*, (7), 726-753.

22. Sun, X.; Zhang, N. Cationic polymer optimization for efficient gene delivery. *Mini-Rev. Med. Chem.* **2010,** *10*, 108-125.

23. Mao, S.; Sun, W.; Kissel, T. Chitosan-based formulations for delivery of DNA and siRNA. *Adv. Drug Delivery Rev.* **2010,** *62*, (1), 12-27.

24. Gautam, A.; Waldrep, C. J.; Densmore, C. L. Delivery systems for pulmonary gene therapy. *Am. J. Respir. Med.* **2002,** *1*, 35-46.

25. Densmore, C. L. Advances in noninvasive pulmonary gene therapy. *Curr. Drug Delivery* **2006,** *3*, 55-63.

26. Elfinger, M.; Geiger, J.; Hasenpusch, G.; Üzgün, S.; Sieverling, N.; Aneja, M. K.; Maucksch, C.; Rudolph, C. Targeting of the b2-adrenoceptor increases nonviral gene delivery to pulmonary epithelial cells *in vitro* and lungs *in vivo*. *J. Controlled Release* **2009,** *135*, (3), 234-241.

27. Mizuno, T.; Mohri, K.; Nasu, S.; Danjo, K.; Okamoto, H. Dual imaging of pulmonary delivery and gene expression of dry powder inhalant by fluorescence and bioluminescence. *J. Control. Release* **2009,** *134*, (2), 149-154.

28. Kim, T. I.; Baek, J. U.; Yoon, J. K.; Choi, J. S.; Kim, K.; Park, J. S. Synthesis and characterization of a novel arginine-grafted dendritic block copolymer for gene delivery and study of its cellular uptake pathway leading to transfection. *Bioconjugate Chem.* **2007,** *18*, (2), 309-17.

29. Stern, M.; Ulrich, K.; Geddes, D. M.; Alton, E. W. F. W. Poly (D, L-lactide-co-glycolide)/DNA microspheres to facilitate prolonged transgene expression in airway epithelium *in vitro*, *ex vivo* and *in vivo*. *Gene Ther.* **2003,** *10*, (16), 1282-1288.

30. Mohri, K.; Okuda, T.; Mori, A.; Danjo, K.; Okamoto, H. Optimized pulmonary gene transfection in mice by spray-freeze dried powder inhalation. *J. Control. Release* **2010,** *144*, (2), 221-226.

31. Nguyen, J.; Xie, X.; Neu, M.; Dumitrascu, R.; Reul, R.; Sitterberg, J.; Bakowsky, U.; Schermuly, R.; Fink, L.; Schmehl, T.; Gessler, T.; Seeger, W.; Kissel, T. Effects of cell-penetrating peptides

and pegylation on transfection efficiency of polyethylenimine in mouse lungs. *J. Gene Med.* **2008,** *10*, (11), 1236-1246.

32. Jiang, H.-L.; Kim, T.-H.; Kim, Y.-K.; Park, I.-Y.; Cho, M.-H.; Cho, C.-S. Efficient gene delivery using chitosan-polyethylenimine hybrid systems. *Biomed. Mater.* **2008,** *3*, (2), 025013.

33. Kleemann, E.; Jekel, N.; Dailey, L. A.; Roesler, S.; Fink, L.; Weissmann, N.; Schermuly, R.; Gessler, T.; Schmehl, T.; Roberts, C. J.; Seeger, W.; Kissel, T. Enhanced gene expression and reduced toxicity in mice using polyplexes of low-molecular-weight poly(ethylene imine) for pulmonary gene delivery. *J. Drug Targeting* **2009,** *17*, (8), 638-651.

34. Nielsen, E.; Nielsen, J.; Becker, D.; Karlas, A.; Prakash, H.; Glud, S.; Merrison, J.; Besenbacher, F.; Meyer, T.; Kjems, J.; Howard, K. Pulmonary gene silencing in transgenic EGFP mice using aerosolised chitosan/siRNA nanoparticles. *Pharm. Res.* **2010,** *27*, (12), 2520-2527.

35. Jiang, H.-L.; Xu, C.-X.; Kim, Y.-K.; Arote, R.; Jere, D.; Lim, H.-T.; Cho, M.-H.; Cho, C.-S. The suppression of lung tumorigenesis by aerosol-delivered folate-chitosan-graft-polyethylenimine/Akt1 shRNA complexes through the Akt signaling pathway. *Biomaterials* **2009,** *30*, (29), 5844-5852.

36. Jere, D.; Jiang, H.-L.; Kim, Y.-K.; Arote, R.; Choi, Y.-J.; Yun, C.-H.; Cho, M.-H.; Cho, C.-S. Chitosan-*graft*-polyethylenimine for Akt1 siRNA delivery to lung cancer cells. *Int. J. Pharm.* **2009,** *378*, (1-2), 194-200.

37. Zamora-Avila, D. E.; Zapata-Benavides, P.; Franco-Molina, M. A.; Saavedra-Alonso, S.; Trejo-Avila, L. M.; Resendez-Perez, D.; Mendez-Vazquez, J. L.; Isaias-Badillo, J.; Rodriguez-Padilla, C. WT1 gene silencing by aerosol delivery of PEI-RNAi complexes inhibits B16-F10 lung metastases growth. *Cancer Gene Ther.* **2009,** *16*, (12), 892-899.

38. Günther, M.; Lipka, J.; Malek, A.; Gutsch, D.; Kreyling, W.; Aigner, A. Polyethylenimines for RNAi-mediated gene targeting *in vivo* and siRNA delivery to the lung. *Eur. J. Pharm. Biopharm.* **2011,** *77*, (3), 438-449.

39. Merkel, O. M.; Beyerle, A.; Librizzi, D.; Pfestroff, A.; Behr, T. M.; Sproat, B.; Barth, P. J.; Kissel, T. Nonviral siRNA delivery to the lung: Investigation of PEG-PEI polyplexes and their *in vivo* performance. *Mol. Pharmaceutics* **2009,** *6*, (4), 1246-1260.

40. Beyerle, A.; Braun, A.; Merkel, O.; Koch, F.; Kissel, T.; Stoeger, T. Comparative *in vivo* study of poly(ethylene imine)/siRNA complexes for pulmonary delivery in mice. *J. Controlled Release* **2011,** *151*, (1), 51-56.

41. Antipina, M. N.; Gainutdinov, R. V.; Rachnyanskaya, A. A.; Tolstikhina, A. L.; Yurova, T. V.; Khomutov, G. B. Studies of nanoscale structural ordering in planar DNA complexes with amphiphilic mono- and polycations. *Surf. Sci.* **2003,** *532-535*, (0), 1025-1033.

42. Chou, L. Y. T.; Ming, K.; Chan, W. C. W. Strategies for the intracellular delivery of nanoparticles. *Chem. Soc. Rev.* **2011,** *40*, (1), 233-245.

43. Nafee, N.; Taetz, S.; Schneider, M.; Schaefer, U. F.; Lehr, C.-M. Chitosan-coated PLGA nanoparticles for DNA/RNA delivery: Effect of the formulation parameters on complexation and transfection of antisense oligonucleotides. *Nanomedicine* **2007,** *3*, (3), 173-183.

44. Rejman, J.; Oberle, V.; Zuhorn, I. S.; Hoekstra, D. Size-dependent internalization of particles via the pathways of clathrin- and caveolae-mediated endocytosis. *Biochem. J.* **2004,** *377*, (1), 159-169.

45. Lam, A. P.; Dean, D. A. Progress and prospects: Nuclear import of nonviral vectors. *Gene Ther.* **2010,** *17*, (4), 439-447.

46. De Smedt, S. C.; Demeester, J.; Hennink, W. E. Cationic polymer based gene delivery systems. *Pharm. Res.* **2000,** *17*, (2), 113-126.

47. Meyer, M.; Dohmen, C.; Philipp, A.; Kiener, D.; Maiwald, G.; Scheu, C.; Ogris, M.; Wagner, E. Synthesis and biological evaluation of a bioresponsive and endosomolytic siRNA-polymer conjugate. *Mol. Pharmaceutics* **2009,** *6*, (3), 752-762.

48. Remaut, K.; Sanders, N. N.; De Geest, B. G.; Braeckmans, K.; Demeester, J.; De Smedt, S. C. Nucleic acid delivery: Where material sciences and bio-sciences meet. *Mater. Sci. Eng., R* **2007,** *58*, (3-5), 117-161.

49. Crommelin, D. J. A.; Storm, G.; Jiskoot, W.; Stenekes, R.; Mastrobattista, E.; Hennink, W. E. Nanotechnological approaches for the delivery of macromolecules. *J. Controlled Release* **2003,** *87*, (1-3), 81-88.

50. Sanders, N.; Rudolph, C.; Braeckmans, K.; De Smedt, S. C.; Demeester, J. Extracellular barriers in respiratory gene therapy. *Adv. Drug Delivery Rev.* **2009,** *61*, (2), 115-127.

51. Ravi Kumar, M. N. V.; Bakowsky, U.; Lehr, C. M. Preparation and characterization of cationic PLGA nanospheres as DNA carriers. *Biomaterials* **2004,** *25*, (10), 1771-1777.

52. Koby, G.; Ofra, B.; Dganit, D.; Marcelle, M. Poly(D,L-lactide-co-glycolide acid) nanoparticles for DNA delivery: Waiving preparation complexity and increasing efficiency. *Biopolymers* **2007,** *85*, (5-6), 379-391.

53. Sahoo, S.; Labhasetwar, V., Biodegradable PLGA/PLA nanoparticles for anti-cancer therapy. In *Nanotechnol. Cancer Ther.*, CRC Press: 2007; Vol. null.

54. Panyam, J.; Labhasetwar, V. Biodegradable nanoparticles for drug and gene delivery to cells and tissue. *Adv. Drug Delivery Rev.* **2003,** *55*, (3), 329-347.

55. Basarkar, A.; Devineni, D.; Palaniappan, R.; Singh, J. Preparation, characterization, cytotoxicity and transfection efficiency of poly(dl-lactide-co-glycolide) and poly(dl-lactic acid) cationic nanoparticles for controlled delivery of plasmid DNA. *Int. J. Pharm.* **2007,** *343*, (1-2), 247-254.

56. Luten, J.; van Nostrum, C. F.; De Smedt, S. C.; Hennink, W. E. Biodegradable polymers as non-viral carriers for plasmid DNA delivery. *J. Controlled Release* **2008,** *126*, (2), 97-110.

57. Perez, C.; Sanchez, A.; Putnam, D.; Ting, D.; Langer, R.; Alonso, M. J. Poly(lactic acid)-poly(ethylene glycol) nanoparticles as new carriers for the delivery of plasmid DNA. *J. Controlled Release* **2001,** *75*, (1-2), 211-224.

58. Baoum, A.; Dhillon, N.; Buch, S.; Berkland, C. Cationic surface modification of PLG nanoparticles offers sustained gene delivery to pulmonary epithelial cells. *J. Pharm. Sci.* **2010,** *99*, (5), 2413-2422.

59. Twaites, B.; Alarcón, C. d. l. H.; Alexander, C. Synthetic polymers as drugs and therapeutics. *J. Mater. Chem.* **2005,** *15*, (4), 441.

60. Castanotto, D.; Rossi, J. J. The promises and pitfalls of RNA-interference-based therapeutics. *Nature* **2009,** *457*, (7228), 426-433.

61. Merkel, O. M.; Kissel, T. Nonviral pulmonary delivery of siRNA. *Acc. Chem. Res.* **2011,** *45(7)*, (7), 961-970.

62. Wang, Y.; Li, Z.; Han, Y.; Liang, L. H.; Ji, A. Nanoparticle-based delivery system for application of siRNA *in vivo*. *Curr. Drug Metab.* **2010,** *11*, (2), 182-196.

63. Ballarín-González, B.; Thomsen, T. B.; Howard, K. A. Clinical translation of RNAi-based treatments for respiratory diseases. *Drug Delivery Transl. Res.* **2013,** *3*, (1), 84-99.

64. Burnett, J. C.; Rossi, J. J.; Tiemann, K. Current progress of siRNA/shRNA therapeutics in clinical trials. *Biotechnol. J.* **2011,** *6*, (9), 1130-1146.

65. Fujita, Y.; Takeshita, F.; Kuwano, K.; Ochiya, T. RNAi therapeutic platforms for lung diseases. *Pharmaceuticals* **2013,** *6*, (2), 223-250.

66. Ge, Q.; Evans, D.; Xu, J. J.; Yang, H. H.; Lu, P. Y., Pulmonary delivery of small interfering RNA for novel therapeutics. In *Delivery Technologies for Biopharmaceuticals: Peptides, Proteins, Nucleic Acids and Vaccines* John Wiley & Sons, Ltd: 2009; pp 269-289.

67. Lam, J. K.-W.; Liang, W.; Chan, H.-K. Pulmonary delivery of therapeutic siRNA. *Adv. Drug Delivery Rev.* **2012,** *64*, (1), 1-15.

68. Jeong, J. H.; Mok, H.; Oh, Y.-K.; Park, T. G. siRNA conjugate delivery systems. *Bioconjugate Chem.* **2009,** *20*, (1), 5-14.

69. Park, K.; Yang, J.-A.; Lee, M.-Y.; Lee, H.; Hahn, S. K. Reducible hyaluronic acid-siRNA conjugates for target specific gene silencing. *Bioconjugate Chem.* **2013,** *24*, (7), 1201-1209.

70. Lee, S. H.; Mok, H.; Lee, Y.; Park, T. G. Self-assembled siRNA-PLGA conjugate micelles for gene silencing. *J. Controlled Release* **2011,** *152*, (1), 152-158.

71. Jung, S.; Lee, S. H.; Mok, H.; Chung, H. J.; Park, T. G. Gene silencing efficiency of siRNA-PEG conjugates: Effect of PEGylation site and PEG molecular weight. *J. Controlled Release* **2010,** *144*, (3), 306-313.

72. Choi, S. W.; Lee, S. H.; Mok, H.; Park, T. G. Multifunctional siRNA delivery system: Polyelectrolyte complex micelles of six-arm PEG conjugate of siRNA and cell penetrating peptide with crosslinked fusogenic peptide. *Biotechnol. Prog.* **2009,** *26*, (1), 57-63.

73. Kim, S. H.; Jeong, J. H.; Lee, S. H.; Kim, S. W.; Park, T. G. Local and systemic delivery of VEGF siRNA using polyelectrolyte complex micelles for effective treatment of cancer. *J. Controlled Release* **2008,** *129*, (2), 107-116.

74. Kim, S. H.; Jeong, J. H.; Lee, S. H.; Kim, S. W.; Park, T. G. LHRH receptor-mediated delivery of siRNA using polyelectrolyte complex micelles self-assembled from siRNA-PEG-LHRH conjugate and PEI. *Bioconjugate Chem.* **2008,** *19*, (11), 2156-2162.

75. Lee, S. H.; Kim, S. H.; Park, T. G. Intracellular siRNA delivery system using polyelectrolyte complex micelles prepared from VEGF siRNA-PEG conjugate and cationic fusogenic peptide. *Biochem. Biophys. Res. Commun.* **2007,** *357*, (2), 511-516.

76. Kim, S. H.; Jeong, J. H.; Lee, S. H.; Kim, S. W.; Park, T. G. PEG conjugated VEGF siRNA for anti-angiogenic gene therapy. *J. Controlled Release* **2006,** *116*, (2), 123-129.

77. Oishi, M.; Nagasaki, Y.; Itaka, K.; Nishiyama, N.; Kataoka, K. Lactosylated poly(ethylene glycol)-siRNA conjugate through acid-labile β-thiopropionate linkage to construct pH-sensitive polyion complex micelles achieving enhanced gene silencing in hepatoma cells. *J. Am. Chem. Soc.* **2005,** *127*, (6), 1624-1625.

78. Oishi, M.; Sasaki, S.; Nagasaki, Y.; Kataoka, K. pH-responsive oligodeoxynucleotide (ODN)-poly(ethylene glycol) conjugate through acid-labile β-thiopropionate linkage: Preparation and polyion complex micelle formation. *Biomacromolecules* **2003,** *4*, (5), 1426-1432.

79. Lee, J.-S.; Green, J. J.; Love, K. T.; Sunshine, J.; Langer, R.; Anderson, D. G. Gold, poly(β-amino ester) nanoparticles for small interfering RNA delivery. *Nano Lett.* **2009,** *9*, (6), 2402-2406.

80. Giljohann, D. A.; Seferos, D. S.; Prigodich, A. E.; Patel, P. C.; Mirkin, C. A. Gene regulation with polyvalent siRNA-nanoparticle conjugates. *J. Am. Chem. Soc.* **2009,** *131*, (6), 2072-2073.

81. Medarova, Z.; Pham, W.; Farrar, C.; Petkova, V.; Moore, A. *In vivo* imaging of siRNA delivery and silencing in tumors. *Nat. Med.* **2007,** *13*, (3), 372-377.

82. Singh, N.; Agrawal, A.; Leung, A. K. L.; Sharp, P. A.; Bhatia, S. N. Effect of nanoparticle conjugation on gene silencing by RNA interference. *J. Am. Chem. Soc.* **2010,** *132*, (24), 8241-8243.

83. Derfus, A. M.; Chen, A. A.; Min, D.-H.; Ruoslahti, E.; Bhatia, S. N. Targeted quantum dot conjugates for siRNA delivery. *Bioconjugate Chem.* **2007,** *18*, (5), 1391-1396.

84. Nishina, K.; Unno, T.; Uno, Y.; Kubodera, T.; Kanouchi, T.; Mizusawa, H.; Yokota, T. Efficient *in vivo* delivery of siRNA to the liver by conjugation of α-tocopherol. *Mol. Ther.* **2008,** *16*, (4), 734-740.

85. Heredia, K. L.; Nguyen, T. H.; Chang, C.-W.; Bulmus, V.; Davis, T. P.; Maynard, H. D. Reversible siRNA-polymer conjugates by RAFT polymerization. *Chem. Commun.* **2008**, (28), 3245-3247.

86. Rozema, D. B.; Lewis, D. L.; Wakefield, D. H.; Wong, S. C.; Klein, J. J.; Roesch, P. L.; Bertin, S. L.; Reppen, T. W.; Chu, Q.; Blokhin, A. V.; Hagstrom, J. E.; Wolff, J. A. Dynamic polyconjugates for targeted *in vivo* delivery of siRNA to hepatocytes. *Proc. Natl. Acad. Sci. U.S.A.* **2007,** *104*, (32), 12982-12987.

87. Moschos, S. A.; Jones, S. W.; Perry, M. M.; Williams, A. E.; Erjefalt, J. S.; Turner, J. J.; Barnes, P. J.; Sproat, B. S.; Gait, M. J.; Lindsay, M. A. Lung delivery studies using siRNA conjugated to TAT(48−60) and penetratin reveal peptide induced reduction in gene expression and induction of innate immunity. *Bioconjugate Chem.* **2007,** *18*, (5), 1450-1459.

88. Juliano, R. L. Intracellular delivery of oligonucleotide conjugates and dendrimer complexes. *Ann. N. Y. Acad. Sci.* **2006,** *1082*, (1), 18-26.

89. Muratovska, A.; Eccles, M. R. Conjugate for efficient delivery of short interfering RNA (siRNA) into mammalian cells. *FEBS Lett.* **2004,** *558*, (1-3), 63-68.

90. Ameres, S. L.; Martinez, J.; Schroeder, R. Molecular basis for target RNA recognition and cleavage by human RISC. *Cell* **2007,** *130*, (1), 101-112.

91. Dhananjay, J.; Rohidas, A.; Hu-Lin, J.; You-Kyoung, K.; Myung-Haing, C.; Chong-Su, C. Bioreducible polymers for efficient gene and siRNA delivery. *Biomed. Mater.* **2009,** *4*, (2), 025020.

92. Kurtoglu, Y. E.; Navath, R. S.; Wang, B.; Kannan, S.; Romero, R.; Kannan, R. M. Poly(amidoamine) dendrimer-drug conjugates with disulfide linkages for intracellular drug delivery. *Biomaterials* **2009,** *30*, (11), 2112-2121.

93. Pouton, C. W.; Seymour, L. W. Key issues in non-viral gene delivery. *Adv. Drug Delivery Rev.* **2001,** *46*, (1-3), 187-203.

94. Rytting, E.; Nguyen, J.; Wang, X.; Kissel, T. Biodegradable polymeric nanocarriers for pulmonary drug delivery. *Expert Opin. Drug Delivery* **2008,** *5*, (6), 629-639.

95. Patton, J. S.; Byron, P. R. Inhaling medicines: Delivering drugs to the body through the lungs. *Nat. Rev. Drug Discovery* **2007,** *6*, (1), 67-74.

96. Gill, D. R.; Davies, L. A.; Pringle, I. A.; Hyde, S. C. The development of gene therapy for diseases of the lung. *CMLS, Cell. Mol. Life Sci.* **2004,** *61*, (3), 355-368.

97. Kolb, M.; Martin, G.; Medina, M.; Ask, K.; Gauldie, J. Gene therapy for pulmonary diseases. *Chest* **2006,** *130*, (3), 879-884.

98. Väyrynen, O. Proinflammatory cytokines modify the expression of surfactant proteins: Study in perinatal rabbit lung. Dissertation, University of Oulu, Finland, Oulu, 2003.

99. Duncan, J. E.; Whitsett, J. A.; Horowitz, A. D. Pulmonary surfactant inhibits cationic liposome-mediated gene delivery to respiratory epithelial cells *in vitro*. *Hum. Gene Ther.* **1997,** *8*, (4), 431-438.

100. Ernst, N.; Ulrichskötter, S.; Schmalix, W. A.; Rädler, J.; Galneder, R.; Mayer, E.; Gersting, S.; Plank, C.; Reinhardt, D.; Rosenecker, J. Interaction of liposomal and polycationic transfection complexes with pulmonary surfactant. *J. Gene Med.* **1999,** *1*, (5), 331-340.

101. Rudolph, C.; Lausier, J.; Naundorf, S.; Müller, R. H.; Rosenecker, J. *In vivo* gene delivery to the lung using polyethylenimine and fractured polyamidoamine dendrimers. *J. Gene Med.* **2000,** *2*, (4), 269-278.

102. Tsan, M.-F.; Tsan, G. L.; White, J. E. Surfactant inhibits cationic liposome-mediated gene transfer. *Hum. Gene Ther.* **1997,** *8*, (7), 817-825.

103. Pack, D. W.; Hoffman, A. S.; Pun, S.; Stayton, P. S. Design and development of polymers for gene delivery. *Nat. Rev. Drug Discovery* **2005,** *4*, (7), 581-593.

104. Hillaireau, H.; Couvreur, P. Nanocarriers' entry into the cell: Relevance to drug delivery. *Cell. Mol. Life Sci.* **2009,** *66*, (17), 2873-2896.

105. Peach, M. S.; Kumbar, S. G.; Brown, J. L.; Laurencin, C. T. Recent developments in nanoparticle based targeted delivery of chemotherapeutics. *Curr. Bioact. Compd.* **2009,** *5*, (3), 170-184.

106. Singh, P.; Gupta, U.; Asthana, A.; Jain, N. K. Folate and folate-PEG-PAMAM dendrimers: Synthesis, characterization, and targeted anticancer drug delivery potential in tumor bearing mice. *Bioconjugate Chem.* **2008,** *19*, (11), 2239-2252.

107. Cheng, C. J.; Saltzman, W. M. Enhanced siRNA delivery into cells by exploiting the synergy between targeting ligands and cell-penetrating peptides. *Biomaterials* **2011,** *32*, (26), 6194-6203.

108. Saeed, A. O.; Magnusson, J. P.; Moradi, E.; Soliman, M.; Wang, W.; Stolnik, S.; Thurecht, K. J.; Howdle, S. M.; Alexander, C. Modular construction of multifunctional bioresponsive cell-targeted nanoparticles for gene delivery. *Bioconjugate Chem.* **2011,** *22*, (2), 156-168.

109. Saovapakhiran, A.; D'Emanuele, A.; Attwood, D.; Penny, J. Surface modification of PAMAM dendrimers modulates the mechanism of cellular internalization. *Bioconjugate Chem.* **2009,** *20*, (4), 693-701.

110. Gillies, E. R.; Fréchet, J. M. J. pH-responsive copolymer assemblies for controlled release of doxorubicin. *Bioconjugate Chem.* **2005,** *16*, (2), 361-368.

111. Eliyahu, H.; Barenholz, Y.; Domb, A. J. Polymers for DNA delivery. *Molecules* **2005,** *10*, 34-64.

112. Manoharan, M. RNA interference and chemically modified small interfering RNAs. *Curr. Opin. Chem. Biol.* **2004,** *8*, (6), 570-579.

113. Montier, T.; Delépine, P.; Pichon, C.; Férec, C.; Porteous, D. J.; Midoux, P. Non-viral vectors in cystic fibrosis gene therapy: Progress and challenges. *Trends Biotechnol.* **2004,** *22*, (11), 586-592.

114. Goel, A.; Sahni, J.; Ali, J.; Baboota, S. Exploring targeted pulmonary delivery for treatment of lung cancer. *Int. J. Pharm. Invest.* **2013,** *3*, (1), 8-14.

115. Oversteegen, L. Inhaled medicines: Product differentiation by device. *Innovations Pharm. Technol.* **2008,** *26*, 62-65.

116. Labiris, N. R.; Dolovich, M. B. Pulmonary drug delivery. Part II: The role of inhalant delivery devices and drug formulations in therapeutic effectiveness of aerosolized medications. *Br. J. Clin. Pharmacol.* **2003,** *56*, (6), 600-612.

117. Zhang, J.; Wu, L.; Chan, H.-K.; Watanabe, W. Formation, characterization, and fate of inhaled drug nanoparticles. *Adv. Drug Delivery Rev.* **2011,** *63*, (6), 441-455.

118. Marijani, R.; Shaik, M. S.; Chatterjee, A.; Singh, M. Evaluation of metered dose inhaler (MDI) formulations of ciclosporin. *J. Pharm. Pharmacol.* **2007,** *59*, (1), 15-21.

119. Covar, R. A.; Gelfand, E. W. Pressurized metered-dose inhalers versus dry-powder inhalers - Advantages and disadvantages. *US Respiratory Disease* **2008,** *4*, (2), 48-53.

120. Bell, J.; Newman, S. The rejuvenated pressurised metered dose inhaler. *Expert Opin. Drug Delivery* **2007,** *4*, (3), 215-234.

121. Wu, L.; da Rocha, S. R. P. Applications of the atomic force microscope in the development of propellant-based inhalation formulations. *KONA Powder and Particle Journal* **2008,** *26*, 106-128.

122. Rogueda, P. G.; Traini, D. The nanoscale in pulmonary delivery. Part 2: Formulation platforms. *Expert Opin. Drug Delivery* **2007,** *4*, (6), 607-620.

123. da Rocha, S. R. P.; Bharatwaj, B.; Saiprasad, S., Science and Technology of Pressurized Metered-Dose Inhalers. In *Controlled Pulmonary Drug Delivery* Smyth, H. D. C.; Hickey, A. J., Eds. Springer New York: 2011; pp 165-201.

124. Rogueda, P. Novel hydrofluoroalkane suspension formulations for respiratory drug delivery. *Expert Opin. Drug Delivery* **2005,** *2*, (4), 625-638.

125. Mazhar, S. H. R. A.; Chrystyn, H. Salbutamol relative lung and systemic bioavailability of large and small spacers. *J. Pharm. Pharmacol.* **2008,** *60*, (12), 1609-1613.

126. Vervaet, C.; Byron, P. R. Drug-surfactant-propellant interactions in HFA-formulations. *Int. J. Pharm.* **1999,** *186*, (1), 13-30.

127. Smyth, H. D. C. The influence of formulation variables on the performance of alternative propellant-driven metered dose inhalers. *Adv. Drug Delivery Rev.* **2003,** *55*, (7), 807-828.

128. Williams III, R. O.; Liu, J. Formulation of a protein with propellant HFA 134a for aerosol delivery. *Eur. J. Pharm. Sci.* **1999,** *7*, (2), 137-144.

129. Wu, L.; da Rocha, S. R. P. Biocompatible and biodegradable copolymer stabilizers for hydrofluoroalkane dispersions: A colloidal probe microscopy investigation. *Langmuir* **2007,** *23*, (24), 12104-12110.

130. Wu, L.; Peguin, R. P. S.; da Rocha, S. R. P. Understanding solvation in hydrofluoroalkanes: *Ab Initio* calculations and chemical force microscopy. *J. Phys. Chem. B* **2007,** *111*, (28), 8096-8104.

131. Peguin, R. P. S.; da Rocha, S. R. P. Solvent-solute interactions in hydrofluoroalkane propellants. *J. Phys. Chem. B* **2008,** *112*, (27), 8084-8094.

132. Bains, B. K.; Birchall, J. C.; Toon, R.; Taylor, G. *In vitro* reporter gene transfection via plasmid DNA delivered by metered dose inhaler. *J. Pharm. Sci.* **2010,** *99*, (7), 3089-3099.

CHAPTER 3

Solvation in Hydrofluoroalkanes: How can Ethanol Help?

3.1 Introduction

Pressurized metered dose inhalers (pMDIs) are the most widely used portable oral inhalation (OI) devices,[1, 2] and are usually associated with high compliance.[3, 4] pMDIs also offer an efficacious and convenient way of delivering drugs to the lungs for cases where repeated administration is necessary,[5] and in disease states where moderate to high inspiratory flows cannot be achieved by the patient,[6] as the aerosol formation in pMDIs is independent of inhalation effort.[2] In a typical pMDI, the compressed liquid propellant, which is in equilibrium with its vapor, makes up 98% of the formulation. pMDI formulations contain drugs either in solution, where the therapeutic is dissolved in the liquid propellant, usually with the help of a cosolvent, or in suspension, where drug crystals or amorphous drug particles are dispersed in the liquid propellant, usually with the aid of excipients including surfactants and cosolvents.[2, 7]

Hydrofluoroalkanes (HFAs) are fluorinated short-chain alkanes with low degree of hydrogen substitution,[8] which were introduced as propellants in pMDIs in the late 80's due to the phasing out of chlorofluorocarbons (CFCs).[9] HFAs are significantly less environmentally damaging than the fully halogenated CFCs.[10] HFA-227 (1,1,1,2,3,3,3-heptafluoropropane) and HFA-134a (1,1,1,2-tetrafluoroethane) are the two propellants currently used in commercial pMDIs.[8, 11] They have been selected based on several criteria, including biological compatibility and inertness.[12] However, due to their unique chemistry,[10] HFAs have significantly different solvent properties compared to CFCs,[8]

including larger dielectric constant and dipole moment.[13] HFAs have a dual character, being somewhat lipophobic, and at the same time hydrophobic.[11, 14] Thus, most therapeutics of interest, and excipients used in previous CFC formulations have very low solubility in HFAs.[10, 12]

In order to overcome solubility limitations, the industry has resorted to a large extent to the use of cosolvents, especially ethanol,[12] not only as a solubility enhancer for drugs in the development of solution formulations, but also as solubility enhancer for other excipients, for both solution and suspension formulations.[12, 15] However, there are also many issues associated with the use of ethanol.[1, 7, 12, 15, 16] In solution-based formulations, ethanol may reduce the chemical stability of the system, and depending on its concentration, the presence of such low volatile compound mixed with the propellant can adversely impact the aerosol characteristics of the formulation.[12, 13, 17] In suspension-based formulations, ethanol may also affect its physical stability and aerosol performance of the device.[1, 18] In spite of these challenges, ethanol is still widely employed in suspension-based formulations so as to help enhancing the solubility of surfactant molecules, which are required to improve the physical stability of drug particles dispersed in the propellants,[17] and thus the quality of the corresponding aerosol.[3, 7]

While the enhancement of the solubility of surfactants in HFAs upon the addition of ethanol is understood, and well documented,[2, 18, 19] the ability of ethanol to enhance the solvation of surfactant tail groups in HFAs, a pre-requisite for particle stabilization upon surfactant adsorption,[12, 20, 21] is less clear.

The goal of this work was thus to investigate the ability of cosolvent ethanol to enhance the solvation of HFAs towards moieties relevant to pMDI formulations, such as those containing alkyl, ether, and ester groups. In order to achieve this objective, the cohesive the force between candidate moieties was measured using chemical force microscopy (CFM) in mixtures of 2H, 3H-perfluoropentane (HPFP) – an excellent model for propellant HFAs, which is a liquid at ambient conditions[8, 10] – and ethanol, at different volume fractions. Johnson-Kendall-Roberts (JKR) theory was used to model the CFM results, and to gain insight on the contribution of ethanol as a solvation enhancer. This work is novel because, for the first time, the enhancement in solvent capacity of HFAs upon the addition of cosolvent ethanol is being addressed quantitatively and systematically. This is of importance as ethanol is a commonly used cosolvent in HFA-based pMDI formulations. The results obtained from this work as a function of the chemistry of the moieties (alkyl, ether, and ester groups) are also novel and of relevance as they can help in the design of HFA-philic compounds, including surfactants and stabilizers, which may be used in the development of more efficient suspension-based pMDI formulations. Finally, the results from this work help us evaluate the potential and limitations of predictive tools in understanding solvation in such novel and challenging fluids, the HFAs.

3.2 Experimental Section

3.2.1 Materials

n-Octyltrichlorosilane (C8TS, > 95%), 3-Methoxypropyltrimethoxysilane (COCTS, > 95%), and Acetoxypropyltrimethoxysilane (COOCTS, >95%) were purchased from

Gelest Inc. The molecular structures of these silanes that contain tail groups (alkyl, ether, and ester moieties) relevant to pMDIs are shown as insets in Figure 3.1. Ethanol (100%, 200 proof) was purchased from Decon Labs. 2H, 3H-perfluoropentane (HPFP, 98%) was purchased from DuPont™ TMC Ind. Inc. Sulfuric acid (H_2SO_4, 95.8%) and toluene (HPLC grade, < 40 ppm of water, 99.9%) were purchased from Fisher Scientific. Hydrogen peroxide (H_2O_2, 30% solution) was purchased from EMD Chemicals Inc. Hydrochloric acid (HCl, 37%) was purchased from Mallinckrodt Chemicals. Deionized water (DI-water, resistivity of 18.2 MΩ.cm) was obtained from a NANOpure® DIamond™ UV ultrapure water system (Barnstead International). Silicon nitride (Si_3N_4) triangular soft contact mode cantilevers with wedged tips were purchased from Budget Sensors (Model: SiNi). The spring constant and the tip radius reported by the manufacturer are 0.06 $N.m^{-1}$ and < 15 nm, respectively. For tips within the same batch, the spring constant determined in our laboratory was found to be in the range 0.051 - 0.069 $N.m^{-1}$, and the tip radius 10 - 16 nm. Among the tips evaluated, the spring constant was determined by measuring their resonant frequency[22] using the NanoScope Image software, considering the dimensions, density, and elastic modulus as constant in the calculations. The tip radii were measured using a TGT01 calibration silicon grating template (MikroMasch), and the Scanning Probe Image Processor (SPIP software, version 3.2.7.0, Image Metrology A/S) as described earlier.[20]

3.2.2 Pretreatment of substrates and atomic force microscopy (AFM) tips

Microscope cover glasses (22 x 22-2, from Fisher Scientific) were used as substrates. For removing surface impurities, they were immersed in 5% (v/v) HCl

aqueous solution for 4 h, rinsed with DI-water, and immersed in DI-water overnight, followed by drying in oven. They were then degreased in ethanol for 15 min using a sonication bath (VWR, P250D, set to 180 W), dried in air flow, and placed in freshly prepared piranha solution (70/30 v/v H_2SO_4/H_2O_2)[20] for 40 min. The Si_3N_4 cantilevers were rinsed with ethanol, blown with a light stream of air, and immersed in freshly prepared piranha solution for 5 min. The glass substrates and Si_3N_4 tips were subsequently rinsed with DI-water, ethanol, blown with a light stream of air, and dried in vacuum oven for 1 h before the surface chemical modification with silanes.

3.2.3 Surface chemical modification of substrates and Si_3N_4 tips by solution deposition

Dried glass substrates and Si_3N_4 tips were immersed in a 5 mM solution of C8TS, or COCTS, or COOCTS in toluene for 4 h at room temperature. Compact and ordered monolayers of silane molecules on glass surfaces are known to be formed by solution deposition (after ca. 1.5 h).[23] Similar success has been achieved on surfaces of Si_3N_4 tips (after ca. 1 h)[24]. The substrates and Si_3N_4 tips were washed vigorously in toluene after deposition, blown in a light stream of air, kept for 1 h in the vacuum oven, followed by storage in the desiccator overnight before the CFM experiments. Our previous works[20, 25] show that monolayers with excellent quality are formed using the earlier described protocol.

3.2.4 Chemical force microscopy (CFM)

The adhesion force between the silane-modified Si_3N_4 tip and glass substrate was determined at room temperature using a PicoSPM LE AFM (Molecular Imaging/Agilent Technologies). It is worth noticing that in our work, F_{ad} is truly a cohesive force – forces are measured between tip and substrates modified with the same silane.[12, 26] However, for consistency with the CFM literature,[27-31] we will use the word adhesion instead. All cantilever deflection-distance curves were obtained using a sealed liquid cell filled with a freshly prepared mixture of HPFP/ethanol (100/0, 90/10, 70/30, 50/50, 30/70, 20/80, 10/90, 0/100 v/v). HPFP is a liquid at ambient conditions that, because it has similar properties to HFAs, it has been extensively used as a model to propellants HFAs,[7, 8, 14, 19, 20, 25] and is required in CFM measurements, as the experiments cannot be performed with propellants. The cell was sealed by ring-shaped elastic on the bottom, and a ring-shaped film on the top.[32] Prior the measurements, the cell was thoroughly washed with ethanol and rinsed with the respective HPFP/ethanol mixture. To avoid deviations due to solvent evaporation, the whole HPFP/ethanol mixture was constantly replaced by a freshly prepared mixture in the liquid cell. F_{ad} measurements took place during the approach/retract cycles in nine different contact points, which were randomly distributed on the surface of the substrate 6000 × 6000 nm and with speed of 1 second per cycle. At each contact point, 25 deflection-distance curves were recorded, and corrected by the slope of the curve. F_{ad} was calculated as the product between the cantilever deflection and the spring constant of the tip.[20, 28] Histograms of calculated F_{ad} were fit to Gaussian distribution, from which the average F_{ad} and deviation was obtained.

3.2.5 Modeling the adhesion force and molecular simulation

The F_{ad} between the chemically modified tip and substrate in liquid environment was calculated using the JKR theory[29, 30] – Equation (1):

$$F_{ad} = \frac{3}{2} . \pi . R . W_{tms} \quad (1)$$

where R is the radius of curvature of the tip, and W_{tms} is the work per unit of area required to separate the modified tip (*t*) and substrate (*s*) in the solvent medium (*m*). The JKR theory is based on the balance between interfacial and elastic distortion energies,[29] on the assumption of perfect elastic interaction and frictionless interface, and on thermodynamic equilibrium.[33] Changes in chain conformation of the sample create a disordered monolayer on the tip and substrate, which are only considered in models that account for plastic deformations.[34]

W_{tms} was estimated based on individual interfacial free energies between the modified tip and the medium (γ_{tm}), that between the substrate and the medium (γ_{sm}), and that between the modified substrate and tip (γ_{st})[15] – Equation (2):

$$W_{tms} = \gamma_{tm} + \gamma_{sm} - \gamma_{st} \quad (2)$$

In this work, considering that the modified tip and substrate have the same surface functional groups, then $\gamma_{st} \approx 0$, and $\gamma_{sm} = \gamma_{tm}$[30], and thus, Equation (2) becomes Equation (3):

$$W_{tms} = 2\gamma_{sm} = 2\gamma_{tm} = 2\gamma_{12} \quad (3)$$

γ_{12} represents the interfacial free energy between the tail of the silane (1) (it contains the chemical moiety of interest – alkyl, ether, or ester) and the liquid medium (2) (HPFP/ethanol mixture). HPFP is a liquid model for propellant HFAs.[7, 8, 14, 19, 20, 25] γ_{12} was calculated using the Girifalco-Good-Fowkes approach[35] – Equation (4):

$$\gamma_{12} = \gamma_1 + \gamma_2 - 2\left(\gamma_1^{\,d}\gamma_2^{\,d}\right)^{1/2} - 2\left(\gamma_1^{\,p}\gamma_2^{\,p}\right)^{1/2} \quad (4)$$

where γ_1 and γ_2 are the total surface free energies of the silane tail, and that of the liquid medium, respectively, in equilibrium with the saturated vapor phase. The upper scripts d and p represent, the dispersive and polar contributions of surface free energy, respectively.

The total surface free energies $\left(\gamma_i^{\,t}\right)$ for the C8 moiety, ethanol and HPFP were obtained from the literature as 21.6 (from n-octane),[36] 21.4,[37] and 13.6 mN.m^{-1},[8] respectively. For COC and COOC moieties, the total surface free energies were calculated using the Beerbower correlation[38] – Equation (5):

$$\gamma_i^{\,t} = \left[\delta_d^2 + 0.632\,\delta_p^2 + 0.632\,\delta_h^2\right] \Big/ \left[13.9\,(1/V_m)^{1/3}\right] \quad (5)$$

where δ's are the Hansen Solubility Parameters: δ_d is the dispersive, δ_p the polar, and δ_h, the hydrogen bonding contributions [(cal.mol^{-3})$^{1/2}$]. Those were calculated

using the expanded table of Beerbower's group contribution.[39] V_m represents the molar volume, estimated using Fedor's group contribution.[40]

For the C8 moiety and ethanol, the dispersive contribution of surface free energy $\left(\gamma_i^{\,d}\right)$ was taken from literature as 21.6 [36] (same as $\gamma_i^{\,t}$ of n-octane, since $\gamma_i^{\,p} = 0$ [35]) and 18.8 mN.m^{-1} [37] respectively. For COC and COOC moieties, $\gamma_i^{\,d}$ was calculated using Panzer correlation[38] – Equation (6):

$$\gamma_i^{\,d} = 0.0715 V_m^{\,1/3} \delta_d \tag{6}$$

The polar contribution of the surface free energy $\left(\gamma_i^{\,p}\right)$ was estimated using the Fowkes approach[41] – Equation (7):

$$\gamma_i^{\,t} = \gamma_i^{\,d} + \gamma_i^{\,p} \tag{7}$$

No suitable experimental information or correlation was found to model the dispersive or polar contributions for HPFP. These values were thus used as fitting parameters, which also served to shine light into the relative contributions of the dispersive/polar forces of HFAs in the solvation of the moieties containing alkyl, ether, and ester groups, as discussed later.

γ (total , dispersive and polar contributions) for the HPFP/ethanol mixture were calculated using a simple (ideal) mixing rule[42] – Equation (8), where the parameter Φ represents the volume fraction:

$$\gamma = \sum_{i}^{m} \Phi_i \gamma_i \tag{8}$$

The properties required in the calculation of the normalized adhesion force (F_{ad}/R) using the JKR theory (along with the parameters obtained as discussed earlier) are listed in Table 3.1. The total surface free energy calculated for COC and COOC moieties is comparable to the original silanes (22.7 and 25.7 mN.m^{-1}, respectively).[43, 44]

Table 3.1. Molar volume, solubility parameters, and surface free energies for the chemistries used in this work. These values were used in the calculation of F_{ad}/R with the JRK theory.

Chemistry	Molar Volume (V_m, cm^3.mol^{-1})	Solubility Parameters (MPa$^{1/2}$)				Surface Free Energy (mN.m^{-1})			F_{ad}/R (mN.m^{-1}) in pure HPFP	
		δ_d	δ_p	δ_h	δ_t [(a)]	γ^d	γ^p	γ^t	CFM	JKR
C8 moiety	-	-	-	-	-	21.6	0.0	21.6	83.6 ± 32.1	77.8
COC moiety	85.6	15.1	4.9	4.7	16.6	17.2	2.3	19.5	20.1 ± 2.7	20.0
COOC moiety	99.8	14.0	4.9	7.2	16.5	15.5	3.9	19.4	9.1 ± 1.9	11.0
Ethanol	-	-	-	-	-	18.8	2.6	21.4	-	-
HPFP	-	-	-	-	-	8.4[(b)]	5.2[(b)]	13.6	-	-

[(a)] $\delta_t^2 = \delta_d^2 + \delta_p^2 + \delta_h^2$ [39]

[(b)] It was used as a fitting parameter as no literature/correlation is available for its estimation.

Molecular simulation was carried out using Gaussian 09.[45] Full geometric optimization was performed at the semi-empirical PM6 level of theory. PM6 was used as it has been shown to be a good choice for studying systems governed by hydrogen bonds,[46] and it is computationally less expensive than more accurate models such as second order Møller Plesset (MP2), thus permitting the study of cluster systems as large as the one shown here.[47]

3.3 Results and Discussion

CFM is a variation of AFM that utilizes functionalized tips and substrates in order to determine the cohesive forces (F_{ad}) between chemical groups.[29] The chemical modification on the surfaces can be performed by self-assembled monolayers (SAMs) of covalently attached organosilanes.[15, 24] SAMs of a large enough number of carbons in the tail group are expected to be highly oriented and ordered upon deposition, irrespective of the functional groups at the end of the monolayer.[48] F_{ad} is a direct measurement of the enthalpic penalty for creating interfaces between modified tip and solvent (and modified substrate and solvent as well) at the moment that the tip-substrate contact is broken due to retraction of the cantilever.[20] Small F_{ad} is obtained when the moieties on tip and substrate are well solvated; conversely, large F_{ad} are observed when the interaction between solvent and moieties is not as favorable.[20] Thus, F_{ad} has been used to evaluate the solvation ability of non-polar and polar solvents,[30] being a good predictor of solvation forces.[3, 19, 20, 25]

In what follows, the experimental results of the normalized cohesive forces (F_{ad}/R) from CFM measurements, and the modeling of those results using the JKR theory for alkyl (C8), ether (COC), and ester (COOC) moieties in the presence of different volume fractions of the cosolvent ethanol mixed with liquid HPFP are discussed. The C8 moiety was selected as the baseline moiety, as it represents the tail groups of surfactants currently used in commercial pMDI formulations, e.g. oleic acid and sorbitan trioleate.[12, 17] Alkyl-based surfactants, such as oleic acid and sorbitan trioleate have very low solubility in HFAs,[17] and are poorly solvated by HFAs alone, being unable to stabilize drug suspensions in HFAs.[7, 12, 20] The COC and COOC

moieties contain more polar groups, which provide possible sites to form strong polar interactions with the HFAs.[15] The COC moiety is representative of compounds such as poly(ethylene glycol) (PEG) which is currently being used as an excipient in Symbicort®, a commercial HFA-based pMDI formulation.[12] The COOC moiety is representative of biodegradable polymers such as poly(lactic acid) (PLA), which has been investigated as potential stabilizers in HFAs.[3, 19, 25]

3.3.1 Solvation in HFAs without the presence of ethanol

The F_{ad}/R for C8/C8, COC/COC, and COOC/COOC in HPFP determined from the CFM measurements was 83.6 ± 32.1, 20.1 ± 2.7, and 9.1 ± 1.9 $mN.m^{-1}$, respectively – the results are shown in Table 3.1. The trend observed here is in agreement with that previously reported by our group.[15, 20] These F_{ad} results are relevant, as they provide a quantitative scale of solvation in HFAs, where the reference state – ideal solvation – is that of $F_{ad}/R \approx 0$ $mN.m^{-1}$.[20] The results obtained here can thus be correlated with the ability of the semi-fluorinated solvents to solvate the candidate compounds containing alkyl, ether, and ester moieties. The COOC moiety was found to be the most HFA-philic, followed by the COC fragment. The C8 moiety, the control group, was observed to be poorly solvated by HPFP, as expected. These results suggest that the COOC moiety would be the best candidate in screening inter-particle forces in HFA suspension-based formulations.

It is interesting to note that the JRK theory can be used to estimate the F_{ad}/R, and equally as important, that the theory shows a trend similar to that observed in the CFM experiments – values are summarized in Table 3.1. The favorable (and

enhanced) enthalpic interactions between HFA and COOC and COC fragments captured experimentally and with the JRK theory are expected due to the presence of the more polar oxygen-containing groups, which are capable of interact with the HPFP.[12, 20, 25] The dipole moment of HPFP is very similar to that of HFA-227 and HFA-134a,[12] the two propellants approved for inhalation use.[11, 21] At the same time, the significant dipole and also the presence of bulkier fluorine atoms, negatively impact the ability of semi-fluorinated propellants to solvate non-polar tails such as C8.[20, 21, 25] The results obtained here are in line with previous *ab-initio* calculations,[20, 25] which showed a more favorable binding energy (E_b) between HFA and fragments with increasing polarity.

3.3.2 Solvation in HFAs in the presence of ethanol

The F_{ad}/R for the candidate tails measured in HPFP/ethanol mixtures was also determined. Experimental and calculated (JKR) results are summarized in Figure 3.1 – the F_{ad}/R decreases upon increasing the volume fraction of ethanol in the liquid mixture with HPFP. The same trend is seen for all moieties. These results suggest that ethanol indeed has the ability to enhance the solvent environment for all compounds containing alkyl, ether, and ester moieties investigated here, as detected by a reduction in the cohesive forces.

At 15% (v/v) ethanol, which is in the upper range of volume fraction of ethanol used in commercial HFA-based pMDI formulations,[49, 50] the F_{ad}/R was reduced to 55 $mN.m^{-1}$ (34 %) for C8, 7.5 $mN.m^{-1}$ for COC (63 %), and down to 3 $mN.m^{-1}$ for COOC tails (67 %).

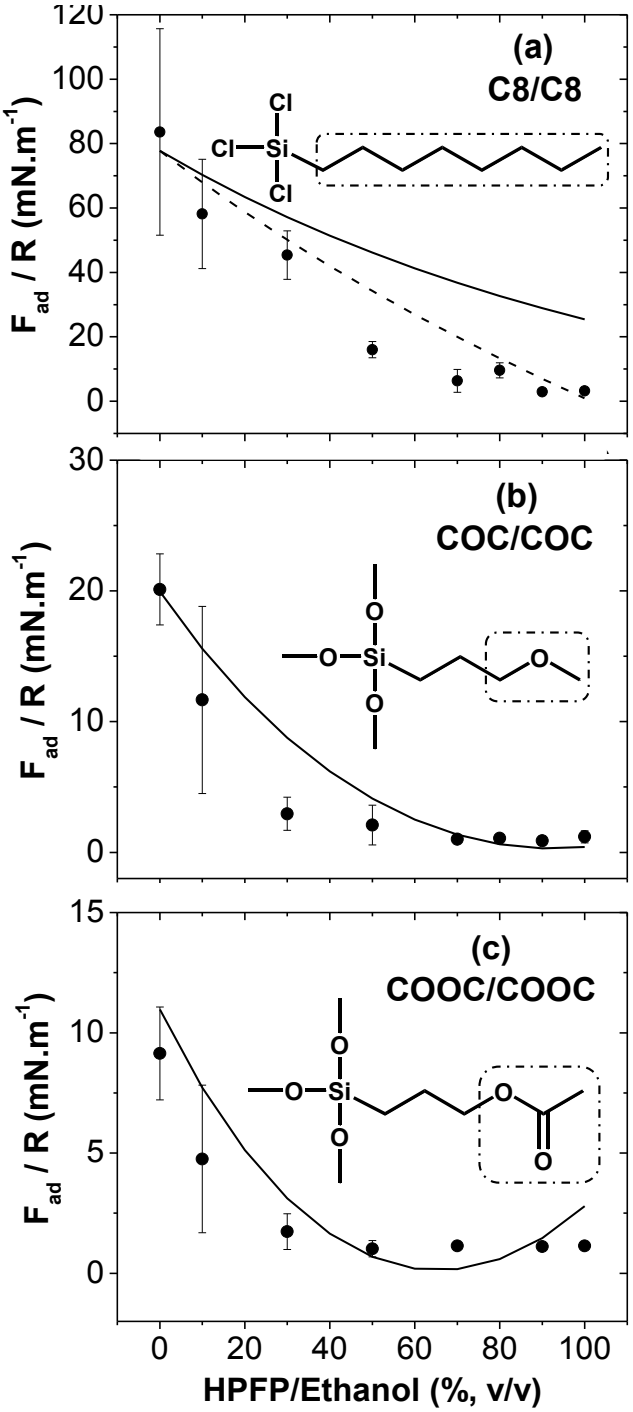

Figure 3.1. Effect of the volume fraction of ethanol on the F_{ad}/R of **(a)** alkyl (C8)- ; **(b)** ether (COC)- ; **(c)** ester (COOC)-based moieties. (•) CFM measurements were at 298 K and in HPFP/ethanol mixtures; (—) F_{ad}/R calculated using the JKR theory, considering γ_d = 18.8, γ_p = 2.6, and γ_t = 21.4 mN.m^{-1} for ethanol; and (- - -) F_{ad}/R calculated using the JKR theory, considering for ethanol: γ_d = 18.8, γ_p = 0.0, and γ_t = 18.8 mN.m^{-1}. *Insets:* Molecular structures of **(a)** C8TS; **(b)** COCTS; and **(c)** COOCTS. The moieties of interest are shown in brackets.

While the F_{ad}/R numbers have not been quantitatively correlated with the ability of surfactants to stabilize particle-suspensions in HFAs, i.e., no threshold number has been attributed to a region of stability vs. a region of instability, a reduced cohesive force between drug particles due to the introduction of surfactants in HFAs has been demonstrated to correlated with enhanced particle dispersibility, and improved aerosol performance of the corresponding formulation.[19, 51]

It can also be seen that the presence of ethanol has a much greater impact in the systems containing COC- and COOC-based moieties, than in that containing the C8 groups. It can be also seen that, even at high volume fractions of ethanol, the F_{ad}/R, especially for C8, falls very far from that expected in case of ideal solvation ($F_{ad}/R \approx 0$ mN.m^{-1}).[20] A volume fraction of ethanol of 48% is required in the C8/C8 system in order to achieve the same level of solvation observed for the system with COC/COC and no ethanol, and 80% to reach F_{ad}/R values for COOC/COOC in pure HPFP. However, such high amounts of ethanol in pMDI formulations are not practical, since it has been shown that the presence of such high concentrations of non-volatile excipients mixed with HFA dramatically (and negatively) impacts the aerosol performance of both solution[13, 49] and suspension formulations,[1, 18] as the vapor pressure of the mixture is significantly reduced.[7, 49]

The results presented here suggest, therefore, that in the range in which ethanol may find use in commercial HFA-based formulations (0 - 15% v/v),[49, 50] its ability to enhance the solvation capacity of HFA is very limited for excipients containing alkyl (non-polar) fragments, such as is the case of most surfactants in FDA-approved pMDI formulations.[12] It is interesting to put the results observed here in perspective with

particle-particle force interactions obtained in liquid HFPF in the presence of surfactant and ethanol. The adhesive forces between salbutamol particles was shown to be suppressed upon the addition of 7% (v/v) ethanol in HPFP by about 87% when in presence of 1 mM oleic acid (surfactant with alkyl tails).[19] However, that system still exhibited very fast flocculation of the formulation in HFA, indicating that such reductions in particle forces or F_{ad}/R are not enough to enhance the solvation of alkyl tails to levels required for particle stabilization in propellant HFAs.

3.3.3 F_{ad}/R in presence of ethanol – analysis from CFM measurements and JKR theory

In the JKR model, the interaction forces are only considered inside the contact region between tip and planar surface of the substrate, and therefore, this model is better applied in the case of soft samples with large adhesion, and tips with large radius of curvature.[27] However, this theory yields satisfactory results for other systems as well.[24, 27, 30] While limitations in the theory do exist, the JKR model is known to provide better overall agreement with F_{ad} when compared to other theories, such as Derjaguin-Muller-Toporov (DMT) and Hertz,[33] and was thus employed in this work. The F_{ad}/R results determined from JKR theory are shown in Figure 3.1 (lines).

Overall, the JRK results correlate well with those determined by CFM – compare solid line against the symbols in Figure 3.1a, 3.1b, and 3.1c, when the dispersive and polar contributions of surface free energy of HPFP were set to 61.8 and 38.2 %, respectively (Table 3.1). The best agreement between theory and experiment was found for the ether moiety (Figure 3.1b). For the COOC moiety, a minimum in the

calculated F_{ad}/R was predicted at around 65% (v/v) ethanol in HPFP, representing a qualitatively different trend compared to that observed experimentally. This may be at least in part explained based on the strong polar nature of the interactions between HPFP and ethanol, and that between the solvents and the ester group of the moiety in question, which may not be accurately captured by the theory or the simple mixing rules used in our calculations.

The agreement between the F_{ad}/R from the JKR theory and the CFM experiments as a function of the HPFP/ethanol ratio for the alkyl moiety, on the other hand, was observed to be inadequate – compare the solid line against symbols in Figure 3.1a. One hypothesis for this behavior is that the very polar ethanol molecules, when in presence of non-polar moieties, such as the alkyl-based fragments evaluated in this work, will tend to enhance the polar interactions among themselves, so as to minimize the energy of the system. According to this hypothesis, the non-polar part of the ethanol molecules (CH_3-CH_2-) will be the ones predominantly interacting with the alkyl tails; i.e., ethanol/C8 interactions in that case would resemble much more the interaction between two non-polar molecules, than between a highly polar and a non-polar group. Such behavior is not well captured by the theory in question, as the interfacial energy used in the calculation of F_{ad} is highly affected by the distribution of polar and dispersive contributions of the solvent and tail groups – Equations (3) and (4).

This hypothesis was tested via molecular simulations, and the result is presented in Figure 3.2a and 3.2b. In this simulation, a central propane molecule (representing the non-polar alkyl group) is left to interact with a cluster of methanol molecules. Methanol was chosen instead of ethanol to prove the point in question in a more

obvious way (methanol is a more polar short molecule which magnifies the dipole-driven interactions), and in order to reduce the computational effort of the simulation. Starting with a cluster of methanol molecules distributed around a central alkyl group – Figure 3.2a – it can be observed that the polar molecules preferentially interact with each other – Figure 3.2b. The methanol molecules form a cluster, and at the same time orient themselves in a way so as to have their polar hydroxyl groups pointing away from the non-polar alkyl groups. Based on this observation, the F_{ad}/R was recalculated using the JKR theory, except that now the nature of solvation was considered purely dispersive; i.e., the dispersive, polar, and total contributions of surface free energy of ethanol was set to 18.8, 0.0, and 18.8 $mN.m^{-1}$, respectively. The results from this calculation are shown in Figure 3.1a – dashed line. It can be observed that the F_{ad}/R calculated in this way agrees much better with the experimental values, thus suggesting that the dispersion forces of ethanol are indeed of great relevance to the solvation of the alkyl tails.

This potential structuring effect of ethanol seen in the system discussed earlier seems to be related to that observed in previous works on the solubility of solutes in water/ethanol mixtures (ethanol was also being used as cosolvent).[52-54] There is an enhancement of the hydrophilic interactions between the hydroxyl groups from ethanol, which work as promoters of hydrophobic interactions[54], i.e., dispersive interactions between alkyl groups and non-polar segment from ethanol. In fact, it has been reported that ethanol can form hydrophobic interactions with the exposed alkyl residues of proteins.[53] A further increase in ethanol concentration makes the structuring effect on the solvent even more relevant,[53] behavior that we have also in the F_{ad} measurements

between C8/C8 tails, as evidenced by the more pronounced deviation between experimental and calculated F_{ad}/R observed as the volume fraction of ethanol (cosolvent) mixed with HPFP (solvent) increased.

3.4 Conclusions

In this work we investigated the ability of cosolvent ethanol in HPFP/ethanol mixtures to enhance the solvation of compounds containing alkyl, ether, and ester moieties, which are of relevance to HFA-based pMDI formulations. CFM was used to determine the F_{ad} between surfaces containing the moieties of interest (alkyl, ether, and ester) in HPFP/ethanol liquid mixtures with varying volume fractions of ethanol. HPFP was used as liquid model for HFAs in the CFM measurements. The normalized adhesion force (F_{ad}/R) in HPFP was thus used as a measure of the solvation forces.

The CFM experimental results show that ethanol is indeed capable of enhancing the solvation of all fragments, and that the solvation increases as the volume fraction of ethanol increases. However, for the alkyl moiety, volume fractions of ethanol much larger than those typically employed in commercial formulations (< 15%) are required to achieve a level of solvation comparable to that of the ether moiety in pure HPFP. The effect of ethanol in the solvation of the ether fragment is much more pronounced (same for the ester fragment), thus suggesting the potential of ethanol to be applied in PEG-based pMDIs. The F_{ad}/R was calculated using the JKR theory, which shows the potential for modeling the CFM experimental results. F_{ad}/R determined by JKR theory suggests a strong dispersive contribution to the solvation of the alkyl tails in HPFP/ethanol mixtures. Thus, the results help us evaluate the potential and limitation

of predictive tools in understanding solvation in HFAs, such novel and challenging fluids. Because ethanol is a commonly used cosolvent in HFA-based pMDI formulations, the results obtained in this work as a function of the chemistry of the moieties (alkyl, ether, and ester groups) is of relevance as they may help design HFA-philic compounds, including surfactants and stabilizers, which may be used in the development of more efficient suspension-based pMDI formulations.

3.5 Declarations

Conflict of interest. The author(s) declare(s) that they have no conflicts of interest to disclose.

Funding. This work was supported by NSF-CBET [grant # 0933144] and funds from Wayne State University.

This chapter is based on the published manuscript: **Conti, D. S.**; Grashik, J.; Yang, L.; Wu, L.; da Rocha, S. R. P. Solvation in hydrofluoroalkanes: How can ethanol help? *Journal of Pharmacy and Pharmacology* **2011**, 64, (9), 1236-1244.

3.6 References

1. Marijani, R.; Shaik, M. S.; Chatterjee, A.; Singh, M. Evaluation of metered dose inhaler (MDI) formulations of ciclosporin. *J. Pharm. Pharmacol.* **2007,** *59*, (1), 15-21.
2. Bell, J.; Newman, S. The rejuvenated pressurised metered dose inhaler. *Expert Opin. Drug Delivery* **2007,** *4*, (3), 215-234.
3. Wu, L.; Bharatwaj, B.; Panyam, J.; da Rocha, S. Core-shell particles for the dispersion of small polar drugs and biomolecules in hydrofluoroalkane propellants. *Pharm. Res.* **2008,** *25*, (2), 289-301.

4. Kwok, P. C. L.; Chan, H.-K. Electrostatics of pharmaceutical inhalation aerosols. *J. Pharm. Pharmacol.* **2009,** *61*, 1587-1599.

5. Bains, B. K.; Birchall, J. C.; Toon, R.; Taylor, G. *In vitro* reporter gene transfection via plasmid DNA delivered by metered dose inhaler. *J. Pharm. Sci.* **2010,** *99*, (7), 3089-3099.

6. Broedersa, M. E. A. C.; Sanchisb, J.; Levyc, M. L.; Graham K. Cromptond; Dekhuijzena, P. N. R. The ADMIT series – Issues in inhalation therapy. 2) Improving technique and clinical effectiveness. *Prim. Care Respir. J.* **2009,** *18*, (2), 76-82.

7. Rogueda, P. Novel hydrofluoroalkane suspension formulations for respiratory drug delivery. *Expert Opin. Drug Delivery* **2005,** *2*, (4), 625-638.

8. Rogueda, P. G. A. HPFP, a model propellant for pMDIs. *Drug Dev. Ind. Pharm.* **2003,** *29*, (1), 39-49.

9. Myrdal, P. B.; Karlage, K. L.; Stein, S. W.; Brown, B. A.; Haynes, A. Optimized dose delivery of the peptide cyclosporine using hydrofluoroalkane-based metered dose inhalers. *J. Pharm. Sci.* **2004,** *93*, (4), 1054-1061.

10. Paul, A.; Griffiths, P. C.; James, R.; Willock, D. J.; Rogueda, P. G. Explaining the phase behaviour of the pharmaceutically relevant polymers poly(ethylene glycol) and poly(vinyl pyrrolidone) in semi-fluorinated liquids. *J. Pharm. Pharmacol.* **2005,** *57*, (8), 973-980.

11. Gaur, P. K.; Mishra, S.; Gupta, V. B.; Rathod, M. S.; Purohit, S.; Savla, B. A. Targeted drug delivery of Rifampicin to the lungs: Formulation, characterization, and stability studies of preformed aerosolized liposome and in situ formed aerosolized liposome. *Drug Dev. Ind. Pharm.* **2010,** *36*, (6), 638-646.

12. da Rocha, S. R. P.; Bharatwaj, B.; Saiprasad, S., Science and Technology of Pressurized Metered-Dose Inhalers. In *Controlled Pulmonary Drug Delivery* Smyth, H. D. C.; Hickey, A. J., Eds. Springer New York: 2011; pp 165-201.

13. Smyth, H. D. C. The influence of formulation variables on the performance of alternative propellant-driven metered dose inhalers. *Adv. Drug Delivery Rev.* **2003,** *55*, (7), 807-828.

14. Cote, M.; Rogueda, P. G. A.; Griffiths, P. C. Effect of molecular weight and end-group nature on the solubility of ethyle ethylene oxide oligomers in 2H,3H-decafluoropentane an and its fully fluorinated analogue, perfluoropentane. *J. Pharm. Pharmacol.* **2008,** *60*, 593-599.

15. Wu, L.; da Rocha, S. R. P. Applications of the atomic force microscope in the development of propellant-based inhalation formulations. *KONA Powder and Particle Journal* **2008,** *26*, 106-128.

16. Mazhar, S. H. R. A.; Chrystyn, H. Salbutamol relative lung and systemic bioavailability of large and small spacers. *J. Pharm. Pharmacol.* **2008,** *60*, (12), 1609-1613.

17. Vervaet, C.; Byron, P. R. Drug-surfactant-propellant interactions in HFA-formulations. *Int. J. Pharm.* **1999,** *186*, (1), 13-30.

18. Williams III, R. O.; Liu, J. Formulation of a protein with propellant HFA 134a for aerosol delivery. *Eur. J. Pharm. Sci.* **1999,** *7*, (2), 137-144.

19. Wu, L.; da Rocha, S. R. P. Biocompatible and biodegradable copolymer stabilizers for hydrofluoroalkane dispersions: A colloidal probe microscopy investigation. *Langmuir* **2007,** *23*, (24), 12104-12110.

20. Wu, L.; Peguin, R. P. S.; da Rocha, S. R. P. Understanding solvation in hydrofluoroalkanes: *Ab Initio* calculations and chemical force microscopy. *J. Phys. Chem. B* **2007,** *111*, (28), 8096-8104.

21. Peguin, R. P. S.; da Rocha, S. R. P. Solvent-solute interactions in hydrofluoroalkane propellants. *J. Phys. Chem. B* **2008,** *112*, (27), 8084-8094.

22. Burnham, N. A.; et al. Comparison of calibration methods for atomic-force microscopy cantilevers. *Nanotechnology* **2003,** *14*, (1), 1-6.

23. Banga, R.; Yarwood, J.; Morgan, A. M.; Evans, B.; Kells, J. FTIR and AFM studies of the kinetics and self-assembly of alkyltrichlorosilanes and (perfluoroalkyl)trichlorosilanes onto glass and silicon. *Langmuir* **1995,** *11*, (11), 4393-4399.

24. Ito, T.; Namba, M.; Bühlmann, P.; Umezawa, Y. Modification of silicon nitride tips with trichlorosilane self-assembled monolayers (SAMs) for chemical force microscopy. *Langmuir* **1997,** *13*, (16), 4323-4332.

25. Peguin, R. P. S.; Wu, L.; da Rocha, S. R. P. The ester group: How hydrofluoroalkane-philic is it? *Langmuir* **2007,** *23*, (16), 8291-8294.

26. Gerberich, W. W.; Cordill, M. J. Physics of adhesion. *Rep. Prog. Phys.* **2006,** *69*, (7), 2157-2203.

27. Butt, H.-J.; Cappella, B.; Kappl, M. Force measurements with the atomic force microscope: Technique, interpretation and applications. *Surf. Sci. Rep.* **2005,** *59*, (1-6), 1-152.

28. Takano, H.; Kenseth, J. R.; Wong, S.-S.; O'Brie, J. C.; Porter, M. D. Chemical and biochemical analysis using Scanning Force Microscopy. *Chem. Rev.* **1999,** *99*, (10), 2845-2890.

29. Noy, A.; Vezenov, D. V.; Lieber, C. M. Chemical Force Microscopy. *Annu. Rev. Mater. Sci.* **1997,** *27*, (1), 381-421.

30. Noy, A.; Frisbie, C. D.; Rozsnyai, L. F.; Wrighton, M. S.; Lieber, C. M. Chemical Force Microscopy: Exploiting chemically-modified tips to quantify adhesion, friction, and functional group distributions in molecular assemblies. *J. Am. Chem. Soc.* **1995,** *117*, (30), 7943-7951.

31. Vezenov, D. V.; Noy, A.; Ashby, P. Chemical force microscopy: Probing chemical origin of interfacial forces and adhesion. *J. Adhes. Sci. Technol.* **2005,** *19*, (3), 313-364.

32. Zhikharev, A. V. A gas-liquid cell for scanning probe microscopes. *Instrum. Exp. Tech.* **2004,** *47*, (6), 829-832.

33. Patrick, D. L.; Flanagan; Kohl, P.; Lynden-Bell, R. M. Atomistic molecular dynamics simulations of chemical force microscopy. *J. Am. Chem. Soc.* **2003,** *125*, (22), 6762-6773.

34. Lee, D. H. Phase state effect on adhesion behavior of self-assembled monolayers. *Langmuir* **2004,** *20*, (19), 8124-8130.

35. Hiemenz, P. C.; Rajagopalan, R., *Principles of Colloid and Surface Chemistry*. 3rd ed.; Marcel Dekker, Inc.: New York, 1997.

36. Adamson, A. W.; Gast, A. P., *Physical Chemistry of Surfaces*. John Wiley & Sons, Inc.: New York, 1997.

37. Surface Tension Components and Molecular Weight of Selected Liquids, In *Accu Dyne Test*^{TM}, http://www.accudynetest.com (accessed 16 June 2011): 2009.

38. Koenhen, D. M.; Smolders, C. A. The determination of solubility parameters of solvents and polymers by means of correlations with other physical quantities. *J. Appl. Polym. Sci.* **1975,** *19*, (4), 1163-1179.

39. Hansen, C. M., *Hansen Solubility Parameters: A User's Handbook*. CRC Press Taylor & Francis Group: Boca Raton, 2007.

40. Krevelen, D. W.; Nijenhuis, K., *Properties of Polymers: Their Correlation with Chemical Structure; Their Numerical Estimation and Prediction from Additive Group Contributions*. Elsevier: Amsterdam, 2009.

41. Oss, C. J. V.; Good, R. J. Surface tension and the solubility of polymers and biopolymers: The role of polar and apolar interfacial free energies. *J. Macromol. Sci., Part A: Pure Appl.Chem.* **1989,** *26*, (8), 1183-1203.

42. Prausnitz, J. M.; Lichetenthaler, R. N.; Azevedo, E. G. d., *Molecular Thermodynamics of Fluid-Phase Equilibria*. 3rd ed.; Prentice Hall PTR: New Jersey, 1999.

43. Guidechem, (3-Methoxypropyl)trimethoxysilane. In *Online Chemical Database*, http://www.guidechem.com (accessed 6 June 2011): 2011.

44. LookChem, 3-(Trimethoxysilyl)propyl acetate,. In *Online Chemical Database*, http://www.lookchem.com (accessed 6 June 2011): 2008.

45. Frisch, M. J.; Trucks, G. W.; Schlegel, H. B.; Scuseria, G. E.; Robb, M. A.; Cheeseman, J. R.; Scalmani, G.; Barone, V.; Mennucci, B.; Petersson, G. A.; Nakatsuji, H.; M. Caricato, X. L., H. P. Hratchian, A. F. Izmaylov, J. Bloino, G. Zheng, J. L. Sonnenberg, M. Hada, M. Ehara, K. Toyota, R. Fukuda, J. Hasegawa, M. Ishida, T. Nakajima, Y. Honda, O. Kitao, H. Nakai, T. Vreven, J. A. Montgomery, Jr., J. E. Peralta, F. Ogliaro, M. Bearpark, J. J. Heyd, E. Brothers, K. N. Kudin, V. N. Staroverov, R. Kobayashi, J. Normand, K. Raghavachari, A. Rendell, J. C. Burant, S. S. Iyengar, J. Tomasi, M. Cossi, N. Rega, J. M. Millam, M. Klene, J. E. Knox, J. B. Cross, V. Bakken, C. Adamo, J. Jaramillo, R. Gomperts, R. E. Stratmann, O. Yazyev, A. J. Austin, R. Cammi, C. Pomelli, J. W. Ochterski, R. L. Martin, K. Morokuma, V. G. Zakrzewski, G. A. Voth, P. Salvador, J. J. Dannenberg, S. Dapprich, A. D. Daniels, Ö. Farkas, J. B. Foresman, J. V. Ortiz, J. Cioslowski, and D. J. Fox *Gaussian 09, Revision A.1*, Gaussian Inc.: Wallingford CT, 2009.

46. Řezáč, J.; Fanfrlík, J. i.; Salahub, D.; Hobza, P. Semiempirical quantum chemical PM6 method augmented by dispersion and h-bonding correction terms reliably describes various types of noncovalent complexes. *J. Chem. Theory Comput.* **2009,** *5*, (7), 1749-1760.

47. Stewart, J. Optimization of parameters for semiempirical methods V: Modification of NDDO approximations and application to 70 elements. *J. Mol. Model.* **2007,** *13*, (12), 1173-1213.

48. Ulman, A. Formation and structure of self-assembled monolayers. *Chem. Rev.* **1996,** *96*, (4), 1533-1554.

49. Gupta, A.; Stein, S. W.; Myrdal, P. B. Balancing ethanol cosolvent concentration with product performance in 134a-based pressurized metered dose inhalers. *J. Aerosol Med.* **2003,** *16*, (2), 167-174.

50. Mitchell, J.; Nagel, M.; Avvakoumova, V.; MacKay, H.; Ali, R. The Abbreviated Impactor Measurement (AIM) concept. Part II - Influence of evaporation of a volatile component - Evaluation with a "Droplet-Producing" pressurized metered dose inhaler (pMDI) - Based formulation containing ethanol as cosolvent. *AAPS Pharm Sci Tech* **2009,** *10*, (1), 252-257.

51. Wu, L.; Al-Haydari, M.; da Rocha, S. R. P. Novel propellant-driven inhalation formulations: Engineering polar drug particles with surface-trapped hydrofluoroalkane-philes. *Eur. J. Pharm. Sci.* **2008,** *33*, (2), 146-158.

52. Li, A.; Yalkowsky, S. H. Solubility of organic solutes in ethanol/water mixtures. *J. Pharm. Sci.* **1994,** *83*, (12), 1735-1740.

53. Castronuovo, G.; Elia, V.; Moniello, V.; Velleca, F.; Perez-Casas, S. Effect of a cosolvent on the hydrophobic interactions. A calorimetric study of alkane-m,n-diols in concentrated aqueous solutions of ethanol. *Phys. Chem. Chem. Phys.* **1999,** *1*, (8), 1887-1892.

54. Castronuovo, G.; Elia, V.; Niccoli, M.; Velleca, F. Calorimetric studies of hydrophobic interactions of alkanols in concentrated aqueous solutions of glucose: Implications for the mechanism of protein stabilization by sugars. *Thermochim. Acta* **2002,** *389*, (1-2), 1.

CHAPTER 4

Propellant-based Inhalers for the Non-invasive Delivery of Genes via Oral Inhalation

4.1 Introduction

There is tremendous potential in targeting genes to the lungs.[1-3] Asthma, cystic fibrosis, chronic obstructive pulmonary disease (COPD), emphysema, and lung cancer are just some of the many examples of pulmonary diseases that can be potentially treated by gene therapy.[1, 2, 4-6] However, there are several challenges associated with the formulation and regional delivery of genes via oral inhalation (OI),[1] the preferred mode of administration of therapeutics to the lungs.

The mucus layer in the airways and the lung surfactant in the alveolar region represent important extracellular barriers to the delivery of genes to the respiratory tract.[7, 8] As transfection with free DNA is not efficient, the choice of the gene carrier system is also of great relevance.[9] For polymeric carriers, the polymer chemistry, and the physical properties of the polymer-DNA complexes (polyplexes), including their size, surface charge, and DNA loading greatly affect the transfection efficiency.[10, 11] In addition, those parameters also influence the uptake and trafficking of the gene carriers and the release of DNA in the cellular environment, which are examples of intracellular barriers that need to be overcome.[12] The choice of the aerosolization technique is also expected to influence the transfection efficiency as the dose and location where the polyplexes will be delivered depend on device characteristics and particle engineering.[5, 13, 14]

The ideal scenario in terms of gene delivery to the lungs would be for both patients and health care providers to be able to choose from a host of different delivery devices, as patient compliance and device suitability depends on the patient and disease state/condition. Nucleic acids can be potentially delivered to the lungs via nebulizers, dry powder inhalers (DPIs) or pressurized metered dose inhalers (pMDIs).[15] Nebulization has many advantages,[5, 13, 15, 16] but it is less efficient and less convenient than portable devices.[5] Therapeutically active molecules can also be delivered to the lungs by DPIs. The delivery of such molecules using DPIs have several advantages, including the fact that DPIs are propellant-free, portable, simple use, have good shelf-life, and reduced time of administration.[17] Some studies have demonstrated the potential of liposomal gene powders,[17] and also of gene powders prepared by supercritical CO_2 using chitosan (CS) as non-viral carriers for use in DPIs.[18, 19] However, there are also some disadvantages associated with the delivery of genes with DPIs, as for example potential problems in dose uniformity, dependency on patient's inspiratory flow rate, and less protection from environmental effects.[20]

Genes can also be delivered to the lungs using pMDIs. However, pMDIs have received considerably less attention than DPIs and nebulizers. The only work discussing gene delivery in hydrofluoroalkane (HFA)-based pMDIs consists in using surfactant-coated DNA particles prepared by reverse microemulsion.[13] However, liposomes were needed during transfection to improve the *in vitro* transfection efficiency of the particles used in the formulation. In spite of the limited amount of work on pMDIs, such devices offer a potentially more efficacious and convenient alternative than DPIs and nebulizers, especially for repeat administration,[13] and serve as a complementary

strategy to other devices. pMDIs are also simple to use, have high compliance, and are extensively used for drug delivery to the lungs.[21, 22] Nevertheless, it has been shown to be difficult to stabilize particle dispersions in the low dielectric propellant HFA,[21, 22] and this is an extra challenge compared to DPIs and nebulizers in terms of the preparation of gene carriers for lung delivery. Particles for pMDI formulations need not only to be within the appropriate size range for deep deposition to the lungs,[23] but they must also have an appropriate surface chemistry to be efficiently dispersed in the propellant HFAs, so as to prevent particle aggregation, which may negatively impact the aerosol characteristics of the pMDIs.[21, 22, 24]

In this work we propose a propellant-based, portable formulation for the OI delivery of genes, which addresses some of the challenges mentioned earlier. We discuss the effect of the characteristics of the chosen polymer carrier (chitosan, CS) on the properties of the polyplexes. The aerosol characteristics of the pMDIs containing the engineered core-shell particles (polyplexes as core and a co-oligomer as shell) are also reported. Finally, we demonstrate the ability of the engineered particles containing the polyplexes to transfect a model lung alveolar epithelium cells *in vitro* before and after exposure to the hydrofluoroalkane (HFA) propellant used in the pMDIs, and the long term stability of the particles in the propellant and their morphology after actuation. This work is relevant as pMDIs are the least expensive and most widely used portable OI devices for the delivery of therapeutics to the lungs, and due to the fact that new gene-based therapies are expected to continue to be developed to treat medically relevant respiratory diseases. The relevance of this work also stems from the fact that most of the work related to OI delivery of genes to the lungs has focused on DPIs[15, 18,

[19, 25, 26] and nebulizers,[15, 16, 27, 28] and only one other report in the literature has addressed the formulation and delivery of genes using HFA-based pMDIs.[13]

4.2 Experimental Section

4.2.1 Materials

Chitosan (CS) 100 - 300 kDa with 80% degree of deacetylation (DDA), Activated Calf Thymus DNA (10-15 million Da; 18,940 bp), Ninhydrin reagent 2% solution, Water Molecular Biology Reagent (MBR, filtered, sterile, DNase, RNase and protease free), Lysozyme from chicken egg white (69,000 units per mg solid), 3,6-dimethyl-1,4-dioxane-2,5-dione (lactide, LA), Tin(II) 2-ethylhexanoate (Stannous octoate, $SnOct_2$, 95%), 2,5-dihydroxybenzoic acid (DHB, 98%), and DNase I (552 Kunitz per mg solid) were purchased from Sigma-Aldrich. Plasmid DNA (pDNA) gWIz-GFP (5,757 bp) was purchased from Aldevron. PicoGreen® dsDNA reagent, Dulbecco's Modified Eagle Medium 1X high glucose (DMEM, with and without phenol red), TrypLE™ Express Stable Trypsin and Penicillin-Streptomycin were purchased from Invitrogen. Serum Advantage FBS non-heat inactivated was purchased from Atlanta Biologicals. TransFast™ Transfection Reagent, MTS [(3-(4,5-dimethylthiazole-2-yl)-5-(3-carboxymethoxyphenyl)-2-(4-sulfophenyl)-2H-tetrazolium, inner salt] and PMS (phenazine methosulfate) were purchased from Promega. Culture flasks (75 cm^2, Cellstar), 24 and 96-well culture plate (Corning) were purchased from VWR. 2H, 3H-perfluoropentane (HPFP, 98%) was purchased from DuPont™ TMC Ind. Inc. Hydrofluoroalkane 1,1,1,2,3,3,3-heptafluoropropane (HFA-227, pharma grade, 99.99%) was a gift from Solvay Fluor. Actuators from Ventolin HFA® (Glaxo Smithkline) were

used in the cascade impaction studies. Glacial acetic acid (100%), hydrogen peroxide (31.4%), hydrochloric acid (37.2%), acetonitrile (ACS grade, 99.9%), toluene (HPLC grade, 99.9%), sodium acetate anhydrous (99%) and phosphate buffered saline (PBS, 10X solution) were purchased from Fisher Chemicals. Sodium sulfate anhydrous (99%) and acetone (ACS grade 99.5%) were purchased from EMD Chemicals. Chitosanase Streptomyces sp. N174 (10 units per 100µL) was purchased from Calbiochem EMD Biosciences. Sodium hydroxide (99%) and ethyl acetate (99.5%) were purchased from Mallinckrodt Chemicals. Ethanol (200 proof) was purchased from Decon Labs. Deionized water (DI-water, resistivity of 18.2 MΩ.cm) was obtained from NANOpure® DIamond™ UV ultrapure water system (Barnstead International). Deuterated dimethyl sulfoxide (DMSO-d6, 99.9%) was purchased from Cambridge Isotope Lab. Inc. Silicon nitride V-shape contact mode cantilevers with integrated pyramidal tips were purchased from Budget Sensors.

4.2.2 Depolymerization and characterization of chitosan (CS) for CS-DNA nanoparticles

Large molecular weight (Mw) CS was depolymerized for the preparation of the polyplexes.[29] Briefly, 1 g of CS was dissolved in 100 mL of DI-water with 2 mL glacial acetic acid, under heating (50°C) and magnetic stirring (3 h). Hydrogen peroxide (1 mL) was added to the solution, and the depolymerization proceeded at 50°C. The solution was allowed to cool down in a cold water bath, and the pH was adjusted to neutral using a 3M sodium hydroxide solution. The depolymerized CS was collected as a precipitate by centrifugation (5,000 rpm - 2,800 xg), washed with DI-water and acetone, and dried

in air at room temperature. The Mw of depolymerized and as received CS was determined by viscometry.[30] Samples with different CS concentrations were prepared in 0.2 M acetic acid / 0.1 M sodium acetate aqueous solution at pH 4.4, and filtered using 0.2 µm filter (non-sterile, Nylon-membrane, PP-housing from Cole-Parmer). Their relative (η_{rel}) and specific (η_{sp}) viscosities were calculated based on the efflux times using an Ubbelohde viscometer (OC-C938, Cole-Parmer) at 30°C as follows:[31]

$$\eta_{rel} = (t_{solution}) \div (t_{solvent})$$

$$\eta_{sp} = \eta_{rel} - 1$$

The intrinsic viscosity [η] was determined as the intersection point at zero concentration of the inherent (η_{inh}) and reduced (η_{red}) viscosities (graphic method) using five different CS concentrations, according to these equations[31] below, where C is the concentration in $g.mL^{-1}$.

$$\eta_{inh} = (\ln \eta_{rel}) \div C$$

$$\eta_{red} = \eta_{sp} \div C$$

The [η] was also calculated using the Solomon-Ciutâ approximation[32] which requires only one CS concentration: $[\eta] = \{ [2.\eta_{sp} - 2.\ln(\eta_{rel})]^{1/2} \} \div C$. Due to the agreement between the [η] values obtained from these two approaches in the initial studies, the Solomon-Ciutâ approximation was chosen for the remainder of the experiments. The Mw was calculated based on Mark-Houwink-Kuhn-Sakurada

(MHKS)[32] equation $[\eta] = k.Mw^a$ with $k = 8.02 \times 10^{-3}$ mL.g^{-1} and $a = 0.960$. The constants *k* and *a* are specific for each CS-solvent system, and they were estimated from the knowledge of the DDA, type of solvent, pH and temperature, using equations from the literature.[30]

4.2.3 Preparation and characterization of CS-DNA nanoparticles (NPs)

4.2.3.1 Preparation of polyplexes. Complex coacervation was used to prepare CS-DNA NPs.[33] Briefly, CS (100 - 500 µg.mL^{-1} in 5mM sodium acetate buffer at pH 5.5, filtered with 0.2 µm filter), and DNA solutions (60 - 100 µg.mL^{-1} in 5mM sodium sulfate) were initially preheated to 55°C in a water bath. CS solution (100 µL) was gradually added to the DNA solution (100 µL) while vortexing at high speed for 45 s. The CS-DNA NPs suspension was kept at room temperature for 30 min before use, to assure the complete formation of the polyplexes. The number of phosphate groups (P) in the DNA content, and the number of amine groups (N) in the CS content used during complexation was determined based on CS Mw and DDA, number of base pairs (bp) of the DNA, and concentrations of CS and DNA solutions. The nominal N/P ratio was calculated using that information.[34] CS-DNA NPs were collected as precipitate by centrifugation (14,000 rpm - 21,500 xg for 1.5 h), and the supernatant was used for determination of free DNA and CS contents, which allowed a more precise characterization of the N/P ratio (actual N/P ratio), and encapsulation efficiency. The CS-DNA NPs were gently re-dispersed in 0.5 mL MBR-water using a probe sonicator (OmniRuptor 250) at 25 W for 5 s. The NPs suspension was used for further characterization and other preparations. The encapsulation efficiency of DNA and CS

was indirectly determined by measuring the difference between the total DNA and CS contents added during the complex coacervation, and the amount of non-entrapped DNA and CS remaining in the aqueous supernatant.[35] The supernatant was analyzed using PicoGreen® Assay (for the non-entrapped DNA) in a Fluorescence/Spectrometer (Parkin Elmer LS50B), and Ninhydrin reagent[36] (for the non-entrapped CS) in a UV-Visible Spectrophotometer (Cary 50 Bio). The amount of DNA and CS in the NPs was calculated according to linear calibration curves.

4.2.3.2 Size and morphology. Malvern ZetaSizer (Nano ZS) was used to evaluate the size and zeta potential of the CS-DNA NPs. The samples were diluted 1:10 in DI-water, and the measurements were performed in quintuplicate, at 25°C, using the refractive index, viscosity and dielectric constant of pure water.[37] The Smoluchowski Model was used to determine the zeta potential.[38] Scanning Electronic Microscopy (SEM, Hitachi S-2400, 25kV) and Atomic Force Microscopy (AFM, Pico LE, Molecular Imaging) were used to investigate the morphology of the polyplexes. For SEM imaging, several drops of CS-DNA NPs suspension in water were placed on a cover glass slip, allowed to dry overnight, and sputter-coated with gold (Ernest Fullan) for 40 s.[21] Image J software (version 1.42 q, National Institutes of Health, NIH) was used to estimate the size of the polyplexes from the SEM images. The histogram of the measured NPs diameter (> 400 particles) was fit to a Gaussian distribution, from which an average size and deviation was obtained. For AFM imaging, 20 µL of the freshly prepared CS-DNA NPs suspension was incubated on a freshly cleaved mica surface for 5 min, so as to allow the binding of the polyplexes on the substrate.[39] The excess of liquid was then removed

by washing with DI-water, the system was left to dry at room temperature under air flow, and the images were obtained using Si_3Ni_4 V-shape cantilever in contact mode.[39]

4.2.3.3 DNA encapsulation efficiency. Chitosanase/lysozyme digestion was used to directly determine the DNA encapsulation efficiency in CS-DNA polyplexes.[39, 40] These results were compared to the indirect DNA loading obtained from the determination of free DNA and CS contents in the supernatant after complexation as described earlier. CS is susceptible to chitosanase and lysozyme digestion – lysozyme degrades sites near the N-acetylated glucosamine, and chitosanase attacks the sequences of three consecutive deacetylated units.[40] CS-DNA NPs (100 µL) were incubated at 37°C for 6 h with 80 µL chitosanase (0.625 $U.mL^{-1}$) in 50/50 (v/v) 50 mM sodium acetate buffer at pH 5.5 / glycerol, and 20 µL lysozyme (1000 $U.mL^{-1}$) in 50 mM sodium acetate buffer at pH 5.5,[39, 40] followed by DNA quantification using PicoGreen® Assay.

4.2.4 Synthesis and characterization of oligo(lactide)-*grafted*-CS (OLA-*g*-CS) co-oligomer

The preparation of water soluble, low Mw CS, followed by the synthesis of OLA-*g*-CS co-oligomer was performed according to a modified method from literature.[21] Details about methods, results and discussion can be found in Appendix A.

4.2.5 Preparation and characterization of CS-DNA core-shell particles

4.2.5.1 Preparation of core-shell particles. Emulsification diffusion was employed to prepare core-shell particles containing CS-DNA NPs.[21] Briefly, 25 mg OLA-*g*-CS was

dissolved in 0.5 mL DI-water, and CS-DNA NPs (50 - 300μg.mL^{-1}) were dispersed in another 0.5 mL of DI-water. The OLA-*g*-CS solution and the dispersion containing the polyplexes were combined and emulsified in 19 mL of ethyl acetate using a sonication bath (VWR, P250D, set to 180 W) for 5 min at 15 - 20°C, producing water-in-oil (W/O) emulsion. This emulsion was subsequently added to a large volume of ethyl acetate (180 mL). Core-shell particles (OLA-*g*-CS as the shell, and CS-DNA NPs as the core) were thus formed, collected by centrifugation (5,000 rpm - 2,800 xg, 15min) and dried in air at room temperature.

4.2.5.2 Size and morphology. SEM (Hitachi S-2400) was used to evaluate the size and morphology of the core-shell particles. A small amount of the particles was dispersed in HPFP using a sonication bath (VWR, P250D, set to 180 W, at 15 - 20°C) and several drops of the suspension were placed on a cover glass slip, allowed to dry, and sputter-coated with gold for 40 s (Ernest Fullan) before SEM imaging. Image J was used to determine the size from SEM images (> 200 particles) using similar procedure as described earlier. Dynamic Light Scattering (DLS) was also used to evaluate the size of CS-DNA core-shell particles. Samples were prepared in HPFP, a model HFA that is liquid at ambient conditions.[21] The measurements were performed in triplicate, at 25°C, using the refractive index, viscosity and dielectric constant of pure HFPF in the calculations.[41] The morphology of the core-shell particles was also investigated by Transmission Electronic Microscopy (TEM, JEOL JEM-2010). A drop of the particles dispersion in HPFP was placed on a 200-mesh copper grid and allowed to dry before TEM imaging.

4.2.5.3 DNA loading in core-shell particles. Chitosanase/lysozyme digestion was also utilized to quantify the DNA loading in the core-shell particles, and on the stages of the Andersen Cascade Impactor (ACI, discussed next). The procedure was similar to that described earlier for quantification of the amount of DNA encapsulated in the polyplexes. Because the OLA-*g*-CS (the co-oligomer shell) is water soluble, the core-shell particles quickly break down, forming a homogeneous aqueous solution of the co-oligomer,[21] with dispersed polyplexes. The method then proceeded as described earlier for CS-DNA NPs, except that core-shell particles were incubated with the enzymes instead of the NPs alone.

4.2.6 Preparation of pMDI formulations and evaluation of their physical stability

An exact mass of core-shell particles containing CS-DNA NPs was weighed into pressure proof glass vials (8412-B, West Pharmaceutical Services), and crimp-sealed with a metering valve (63 µL, EPDM Spraymiser, 3M Inc.). A known amount of HFA-227 was added with the help of a manual syringe pump (HiP, 50-6-15), and a home-built high pressure aerosol filler, to make 2 $mg.mL^{-1}$ concentration of CS-DNA core-shell particles in the propellant HFA-227. The dispersions were sonicated (VWR, P250D, set to 180 W, at 15 - 20°C) in order to break up any large aggregates. The physical stability was investigated by visually monitoring the quality of the dispersion as function of time after mechanical energy input ceased.

4.2.7 Aerosol characteristics

The aerosol properties of the CS-DNA core-shell particles and CS-DNA NPs alone in pMDI formulations were determined with an Andersen Cascade Impactor (ACI, CroPharm, Inc.) fitted with a USP induction port and operated at a flow rate of 28.3 $L.min^{-1}$, at 298 K and 45% relative humidity.[21, 22] The pMDI formulations containing core-shell particles loaded with CS-DNA NPs were prepared as described in Section 4.2.6. pMDI formulations containing CS-DNA NPs alone were prepared as follows: CS-DNA NPs re-dispersed in 0.5 mL MBR-water were frozen in liquid N_2 and lyophilized (Labconco Freeze Zone 1) at 0.05 mbar and -47°C for 48 h. The solid obtained was placed into a pressure proof glass vial (8412-B, West Pharmaceutical Services), and crimp-sealed with a metering valve (63 µL, EPDM Spraymiser, 3M Inc.). A known amount of HFA-227 was subsequently added, so that the total amount of CS-DNA NPs was the same as in the formulations prepared with CS-DNA core-shell particles. The dispersions were sonicated (VWR, P250D, set to 180 W, at 15 - 20°C) in order to break up any large aggregates. Before each test, five shots were first fired to waste. Subsequently, twenty shots were released into the ACI, with an interval of 10 s between each actuation.[22] Three independent canisters were tested for each formulation. After each run, the ACI was disassembled and the actuator, induction port (IP) and the stages were rinsed thoroughly with 20 mL of DI-water. The aqueous solution relative to each part of the ACI was frozen separately in liquid N_2, and lyophilized (Labconco Freeze Zone 1, 0.05 mbar, -47°C) for 48 h. The powder collected was dissolved in 150 µL of 50 mM sodium acetate buffer at pH 5.5, and incubated at 37°C for 6 h with 80 µL chitosanase (0.625 $U.mL^{-1}$) in 50/50 (v/v) 50 mM sodium acetate buffer at pH 5.5 /

glycerol, and 20 µL lysozyme (1000 $U.mL^{-1}$) in 50 mM sodium acetate buffer at pH 5.5. After the chitosanase/lysozyme digestion, the amount of free DNA was quantified by PicoGreen® Assay, and the DNA content in each stage of the device thus determined. The fine particle fraction (FPF), mass median aerodynamic diameter (MMAD), and geometric standard deviation (GSD) were calculated. FPF is defined as the mass of DNA on the respirable stages of the impactor (from stage 3 to filter) over the total mass of the DNA released into the device (from IP to filter, excluding the amount remaining in the actuator).[42] The cumulative DNA mass fraction into the device (stage 0 to filter) was calculated, and a graph of cut-off diameter of each stage (*x* axis, log 10 scale) versus the cumulative DNA mass fraction (*y* axis, probability scale) was plotted, and fitted linearly. The MMAD was determined as the particle size at which the line crossed the 50% mark, and GSD was defined as the ratio between the particle size at 84.1% mark and at 50% mark.[43] The single % dose per actuation was calculated by dividing the total mass of the formulation found in the ACI (from actuator to filter) to the nominal expected dose emitted during each run (in this case twenty),[22] which can be calculated based on the volume of the reservoir and the concentration of DNA loaded per volume of solvent.

4.2.8 *In vitro* transfection

A549 cells (human lung adenocarcinoma cell line, an *in vitro* model of Type II alveolar epithelium)[44] were seeded in a 75 cm^2 cell culture flask and subcultured until approximately 90% confluence. The cell culture medium (DMEM supplemented with 10% FBS and 1% antibiotics) was changed every two days. The cells were seeded on

24-well culture plate at density of 5×10^4 cells per well, and cultured in 0.5 mL DMEM supplemented with 10% FBS and 1% antibiotics for 24 h at 37°C and 5% CO_2 (Thermo Scientific Incubator, NAPCO 8000WJ). The cells were rinsed with 1X PBS twice, and transfection was initiated by adding 0.2 mL of transfection mixture containing CS-DNA NPs alone or CS-DNA core-shell particles (both equivalent to 0.25 µg DNA per well) in DMEM at pH 6.9 (without phenol red, antibiotics and serum). After 6 h of incubation, the cells were overlaid with 0.3 mL DMEM (without phenol red, supplemented with 10% FBS and 1% antibiotics) and incubated at 37°C and 5% CO_2. Free DNA was used as negative control, and DNA complexed with TransFast™ Transfection Reagent was used as positive control. The biological functionality of the reporter pDNA gWIz-GFP was investigated at 48 h post-transfection using a Fluorescence Microscope (Zeiss Imager Z1, Axio Cam MRm). The experiments were performed at 48 h based on the protocol suggested by the supplier of the transfection agent used as positive control.[45] All experiments were carried out in duplicate. The effect of the propellant HFA-227 on the biological activity of the pDNA was also investigated. CS-DNA NPs (alone and engineered as core-shell particles, both prepared as pMDI formulations at same pDNA concentration) were stored in HFA-227 at 298K and saturation pressure of the propellant. After 6 weeks, the HFA-227 propellant was slowly released by depressurization (removal of the gas phase), and the particles were allowed to dry at room temperature, following dispersion of the particles in 0.6 mL MBR-water. This solution was used in transfection experiments (equivalent to 0.25 µg DNA per well) in A549 cells, following similar protocol as explained earlier to determine the effect of storage under the compressed HFA environment.

4.2.9 *In vitro* cytotoxicity

A549 cells were seeded on 96-well culture plate (5×10^3 cells per well) and cultured in 100 µL DMEM supplemented with 10% FBS and 1% antibiotics for 24 h at 37°C and 5% CO_2. Cells were rinsed with 1X PBS twice, and it was added a culture medium containing CS-DNA NPs at varying concentrations of CS (5 - 100 $\mu g.mL^{-1}$), or OLA-*g*-CS (0.5 - 13.5 $mg.mL^{-1}$), or CS-DNA core-shell particles (5 - 100 $\mu g.mL^{-1}$ CS from NPs, and 0.5 - 13.5 $mg.mL^{-1}$ OLA-*g*-CS). The concentration of CS-DNA NPs and OLA-*g*-CS co-oligomer used in the experiments fall within the ranged used in the transfection and the ACI studies. The cells were incubated in these solutions for 15 h (overnight) at 37°C and 5% CO_2. This time was chosen based on previous literature, which have shown that CS-based polyplexes[46-49] and OLA-*g*-CS[21] are not cytotoxic at least up to 24 h. The cells were then rinsed with 1X PBS twice, and the medium containing the particles was replaced by 100 µL culture medium (particle free) and 20 µL MTS/PMS cell proliferation assay. The cells were allowed to incubate in this mixture for 4h at 37°C and 5% CO_2. MTS is bioreduced into formazan (which is soluble in the culture medium) by dehydrogenase enzymes found in metabolically active cells into formazan, which is soluble in the culture medium.[21] The absorbance of the formazan at 490 nm was measured directly from the 96-well culture plate (Molecular Devices, Spectra Max 250). This quantity is directly proportional to the number of living cells in the culture. Cell viability (%) is defined as the ratio of the absorbance between the treated (with particles) and untreated cells (control).

4.2.10 Stability of CS-DNA polyplexes and integrity of gWIz GFP pDNA

DNase I assay was performed in order to assess the protection of complexed gWIz GFP pDNA against nuclease degradation. Freshly prepared CS-DNA NPs at N/P ratio of 7, equivalent to 5 μg pDNA, were incubated with different concentrations of DNase I, model enzyme,[50] at 37°C for 15 min. The reaction was stopped by heat inactivation: 60°C for 15 min,[51] in presence of 0.5 M EDTA, at 5 μL per 1 U DNase.[52] CS-DNA NPs were collected by centrifugation (14,000 rpm - 21,500 xg for 1.5 h), and incubated with chitosanase/lysozyme at same conditions as described in Section 4.2.3.3, for DNA release. Samples were loaded in 1% (w/v) agarose gel (SeaKem® LE Agarose, Lonza) in TAE buffer 1X with 0.5 $\mu g.mL^{-1}$ ethidium bromide (10 $mg.mL^{-1}$ solution, Promega). Free pDNA, and CS-DNA NPs without exposure to DNase I were used as controls. The electrophoresis was performed at 100 V (E0160-VWR Mini Gel Electrophoresis) for 45 min, the pDNA-dye migration was observed under UV irradiation (FOTO/Analyst® Investigator/Eclipse with UV Transilluminator, Fotodyne Inc.) and the images were recorded using the FOTO/Analyst® PC Image software (v.5).

The integrity of the gWIz-GFP pDNA after complexation with CS, core-shell particles preparation, and storage in propellant HFA, was also analyzed by gel electrophoresis, following the protocol described earlier. 100 μL samples of CS-DNA polyplexes alone at N/P ratio of 7, and CS-DNA polyplexes formulated as core-shell particles, which were freshly prepared and stored in HFA-227 at 298K and saturation pressure of the propellant, were incubated with chitosanase/lysozyme under same conditions as described in Section 4.2.3.3 for DNA release. Free pDNA as received and the same particles without exposure to the enzymes were used as controls.

4.3 Results and Discussion

4.3.1 Depolymerization and characterization of CS for preparation of CS-DNA NPs

The Mw of CS has a strong influence on its physicochemical and biological properties.[34] The Mw has been also shown to modulate the transfection efficiency *in vitro*[33] and *in vivo*.[18, 33, 37] The literature brings several examples of *in vitro* transfection studies with CS-DNA NPs using medium/high Mw CS (40 - 600 kDa),[38, 40] and also low Mw CS (1 - 50 kDa).[33, 53] Based on those previous works, CS with Mw varying between 10 and 100 kDa,[53] when considered in combination with other relevant parameters such as DDA, N/P ratio, pH and serum content of the culture medium, and cell type,[34] seem to optimize *in vitro* gene expression of polyplexes between CS and DNA.

Low Mw CS can be easily prepared by random depolymerization using hydrogen peroxide as free radical generator.[29] The acidity of the solution and temperature cause decomposition of the hydrogen peroxide ($H_2O_2 \rightarrow H^+ + HOO^-$), producing unstable perhydroxyl anions (HOO^-), which decompose in powerful oxidants – the hydroxyl radicals (HO•) – abstracting hydrogen from carbons ($RH + HO\bullet \rightarrow R\bullet + H_2O$).[54] These H-abstractions lead to cleavage of 1,4-β-D-glucoside bonds in CS chains, decreasing its Mw.[29, 54] Parameters as the acidity and concentration of H_2O_2, temperature, and reaction time all affect the final Mw of CS, and can be used to control the depolymerization process.[29, 54]

Before starting the CS depolymerization, the Mw for non-depolymerized CS was determined using viscometry.[30, 31] The Mw was related to the intrinsic viscosity [η] by the MHKS equation,[32] and the [η] was calculated by the graphical method,[31] and using

the Solomon-Ciutâ approximation.[32] Figure 4.1a shows how the [η] for non-depolymerized CS was determined using the graphical method.

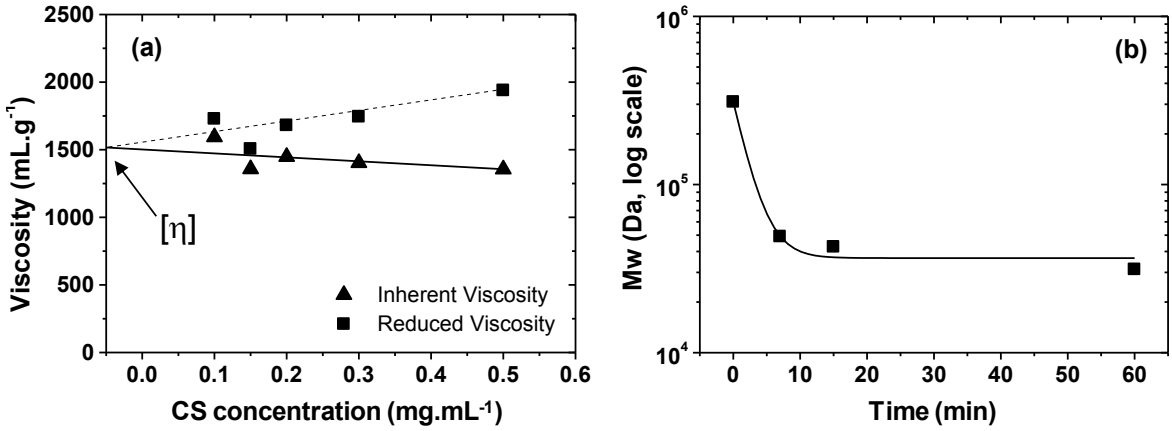

Figure 4.1. **(a)** Plot for the determination of intrinsic viscosity [η] of non-depolymerized CS (310 kDa, 80% DDA) based on inherent and reduced viscosities; **(b)** Exponential reduction in the Mw of CS (80% DDA) according to the depolymerization time.

The results indicate that the [η] of non-depolymerized CS with 80% DDA was 1524 $mL.g^{-1}$. The [η] calculated by Solomon-Ciutâ approximation was 1520 $mL.g^{-1}$, in agreement with the graphical method. From the [η] results, the Mw of non-depolymerized CS with 80% DDA (ca. 1464 amine and 366 acetyl units) was determined to be 310 kDa, in agreement with the results provided by the manufacturer. Because the [η] obtained by the Solomon-Ciutâ approximation was in good agreement to the more laborious graphical method, this approximation was used for all other determinations. Thus, in order to prepared CS with Mw between 10 and 100 kDa, large Mw CS (310 kDa, 80% DDA) was depolymerized using 2% CH_3COOH and 1% H_2O_2 (v/v) at 50°C for 7, 15 and 60 min. The Mw of depolymerized CS was found to be 49, 42 and 31kDa, respectively, as shown in Figure 4.1b.

CS depolymerizes very quickly in the first few minutes of reaction, leveling off after only 11 min (Figure 4.1b). Such exponential reduction of Mw is observed due to the rapid decrease in the solution's viscosity.[54] No significant change in the DDA of CS was expected under such relatively mild reaction conditions (low CH_3COOH and H_2O_2 concentrations, low temperature and short reaction times).[31, 54] Indeed, the DDA of 31 kDa CS, which is the one obtained using the longest depolymerization time, was determined by ^{1}H-NMR to be 77% (141 amine and 41 acetyl units), which is very close to the non-depolymerized / as received CS. Details about these results can be found in Appendix A. In addition, we also show (discussion in the Appendix A) that even for stronger reaction conditions used in the depolymerization of CS for the OLA-*g*-CS co-oligomer synthesis, the DDA does not change appreciably (also 77%). The DDA is an important quantity as it relates to the overall positive charge density of CS, and it is thus expected to have an effect on the transfection efficiency.[34, 55]

4.3.2 Preparation and characterization of CS-DNA NPs

4.3.2.1 Preliminary screening. In order to prepare CS-DNA polyplexes with small size (diameters around 200 nm or smaller), enhanced colloidal stability, and also good *in vitro* transfection efficiency in A549 cells, we performed a series of preliminary experiments that involved the preparation of polyplexes with varying CS Mw and N/P ratio. The polyplexes were characterized according to their size and zeta potential (ζ), and their ability to transfect A549 cells (good/poor). Calf Thymus DNA (18,940 bp long) and a pDNA encoding for green fluorescent protein (gWIz-GFP; 5,757 bp long) were chosen as models for this screening step. The use of two different DNAs (plasmid vs. linear, and with different number of bp) is relevant in terms of the applicability of the

proposed methodology for the delivery of a broad range of genes to the lungs, since it has been shown that efficient gene transfer can be achieved using large pDNA (up to 20.2 kbp in size)[56] and DNA in the linear form.[57] A brief discussion on the effect of the different variables is provided next.

The Mw of CS has a strong effect on the size of the polyplexes.[58] Literature has shown that it is possible to obtain smaller polyplexes with lower Mw CS.[58, 59] This can be attributed to the higher solubility and flexibility of the shorter CS chains in solution.[59] During the preliminary screening, our results indicated that the size of CS-DNA NPs decreased as the Mw CS decreased – e.g. the size of the polyplexes formed with Calf Thymus DNA, CS 80% DDA, and nominal N/P ratio of 6 decreased from 547 ± 92 nm to 183 ± 51 nm when the CS Mw was reduced from 310 to 31 kDa.

The size of the polyplexes is also influenced by the N/P ratio, and an increase in N/P ratio usually yields polyplexes with smaller diameters.[40] During our preliminary screening using CS (31 kDa, 80% DDA) and gWIz-GFP DNA, a size reduction from 229 ± 93 nm to 181 ± 62 nm was observed when the nominal N/P ratio increased from 5 to 7. The N/P ratio is also known to have a significant impact on *in vitro* transfection. N/P ratios that are too low typically yield physically unstable polyplexes, and poor *in vitro* transfection.[34] More stable dispersions of polyplexes can be obtained at higher N/P ratios.[40] Our preliminary results are in agreement with this trend. Polyplexes (CS 31 kDa, 80% DDA, gWIz-GFP DNA) showed poor *in vitro* transfection in A549 cells at nominal N/P ratio of 2 and 4. These polyplexes had lower zeta potential (ζ = + 13 ± 1 mV at N/P ratio of 2; and ζ = + 16 ± 1 mV at N/P ratio of 4), and were physically unstable (aggregated) in aqueous medium even at short times, as observed

during the DLS measurements. *In vitro* transfection improved when the nominal N/P ratio increased to 5 and 7, with ζ = + 23 ± 1 mV; and ζ = + 22 ± 6 mV, respectively. Collectively, these results indicate that the Mw and N/P ratio may be used as parameters to optimized *in vitro* transfection in A549 cells.

4.3.2.2 CS-DNA NPs selected for further studies. Polyplexes containing Calf Thymus and gWIz-GPF DNA, prepared with CS 31 kDa and 80% DDA, and possessing similar size and zeta potential to each other were selected for further studies. The properties of these polyplexes are shown in Table 4.1. Additional details about the properties of CS-DNA polyplexes obtained during the preliminary screening that lead to the selection above can be found in Appendix A.

Table 4.1. DNA and CS encapsulation efficiency (EE), particle size, and zeta potential of the CS-DNA NPs selected for further studies. The characteristics of the CS (Mw and DDA), nominal and actual N/P ratio are also shown.

CS Mw (kDa)	CS DDA (%)	Type of DNA	Nominal N/P ratio	DNA EE (%)	CS EE (%)	Actual N/P ratio	Particle Size (nm)	Zeta Potential (mV)
31	80	Calf Thymus	6	90 ± 8	79 ± 19	5	183 ± 51	21 ± 4
31	80	gWIz-GFP	7	95 ± 3	70 ± 8	5	181 ± 62	22 ± 6

Results in mean ± s.d. for n = 5 (five independent polyplexes preparations, and s.d. = standard deviation).

In order to better characterize the polyplexes, the encapsulation efficiency (EE) of DNA and CS was determined, and are presented in Table 4.1. The results show that the DNA EE, calculated based on the amount of free DNA measured in the supernatant after complexation – the indirect method described in Section 4.2.3.1 – was 90% for

Calf Thymus and 95% for gWIz-GFP DNA. The DNA EE determined after chitosanase/lysozyme digestion (direct method described in Section 4.2.3.3) was 96 ± 5% for both types of DNA. These results are in agreement with each other, indicating that almost all DNA was trapped within the NPs, and also serve to validate both methods for determining the DNA EE. High DNA EE is typically reported in the literature.[39, 40, 58] The CS EE, on the other hand, was much smaller (70 - 80%, Table 4.1). Similar findings have been reported in the previous works.[39, 40]

Based on the EE results, the N/P ratio of the polyplexes after complexation was (re)calculated. The actual N/P ratio was determined to be 5 (Table 4.1). Although these results indicate a decrease in the N/P ratio, ζ around + 21 mV suggests that the CS-DNA NPs have high enough charge density to provide good colloidal stability.[53, 58] Given the deviation in EE, especially for CS, it seems that a nominal N/P ratio is not sufficient information when discussing the effect of such variable on the transfection efficiency. Instead, an actual N/P ratio, which takes into account the DNA and CS EE, seems to be more appropriate, along with experimental information on the ζ and stability of the polyplexes.

In order to provide efficient gene transfer, polyplexes must have well-defined properties to overcome the intracellular barriers.[55] The size of the polyplexes plays a key role in this process. Since the uptake happens by endocytosis, some studies suggest that the size of NPs should be limited to diameters smaller than 150 nm.[39, 60] However, several reports demonstrate that polyplexes may efficiently transfect cells *in vitro* with NPs with a much broader size range.[33, 48, 58, 61-63] It is clear, therefore, that apart from particle size, other biological and biophysical parameters play important role

in the transfection process.[60] The results in Table 4.1 show that the size of CS-DNA NPs (Calf Thymus and gWIz-GFP DNA) obtained in this work was around 182 nm. Similar diameters have been reported in the literature.[33, 58] It interesting to also note that, based on our results, the type and size of the DNA does not seem to exert a large influence on the size and/or ζ of the resulting polyplexes, as has been shown in other studies.[40] The morphology and size of the selected CS-DNA NPs was further characterized by SEM and AFM, and the results are shown in Figure 4.2.

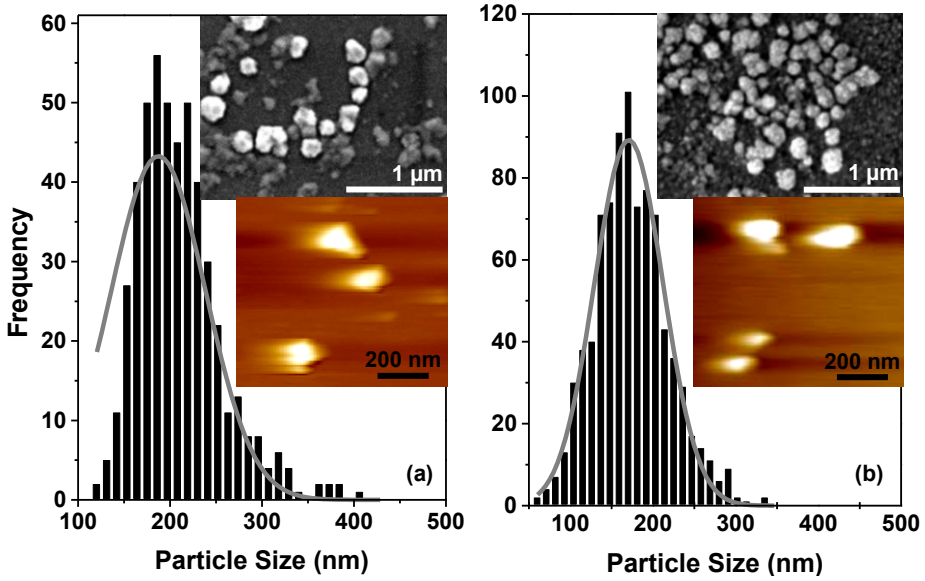

Figure 4.2. Histograms and Gaussian fits to the particle size distributions obtained from the SEM images of the CS-DNA NPs prepared with CS (31 kDa, 80% DDA) and **(a)** Calf Thymus DNA at nominal N/P ratio of 6; or **(b)** gWIz-GFP DNA at nominal N/P ratio of 7. *Insets:* SEM and AFM images of the CS-DNA NPs.

CS-DNA polyplexes exhibited somewhat spherical morphology, as reported in the literature.[37, 39, 60] While spheroids, toroids and rods are the most common morphologies for polyplexes, other less defined shapes, such as rings and flower-like can be also observed.[64] The size of the CS-DNA NPs estimated from the SEM using Image J images was 187 ± 51 nm for NPs containing Calf Thymus DNA at nominal N/P

ratio of 6, and 171 ± 41 nm for NPs containing gWIz-GFP DNA at nominal N/P ratio of 7, showing excellent agreement with the DLS results presented in Table 4.1.

4.3.3 Preparation and characterization of core-shell particles loaded with CS-DNA NPs

In order to efficiently deliver genes to the lungs using propellant-based OI formulations, several hindrances need to be overcome. One of the foremost challenges that need to be addressed is pertaining to the aerodynamic size of the particles. For optimal deep lung deposition, the particle size needs to be between 1 and 5 μm,[65] a range that falls far from the size of the DNA-polymer nanocomplexes being studied here (ca. 200 nm). Secondly, the polyplexes need to be well dispersed in the propellant for optimum aerosol performance.[21, 66] Because steric mechanisms are thought to dominate the stability of colloidal aggregates in the low dielectric HFAs, the relatively high surface charge of the polyplexes is thus expected to be another challenge in the formulation of the colloidal particles.[67] We propose, therefore, to engineer core-shell particles with the polyplexes as the core, and the shell being employed to generate micron-sized particles that are structurally stable in the propellant (shell not soluble in HFA), and yet break down in aqueous solutions (shell soluble in water). The shell is also designed so as to sterically-stabilize the dispersions in HFAs (the shell contains HFA-philic groups that reduce particle-particle interactions). Core-shell particles containing CS-DNA NPs as core (with Calf Thymus or gWIz-GFP DNA), and OLA-*g*-CS co-oligomer as shell, were thus prepared by emulsification-diffusion.

Polyplexes were dispersed in aqueous solution containing the co-oligomer, which was subsequently emulsified into ethyl acetate. The emulsification process was aided by the presence of the co-oligomer, which is active at the water/ethyl acetate interface.[21] The emulsion was diluted into an excess of the organic phase, and the water, which has high solubility in the organic phase, diffused from within the emulsion droplets, thus templating the micron-sized particles containing the polyplexes as core and the OLA-*g*-CS co-oligomer as shell. The oligo(LA) units grafted on the low Mw CS are relevant in the proposed formulation as they are well solvated by HFAs, and are capable of improving dispersion stability in the propellants used in pMDIs.[24, 66, 67]

The DNA loading efficiency (% DNA that was entrapped from the initial amount added in the dispersion) into core-shell particles was measured (n = 5, five independent experiments) using PicoGreen® Assay after chitosanase/lysozyme digestion, and it was found to be very high: 73 ± 8% (gWIz-GFP DNA) and 90 ± 5% (Calf Thymus DNA), both w/w. CS-DNA core-shell particles were characterized by SEM and TEM for size and morphology (Figure 4.3) before loading into pMDI formulations.

The SEM images indicate that the core-shell particles have spherical morphology, as expected, since they were templated by emulsion droplets. In addition, they were fairly polydisperse, with geometric diameters estimated to be 1.1 ± 0.8 μm and 0.8 ± 0.3 μm, for core-shell particles prepared with Calf Thymus and gWIz-GFP DNA, respectively. In good agreement with the SEM results, DLS experiments revealed that the size of the core-shell particles dispersed in HPFP was 0.8 ± 0.2 μm (Calf Thymus DNA) and 1.4 ± 0.1 μm (gWIz-GFP DNA). TEM images (*insets* in Figure 4.3) corroborate the presence of the polyplexes within the OLA-*g*-CS co-oligomer.

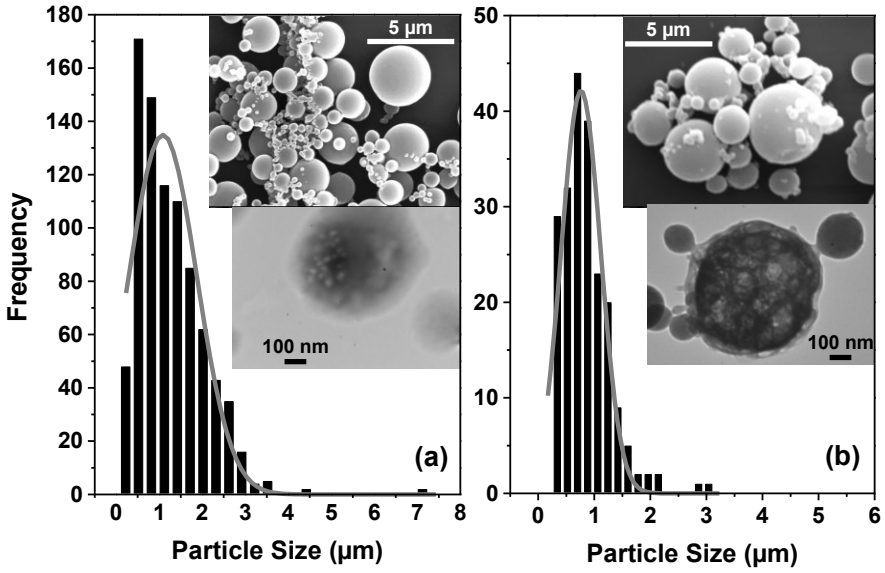

Figure 4.3. Histograms and Gaussian fits to the particle size distributions obtained from the SEM images of the core-shell particles loaded with CS-DNA NPs prepared with CS (31 kDa, 80% DDA) and **(a)** Calf Thymus DNA at nominal N/P ratio of 6; or **(b)** gWIz-GFP DNA at nominal N/P ratio of 7. *Insets:* SEM and TEM images of the CS-DNA core-shell particles.

4.3.4 Physical stability of the CS-DNA core-shell particles in propellant HFA

Core-shell particles containing the CS-DNA NPs had their physical stability qualitatively evaluated in HFA-227 propellant through sedimentation rate experiments at 298 K and saturation pressure of the propellant. CS-DNA core-shell particles were weighed, placed into pressure proof glass vials, and crimp sealed. A known volume of the propellant was then added to make 2 $mg.mL^{-1}$, and the system dispersed with the aid of sonication bath. The stability of the formulations was determined as the creaming/sedimentation rate as a function of the time after stopping the mechanical energy input.[21, 22] During these experiments, digital images were taken, and the results are shown as *insets* in Figure 4.4.

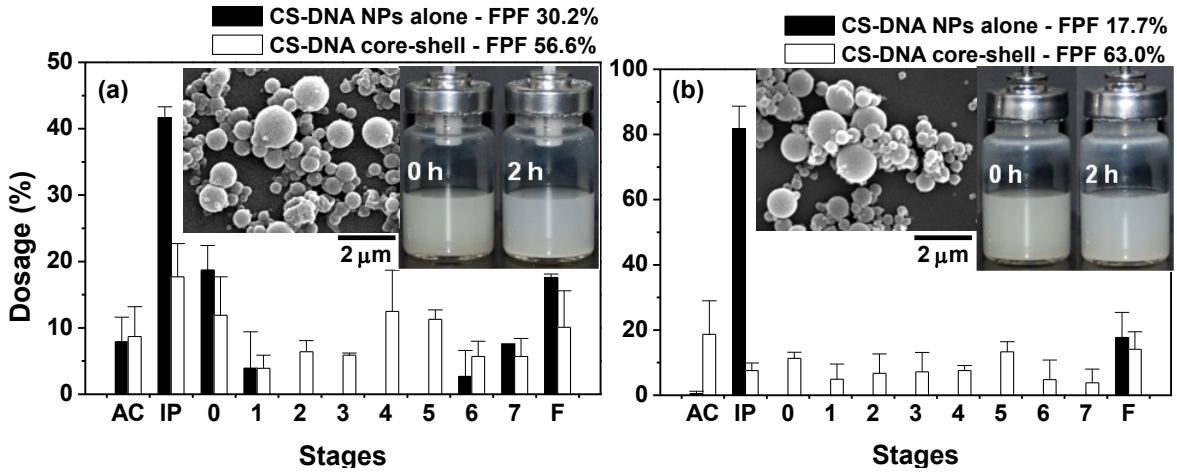

Figure 4.4. Aerodynamic characteristics of the CS-DNA NPs alone and engineered as core-shell particles. Polyplexes prepared with CS (31 kDa, 80% DDA) and **(a)** gWIz-GFP DNA at nominal N/P ratio of 7; or **(b)** Calf Thymus DNA at nominal N/P ratio of 6. pMDI formulations in HFA-227 at 298 K, and saturation pressure of the propellant. CS-DNA core-shell particles at 2 $mg.mL^{-1}$ of propellant, and DNA concentration ca. 4 $\mu g.mL^{-1}$ (Calf Thymus) and ca. 6 $\mu g.mL^{-1}$ (gWIz-GFP) for all formulations. AC, IP and F refer to actuator, induction port and filter, respectively. *Insets:* Core-shell particles loaded with CS-DNA polyplexes – dispersion stability of freshly prepared pMDI formulations (*right*), and SEM of particles actuated from pMDIs after one year of storage (*left*).

The pMDI formulations of CS-DNA core-shell particles (containing gWIz-GFP DNA, *inset* in Figure 4.4a; or Calf Thymus DNA, *inset* in Figure 4.4b) showed excellent physical stability. A small precipitated layer of the core-shell particles could be clearly observed after 2 h. However, such precipitated layers could be easily redispersed by simply shaking the formulation, which indicates that the core-shell particles did not form irreversible aggregates. Easily redispersible aggregates have also been found in pMDI formulations prepared with surfactant-coated pDNA particles in HFA-134a.[13] However, those particles were suspended in the propellant in presence of ethanol, a co-solvent presumably necessary to enhance the solvation of the alkane groups that make the surfactant coat around the pDNA particles.

These results demonstrate that the OLA-*g*-CS co-oligomer shell was able to enhance the physical stability of the CS-DNA NPs in HFA-227. This improved stability

can be attributed to the ability of the HFA to solvate the oligo(LA) side chains of the co-oligomer shell.[24, 66, 67] These results are in sharp contrast to the poor stability of the formulations prepared with CS-DNA NPs alone (using either Calf Thymus or gWIz-GFP DNA). Those formulations were observed not to be completely dispersible (large aggregates formed for NPs containing gWIz-GFP DNA), or settled immediately after sonication stopped (NPs prepared with Calf Thymus DNA). This lack of physical stability is expected as particle-particle attractive interactions dominate over (any potential) electrostatic repulsions in the low dielectric HFAs, as no steric barrier is present when the particles are not coated by the HFA-philic shell.[68, 69] CS-DNA core-shell particles in HFA-227 after one year of storage at 298 K and saturation pressure of the propellant were actuated on the surface of a container, and the particles were re-suspended in HPFP according to procedure described in Section 4.2.5.2, and imaged using SEM. The results are shown as *insets* in Figure 4.4, and reveal that the core-shell particles were stable upon storage and actuation, retaining their overall morphology and size compared to those freshly prepared – those not contacted with the propellant – SEM *insets* in Figure 4.3.

4.3.5 Aerosol characteristics

ACI was used to quantitatively characterize the aerosol properties of the pMDI formulations containing the polyplexes. Such formulations were prepared using CS-DNA NPs alone or polyplexes engineered as core-shell particles (same conditions as discussed in Section 4.3.4) in HFA-227 propellant. During the cascade impaction tests, the particles are deposited on the different stages depending on their aerodynamic size.

The results shown in Table 4.2 thus serve as an *in vitro* metric for lung deposition efficiency. The DNA content deposited on the ACI stages was determined using chitosanase/lysozyme digestion followed by PicoGreen® Assay as described earlier.

Table 4.2. Aerodynamic characteristics of the CS-DNA NPs alone and engineered as core-shell particles. Polyplexes prepared with CS (31 kDa, 80% DDA), and pMDI formulations in HFA-227 at 298 K and saturation pressure of the propellant. CS-DNA core-shell particles at 2 $mg.mL^{-1}$ of propellant. DNA concentration ca. 4 $\mu g.mL^{-1}$ (Calf Thymus) and ca. 6 $\mu g.mL^{-1}$ (gWIz-GFP) for all formulations. Results in µg DNA ± s.d. (s.d. = standard deviation) for n = 3 (three independent runs) and twenty actuations each.

Stages	CS-DNA NPs containing gWIz-GFP DNA at nominal N/P ratio of 7		CS-DNA NPs containing Calf Thymus DNA at nominal N/P ratio of 6	
	Polyplexes alone	Polyplexes loaded in core-shell particles	Polyplexes alone	Polyplexes loaded in core-shell particles
Actuator	0.2 ± 0.0	1.1 ± 0.4	0.0 ± 0.1	1.4 ± 0.9
Induction Port	1.0 ± 0.4	3.0 ± 2.6	5.5 ± 2.9	0.8 ± 0.7
Stage 0 (9.0-10.0 µm)	0.4 ± 0.1	2.3 ± 2.5	0.0 ± 0.0	1.1 ± 0.9
Stage 1 (5.8-9.0 µm)	0.1 ± 0.2	0.6 ± 0.4	0.0 ± 0.0	0.8 ± 0.8
Stage 2 (4.7-5.8 µm)	0.0 ± 0.0	0.9 ± 0.5	0.0 ± 0.0	1.0 ± 1.0
Stage 3 (3.3-4.7 µm)	0.0 ± 0.0	0.9 ± 0.7	0.0 ± 0.0	0.8 ± 1.0
Stage 4 (2.1-3.3 µm)	0.0 ± 0.0	2.7 ± 2.4	0.0 ± 0.0	0.8 ± 0.6
Stage 5 (1.1-2.1 µm)	0.0 ± 0.0	1.8 ± 1.3	0.0 ± 0.0	1.2 ± 0.9
Stage 6 (0.7-1.1 µm)	0.1 ± 0.1	0.7 ± 0.2	0.0 ± 0.0	0.8 ± 1.0
Stage 7 (0.7-0.4 µm)	0.2 ± 0.1	0.7 ± 0.1	0.0 ± 0.0	0.6 ± 0.7
Filter (0.0-0.4 µm)	0.4 ± 0.2	1.2 ± 0.2	1.0 ± 0.0	1.2 ± 0.8
FPF (%)	30.2 ± 2.6	56.6 ± 10.6	17.7 ± 7.6	63.0 ± 6.8
MMAD (µm)	1.3 ± 0.3	2.2 ± 0.8	- *	2.0 ± 0.5
GSD	- *	4.1 ± 0.3	- *	4.7 ± 1.1

* These values could not be calculated due to poor mass distribution on the ACI stages.

The ACI results revealed a FPF of 57% for formulations prepared with CS-DNA core-shell particles using gWIz-GFP DNA, and a FPF of 63% for those with Calf Thymus DNA. As expected, the FPF was lower for formulations prepared with polyplexes alone (no co-oligomer shell): 30% for those with gWIz-GFP DNA, and 18%

for those with Calf Thymus DNA. FPF is a measure of the therapeutically beneficial portion of the inhaled mass of the formulation capable of reaching the lower respiratory tract,[70] and thus indicate that the core-shell formulations are performing significantly better than those without the co-oligomer shell. The somewhat high value of FPF (30%) for formulations prepared with polyplexes containing gWIz-GFP DNA may reflect the fact that the NPs had the opportunity to aggregate in clusters of larger diameters in the propellant, as observed during the physical stability experiments, thus attaining a more appropriate size range, closer to the expected optimum between 1 and 5 μm.[23] The formation of such aggregates is undesirable, however, since it is uncontrollable, may affect the delivery dosage,[71] and possibly their interactions with the lung epithelial cells.[72] The results from Table 4.2, expressed as percentages, are shown in Figure 4.4.

As seen in Figure 4.4, polyplexes alone were found to be entrapped mostly in the IP, stage 0 and filter, showing a very poor mass distribution along the other ACI stages, possibly due to widespread aggregation of the NPs in the propellant, because of the absence of a stabilizing shell. On the other hand, pMDI formulations prepared with polyplexes engineered as core-shell particles showed a much better distribution of the DNA on the ACI stages, and also significantly less DNA entrapment in the IP. In addition, the MMAD of the CS-DNA core-shell particles falls within the values suggested as appropriate for particle size distribution of aerosolized substances – 1 to 5 μm.[23] The % DNA released per actuation was > 90% for CS-DNA polyplexes loaded in core-shell particles (for both types of DNA). On the other hand, CS-DNA polyplexes formulated alone in pMDIs exhibited a % DNA released per actuation of ca. 30% for gWIz-GFP DNA, and ca. 80% for Calf Thymus DNA. However, it is worth to mention here that this

somewhat high value for polyplexes alone (80%) is not related to the respirable stages (0 to filter), and mostly from the DNA entrapped in the IP, which is not part of the respirable fraction – Figure 4.4a.

The results discussed earlier may be compared with those from pMDI formulations containing surfactant-coated pDNA particles prepared in HFA134a containing ethanol as co-solvent, and tested in an eight-stage ACI.[13] Although the aerosol characteristics (FPF and MMAD) were not reported in that study, SEM images of the particulates deposited on the ACI stages revealed particles with variable diameters (< 10 μm with some agglomeration), but with a large fraction deposited on the stages four and five, suggesting that those particles were within the respirable size range.[13]

In summary, the aerosol characteristics of the formulations containing CS-DNA NPs entrapped within the HFA-philic and biodegradable shell are significantly and statistically better (FPF tested with One-Way ANOVA, *p*-values < 0.05) than those observed for the polyplexes alone. These results indicate that the co-oligomer shell helps reduce the forces between the polyplexes, thus improving the colloidal stability of the particles in the propellant, and ultimately the aerosol characteristics. We have observed (and also confirmed by colloidal probe microscopy measurements) such screening effect in other systems stabilized by the LA-based polymers,[24, 66, 67] and that physical stability in the propellant correlates well with the aerosol characteristics, that is, pMDI formulations showing good dispersion stability also show good aerosol characteristics.

4.3.6 *In vitro* transfection

The transfection efficiency of the polyplexes alone and engineered as core-shell particles was qualitatively evaluated *in vitro* by detecting the expression of a green fluorescence protein in A549 cells, a type II alveolar epithelial cell line,[73] using fluorescence microscope. The results were compared with controls, both negative (free pDNA) and positive (TransFast™). The concentration of the reporter pDNA was kept constant for all systems, at 0.25 μg DNA per well. The results are shown in Figure 4.5.

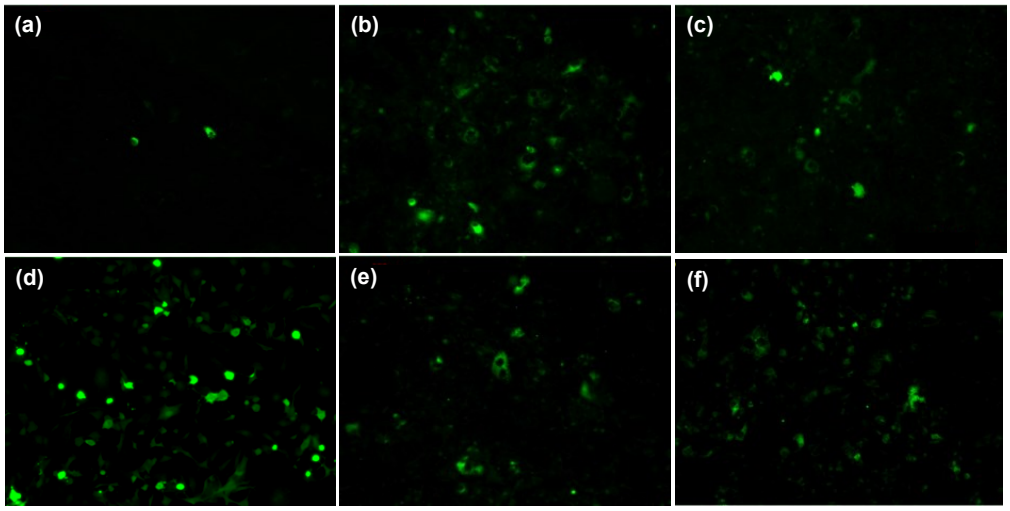

Figure 4.5. Fluorescence microscope images of A549 cells transfected *in vitro* with **(a)** free DNA (negative control); **(b)** CS-DNA NPs; **(c)** Core-shell particles loaded with CS-DNA NPs; **(d)** TransFast™ Transfection Reagent (positive control); **(e)** CS-DNA core-shell particles and **(f)** CS-DNA NPs after 6 weeks of storage in HFA-227 at 298 K and saturation pressure of the propellant. CS-DNA polyplexes prepared with CS (80% DDA, 31 kDa) and gWIz-GFP DNA at nominal N/P ratio of 7. Dosage of 0.25 μg DNA per well. All images at 10x magnification.

CS-DNA NPs alone and those engineered as core-shell particles (Figure 4.5b and 4.5c) showed an intermediate level of *in vitro* transfection efficiency compared to negative and positive controls (Figure 4.5a and 4.5d). The similarity of the results shown in Figure 4.5b and 4.5c indicates that the neither the co-oligomer shell nor the engineering steps for the preparation of the core-shell particles interfere in the

transfection process/biological activity of the pDNA. It is also important to mention that DLS measurements of the CS-DNA core-shell particles in DMEM revealed that the size of the polyplexes does not change significantly (One-Way ANOVA, *p*-values < 0.05) in the presence of the co-oligomer (compared to the size before formation of core-shell particles). It can be concluded, therefore, that the shell is performing its role of providing integrity to the particles while dispersed in the propellant, and at the same time breaking down in aqueous media, subsequently releasing the CS-DNA NPs to initiate the transfection process. This water solubility of the co-oligomer shell is an important property that should help the NPs to rapidly disperse in the deep lung, avoiding potential macrophage uptake.[23] Aqueous solubility should also aid in the removal of the co-oligomer from the lung tissue, thus minimizing any cytotoxic effects.[74] Combined, these results suggest that the selected CS (Mw, DDA), in combination with N/P ratio and other parameters discussed earlier, provide the appropriate characteristics for the polyplexes in the form of core-shell particles to overcome the intracellular barriers and successfully transfect the A549 cells *in vitro*. Surfactant-coated pDNA particles (5 µg pDNA per well) formulated in pMDIs have also been shown to transfect A549 cells *in vitro*.[13] However, 1,2-dioleoyl-3-trimethylammonium-propane (DOTAP, a cationic liposome dispersed in the culture medium) was required to aid in the transfection process,[13] as free pDNA is not expected to show enhanced efficiency.

Another result of great relevance is the fact that CS-DNA NPs (alone and engineered as core-shell particles) were able to successfully transfect A549 cells even after six weeks of storage in HFA-227, as shown in Figure 4.5e and 4.5f, indicating that the propellant does not have any effect on the biological functionality of the pDNA. This

finding is in agreement with a previous report,[13] which demonstrated that the *in vitro* transfection efficiency of surfactant-coated pDNA particles in A549 cells (with the help of DOTAP in the culture medium) is not altered after contacting pDNA particles with HFA-134a propellant.

4.3.7 *In vitro* cytotoxicity

The evaluation of cell viability is a useful method to study the *in vitro* cytotoxicity of biomaterials.[21] We tested the *in vitro* cytotoxicity of the polyplexes and co-oligomer on A549 cells using MTS assay, and the results are shown in Figure 4.6a, 4.6b and 4.6c.

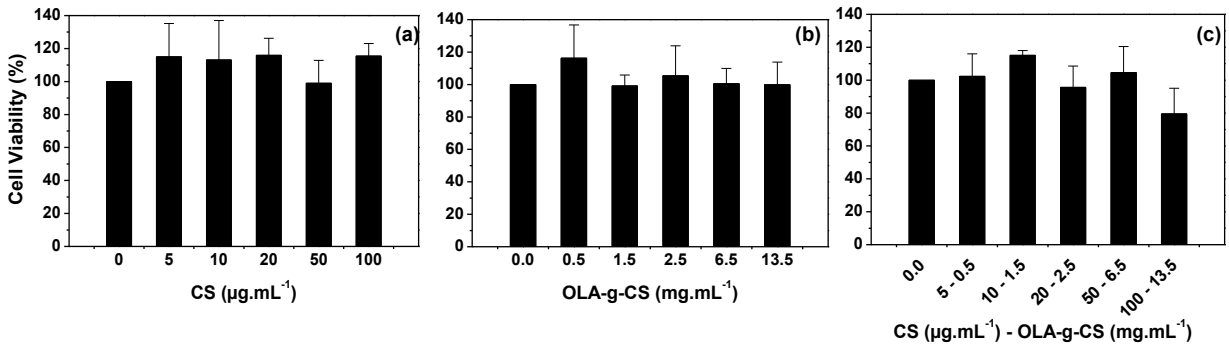

Figure 4.6. Cytotoxicity of **(a)** CS-DNA NPs; **(b)** OLA-*g*-CS co-oligomer; and **(c)** core-shell particles loaded with CS-DNA NPs. Polyplexes prepared with CS (31kDa, 80% DDA) and gWIz-GFP DNA at nominal N/P ratio of 7. All experiments carried out in A549 cell line.

When assayed independently, neither CS-DNA polyplexes nor OLA-*g*-CS co-oligomer reduce the cell viability of A549 cells within the concentration range investigated. Even at high CS concentration (100 μg.mL^{-1}), the cell viability was around 100%. The OLA-*g*-CS co-oligomer was also found to be non-toxic. Cell viability was close to 100% up to extremely high concentration (13.5 mg.mL^{-1}). The results presented here are in agreement with previous studies that also have indicated CS and

CS-based polymers to be fairly non-toxic on lung cells at moderate to high concentrations.[21, 75] This is indeed one of the main advantages in using CS for gene therapy applications. This is indeed one of the main advantages in using CS for gene therapy applications.

The results shown in Figure 4.6c indicate, however, that the viability of the lung alveolar epithelium cells can be impacted when they are exposed to CS-DNA NPs and co-oligomer at the same time, even at concentrations demonstrated to be non-toxic when each one is tested independently. However, toxicity is only observed at extremely high concentrations of co-oligomer (6.5 and 13.5 $mg.mL^{-1}$), which correspond to 361 and 750 actuations from a 2 $mg.mL^{-1}$ pMDI formulation, respectively, considering the ACI results shown earlier and that the particles emitted from a single actuation would be diluted in the lung alveolar fluid estimated to be 7 mL.[76, 77] There results fare very well compared to the pMDI formulations containing surfactant-coated pDNA, where the viability of A549 cells was reduced to 60-70% upon contacting with equivalent dosage from 80 actuations.[13] However, since those formulations were aerosolized directly on the cells, the cold-freon effect might have contributed to reduction in cell viability, as well as the presence of DOTAP in the cell culture medium.[13]

4.3.8 Stability of CS-DNA polyplexes and integrity of gWlz GFP pDNA

The protective efficacy of the pDNA against DNase I, upon complexation with the positively charged polymer (CS) was evaluated by gel electrophoresis. CS-DNA polyplexes were incubated with different concentrations of DNase I, followed by release of the pDNA after digestion of CS by chitosanase/lysozyme. The results are shown in Figure 4.7a. The integrity of the pDNA after complexation with CS, core-shell particle

formation, and storage in HFA-227 propellant, was also analyzed by gel electrophoresis. Particles in suspension were incubated with chitosanase/lysozyme for CS digestion, thus releasing the pDNA, whose structure was compared to free pDNA (control) as received. The results are shown in Figure 4.7b.

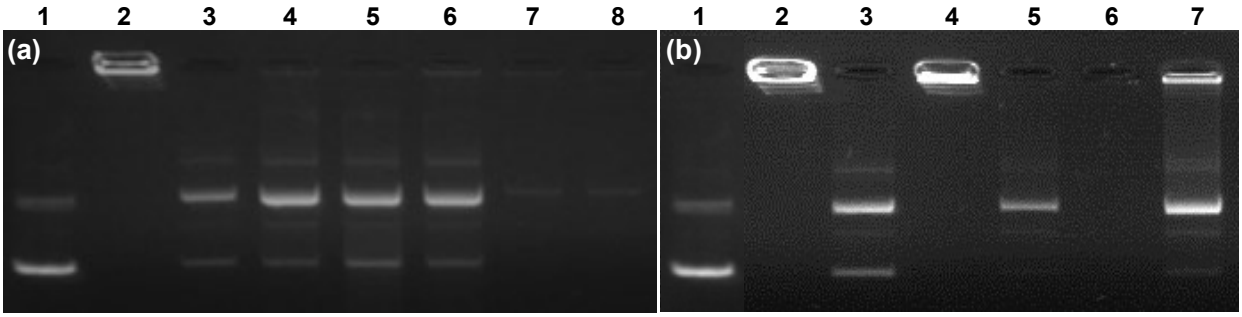

Figure 4.7. **(a)** Gel electrophoresis for evaluation of the stability of complexed gWIz-GFP pDNA after exposure of the CS-DNA NPs to DNase I: free pDNA (control, *lane 1*); CS-DNA NPs freshly prepared before (*lane 2*) and after (*lane 3*) incubation with chitosanase/lysozyme; CS-DNA NPs + DNase I (1 μU *lane 4*, 50 μU *lane 5*, 0.5 U *lane 6*, 1 U *lane 7*, and 2 U *lane 8*) + chitosanase/lysozyme. U means units DNase I per 1μg pDNA. **(b)** Gel electrophoresis for monitoring the integrity of gWIz-GFP pDNA after particle preparation and exposure to propellant HFA: free pDNA (control, *lane 1*); CS-DNA polyplexes freshly prepared before (*lane 2*) and after (*lane 3*) incubation with chitosanase/lysozyme; CS-DNA core-shell particles freshly prepared before (*lane 4*) and after (*lane 5*) incubation with chitosanase/lysozyme; CS-DNA core-shell particles stored in HFA-227 at 298K and saturation pressure of the propellant for 12 days before (*lane 6*) and after (*lane 7*) incubation with chitosanase/lysozyme. All CS-DNA polyplexes at N/P ratio of 7 – same as those used in all other studies.

CS (31 kDa, 80% DDA) was able to successfully protect the gWIz-GFP pDNA against DNase I degradation up to 0.5 U enzyme per 1 μg plasmid (Figure 4.7a). The pDNA recovered from the polyplexes after treatment with DNase I (*lanes 4*, *5* and *6*) showed essentially the same conformation to that not incubated with the endonuclease model (*lane 3*). These results are comparable with those in the literature, which have shown that low Mw CS (22 kDa and 75% DDA)[78] is able to provide protection to DNA against DNase I digestion at 0.5 U per 1 μg DNA. However, upon increasing the concentration of DNase I, the pDNA in the polyplexes was degraded, and only a small

portion of the open circular conformation (upper band, *lanes 7* and *8*) was recovered after CS digestion by chitosanase/lysozyme. This is expected based on the relatively low Mw of CS. It has been shown that even for polyplexes formed with high Mw CS (400 kDa, 85% DDA), protection can only be achieved to concentrations up to around 1 U DNase I per 1 μg DNA.[79] Therefore, considering a range which DNase I assay is usually performed (up to 0.5 U per 1 μg DNA) for polyplexes formed using low Mw CS (20-80 kDa)[78, 80] the polyplexes studied here were able to provide an efficient protection for the GFP pDNA against nuclease degradation, and conform similarly to those reported in the literature.

As seen in Figure 4.7b, polyplexes prepared with CS (31 kDa, 80% DDA, at N/P ratio of 7) effectively retarded the pDNA mobility (*lane 2*). This result is in agreement with the literature, where the ability of CS to condense genetic material has been demonstrated.[33] It can be also observed that the engineering of such polyplexes as core-shell particles did not affect the ability of CS to complex DNA (*lane 4*), and that storage of the polyplexes in propellant HFA (*lane 6*) did not impact the interaction between CS and DNA either. The overall integrity of the active pDNA (combination of the supercoiled – lower band; and open circular – upper band) was largely retained during the studies, as can be concluded by comparing the bands from *lanes 3*, *5* and *7*, with that from free pDNA (*lane 1*). Reduction in the supercoiled form of the pDNA, upon complexation with CS, is mostly associated with the formation of the also active open circular form of the pDNA – see *lane 3*, and to a much lower extent with the increase in the non-active linear form (intermediate band). No significant differences are to be expected in gene expression levels between supercoiled and open circular

conformations, while the linear pDNA is expected to be nearly 90% less efficient than supercoiled form.[19] Such results are expected to be observed upon complexation of pDNA with CS.[53] Further reduction in the supercoiled form into the open circular is observed upon formation of the core-shell structures (*lane 5*). This is also to be expected upon further processing of the polyplexes. Similar observations have been reported during the preparation of CS-DNA particles for DPIs under supercritical CO_2 processing.[19] However, no further increase in the linear form is seen. Most interesting, however, is to note that there are no further changes in the pDNA upon exposure of the core-shell structures containing the polyplexes to propellant HFA, in agreement with the *in vitro* transfection studies, and further suggesting the potential of the proposed platform for the delivery of polyplexes to the lungs.

4.4 Conclusions

In this work we demonstrated that DNA can be successfully formulated in pMDIs. Chitosan (CS)-DNA nanoparticles (NPs) were prepared by complex coacervation, using low Mw CS (31 kDa, 80% DDA). The polyplexes showed high DNA encapsulation efficiency – greater than 90% (w/w), and appropriate size – average diameter less than 200 nm. Using emulsification-diffusion, the polyplexes were successfully encapsulated with high DNA loading efficiency within water soluble, biodegradable and HFA-philic co-oligomer shell – up to 90% (w/w). The chosen particle engineering strategy also allowed us to control the size range of the core-shell particles, which had an average diameter of 1 μm, a key requirement for the generation of aerosols with enhanced deep lung deposition. pMDI formulations of the core-shell particles prepared as dispersions

in HFA-227 propellant showed improved physical stability and excellent aerosol performance (MMAD = 2 μm, and FPF of up to 63%), as measured by ACI. *In vitro* studies revealed that the CS-DNA NPs engineered as core-shell particles were able to transfect A549 cells, even after several weeks of storage in the HFA-227, suggesting that the propellant does not have any effect on the biological functionality of the pDNA. *In vitro* cytotoxicity experiments showed that CS-DNA core-shell particles had no significant cytotoxic effect on A549 cells, even at very high concentrations. All these results, when put in perspective, suggest that formulating polyplexes in core-shell particles is an efficient approach to deliver genes to the lungs using inexpensive and portable pMDIs to treat medically relevant pulmonary diseases, including asthma, COPD and cancer.

4.5 Acknowledgements

Thank you for financial support from the Lung Cancer Research Foundation, and NSF-CBET # 0933144. Thank you for Solvay for the propellant HFA, 3M for the metering valves, Dr. Hüttemann's group (Center for Molecular Medicine and Genetics, School of Medicine at WSU) for access to the Fluorescence Microscope, Dr. Mathew's and Kannan's group (Department of Chemical Engineering and Materials Science at WSU) for access to the Fluorescence/Spectrometer and DLS, respectively, Dr. Verani's group (Department of Chemistry at WSU) for access to the FTIR, Dr. Pile's group (Department of Biological Sciences at WSU) for access to the UV Transilluminator System, and Fernando L. Cassio (Chemistry Institute, University of São Paulo, Brazil) for discussions regarding the synthesis and characterization of the co-oligomer.

This chapter is based on the published manuscript: **Conti, D. S.**; Bharatwaj, B.; Brewer, D.; da Rocha, S. R. P. Propellant-based inhalers for the non-invasive delivery of genes via oral inhalation. *Journal of Controlled Release* **2012**, 157, (3), 406-417.

4.6 References

1. Roy, I.; Vij, N. Nanodelivery in airway diseases: Challenges and therapeutic applications. *Nanomedicine* **2010,** *6*, (2), 237-244.
2. Tang, B. C.; Dawson, M.; Lai, S. K.; Wang, Y.-Y.; Suk, J. S.; Yang, M.; Zeitlin, P.; Boyle, M. P.; Fu, J.; Hanes, J. Biodegradable polymer nanoparticles that rapidly penetrate the human mucus barrier. *Proc. Natl. Acad. Sci. U.S.A.* **2009,** *106*, (46), 19268-19273.
3. Harada-Shiba, M.; Takamisawa, I.; Miyata, K.; Ishii, T.; Nishiyama, N.; Itaka, K.; Kangawa, K.; Yoshihara, F.; Asada, Y.; Hatakeyama, K.; Nagaya, N.; Kataoka, K. Intratracheal gene transfer of adrenomedullin using polyplex nanomicelles attenuates monocrotaline-induced pulmonary hypertension in rats. *Mol. Ther.* **2009,** *17*, (7), 1180-1186.
4. Kolb, M.; Martin, G.; Medina, M.; Ask, K.; Gauldie, J. Gene therapy for pulmonary diseases. *Chest* **2006,** *130*, (3), 879-884.
5. Li, H. Y.; Seville, P. C.; Williamson, I. J.; Birchall, J. C. The use of amino acids to enhance the aerosolisation of spray-dried powders for pulmonary gene therapy. *J. Gene Med.* **2005,** *7*, (3), 343-353.
6. Kushwah, R.; Hu, J., Viral and non-viral vector mediated lung gene therapy. In *Recent Dev. Gene Ther.*, Xiang, J., Ed. Transworld Research Network: Kerala, India, 2007; pp 53-75.
7. Sanders, N.; Rudolph, C.; Braeckmans, K.; De Smedt, S. C.; Demeester, J. Extracellular barriers in respiratory gene therapy. *Adv. Drug Delivery Rev.* **2009,** *61*, (2), 115-127.
8. Gill, D. R.; Davies, L. A.; Pringle, I. A.; Hyde, S. C. The development of gene therapy for diseases of the lung. *CMLS, Cell. Mol. Life Sci.* **2004,** *61*, (3), 355-368.
9. Grigsby, C. L.; Leong, K. W. Balancing protection and release of DNA: Tools to address a bottleneck of non-viral gene delivery. *J. R. Soc. Interface* **2010,** *7*, (Suppl 1), S67-S82.

10. Tiera, M. J.; Winnik, F. M.; Fernandes, J. C. Synthetic and natural polycations for gene therapy: State of the art and new perspectives. *Curr. Gene Ther.* **2006,** *6*, 59-71.

11. Eliyahu, H.; Barenholz, Y.; Domb, A. J. Polymers for DNA delivery. *Molecules* **2005,** *10*, 34-64.

12. Ferrari, S.; Geddes, D. M.; Alton, E. W. F. W. Barriers to and new approaches for gene therapy and gene delivery in cystic fibrosis. *Adv. Drug Delivery Rev.* **2002,** *54*, (11), 1373-1393.

13. Bains, B. K.; Birchall, J. C.; Toon, R.; Taylor, G. *In vitro* reporter gene transfection via plasmid DNA delivered by metered dose inhaler. *J. Pharm. Sci.* **2010,** *99*, (7), 3089-3099.

14. Laube, B. L. The expanding role of aerosols in systemic drug delivery, gene therapy, and vaccination. *Respir. Care* **2005,** *50*, (9), 1161-1176.

15. Birchall, J. Pulmonary delivery of nucleic acids. *Expert Opin. Drug Delivery* **2007,** *4*, (6), 575-578.

16. Arulmuthu, E. R.; Williams, D. J.; Baldascini, H.; Versteeg, H. K.; Hoare, M. Studies on aerosol delivery of plasmid DNA using a mesh nebulizer. *Biotechnol. Bioeng.* **2007,** *98*, (5), 939-955.

17. Seville, P. C.; Kellaway, I. W.; Birchall, J. C. Preparation of dry powder dispersions for non-viral gene delivery by freeze-drying and spray-drying. *J. Gene Med.* **2002,** *4*, (4), 428-437.

18. Mizuno, T.; Mohri, K.; Nasu, S.; Danjo, K.; Okamoto, H. Dual imaging of pulmonary delivery and gene expression of dry powder inhalant by fluorescence and bioluminescence. *J. Control. Release* **2009,** *134*, (2), 149-154.

19. Okamoto, H.; Sakakura, Y.; Shiraki, K.; Oka, K.; Nishida, S.; Todo, H.; Iida, K.; Danjo, K. Stability of chitosan-pDNA complex powder prepared by supercritical carbon dioxide process. *Int. J. Pharm.* **2005,** *290*, (1-2), 73-81.

20. Ashurst, I.; Malton, A.; Prime, D.; Sumby, B. Latest advances in the development of dry powder inhalers. *Pharm. Sci. Technol. Today* **2000,** *3*, (7), 246-256.

21. Wu, L.; Bharatwaj, B.; Panyam, J.; da Rocha, S. Core-shell particles for the dispersion of small polar drugs and biomolecules in hydrofluoroalkane propellants. *Pharm. Res.* **2008,** *25*, (2), 289-301.

22. Bharatwaj, B.; Wu, L.; Whittum-Hudson, J. A.; Rocha, S. R. P. d. The potential for the noninvasive delivery of polymeric nanocarriers using propellant-based inhalers in the treatment of Chlamydial respiratory infections. *Biomaterials* **2010,** *31*, 7376-7385.

23. Patton, J. S.; Byron, P. R. Inhaling medicines: Delivering drugs to the body through the lungs. *Nat. Rev. Drug Discovery* **2007,** *6*, (1), 67-74.

24. Wu, L.; Peguin, R. P. S.; da Rocha, S. R. P. Understanding solvation in hydrofluoroalkanes: *Ab Initio* calculations and chemical force microscopy. *J. Phys. Chem. B* **2007,** *111*, (28), 8096-8104.

25. Mohri, K.; Okuda, T.; Mori, A.; Danjo, K.; Okamoto, H. Optimized pulmonary gene transfection in mice by spray-freeze dried powder inhalation. *J. Control. Release* **2010,** *144*, (2), 221-226.

26. Li, H.-Y.; Birchall, J. Chitosan-modified dry powder formulations for pulmonary gene delivery. *Pharm. Res.* **2006,** *23*, (5), 941-950.

27. Dailey, L. A.; Kleemann, E.; Merdan, T.; Petersen, H.; Schmehl, T.; Gessler, T.; Hänze, J.; Seeger, W.; Kissel, T. Modified polyethylenimines as non viral gene delivery systems for aerosol therapy: Effects of nebulization on cellular uptake and transfection efficiency. *J. Control. Release* **2004,** *100*, (3), 425-436.

28. Rudolph, C.; Müller, R. H.; Rosenecker, J. Jet nebulization of PEI/DNA polyplexes: physical stability and *in vitro* gene delivery efficiency. *J. Gene Med.* **2002,** *4*, (1), 66-74.

29. Tian, F.; Liu, Y.; Hu, K.; Zhao, B. Study of the depolymerization behavior of chitosan by hydrogen peroxide. *Carbohydr. Polym.* **2004,** *57*, (1), 31-37.

30. Kasaai, M. R. Calculation of Mark-Houwink-Sakurada (MHS) equation viscometric constants for chitosan in any solvent-temperature system using experimental reported viscometric constants data. *Carbohydr. Polym.* **2007,** *68*, (3), 477-488.

31. Mao, S.; Shuai, X.; Unger, F.; Simon, M.; Bi, D.; Kissel, T. The depolymerization of chitosan: Effects on physicochemical and biological properties. *Int. J. Pharm.* **2004,** *281*, (1-2), 45-54.

32. Morris, G. A.; Castile, J.; Smith, A.; Adams, G. G.; Harding, S. E. Macromolecular conformation of chitosan in dilute solution: A new global hydrodynamic approach. *Carbohydr. Polym.* **2009,** *76*, (4), 616-621.

33. Yang, X.; Yuan, X.; Cai, D.; Wang, S.; Zong, L. Low molecular weight chitosan in DNA vaccine delivery via mucosa. *Int. J. Pharm.* **2009,** *375*, (1-2), 123-132.

34. Kim, T.-H.; Jiang, H.-L.; Jere, D.; Park, I.-K.; Cho, M.-H.; Nah, J.-W.; Choi, Y.-J.; Akaike, T.; Cho, C.-S. Chemical modification of chitosan as a gene carrier *in vitro* and *in vivo*. *Prog. Polym. Sci.* **2007,** *32*, (7), 726-753.

35. Weil, H.; Guang-hua, C.; Yu-li, W.; Jun-feng, H.; Xu, Z.; Zhong-gao, G. Determination of pDNA encapsulating and loading efficiency of pDNA loaded chitosan nanoparticles PicoGreen-fluorometry and ninhydrin-colorimetry. *Chin. J. Pharm. Anal.* **2010**, (2).

36. Prochazkova, S.; Vårum, K. M.; Ostgaard, K. Quantitative determination of chitosans by ninhydrin. *Carbohydr. Polym.* **1999,** *38*, (2), 115-122.

37. Jean, M.; Smaoui, F.; Lavertu, M.; Methot, S.; Bouhdoud, L.; Buschmann, M. D.; Merzouki, A. Chitosan-plasmid nanoparticle formulations for IM and SC delivery of recombinant FGF-2 and PDGF-BB or generation of antibodies. *Gene Ther.* **2009,** *16*, (9), 1097-1110.

38. Mishra, S.; Heidel, J. D.; Webster, P.; Davis, M. E. Imidazole groups on a linear, cyclodextrin-containing polycation produce enhanced gene delivery via multiple processes. *J. Control. Release* **2006,** *116*, (2), 179-191.

39. Corsi, K.; Chellat, F.; Yahia, L.; Fernandes, J. C. Mesenchymal stem cells, MG63 and HEK293 transfection using chitosan-DNA nanoparticles. *Biomaterials* **2003,** *24*, (7), 1255-1264.

40. Mao, H.-Q.; Roy, K.; Troung-Le, V. L.; Janes, K. A.; Lin, K. Y.; Wang, Y.; August, J. T.; Leong, K. W. Chitosan-DNA nanoparticles as gene carriers: Synthesis, characterization and transfection efficiency. *J. Control. Release* **2001,** *70*, (3), 399-421.

41. Rogueda, P. G. A. HPFP, a model propellant for pMDIs. *Drug Dev. Ind. Pharm.* **2003,** *29*, (1), 39-49.

42. Akapo, S.; Gupta, J.; Martinez, E.; McCrea, C.; Ye, L.; Roach, M. Compatibility and aerosol characteristics of formoterol fumarate mixed with other nebulizing solutions. *Ann. Pharmacother.* **2008,** *42*, (10), 1416-1424.

43. Organisation for Economic Co-operation and Development, Guidance document on acute inhalation toxicity testing. In *Series on Testing and Assessment*, OECD Environment, Health and Safety Publications: Paris, 2009; pp 1-71.

44. Foster, K. A.; Oster, C. G.; Mayer, M. M.; Avery, M. L.; Audus, K. L. Characterization of the A549 cell line as a type II pulmonary epithelial cell model for drug metabolism. *Exp. Cell Res.* **1998,** *243*, (2), 359-366.

45. Promega Corporation, TransFast™ Transfection Reagent. 2009; 'Vol.' Part# TB260, pp 1-17.

46. Sato, T.; Ishii, T.; Okahata, Y. *In vitro* gene delivery mediated by chitosan. Effect of pH, serum, and molecular mass of chitosan on the transfection efficiency. *Biomaterials* **2001,** *22*, (15), 2075-2080.

47. Zhao, Q.-Q.; Chen, J.-L.; Lv, T.-F.; He, C.-X.; Tang, G.-P.; Liang, W.-Q.; Tabata, Y.; Gao, J.-Q. N/P ratio significantly influences the transfection efficiency and cytotoxicity of a polyethylenimine/chitosan/DNA complex. *Biol. Pharm. Bull.* **2009,** *32*, (4), 706-710.

48. Lu, B.; Wang, C.-F.; Wu, D.-Q.; Li, C.; Zhang, X.-Z.; Zhuo, R.-X. Chitosan based oligoamine polymers: Synthesis, characterization, and gene delivery. *J. Control. Release* **2009,** *137*, (1), 54-62.

49. Jiang, H.-L.; Kim, Y.-K.; Arote, R.; Nah, J.-W.; Cho, M.-H.; Choi, Y.-J.; Akaike, T.; Cho, C.-S. Chitosan-graft-polyethylenimine as a gene carrier. *J. Control. Release* **2007,** *117*, (2), 273-280.

50. Li, G.; Liu, Z.; Liao, B.; Zhong, N. Induction of Th1-type immune response by chitosan nanoparticles containing plasmid DNA encoding house dust mite allergen der p 2 for oral vaccination in mice. *Cell. Mol. Immunol.* **2009,** *6*, (1), 45-50.

51. Douglas, K. L.; Piccirillo, C. A.; Tabrizian, M. Effects of alginate inclusion on the vector properties of chitosan-based nanoparticles. *J. Control. Release* **2006,** *115*, (3), 354-361.

52. Raviña, M.; Cubillo, E.; Olmeda, D.; Novoa-Carballal, R.; Fernandez-Megia, E.; Riguera, R.; Sánchez, A.; Cano, A.; Alonso, M. Hyaluronic acid/chitosan-g-poly(ethylene glycol) nanoparticles for gene therapy: An application for pDNA and siRNA delivery. *Pharm. Res.* **2010,** *27*, (12), 2544-2555.

53. Strand, S. P.; Lelu, S.; Reitan, N. K.; de Lange Davies, C.; Artursson, P.; Vårum, K. M. Molecular design of chitosan gene delivery systems with an optimized balance between polyplex stability and polyplex unpacking. *Biomaterials* **2010,** *31*, (5), 975-987.

54. Qin, C. Q.; Du, Y. M.; Xiao, L. Effect of hydrogen peroxide treatment on the molecular weight and structure of chitosan. *Polym. Degrad. Stab.* **2002,** *76*, 211-218.

55. Zhao, X.; Yin, L.; Ding, J.; Tang, C.; Gu, S.; Yin, C.; Mao, Y. Thiolated trimethyl chitosan nanocomplexes as gene carriers with high *in vitro* and *in vivo* transfection efficiency. *J. Control. Release* **2010,** *144*, (1), 46-54.

56. Fink, T. L.; Klepcyk, P. J.; Oette, S. M.; Gedeon, C. R.; Hyatt, S. L.; Kowalczyk, T. H.; Moen, R. C.; Cooper, M. J. Plasmid size up to 20 kbp does not limit effective *in vivo* lung gene transfer using compacted DNA nanoparticles. *Gene Ther.* **2006,** *13*, (13), 1048-1051.

57. Groll, A. v.; Levin, Y.; Barbosa, M. C.; Ravazzolo, A. P. Linear DNA low efficiency transfection by liposome can be improved by the use of cationic lipid as charge neutralizer. *Biotechnol. Prog.* **2006,** *22*, (4), 1220-1224.

58. Huang, M.; Fong, C.-W.; Khor, E.; Lim, L.-Y. Transfection efficiency of chitosan vectors: Effect of polymer molecular weight and degree of deacetylation. *J. Controlled Release* **2005,** *106*, (3), 391-406.

59. Liu, W.; Sun, S.; Cao, Z.; Zhang, X.; Yao, K.; Lu, W. W.; Luk, K. D. K. An investigation on the physicochemical properties of chitosan/DNA polyelectrolyte complexes. *Biomaterials* **2005,** *26*, (15), 2705-2711.

60. Sajomsang, W.; Ruktanonchai, U.; Gonil, P.; Mayen, V.; Opanasopit, P. Methylated N-aryl chitosan derivative/DNA complex nanoparticles for gene delivery: Synthesis and structure-activity relationships. *Carbohydr. Polym.* **2009,** *78*, (4), 743-752.

61. De Smedt, S. C.; Demeester, J.; Hennink, W. E. Cationic polymer based gene delivery systems. *Pharm. Res.* **2000,** *17*, (2), 113-126.

62. Lavertu, M.; Méthot, S.; Tran-Khanh, N.; Buschmann, M. D. High efficiency gene transfer using chitosan/DNA nanoparticles with specific combinations of molecular weight and degree of deacetylation. *Biomaterials* **2006,** *27*, (27), 4815-4824.

63. Ishii, T.; Okahata, Y.; Sato, T. Mechanism of cell transfection with plasmid/chitosan complexes. *Biochim. Biophys. Acta* **2001,** *1514*, (1), 51-64.

64. Wan, L.; You, Y.; Zou, Y.; Oupický, D.; Mao, G. DNA release dynamics from bioreducible poly(amido amine) polyplexes. *J. Phys. Chem. B* **2009,** *113*, (42), 13735-13741.

65. Byron, P. R. Prediction of drug residence times in regions of the human respiratory tract following aerosol inhalation. *J. Pharm. Sci.* **1986,** *75*, (5), 433-438.

66. Peguin, R. P. S.; Wu, L.; da Rocha, S. R. P. The ester group: How hydrofluoroalkane-philic is it? *Langmuir* **2007,** *23*, (16), 8291-8294.

67. Peguin, R. P. S.; da Rocha, S. R. P. Solvent-solute interactions in hydrofluoroalkane propellants. *J. Phys. Chem. B* **2008,** *112*, (27), 8084-8094.

68. Williams III, R. O.; Barron, M. K.; José Alonso, M.; Remuñán-López, C. Investigation of a pMDI system containing chitosan microspheres and P134a. *Int. J. Pharm.* **1998,** *174*, (1-2), 209-222.

69. Jones, S. A.; Martin, G. P.; Brown, M. B. Manipulation of beclomethasone-hydrofluoroalkane interactions using biocompatible macromolecules. *J. Pharm. Sci.* **2006,** *95*, (5), 1060-1074.

70. Mitchell, J. P.; Nagel, M. W.; Wiersema, K. J.; Doyle, C. C. Aerodynamic particle size analysis of aerosols from pressurized metered-dose inhalers: Comparison of Andersen 8-stage cascade impactor, next generation pharmaceutical impactor, and model 3321 aerodynamic particle sizer aerosol spectrometer. *AAPS PharmSciTech* **2003,** *4*, (4), 1-9.

71. Grenha, A.; Seijo, B.; Remuñán-López, C. Microencapsulated chitosan nanoparticles for lung protein delivery. *Eur. J. Pharm. Sci.* **2005,** *25*, (4-5), 427-437.

72. Singh, S.; Shi, T.; Duffin, R.; Albrecht, C.; van Berlo, D.; Höhr, D.; Fubini, B.; Martra, G.; Fenoglio, I.; Borm, P. J. A.; Schins, R. P. F. Endocytosis, oxidative stress and IL-8 expression in human lung epithelial cells upon treatment with fine and ultrafine TiO2: Role of the specific surface area and of surface methylation of the particles. *Toxicol. Appl. Pharmacol.* **2007,** *222*, (2), 141-151.

73. Bur, M.; Lehr, C.-M. Pulmonary cell culture models to study the safety and efficacy of innovative aerosol medicines. *Expert Opin. Drug Delivery* **2008,** *5*, (6), 641-652.

74. Johnston, H. J.; Hutchison, G.; Christensen, F. M.; Peters, S.; Hankin, S.; Stone, V. A review of the *in vivo* and *in vitro* toxicity of silver and gold particulates: Particle attributes and biological mechanisms responsible for the observed toxicity. *Crit. Rev. Toxicol.* **2010,** *40*, (4), 328-346.

75. Kean, T.; Thanou, M. Biodegradation, biodistribution and toxicity of chitosan. *Adv. Drug Delivery Rev.* **2010,** *62*, (1), 3-11.

76. Weibel, E. R., *Morphometry of the Human Lung*. Academic Press: 1963.

77. Stone, K. C.; Mercer, R. R.; Gehr, P.; Stockstill, B.; Crapo, J. D. Allometric relationships of cell numbers and size in the mammalian lung. *Am. J. Resp. Cell Mol.* **1992,** *6*, (2), 235-43.

78. Lee, M.; Nah, J.-W.; Kwon, Y.; Koh, J. J.; Ko, K. S.; Kim, S. W. Water-soluble and low molecular weight chitosan-based plasmid DNA delivery. *Pharm. Res.* **2001,** *18*, (4), 427-431.

79. Centelles, M. N.; Isasi, J. R.; Qian, C.; Campanero, M. A.; Irache, J. M. Influence of the chitosan nature on the transfection efficacy of DNA-loaded nanoparticles after hydrodynamic administration in mice. *J. Microencapsul.* **2010,** *27*, (5), 460-469.

80. Bivas-Benita, M.; Laloup, M.; Versteyhe, S.; Dewit, J.; Braekeleer, J. D.; Jongert, E.; Borchard, G. Generation of toxoplasma gondii GRA1 protein and DNA vaccine loaded chitosan particles: Preparation, characterization, and preliminary *in vivo* studies. *Int. J. Pharm.* **2003,** *266*, (1-2), 17-27.

CHAPTER 5

Dendrimer Nanocarriers and their Aerosol Formulations for siRNA Delivery to the Lung Epithelium

5.1 Introduction

RNA interference (RNAi) promotes silencing of gene expression in a post-transcriptional manner,[1] and its mechanism has been extensively discussed in literature.[2, 3] The delivery of double-stranded small interfering RNA (ds-siRNA, typically consisting of 20 - 27 bp)[4] which target the RNA-induced silencing complex (RISC) located into the cell cytoplasm is a very promising approach with great therapeutic potential to treat many diseases.[1, 5] RNAi-based therapies have been studied as potential for treatment of several medically relevant pulmonary diseases, such as lung cancer,[6, 7] cystic fibrosis,[8, 9] asthma,[10, 11] chronic obstructive pulmonary disease (COPD),[10] respiratory syncytial virus (RSV),[12] and severe acute respiratory syndrome (SARS) viral infection.[13] However, the progress of siRNA delivery targeting locally the lung epithelium has been hampered largely by the lack of adequate nanocarriers capable to overcome the lung's structure, extra and intracellular barriers present in the lung tissue, and formulation challenges related to the route of administration.[1, 14, 15] Therefore, the development of efficient nanocarries to deliver siRNA to the lungs and appropriate formulation strategies is very relevant.

Poly(amidoamine) (PAMAM) dendrimers are dendritic polymers widely studied for biomedical applications.[16] PAMAM dendrimers are highly branched polymers with low polydispersity, high functionality, and provide an ideal structure for construction of

effective drug carriers and gene transfer vehicles.[16, 17] PAMAM dendrimers possess cationic primary amine groups (NH_2) at their surface, which participate in the nucleic acid binding process forming nanoscale dendriplexes. However, these promising vehicles have been less explored for the siRNA delivery to the lungs.[18] Few reports in literature have investigated the *in vitro* knockdown efficiency of siRNA-[4, 19] or antisense oligonucleotide- (AON)[20] delivered to lung cells via dendriplexes, and up-to-date, there is no literature about the use of generation-four amine-terminated (G4NH2) PAMAM to deliver siRNA to lung cells. Nonetheless, besides an adequate nanocarrier for siRNA, its route of administration to the lungs must be equally efficient.

Oral inhalation (OI) is a very promising administration route for siRNA to the pulmonary epithelium, since it provides a direct and non-invasive mean of targeting different regions of the lungs.[21] Pressurized metered dose inhalers (pMDIs) are the most widely used OI devices due to their portability, small size, long shelf life, reliability, ability of use even in patients with diseased lungs (propellant based and not respiratory driven) and low cost.[22] However, to the best of our knowledge, no work has been reported on siRNA delivery to the lungs via pMDIs to date, and most of the *in vivo* studies use either intratracheal or intranasal routes.[1, 14, 23] The most challenger barriers in formulating inhalable siRNAs in pMDIs are pertaining to *(i)* the aerodynamic size of the particles – for optimal deep lung deposition, the particle size needs to be between 0.5 and 5 μm,[57, 145, 146] and thus, nanocarriers > 500 nm trend to be exhaled due to their low inertia;[24] and *(ii)* the quality of the dispersion – the particles must be very well dispersed in the propellant to provide good aerosol performance,[25, 26] i.e., they need to

have an appropriate chemistry to be well-solvated by the propellant to prevent aggregation.[26-28]

In this work we propose a portable propellant-based formulation for the OI delivery of siRNA, which addresses most of the challenges discussed above. We report the preparation and characterization of siRNA-G4NH2 dendriplexes, and evaluate their *in vitro* gene knockdown efficiency in a model lung alveolar epithelium cells stably expressing enhanced green fluorescent protein (eGFP). We propose different formulation strategies for the dendriplexes in pMDIs via encapsulation of those into microparticles formed from oligo(lactide)-*grafted*-chitosan (CSLA) co-oligomer or mannitol sugar alcohol, following evaluation of the aerosol performance. This work is innovative since it discusses the gene knockdown provided by siRNA-G4NH2 dendriplexes in human lung cancer cells, and addresses the formulation of siRNA in pMDIs, which have not been reported in literature yet. Moreover, this work is relevant as pMDIs are the most widely used OI devices to deliver therapeutics to the lungs, and as new siRNA-based therapies to treat medically relevant pulmonary diseases are expected to continue in development.

5.2 Experimental Section

5.2.1 Materials

Generation-four amine-terminated poly(amidoamine) dendrimer (PAMAM G4NH2, 14,215 $g.mol^{-1}$, 64 NH_2 surface groups) was purchased from Dendritech Inc., and provided in methanol (15.35 w/w). Methanol was removed with the help of a rotary evaporator (Buchi R-200). Double-stranded siRNA (ds-siRNA, sense: 5'- AAC UUC

AGG GUC AGC UUG C dTdT -3'; antisense: 5'- GCA AGC UGA CCC UGA AGU U dTdT -3') was purchased from Bioneer Inc. Double-stranded Dicer substrate siRNA (ds-DS-siRNA) targeting eGFP (sense: 5'- p ACC CUG AAG UUC AUC UGC ACC AC cg -3'; antisense: 5'- p CGG UGG UGC AGA UGA ACU UCA GGG UCA -3') and a respective mismatch (Integrated DNA Technologies, IDT) were used in all gene knockdown experiments. Capital letters represent ribonucleotides, underlined bases depict 2′-O-methylribonucleotides, lower case letters represent 2′-deoxyribonucleotides, "p" and "dTdT" depict an additional phosphate at the 5'-end, and thymine overhangs, respectively. Deionized water (DI-water, resistivity of 18.2 MΩ.cm) was obtained from NANOpure® DIamond™ UV ultrapure water system (Barnstead International) and treated with DEPC (0.1% v/v) overnight, following autoclaving. Diethylpyricarbonate (DEPC, high purity grade) and EDTA (0.5 M sterile solution, pH 8, DEPC treated) were purchased from Amresco. A549 cells – human lung adenocarcinoma cell line, an *in vitro* model of Type II alveolar epithelium[29] – were sourced from ATCC® (CCL-185™, passage 82). Gibco® Dulbecco's Modified Eagle Medium (DMEM, high glucose, GlutaMAX™, pyruvate), Gibco® Penicillin-Streptomycin Liquid (AB), Quant-iT™ PicoGreen ®, and Lipofectamine® 2000 Transfection Reagent were purchased from Invitrogen™ Life Technologies Corporation. Fetal Bovine Serum Advantage (FBS, non-heat inactivated, S11050) was purchased from Atlanta Biologicals Inc. Trypsin EDTA 1X (0.25% trypsin, 2.21 mM EDTA in HBSS) Corning® Cellgro® was purchased from Mediatech Inc. CellTiter 96 ® AQueous Non-Radioactive Cell Proliferation Assay (MTS reagent powder) and TransFast™ Transfection Reagent were purchased from Promega Corporation. Phenazine methosulfate (PMS, 95%) was purchased from MP

Biomedicals Inc. eGFP lentiviral particles (LVP-340, 1×10^7 IFU.mL^{-1}, a puromycin gene under Rsv promoter allows the selection of transduced fluorescent positive cells) were purchased from GenTarget Inc. Puromycin dihydrochloride (10 mg.mL^{-1}) was purchased from Toku-E. Cell culture flasks Cellstar® (75 cm^2), 24- and 96-well Costar® cell culture microplates (flat bottom, tissue culture treated, polystyrene, sterile) were purchased from Corning® Inc. 96-well microplate (black, flat bottom shape, polypropylene) was purchased from Greiner Bio One. Ribonuclease A (RNase A, R5503, 43 U.mg^{-1} solid) from bovine pancreas, heparin sodium salt (H4784, 194 U.mg^{-1}) from porcine intestinal mucosa, D-mannitol (minimum 98%), chitosan (CS, 100 - 300 kDa, 80% degree of deacetylation), 3,6-dimethyl-1,4-dioxane-2,5-dione (lactide, LA), Tin(II) 2-ethylhexanoate (Stannous octoate, $SnOct_2$, 95%) were purchased from Sigma-Aldrich. RiboLock® RNase Inhibitor (RI, EO0381, 40 U.μL^{-1}) was purchased from Thermo Scientific. SaeKem® LE Agarose was purchased from Lonza. Ethidium bromide (98%, 10 mg.mL^{-1}) was purchased from IBI Scientific. Tris Base Ultrapure BioReagent (99.5%) was purchased from J.T.Baker. Glacial acetic acid (100%), citric acid anhydrous (100%), phosphate buffered saline (PBS 10X solution), and microscope cover glasses (22 × 22 mm) were purchased from Thermo Fisher Scientific Inc. Tris-HCl 1M pH 8, and TE 20X pH 7.4 buffers were purchased from Boston BioProducts. Dibasic sodium phosphate anhydrous (99%) was purchased from EMD Chemicals Inc. Ethyl acetate (99.5%) was purchased from Mallinckrodt Chemicals. Propellant HFA-277 (Dymel 227 ea/P) was provided by DuPont™. 2H, 3H-perfluoropentane (HPFP, DuPont™ Vertrel® XF) was purchased from TMC Industries Inc. Deuterated dimethyl sulfoxide (DMSO-d6, 99.9%) was purchased from Cambridge

Isotope Laboratories Inc. Multi-75 silicon AFM probes for force modulation and light tapping (75 kHz, 3 $N.m^{-1}$) were purchased from Budget Sensors. Mica sheet was purchased from Ted Pella Inc.

5.2.2 Preparation and characterization of siRNA-G4NH2 dendriplexes

Dendriplexes were formed by mixing equal volumes (10 - 100 μL) of (negatively charged) siRNA (50 - 150 $\mu g.mL^{-1}$ in RNase free DI-water) and (positively charged) PAMAM G4NH2 (150 - 3000 $\mu g.mL^{-1}$ in 20 mM Tris-HCl pH 7.4 buffer RNase free).[19, 30] siRNA solution was added dropwise into the G4NH2 solution under vortex at 3000 rpm (VWR Digital Vortex Mixer) for 1 min. The siRNA-G4NH2 dispersions were kept at room temperature for at least 30 min before any further experiment to assure complete formation of the dendriplexes.[30] The G4NH2 concentration was varied in order to prepare dendriplexes at different N/P ratios – the molar ratio between the primary amine groups (N) from G4NH2 and phosphate groups (P) from siRNA.[31]

siRNA-G4NH2 dendriplexes dispersions (minimum of five independent batches, n = 5) were quantitatively analyzed using PicoGreen® assay[32] in Synergy 2 Microplate Reader (BioTek, VT) for the uncomplexed siRNA content, which was calculated using a linear calibration curve (siRNA concentration *vs.* fluorescent units). PicoGreen® is an ultrasensitive fluorescent nucleic acid stain used to quantify double-stranded DNA (ds-DNA)[32] and ds-siRNA in solution.[33] The siRNA complexation efficiency (CE) was calculated based on the difference between the initial amount of siRNA added during the formation of the dendriplexes, and the non-entrapped free siRNA remaining in the dendriplex dispersion.

Light Scattering (LS, Malvern ZetaSizer Nano ZS) was used to evaluate size (diameter) and zeta potential (ζ) of the siRNA-G4NH2 dendriplexes. Samples were diluted to 80 nM siRNA, and measurements were performed at 25°C using refractive index, viscosity, and dielectric constant of the buffer (for size) or DI-water (for ζ). Dendriplexes were formed in RNase free DI-water for ζ , which was calculated using the Smoluchowski Model.[31] A minimum of three independent batches (n = 3) were used to calculated an average size and ζ.

Scanning Electron Microscopy (SEM, Jeol/EO JSM-6510LV-LGS, 25 kV) and Atomic Force Microscopy (AFM, Pico SPM® LE Molecular Imaging) were used to investigate the morphology of the dendriplexes, which were formed in RNase free DI-water. For SEM imaging, several drops of the siRNA-G4NH2 dispersion were deposited on a microscope cover glass, dried overnight, and sputter-coated with gold (Ernest Fullan) under vacuum for 40 s. The sizes of the dendriplexes were estimated from the SEM images using Image J 1.42q.[34] The histogram of the measured diameters (> 400 particles) was fit to a Gaussian distribution, from which average and standard deviation were calculated. For AFM imaging, 20 μL of siRNA-G4NH2 dendriplexes dispersion was deposited on a freshly cleaved mica sheet and incubated at room temperature for 5 min[35] to allow the binding of the dendriplexes on the substrate. The substrate was then washed with few drops of DI-water, and dried with gentle air flow. AFM images were obtained using a Multi-75 silicon AFM probe in tapping mode.[35]

5.2.3 Gel retardation assay

The capacity of G4NH2 to form complexes with siRNA was also examined by gel electrophoresis. A known volume of the dendriplexes dispersions (equivalent to 300 ng siRNA) was loaded in the slots of casted non-denaturing agarose gel (1.5 % w/v in TAE 1X pH 8.2 buffer) stained with ethidium bromide (0.5 $\mu g.mL^{-1}$). The electrophoresis was performed at 60V (E0160-VWR Mini Gel Electrophoresis) for 40 min, and the siRNA-dye migration was visualized under UV irradiation (FOTO/Analyst® Investigator/Eclipse with UV Transilluminator Fotodyne Inc.). The images were recorded using the FOTO/Analyst® PC Image software (v.5).

5.2.4 RNase protection assay

Three RNase protection assays were performed as followed. *(i)* The determination of the minimal RNase A concentration needed to completely degrade bare siRNA is described in the Appendix B. *(ii)* The effect of the N/P ratio on the protection efficiency against RNase A degradation. Briefly, siRNA-G4NH2 dendriplexes at different N/P ratios were formed in buffer as described earlier, and 6 μL dendriplex dispersions (equivalent to 250 ng siRNA) were incubated with 8 μL RNase A in TE 1X pH 8 buffer (0.162 μg RNase A per 1 μg siRNA) for 6 h at 37°C, following the addition of RiboLock® RNase inhibitor (RI, 1μL = 40 U) and incubation for 30 min at 37°C to stop degradation reaction.[30] Dendriplexes were dissociated by adding 8 μL heparin (455 U per 1 μg siRNA) in TE 1X pH 8 buffer following incubation for 30 min at 37°C. Samples were frozen at -20°C overnight, and the integrity of the siRNA was determined by gel electrophoresis at the same conditions applied for gel retardation assay. *(iii)* The effect

of RNase concentration on the siRNA integrity at a fixed N/P ratio. Briefly, siRNA-G4NH2 dendriplexes at N/P 5 were incubated with increased concentrations of RNase (0.35, 0.7, 1.0, 1.5, and 3.5 μg RNase A per 1 μg siRNA) for 6 h at 37°C, following the treatments with RI and heparin, as described earlier. Appropriate controls (bare siRNA and dendriplexes +/- RNase A, and +/- heparin treatments) were included in all experiments. Heparin decomplexation assay is described in Appendix B.

5.2.5 *In vitro* release

siRNA-G4NH2 dendriplexes at different N/P ratios were formed in buffer as described earlier. A known volume of 0.1 M citrate/phosphate buffer (pH 5 or 7.4, to mimic intracellular endosomes/lysosomes and cytosol,[36] respectively) was added to the dendriplexes dispersion (2.2 μg siRNA) to make 2 mL, and samples were incubated in a water bath at 37°C. Aliquots of 50 μL were taken out at each time point, placed in a black 96-well plate, and frozen at -20°C. The collected samples were quantitatively analyzed using PicoGreen® assay[32] in Synergy 2 Microplate Reader (BioTek, VT) for the amount of siRNA released in each time point, which was calculated using a linear calibration curve (siRNA concentration *vs.* fluorescent units) and taking into account the amount of free and complexed siRNA removed out from the sample in each aliquot of 50 μL. Experiments were performed in triplicates (n = 3).

5.2.6 *In vitro* cytotoxicity

A549 cells (passages 5 - 8 from the original passage provided by ATCC®) were seeded in a 75 cm^2 cell culture flask and subcultured until approximately 90%

confluence. The cell culture medium (DMEM supplemented with 10% FBS and 1% AB, v/v) was changed every two days. Then, the cells were seeded in 96-well culture plate (5×10^3 cells per well) and cultured in 200 μL culture medium for 24 h at 37°C and 5% CO_2 (Thermo Scientific Incubator, NAPCO 8000WJ). For the cytotoxicity of bare PAMAM G4NH2, cells were rinsed with PBS 1X buffer, the medium was replaced by 200 μL of regular culture medium containing increased concentrations of G4NH2 dendrimer (0 - 500 μM), and the cells were kept in the incubator for 48 h at 37°C and 5% CO_2. For the cytotoxicity of dendriplexes, cells were rinsed with PBS 1X buffer, the medium was replaced by 100 μL DMEM only containing increased concentrations of siRNA-G4NH2 dendriplexes at N/P 30 (0 - 25 μM G4NH2, and 0 - 1.25μM siRNA) formed in buffer as described earlier. Cells were kept in the incubator for 6 h at 37°C and 5% CO_2. They were then overlaid with 100 μL of regular culture medium (the dendriplexes were kept in contact with the cells) and incubated for 72 h at 37°C and 5% CO_2. The concentration ranges of G4NH2 and siRNA used in these cytotoxicity experiments were designed in such way that the concentrations of G4NH2 and siRNA applied in all gene knockdown and aerosol characterization fall within that. Equally important, the incubation time in the cytotoxicity experiments falls within the usual time times (24 - 96 h) applied in gene knockdown experiments.[37] The cell viability was assessed by MTS cell proliferation assay.[38] Briefly, cells were rinsed with PBS 1X buffer, and 100 μL DMEM only was added to the cells, followed by 20 μL MTS/PMS solution. Cells were incubated in this DMEM/MTS/PMS mixture for 4 h at 37°C and 5% CO_2. MTS is bioreduced into formazan (which is soluble in the culture medium) by dehydrogenase enzymes found in metabolically active cells.[38] Absorbance of formazan

at 490 nm was measured directly from the 96-well culture plate (Molecular Devices, Spectra Max 250) and is proportional to the number of living cells. Thus, cell viability (%) was calculated as the ratio between the absorbance of treated (incubated with bare G4NH2 or dendriplexes) and untreated (G4NH2 and dendriplexes free) cells.

5.2.7 *In vitro* gene knockdown

In order to evaluate the knockdown efficiency achieved by siRNA-based dendriplexes, A549 cells stably expressing eGFP were developed as detailed in Appendix B. After successfully establishing the eGFP A549 cell line, eGFP knockdown experiments were performed. We tested both, the ds-DS-siRNA targeting eGFP – the positive sequence called siRNA(+), and the eGFP-mismatch ds-DS-siRNA, the scramble or negative sequence called siRNA(–). Dendriplexes at different N/P ratios were formed between G4NH2 and siRNA(+) and siRNA(–) as described earlier. Commercial transfection reagents (Lipofectamine® 2000 and TransFast^{TM})[37, 39] were used as positive controls, and free siRNA (+ and –) was used as a negative control. All eGFP knockdown experiments were performed according to Lipofectamine® 2000 protocol.[37] Firstly, eGFP stable A549 cells (passages 10 - 20 from the original passage provided by ATCC®) were seeded in a 75 cm^2 cell culture flask and subcultured until approximately 90% confluence. The cell culture medium (DMEM supplemented with 10% FBS and 2.5 $\mu g.mL^{-1}$ puromycin selective antibiotic) was changed every two days. Then, the cells were seeded in a 24-well culture plate (50,000 cells per well) and cultured in 500 μL DMEM supplemented with 10% FBS (v/v, no antibiotics) for 24 h at 37°C and 5% CO_2 (Thermo Scientific Incubator, NAPCO 8000WJ). Cells were rinsed

with PBS 1X buffer, and 250 μL transfection medium (DMEM containing siRNA(+) or siRNA(–) equivalent to 20 pmol per well, 80 nM siRNA) was added, and the transfection proceeded for 6 h at 37°C and 5% CO_2. Then, the transfection medium was replaced by 500 μL culture medium (DMEM + 10% FBS, no antibiotics) and the cells were returned to the incubator for 72 h at 37°C and 5% CO_2. Cells were dispersed in 1 mL PBS 1X buffer, and the median fluorescence intensity (MFI) was measured by flow cytometry (FACS, HWCRC 615 – BD LSR II Analyzer in Microscopy) with data from 10,000 to 20,000 cells. Untreated non-eGFP and eGFP stable A549 cells (siRNA or dendriplexes free) were used as controls. The MFI level of eGFP expression in untreated eGFP stable A549 cells was taken as 100%. The % eGFP knockdown efficiency was calculated by correlating the eGFP expression of untreated eGFP stable A549 cells with that from transfected cells.

The effect of the propellant HFA-227 on the biological activity of the siRNA was also investigated. Briefly, a known amount of siRNA (+ and –) dissolved in RNase free DI-water was placed in a pressure proof glass vial, frozen at -20°C overnight, and lyophilized (Labconco Freeze Zone 1) at -47°C and 0.055 mbar for 48 h. The vial was closed with a pressure valve (HiP, 15-11AF1) and the propellant HFA-227 was filled into the vial with the help of a manual syringe pump (HiP, 50-6-15) and a home-built high-pressure filler. The siRNA was stored in HFA-227 at 25°C and saturation pressure of the propellant, simulating a pMDI formulation of bare siRNA. After two months, the propellant HFA-227 was released by depressurization, and the siRNA was allowed to dry at room temperature, following its dissolution in a known volume of RNase A free DI-water, making a siRNA concentration of 10 nmol per 1 mL. As control, an aliquot of

the lyophilized siRNA (+ and –) was kept in a freezer at -20°C instead of being stored in pressurized, liquid HFA. Gene knockdown experiments (as described earlier) were performed with these siRNA sequences (+ and –) to evaluate the effect of storage under a compressed HFA environment. All transfection experiments (siRNA as received, stored in HFA and a freezer) were performed in a minimum of triplicates (n = 3).

5.2.8 Preparation of CSLA microparticles loaded with dendriplexes.

The biodegradable, water soluble, and HFA-philic CSLA co-oligomer was synthesized according to our previous work.[40] CSLA was composed by short segments of lactide – oligo(LA) – grafted onto low Mw CS via ring-opening polymerization.[40] Details about its synthesis and characterization can be found in Appendix B. Emulsification diffusion[40] was employed to prepare core-shell microparticles of CSLA loaded with siRNA-G4NH2 dendriplexes. Briefly, 15 mg CSLA was dissolved in 800 μL RNase free DI-water, and combined with 200 μL dispersion of siRNA-G4NH2 at N/P 10. The mixture (equivalent to 5 - 10 μg siRNA) was emulsified in 19 mL ethyl acetate using sonication bath (VWR, P250D, set to 180 W) for 5 min at 15 - 20°C making a water-in-oil (W/O) emulsion, which was quickly transferred to 180 mL ethyl acetate. Core-shell microparticles loaded with siRNA-G4NH2 (CSLA as shell and dendriplexes as core) were thus formed, collected via centrifugation (5,000 rpm for 20 min) and dried in air-flow at room temperature.

5.2.9 Preparation of mannitol microparticles loaded with dendriplexes

siRNA-G4NH2 at N/P 10 were formed in buffer as described earlier, and 200 μL of the dendriplex dispersion (equivalent to 10 μg siRNA) was combined with 30 mg mannitol previously dissolved in 800 μL RNase free DI-water. The mixture was spray-dried (BUCHI Mini Spray Dryer B-290) using the following parameters: atomizing air flow = 473 $L.h^{-1}$, aspiration = 70%, pump ratio = 5%, nozzle cleaner = 0, inlet temperature = 45°C, outlet temperature = 30 - 33°C. Nitrogen was the atomizing gas, and dry mannitol microparticles loaded with dendriplexes were accumulated in the collection vessel at the end of the glass cyclone.

5.2.10 Characterization of CSLA and mannitol microparticles loaded with dendriplexes

siRNA loading efficiency into microparticles was assessed by densitometry. Briefly, a known amount of particles was dissolved in 200 μL TE 1X pH 8 buffer and incubated at room temperature overnight, so that the water-soluble mannitol or CSLA shell broke down. Next, a known mass of heparin (equivalent to 455 U per 1 μg siRNA, based on the estimation that all siRNA was loaded into the microparticles) was added to the mixture, which was vortexed until heparin dissolution. The system was incubated for 30 min at 37°C, so that the siRNA complexed with the G4NH2 was released (see heparin decomplexation assay in Appendix B). Samples were frozen at -20°C overnight, and gel electrophoresis was performed at conditions applied for gel retardation assay. siRNA content encapsulated into microparticles was quantified by densitometry using Image J 1.42q[34] based on the electrophoresis images.

Densitometry finds application in the quantification of proteins,[8] DNA,[41] and siRNA.[42] Details on this technique can be found in those publications. Appropriate controls were employed – free siRNA mixed with heparin (positive control), and CSLA (or mannitol) mixed with heparin (no siRNA, negative control). Four independent batches (n = 4) of microparticles loaded with dendriplexes were used to calculate the average of siRNA loading. In addition, the integrity of the siRNA after dendriplexes formation and by encapsulation into CSLA or mannitol microparticles was also determined.

The hydrodynamic diameter of the microparticles was assessed by LS. Briefly, particles loaded with siRNA-G4NH2 at N/P 10 were dispersed in HPFP (2 mg per 1 mL) using a sonication bath, and measurements were performed at 25°C using refractive index, viscosity, and dielectric constant of the HPFP, which is a model of propellant HFA that is liquid at ambient conditions.[43] Next, HPFP was evaporated and 1 mL RNase free DI-water was added to the microparticles to break down the CSLA shell (or mannitol) and release the dendriplexes. LS measurements were performed at 25°C using refractive index, viscosity, and dielectric constant of the water, and thus, the hydrodynamic diameter of the dendriplexes was recorded, but at this time, in presence of the CSLA (or mannitol) dissolved in the aqueous medium.

SEM was used to investigate the morphology of the microparticles, which were dispersed in HPFP using a sonication bath. Several drops of the dispersion were deposited on a microscope cover glass, the HPFP was quickly evaporated by using air flow, and the glass was sputter-coated with gold (Ernest Fullan) under vacuum for 40 s, following acquisition of the images via SEM.

5.2.11 Preparation of the pMDI formulations and evaluation of their physical stability

A known mass of microparticles (CSLA or mannitol) encapsulating siRNA-G4NH2 dendriplexes (at N/P 10) was weighed into pressure proof glass vials (8412-B, West Pharmaceutical Services) and crimp-sealed (CroPharm, Inc) with a 63 µL metering valves (EPDM, 3M Drug Delivery Systems). A known volume of propellant HFA-227 was added with the help of a manual syringe pump (HiP, 50-6-15) and a home-built high pressure filler in order to make a 2 $mg.mL^{-1}$ concentration.[40] The particles were dispersed in the propellant using a sonication bath (VWR, P250D, set to 180 W, 15 - 20°C).[40] The physical stability was investigated via sedimentation rate experiment, i.e., by visually monitoring the quality of the dispersions as a function of time after stopping the mechanical energy from the sonication – digital images were taken according to the time.[40] pMDI formulations of bare siRNA-G4NH2 dendriplexes at N/P 10 were attempted, as described in Appendix B. The free dendriplexes were found not to disperse in the propellant.

5.2.12 Aerosol characterization of the pMDI formulations

An eight-stage Andersen Cascade Impactor (ACI, Copley Scientific) fitted with an USP induction port and operated with a flow rate of 28.3 $L.min^{-1}$ at 25°C and 75% relative humidity[44] was used to evaluate the aerosol properties of the pMDI formulations, which were prepared as described earlier. Prior each ACI test, the formulation was completely dispersed using a sonication bath for 10 - 15 min at 15 - 20°C, and five actuations were fired to waste. Next, 50-65 actuations (depending on the

siRNA concentration in the formulation) were fired into the ACI, with an interval of 10 s between each actuation.[40] The ACI was disassembled and had the actuator (AC), induction port (IP), and all stages rinsed with and kept in 20 mL RNase free DI-water for 6 h in order to break down the water soluble CSLA shell (or mannitol) from the microparticles containing siRNA-G4NH2 dendriplexes. Samples were frozen at -20°C overnight, and lyophilized (Labconco Freeze Zone 1) at -47 °C and 0.055 mbar for 48 h. The collected powder was dissolved in 100 μL TE 1X buffer pH 8 and incubated with a known mass of heparin (equivalent to 455 U per 1 μg siRNA – see Appendix B) for 30 min at 37°C, in order to dissociate the siRNA from the PAMAM G4NH2. Samples were frozen (-20°C) overnight, loaded into the slots of non-denaturing agarose gel, following electrophoresis at conditions applied for gel retardation assay. The siRNA content in each ACI stage was quantified by densitometry using Image J 1.42q[34] based on the electrophoresis images and appropriate controls (presence or absence of siRNA, as described earlier). The aerosol characteristics were thus calculated: *(i)* fine particle fraction (FPF – the siRNA content on the respirable stages of the ACI (from stage 3 to filter) over the total siRNA content released into the impactor (from IP to filter) excluding the siRNA content remaining in the actuator);[40] *(ii)* respirable fraction (RF – the siRNA content collected from stage 0 to filter over the total siRNA released into the impactor);[27] *(iii)* % siRNA recovered, and siRNA content in a single puff dose; *(iv)* mass median aerodynamic diameter (MMAD); and *(v)* geometric standard deviation (GSD). MMAD and GSD were calculated as described in the literature.[40] ACI experiments were performed in duplicates (n = 2).

5.2.13 Statistical analysis

One-Way ANOVA in OriginPro 8 SR0 v8.0724 (B724) software was used to perform all statistical analyses. *p* values < 0.05 were considered statistically significant.

5.3 Results and Discussion

5.3.1 Preparation and characterization of siRNA-G4NH2 dendriplexes

siRNA-G4NH2 dendriplexes at different N/P ratios were prepared and characterized with respect to their morphology, size and surface charge according to AFM, SEM and LS. The results are summarized in Table 5.1. Details of the characterization for one N/P ratio (N/P 20), including AFM and SEM micrographs, are shown in Figure 5.1.

Table 5.1. Size of siRNA-G4NH2 dendriplexes determined by LS and SEM as a function of the N/P ratio. Zeta potential (ζ) and siRNA complexation efficiency (CE) are also shown. LS was performed with dendriplexes at 80 nM siRNA, and in 10 mM Tris-HCl pH 7.4 (for size) and pure water (for ζ). Image J was used to estimate the size of the dendriplexes from the SEM images: histograms of the measured diameters (> 400 particles) were fitted to Gaussian distributions, from which the average size and standard deviation was obtained.

N/P ratio	DLS			SEM	siRNA CE (%)
	Size (nm)	PDI	ζ (mV)	Size (nm)	
5	267 ± 115	0.4 ± 0.2	+ 34 ± 9	285 ± 78	97.3 ± 0.6
10	246 ± 63	0.4 ± 0.2	+ 36 ± 7	285 ± 70	96.2 ± 1.5
20	262 ± 85	0.6 ± 0.2	+ 32 ± 4	207 ± 51	97.2 ± 0.6
30	254 ± 52	0.5 ± 0.1	+ 33 ± 3	257 ± 74	97.5 ± 0.8

It was observed that the hydrodynamic diameter of the dendriplexes did not vary substantially with the N/P ratio. The average hydrodynamic diameter from all N/P ratios combined was ca. 257 nm. This value is corroborated by SEM, with an average

diameter of 258 nm. As seen in literature,[35, 45, 46] the size of dendriplexes usually displays significant heterogeneities, as is the case for polyplexes prepared with other cationic polymers. This heterogeneity has been attributed to the electrostatic and entropic nature of the complexation process.[45]

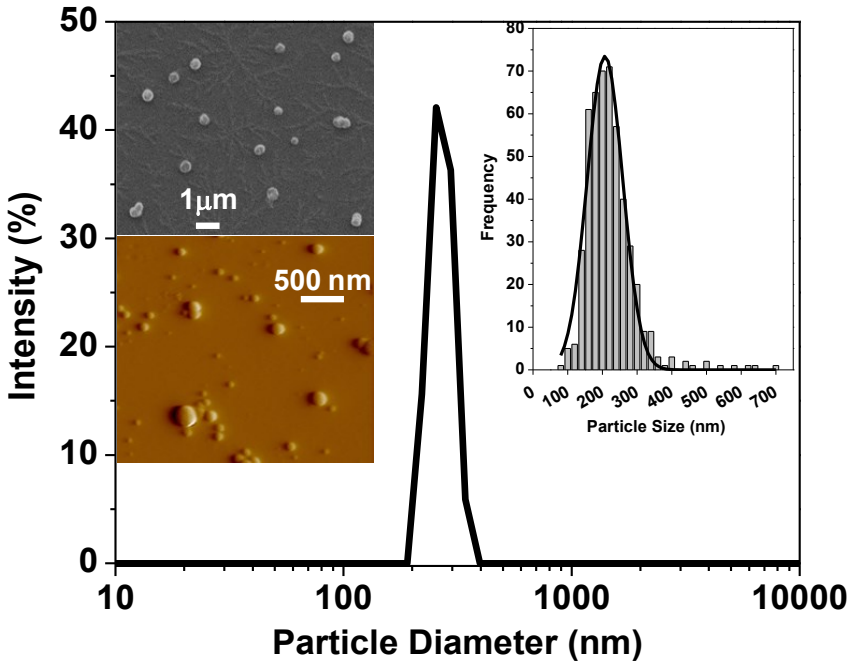

Figure 5.1. Size and morphology of siRNA-G4NH2 dendriplexes at N/P 20 as determined by LS (*main distribution in the center*), SEM (*upper left inset*), and AFM (*lower left inset*). Histogram and Gaussian fit to the diameter distribution obtained from SEM images (> 400 particles) of the dendriplexes is also shown (*upper right inset*).

The overall surface charge of the siRNA-G4NH2 dendriplexes did not show any specific trend as a function of the N/P ratio, with a magnitude of the order of 30 to 40, also in agreement with previous studies of dendriplexes with PAMAM dendrimers.[46]

5.3.2 Gel retardation assay of G4NH2 to siRNA

The ability of G4NH2 to form complexes with siRNA as a function of the N/P ratio was investigated by gel electrophoresis (semi-quantitative) combined with PicoGreen® assay (quantitative). The results are summarized in Table 5.1 and Figure 5.2.

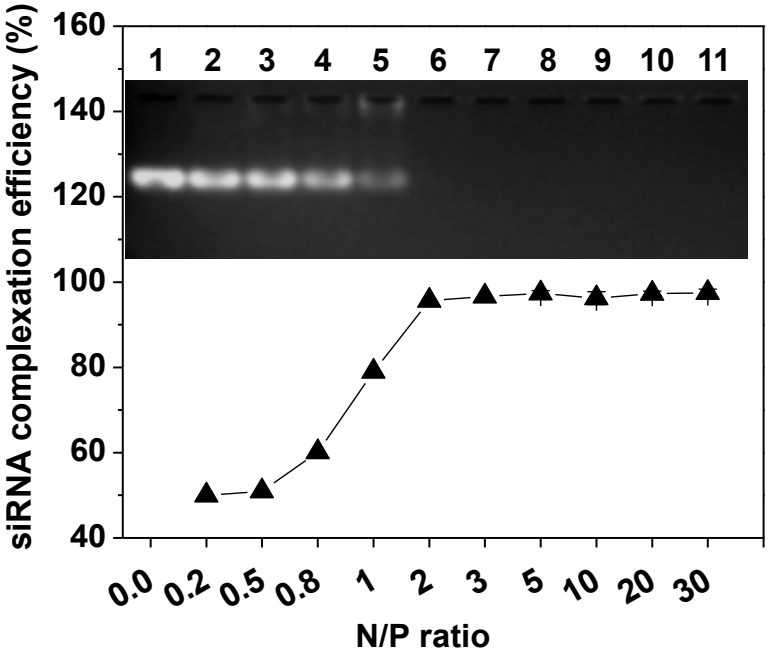

Figure 5.2. siRNA complexation efficiency as a function of the N/P ratio, as quantified by PicoGreen® Assay of residual free siRNA in the dispersion after preparation of the dendriplexes. *Inset:* Non-denaturating agarose gel electrophoresis of the corresponding dendriplexes: N/P 0.2 (*lane 2*), 0.5 (*lane 3*), 0.8 (*lane 4*), 1 (*lane 5*), 2 (*lane 6*), 3 (*lane 7*), 5 (*lane 8*), 10 (*lane 9*), 20 (*lane 10*), 30 (*lane 11*). Untreated siRNA control (300 ng) is shown in *lane 1*.

The complexation efficiency (CE) of G4NH2 to siRNA is seen to be low (< 80%) at N/P < 1. However, almost all siRNA was complexed with the at N/P ratios > 2 (siRNA CE > 95%). These quantitative results assessed by PicoGreen® assay – measuring the uncomplexed siRNA remaining in solution after dendriplex formation – were confirmed by gel electrophoresis (*inset* in Figure 5.2). The siRNA band is seen to disappear in the gel as the N/P ratio increases, indicating that the siRNA was largely

complexed with the PAMAM G4NH2 dendrimer, and thus, was unable to flow through the pores of the gel (compare *lanes 2 - 11*: siRNA-G4NH2 dendriplexes formed at N/P 0.2 - 30, with *lane 1*: untreated siRNA control). Therefore, these results reinforce that highly positively charged PAMAM G4NH2 is able to condense siRNA into NPs very efficiently, since very little uncomplexed siRNA was found to be free in the supernatant after the complexation (N/P > 2). Similar findings have been reported in literature – starting at N/P 2 the relative fluorescence due to free siRNA in the medium after dendriplex formation was 30% (siRNA CE ca. 70%), as measured by ethidium bromide exclusion assay, and no band assigned to free siRNA is visualized in the non-denaturing agarose gel after electrophoresis.[47] In addition, higher siRNA CE (> 90%) have been reported for siRNA-based dendriplexes using cationic PAMAM at different generations (G4, G5, and G6) starting at N/P ratio 4, as quantified by densitometry using gel electrophoresis images.[48]

5.3.3 Protection of siRNA by G4NH2 against RNase degradation

siRNA is vulnerable to degradation by RNases,[49] and one of the important potential advantages in using nanocarriers in siRNA therapeutic technologies is the ability to protect this frail cargo. Thus, in order to evaluate the ability of PAMAM G4NH2 to protect siRNA from RNase degradation, siRNA-G4NH2 dendriplexes were formed at several N/P ratios and incubated with the RNase A (the lowest concentration found to digest bare siRNA completely – 0.162 μg RNase A per 1 μg siRNA – as seen in Appendix B) for 6 h at 37°C, following RNase inhibitor and heparin treatments, and gel electrophoresis so as to release and quantify the non-degraded siRNA. The results are

shown in Figure 5.3. PAMAM G4NH2 is seen to efficiently protect siRNA from RNase A degradation upon complexation. For all tested N/P ratios, the siRNA released from the dendriplexes kept in contact with RNase A (*lanes 3*, *7*, *11*, and *15*) was comparable to the siRNA released from dendriplexes which were not exposed to RNase A (*lanes 5*, *9*, *13*, and *17*, the positive controls).

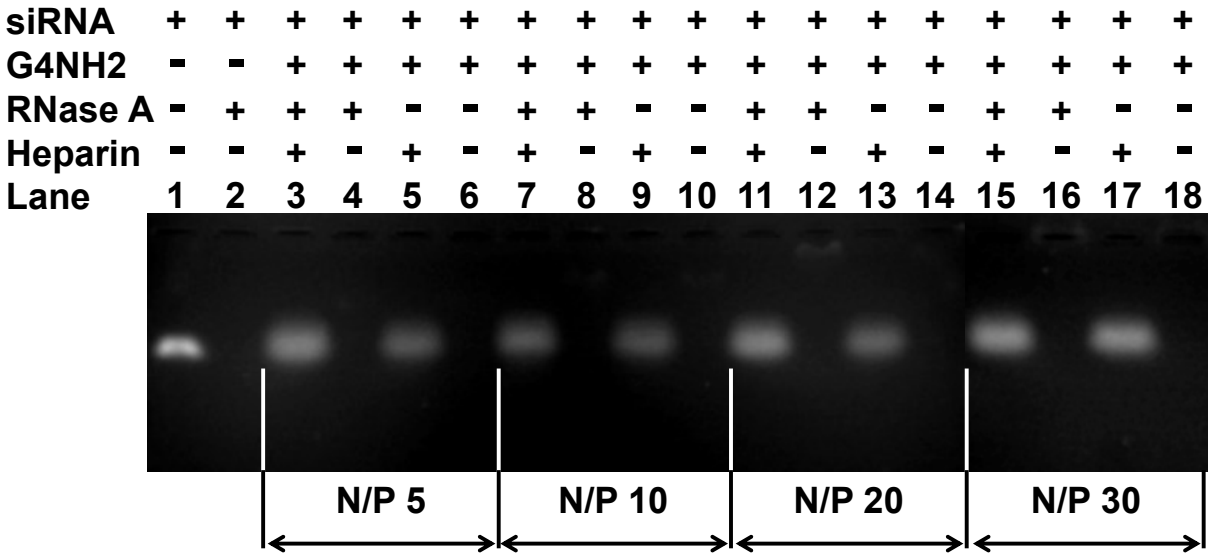

Figure 5.3. RNase protection assay (non-denaturing agarose gel electrophoresis) of the siRNA-G4NH2 dendriplexes as a function of the N/P ratio. Dendriplexes incubated in the absence (-) or presence (+) of the treatments: RNase A (0.162 μg per 1 μg siRNA) for 6 h at 37 °C, followed by 1μL (40 U) RiboLock® RNase inhibitor for 30 min at 37°C to block RNase activity, and heparin (455 U per 1 μg siRNA) for 30 min at 37 °C to dissociate the siRNA from the dendrimer. Aqueous medium: TE buffer 1X pH 8. Untreated siRNA control (300 ng) before (*lane 1*) and after (*lane 2*) incubation with RNase A.

In order to probe the protection efficiency provided by the PAMAM G4NH2 at increasing RNase A concentrations, siRNA-G4NH2 dendriplexes formed at N/P 5 were incubated with increased concentrations of RNase A (0.35, 0.7, 1.0, 1.5, and 3.5 μg per 1 μg siRNA) for 6 h at 37°C, following RNase inhibitor and heparin treatments, and gel electrophoresis. The results are shown in Figure 5.4, and again indicate that the siRNA was sufficiently protected from RNase degradation upon complexation with G4NH2.

Even at this relatively low N/P ratio (N/P 5) the siRNA was well protected when kept in contact with very high concentrations of RNase A (3.5 μg per 1 μg siRNA) – in Figure 5.4, compare the siRNA from dendriplexes incubated in presence (*lane 20*) and absence (*lane 22*) of RNase A. Literature results suggest that this protection ability should hold somewhat till even higher concentrations, as it was observed that 75% of the siRNA integrity is still maintained at RNase A concentrations 7-fold higher than the one studied here (at N/P 10).[50] However, the experimental conditions laid out here were more severe than those reported in other works.[51, 52]

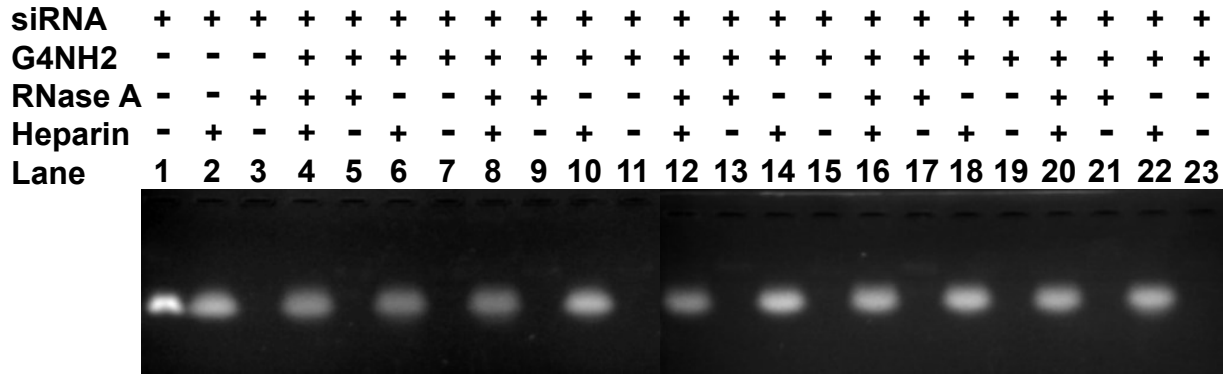

Figure 5.4. RNase protection assay (non-denaturing agarose gel electrophoresis) of the siRNA-G4NH2 dendriplexes (N/P 5) as a function of the RNase A concentration. Dendriplexes incubated in presence (+) or absence (-) of the treatments: RNase A (0.35, 0.7, 1.0, 1.5, and 3.5 μg per 1 μg siRNA, in *lanes 4-7*, *8-11*, *12-15*, *16-19*, *20-23*, respectively) for 6 h at 37°C, followed by 1μL (40 U) RiboLock® RNase inhibitor for 30 min at 37°C to block RNase activity, and heparin (455 U per 1 μg siRNA) for 30 min at 37 °C to dissociate the siRNA from the dendrimer. Aqueous medium: TE buffer 1X pH 8. Untreated siRNA control (250 ng) in *lane 1*, after incubation with heparin (*lane 2*) and 0.35 μg RNase A per 1 μg siRNA (*lane 3*).

5.3.4 *In vitro* release of siRNA from G4NH2

The siRNA release from the dendriplexes was evaluated *in vitro* at 37°C, in citrate/phosphate buffer at pH 5 and 7.4, in order to mimic endosomes/lysosomes and cytosol, respectively.[36] The results are shown in Figure 5.5, and indicate that the siRNA *in vitro* release profile from dendriplexes (N/P 10, 20, and 30) is highly dependent upon

the pH. The release is much slower at acidic medium than at physiological pH. At low pH (< 5) all primary and tertiary amines from G4NH2 are protonated[53] and consequently the electrostatic interactions between the positively charged dendrimer and negatively charged siRNA increase, which results in stronger binding and lower siRNA released at low pH. At physiological pH 7.4 the tertiary amines are deprotonated and only the primary amines are protonated[53] which decreases the electrostatic interactions between siRNA and G4NH2, and as result, the release of the siRNA increases at higher pH.

This degree of compactness observed at lower pH is also manifested on the fact that no burst release is observed at pH 5.0. On the other hand, at physiological pH, a burst release was observed at 1 - 2 days, and it was ca. 3.5% or 5.5 pmol – based on the initial loading of siRNA into dendriplexes. After 3 - 5 days, it was observed that 8 - 10% siRNA was released from the dendriplexes, which corresponds to 13 - 16 pmol. The results in Figure 5.5 show that 48, 24, and 34% of the total siRNA complexed with G4NH2 is released from the dendriplexes at N/P 10, 20, and 30, respectively, after 20 days in citrate/phosphate buffer pH 7.4 at 37°C. While no literature results are available for the *in vitro* release for siRNA from PAMAM-based dendriplexes, we can contrast the results obtained here with the release of oligonucleotides (ON) from PEI polyplexes.[54] At N/P 15 and 40 in PBS pH 7.4 and 37°C, 55% of the ON was released after 20 days for those complexes, which is somewhat similar to the results obtained in our work.

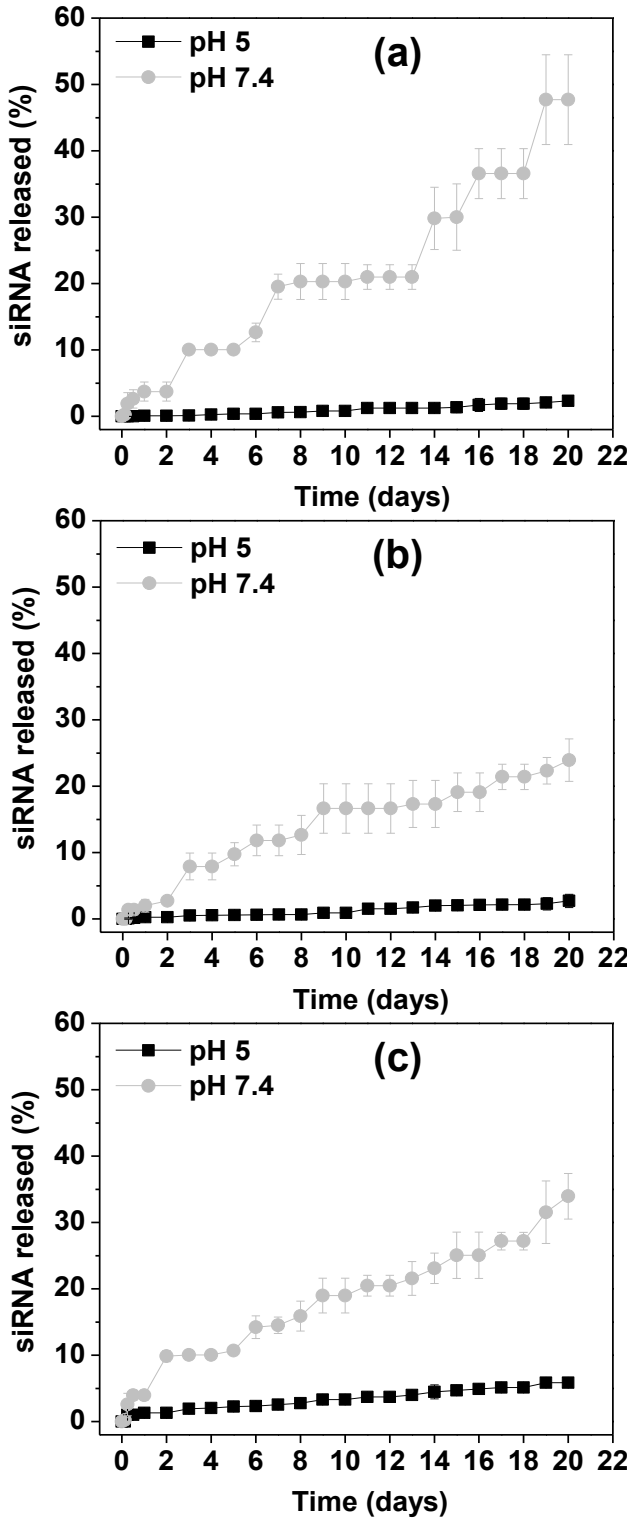

Figure 5.5. *In vitro* release of siRNA from dendriplexes in 0.1 M citrate/phosphate buffer (pH 5 and 7.4, mimicking intracellular endosomes/lysosomes and cytosol, respectively) at 37°C. siRNA-G4NH2 dendriplexes differ by N/P ratio: N/P 10 **(a)**, N/P 20 **(b)**, and N/P 30 **(c)**.

5.3.5 *In vitro* cytotoxicity of G4NH2 and siRNA-G4NH2 dendriplexes

Cationic dendritic polymers, like polypropyleneimine (PPI), polylysine (PLL), and PAMAM may induce significant *in vitro* cytotoxicity due to the high density of cationic groups on their surface.[55] There are many reports discussing the effect of concentration and generation on the toxicity of dendrimers,[17, 35, 55-57] which is a critical factor to be considered when evaluating the potential of dendrimers as nanocarriers for siRNA delivery. In this work, *in vitro* cytotoxicity studies were performed with A549 cells by incubating them with bare G4NH2, and siRNA-G4NH2 dendriplexes at N/P 30, according to the MTS assay.[38] The cell viability results are shown in Figure 5.6.

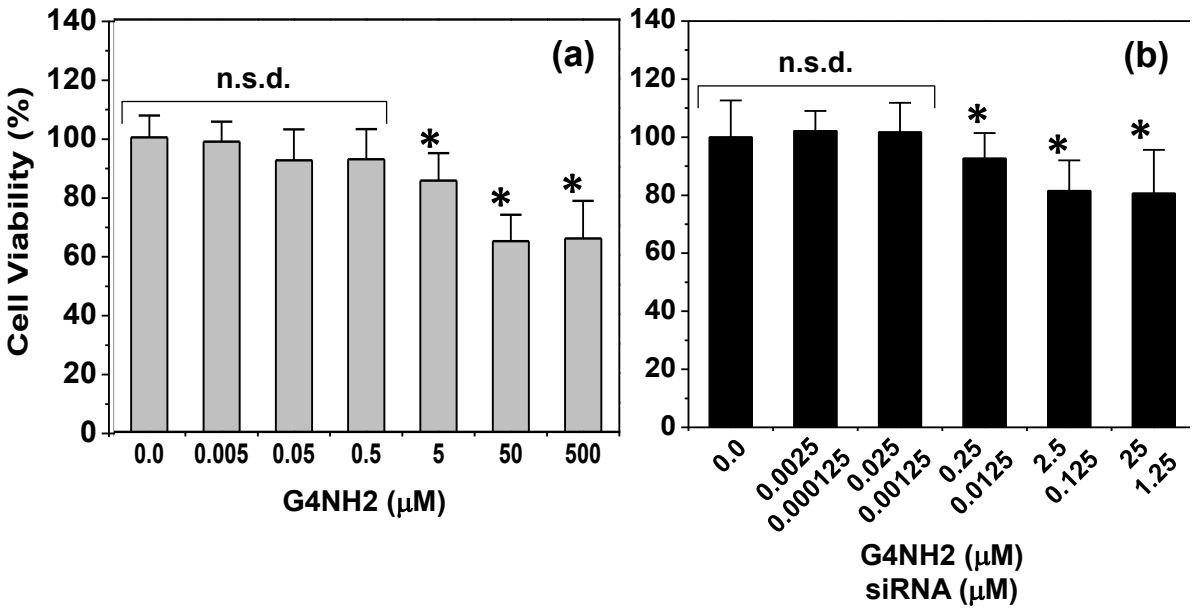

Figure 5.6. *In vitro* cytotoxicity of G4NH2 alone **(a)** and siRNA-G4NH2 dendriplexes at N/P 30 **(b)** in increased concentrations in A549 cell line. ∗ = statistically different compared to untreated cells control; n.s.d. = no statistical difference among them (*p* value < 0.05, One-Way ANOVA).

The results presented in Figure 5.6a indicate that the viability of A549 was > 85% when the cells were in contact with G4NH2 alone for 48 h at concentrations up to 5 μM.

This result is in agreement with previous literature reporting that the viability of A549 cells was > 80% for G4NH2 at low concentrations of 0.7 and 7 μM, as evaluated by MTT assay after 72 h of incubation.[58] Several other works report different cytotoxicity results for PAMAM G4NH2,[47, 56, 57] and thus, the toxicity level of G4NH2 is dependent upon concentration, cell type, and incubation time.[48] PAMAM dendrimers are known to be cytotoxic by causing membrane rupture, substantially related to the formation of cavities in the cellular membrane.[48] Toxicity and other dendritic properties (interactions, mechanisms of cellular uptake, and intracellular fate) are most likely governed by the surface groups.[59]

The toxic effects of siRNA-G4NH2 dendriplexes at N/P 30 (the highest N/P ratio applied in the gene knockdown experiments discussed next) to A549 were also investigated via MTS assay after 72 h contacting the dendriplexes with the cells. The results in Figure 5.6b indicate that the cytotoxicity of the dendriplexes at N/P 30 was low, even at the highest concentration – viability of A549 cells was ca. 80% at 25 and 1.25 μM of G4NH2 and siRNA, respectively. It has been reported in literature that J-774 cells (macrophage-like cell line) showed 90 - 95% viability after 24 h incubation with siRNA-G4NH2 dendriplexes at N/P 10 (0.05 μM siRNA) as measured by MTT assay.[50] Here in our work, at the same 0.05 μM siRNA concentration, A549 cells showed ca. 85% viability. This result is interesting since the time of incubation and N/P ratio were both 3-fold higher than that reported in literature.[50] Other work has reported that the viability of A549 was reduced to 45% when the cells were incubated with G5NH2/ON (0.16 μM ON) dendriplexes at N/P 15 for 4 h, following measure by CellTiter-Blue®.[20] In our work, at similar 0.125 μM siRNA concentration, the cell viability of A549 was ca.

80%. These results are especially relevant and necessary in gene knockdown studies. When working in concentration regions of no toxicity, gene knockdown is not confounded with nonspecific toxicity. At the harshest condition of the *in vitro* cytotoxicity studies, the cell viability of A549 was still ca. 80% after 72 h of incubation with siRNA-G4NH2 dendriplexes at N/P 30 containing 25 and 1.25 μM G4NH2 and siRNA, respectively. In contrast, at the harshest condition of the *in vitro* gene knockdown experiments (discussed next), the A549 cells were incubated for 6 h only, with dendriplexes at N/P 30 containing 1.95 μM and 80 nM G4NH2 and siRNA, respectively. At these latter G4NH2 and siRNA concentrations, the viability of A549 cells was at least ca. 90% (Figure 5.6b), and expected to be even higher at smaller N/P ratios. In addition, cell debris was excluded during FACS analyses, and thus, the small fraction of dead cells due to toxicity (< 10% for the highest N/P ratio) is not expected to interfere in the FACS results.

5.3.6 *In vitro* gene knockdown of siRNA-G4NH2 dendriplexes

FACS of A549 cells stably expressing eGFP was used to investigate the gene silencing efficiency of siRNA-G4NH2 dendriplexes. Lipofectamine® 2000 (LF) and TransFast™ (TF) were the commercial transfection reagents selected as positive controls. TF is originally designed as a transfection reagent for DNA,[39] but it has shown gene suppression ca. 60 - 90% in the *in vitro* delivery of siRNA(+).[60] Bare siRNA was used as the negative control. A549 cells that were not transduced (no eGFP) were used as reference. Cellular debris due to dead or damaged dying cells was gated out during the FACS analyses to prevent any toxic effect of the nanocarriers to mask true

gene knockdown. Transfection of eGFP stable A549 cells was performed with ds-DS-siRNA targeting eGFP, the positive sequence siRNA(+), and an eGFP-mismatch, the scramble negative sequence siRNA(–). The results are shown in Figure 5.7a, and indicate that the gene knockdown efficiency of G4NH2-siRNA(+) dendriplexes (average of 22 - 36%) was intermediate compared to LF (72%), TF (70%), and bare siRNA (2.8%). No statistical difference was found when comparing gene knockdown as a function of the N/P ratio (One-Way ANOVA, *p* value < 0.05).

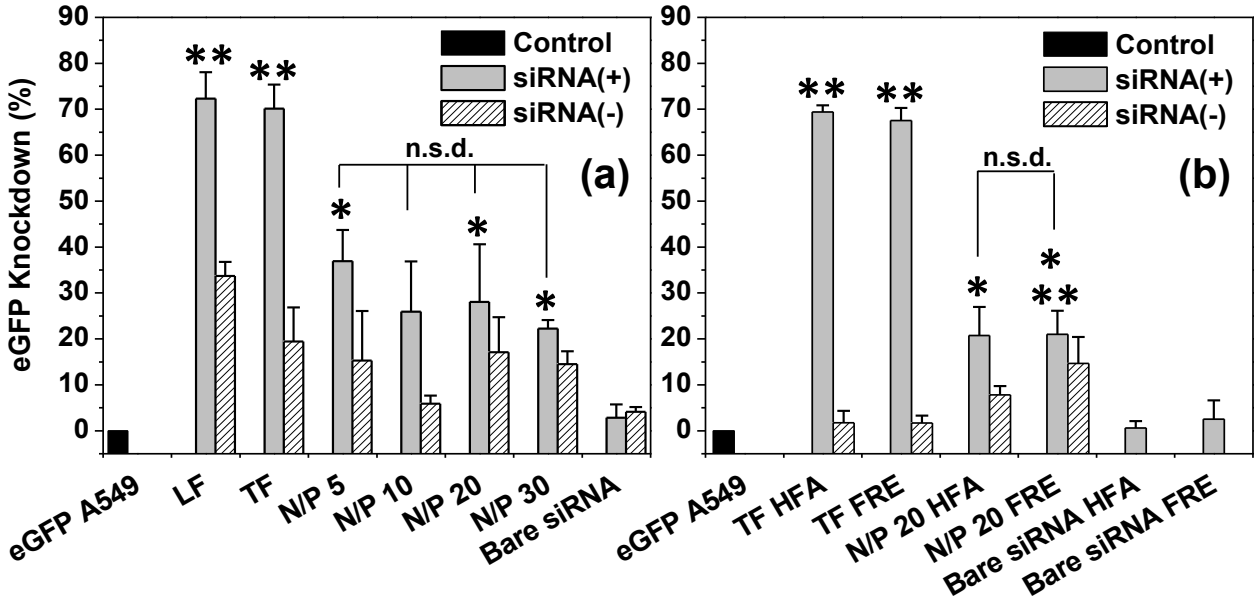

Figure 5.7. *In vitro* knockdown of eGFP expression in A549 cells stably expressing eGFP. siRNA-G4NH2 dendriplexes at N/P 5, 10, 20, and 30, were prepared with **(a)** siRNA as received from the supplier and **(b)** at N/P 20 with lyophilized siRNA stored in HFA-227 (HFA, at 25°C and saturation pressure of the propellant) and in freezer at -20°C (FRE, at 253 K) for 2 months. Specificity of the knockdown (positive siRNA sequence, anti-eGFP) is maintained by comparison to effects with the negative siRNA sequence (scramble). Lipofectamine® 2000 (LF) and TransFast™ (TF) were the commercial transfection reagents used as controls, and bare siRNA was negative control. G4NH2 concentration at N/P 30 corresponds to 1.95 μM, and siRNA concentration in all systems was 80 nM. ∗∗ = statistically different compared to untreated eGFP A549 cells control; ∗ = statistically different compared to eGFP A549 cells treated with bare siRNA; n.s.d. = no statistical difference among them (*p* value < 0.05, One-Way ANOVA).

While no gene knockdown have been reported for dendriplexes on A549 cells up-to-date, we try to contrast our results with the literature for other cell types. For example, siRNA-G4NH2 dendriplexes at N/P 10 caused 12.5 and 22% inhibition of eGFP expression in J-774 (macrophage-like) and T98G (human glioblastoma) cell lines, respectively,[50] and 10% eGFP knockdown in C-166 (mouse yolk sac embryo) cells.[47] Thus, the silencing efficiency obtained with siRNA-G4NH2 dendriplexes on eGFP expressing A549 cells seem to be improved.

A reduction in eGFP expression in A549 cells was also observed when the scramble siRNA(–) was delivered using LF (34%), TF (19.5%), and G4NH2 (6 - 17%) – Figure 5.7a. It has been shown that LF-siRNA(–) complexes cause measurable and undesired gene silencing ca. 10 - 45% in several cell types.[61-63] This unwanted eGFP suppression is most likely due to off-target effects[64] which can be due to toxicity of the nanocarrier,[61] but also depend on the similarity between the nucleotide sequence from the siRNA(–) and short motifs in messenger RNA (mRNA) and other unrelated genes not targeted during the transfection.[64, 65] Off-target effects in RNAi are quite common and an issue of consideration when developing RNAi technologies,[65] but may be hard to avoid,[64] and are still not well understood.[66]

Alterations in gene expression *in vitro* and *in vivo* have been problematic for several types of nanocarriers – e.g. linear and branched PEI,[66, 67] PEG-PEI,[66] PPI,[49, 58] diaminobutane (DAB),[49, 58] and PAMAM.[66, 67] In addition, siRNAs used as negative control for GFP target and deregulate endogenous genes with important roles in many pathways and in different cell lines, even though there are very small homologous region sequences between the siRNA(–) and the mRNA.[64] However, the possible off-

target effects should not annul the tremendous potential of RNAi in the development of siRNA-based therapies.

5.3.7 *In vitro* gene knockdown of siRNA-G4NH2 dendriplexes exposed to propellant HFA

In order to test whether the biological activity of the siRNA was preserved after the formulation in the pMDI (under HFA atmosphere), the gene knockdown activity of dendriplexes formed with siRNA that was lyophilized and stored under HFA-227 at 25°C and saturation pressure of the propellant for two months, was compared to a control (lyophilized but stored at -20°C). Gene knockdown experiments were performed on eGFP A549 cells with dendriplexes at N/P ratio of 20, and the results are shown in Figure 5.7b. The results demonstrate that even after such harsh storage conditions in propellant HFA, the siRNA(+) was still biologically active to silence the eGFP expression in A549 cells – around 69% and 21% eGFP knockdown for TF and dendriplexes at N/P 20, respectively – and low off-target effects were caused by the delivery of siRNA(–). Similar values of eGFP suppression were obtained with the control siRNA(+) that was not stored under HFA-227 – 68% and 21% for TF and N/P 20, respectively. In addition, these results are readily comparable to those reported earlier (Figure 5.7a) for siRNA(+) as received – 70% eGFP knockdown for TF and 28% for N/P 20. Collectively, these results indicate that the biological activity of the siRNA is kept even after long-term exposure in propellant HFA.

5.3.8 Preparation and characterization of microparticles loaded with dendriplexes

There is one major obstacle in the regional delivery of the dendriplexes to the lungs when using OI devices. While the dendriplexes are in the order of nanometers in size, the optimum aerosol size for deep lung deposition is in the micron range (between 0.5 to 5 μm).[68, 69] Particles with an aerodynamic diameter < 0.5 μm may be easily exhaled, while those > 5 μm tend to be deposited in the mouth and throat, ending up in the digestive tract. In the case of pMDIs, another hurdle that needs to be overcome is the physical stabilization of the microparticle dispersions (suspension) in the low dielectric propellant HFA.[25, 26]

It is necessary, therefore, to develop particle engineering strategies capable of forming stable suspension of the dendriplexes in the form of microparticles. We demonstrate in this work two such strategies. One consists in encapsulating the dendriplexes within mannitol microparticles, via spray drying, and the other is the use of a CSLA co-oligomer shell formed during emulsification diffusion. Mannitol was chosen as it is a generally recognized as a safe (GRAS) excipient widely used as bulking agent and non-active carrier in dry powder inhalers.[70] Mannitol particles alone also have shown to have less adhesion/cohesion in propellant HFA, slower sedimentation rates, and superior aerosol performance than other sugars such as lactose.[71] The CSLA co-oligomer was chosen because it is water soluble, degradable and non-HFA soluble – the shell will not disintegrate in HFA but will break down when in contact with the fluid lining the lungs. The ester groups from the oligo(LA) are HFA-philic,[25, 28] and microparticles formed with CSLA shell have shown enhanced physical stability in

propellant HFAs.[26, 27, 40] The size and morphology of the CSLA and mannitol microparticles containing siRNA-G4NH2 dendriplexes at N/P 10 were evaluated by LS and SEM. The results are shown in Figure 5.8.

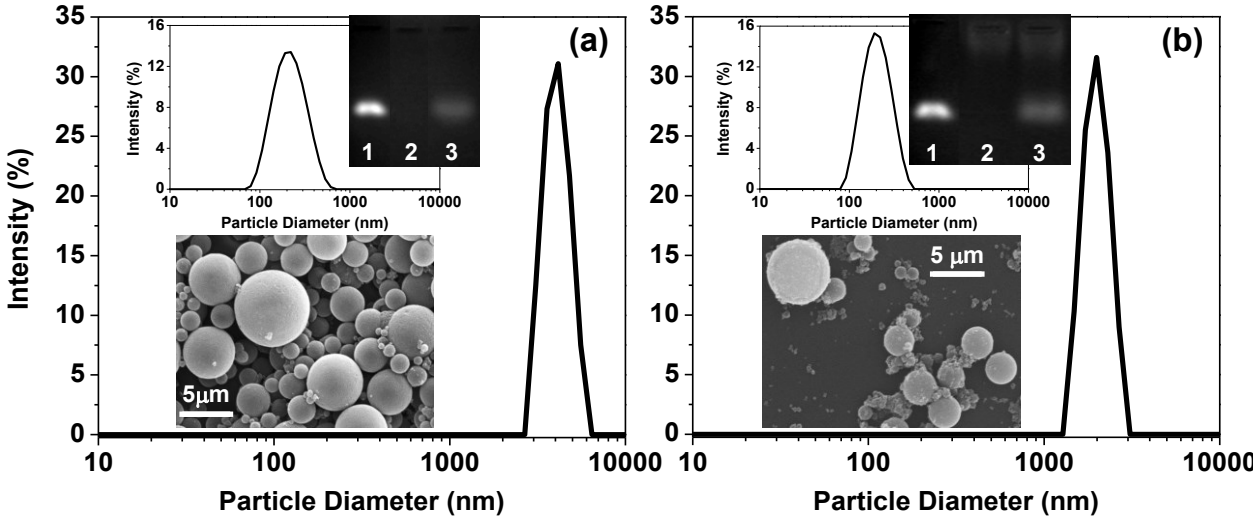

Figure 5.8. Size and morphology of mannitol **(a)** and CSLA **(b)** microparticles loaded with siRNA-G4NH2 dendriplexes at N/P 10 as determined by LS (*main distribution on right*) and SEM (*lower left inset*). Particles were dispersed in HPFP (2 mg.mL^{-1}) to perform LS, and after that, the HPFP was evaporated and 1 mL DI-water was added to dissolve the mannitol or CSLA shell, and LS was performed again, but at this time, the size of the dendriplexes released from the mannitol (or CSLA) was measured by LS (*upper left inset*). Non-denaturing agarose gel electrophoresis (*upper right inset*) show the integrity of the siRNA after its release from mannitol (or CSLA) shell and G4NH2 dendrimer by incubation in aqueous heparin solution (455 U per 1 μg siRNA) for 30 min at 37°C. Untreated siRNA (250 ng) as positive control in *lane 1*; mixture of G4NH2, mannitol (or CSLA) and heparin (but no siRNA) as negative control in *lane 2*; siRNA-G4NH2 dendriplexes at N/P 10 loaded into mannitol (or CSLA) microparticles after incubation with aqueous heparin in *lane 3*.

The hydrodynamic diameter of CSLA and mannitol microparticles measured by LS was found to be 2.0 ± 0.8 μm and 4.6 ± 0.9 μm, respectively – average and standard deviation calculated based on eight (n = 8) independent batches. These results indicate that the dendriplexes-carrying microparticles are in the desired geometric diameter for appropriate deep lung deposition (> 5 - 6 μm).[71, 72] Additionally, the microparticles displayed a spherical morphology (SEM as *inset* in Figure 5.8), which is in agreement

with previous CSLA particles prepared via emulsification diffusion[26, 40] and mannitol spray-dried particles.[73]

It is worthwhile to mention that the size of the dendriplexes was measured by LS after contacting the microparticles with aqueous solution, and it was 236 ± 75 nm and 192 ± 38 nm for CSLA and mannitol, respectively. The size distribution of these dendriplexes is shown as *inset* in Figure 5.8 – average and standard deviation calculated based on five (n = 5) independent experiments. Thus, the hydrodynamic diameter of the dendriplexes released from the shell are readily comparable to those (Table 5.1) before loading into CSLA or mannitol microparticles, and therefore, the process of forming the microparticles does not seem to induce any undesirable irreversible aggregation of the dendriplexes.

The siRNA loading efficiency (% siRNA encapsulated from the initial content in dendriplexes) into CSLA and mannitol microparticles was measured via densitometry using Image J,[34] based on the images obtained from gel electrophoresis using the protocol discussed in Section 5.2.10. siRNA loading efficiency of 49.0 ± 8.4 % was found for CSLA (230 ± 20 ng siRNA per 1 mg CSLA particles), and 25.4 ± 4.0 % (229 ± 47 ng siRNA per 1 mg mannitol particles) for mannitol. The final yield was 65% and 50% (w/w) after emulsification diffusion and spray drying, considering the initial content of CSLA and mannitol, respectively.

The integrity of the siRNA after particle preparation was also evaluated using gel electrophoresis (*inset* in Figure 5.8). The siRNA band after particle preparation was found to be very similar to the untreated siRNA control (compare *lanes 1* and *3*). However, the intensity of the band in *lane 3* – which corresponds to the siRNA released

after breaking down the mannitol or CSLA shell and dissociation from G4NH2 dendrimer – is weaker due to the reduced siRNA loading into the microparticles, as discussed above. Collectively, these results demonstrate the feasibility of encapsulating siRNA-based dendriplexes into CSLA and mannitol microparticles via emulsification diffusion and spray drying processes, respectively. The dendriplexes were successfully loaded into such microparticles (which showed appropriate size for further formulation in pMDIs), conserved their hydrodynamic diameter after particle processing and shell dissolution, and more importantly, the siRNA kept its integrity.

5.3.9 Physical stability of microparticles loaded with dendriplexes in propellant HFA

Sedimentation rate experiments of the microparticles containing dendriplexes at 25°C and saturation pressure of the propellant were performed in order to evaluate their physical stability in propellant HFA. Microparticles were weighed into pressure proof glass vials, crimp sealed with 63 μL metering valves, and a known volume of propellant HFA-227 was added to make 2 $mg.mL^{-1}$. The particles were dispersed with the aid of a sonication bath for 30 min at 15 - 20°C. Stability of the formulations was determined visually via sedimentation/flocculation rate as a function of the time after stopping the mechanical energy input from the sonication bath. Digital images were taken, and the results are presented as *insets* in Figure 5.9.

Dispersions of both CSLA and mannitol microparticles containing siRNA-G4NH2 dendriplexes at N/P 10 in propellant HFA-227 showed excellent physical stability. While some aggregation could be observed onto the walls of the canister and in the bulk

propellant, no strong flocculation or irreversible aggregation was observed (*insets* in Figure 5.9). Aggregates formed due to sedimentation could be easily re-dispersed by simple manual agitation. In the case of CSLA, the improved physical stability compared to dendriplexes alone, which are not dispersible in propellant HFA – Figure B5 in Appendix B, arises due to the enhanced solvation of the ester groups (LA chains) of CSLA by the propellant HFA.[25, 28] In the case of the mannitol, the reasons for the enhanced stability are less clear, but we expect to have an improved density matching to HFA-277 since spherical spray-dried mannitol microparticles produce densities ca. 1.47 - 1.51 $g.cm^{-3}$ (depending on the spray drying conditions)[74] and the density of HFA-227 is 1.39 at 25°C.[43] Moreover, the fact that the cohesive forces for mannitol in HFA are relatively lower compared to other sugars[71] indicates an enhanced solvation of that surface in the propellant, but this is relative to sugars and no comparison with CSLA has been shown.

5.3.10 Aerosol performance of the pMDI formulations with the engineered microparticles

An eight-stage ACI was used to characterize the aerosol properties of the HFA-based formulations containing mannitol and CSLA engineered microparticles with siRNA-G4NH2 dendriplexes (N/P 10) loaded within their core. As described earlier, free dendriplexes (negative control, with no mannitol or CSLA shell) did not disperse at all in propellant HFA-227 – the dendriplexes remained stuck onto the walls of the canister, as seen in Appendix B, and thus ACI tests could not even be performed. The siRNA content for the pMDI formulations was quantified by incubation of the deposited mass of

each ACI stage with RNase free DI-water (which broke down the mannitol or CSLA shell, thus releasing the dendriplexes to the aqueous solution) followed by freezing, lyophilization, heparin decomplexation assay (which dissociates the siRNA from the G4NH2 – Appendix B), gel electrophoresis, and densitometry using the gel images, as described in the previous sections. A summary of the results are shown in Table 5.2.

Table 5.2. Aerosol performance of pMDI formulations prepared with mannitol and CSLA microparticles loaded with siRNA-G4NH2 dendriplexes at N/P 10. All formulations at 2 mg particles per 1 mL of HFA-227 at 25°C and saturation pressure of the propellant. siRNA concentration of 290 - 550 ng.mL^{-1} in formulations prepared with dendriplexes-loaded into mannitol, and 420 - 505 ng.mL^{-1} in those prepared with CSLA. Results in ng siRNA ± deviation for n = 2 (two independent canisters) and 50 - 65 actuations each, from AC to Filter.

Stage	siRNA-G4NH2 dendriplexes loaded into microparticles	
	mannitol	CSLA
Actuator (AC)	74.3 ± 27.6	191.8 ± 13.7
Induction Port (IP)	109.6 ± 87.4	403.1 ± 61.2
Stage 0 (9.0 - 10.0 μm)	38.9 ± 0.4	72.2 ± 17.5
Stage 1 (5.8 - 9.0 μm)	42.9 ± 14.1	44.0 ± 47.6
Stage 2 (4.7 - 5.8 μm)	39.8 ± 22.2	87.5 ± 0.0
Stage 3 (3.3 - 4.7 μm)	43.1 ± 2.2	43.7 ± 28.9
Stage 4 (2.1 - 3.3 μm)	35.1 ± 8.6	112.1 ± 33.3
Stage 5 (1.1 - 2.1 μm)	33.0 ± 6.9	108.5 ± 5.2
Stage 6 (0.7 - 1.1 μm)	33.7 ± 5.6	75.6 ± 52.8
Stage 7 (0.7 - 0.4 μm)	42.8 ± 12.9	99.7 ± 46.9
Filter (0.0 - 0.4 μm)	23.1 ± 32.6	80.7 ± 17.6
FPF (%)	48.9 ± 5.7	46.1 ± 2.5
RF (%)	77.4 ± 9.9	64.3 ± 4.0
Recovery (%)	28.0 ± 10.5	84.8 ± 0.1
Single Puff Dose (ng)	9.5 ± 3.2	26.4 ± 0.7
MMAD (μm)	2.6 ± 0.5	1.9 ± 0.7
GSD	3.8 ± 0.4	3.7 ± 0.1

The FPF, an important aerosol characteristic that serves as a measure of the therapeutically beneficial portion of the inhaled mass of siRNA which would reach the lower respiratory tract,[75] was determined from the ACI results. The FPF for mannitol and CSLA microparticles was determined to be 49% and 46%, respectively, which is

excellent, falling within those of commercial HFA-based pMDIs (30 - 55% on average)[26, 76] even though no optimization of the pMDI formulations was attempted. It is worth noticing that FPF for both formulations were not significantly different (One-Way ANOVA, *p* value < 0.05). The RF – the siRNA content collected from stage 0 to filter over the total siRNA released into the impactor[27] – was found to be a little higher for pMDIs formulated with mannitol microparticles (77%) than those with CSLA (64%), but again, without significant difference (One-Way ANOVA, *p* value < 0.05).

The MMAD and GSD are properties that characterize the particles in the aerosol spray. MMAD represents the aerodynamic diameter on a mass basis, and GSD is a measure of the spread of particle size around this median.[77] As seen in Table 5.2, the MMAD and GSD of the mannitol and CSLA microparticles containing dendriplexes were not significantly different (One-Way ANOVA, *p* value < 0.05) from each other at 2.6 and 1.9 μm, and 3.8 and 3.7 μm on average, respectively. Since large particles with MMAD > 5 μm tend to sediment in the oropharynx and upper airways, and particles with MMAD between 1 and 5 μm tend to be deposited into bronchioles and deeper airways,[15] the results presented here suggest that such microparticles from both strategies – mannitol and CSLA shell – would be able to deliver siRNA to the deep lungs.

The considerable difference between both strategies came in the form of the total siRNA recovered and the siRNA content in a single puff dose, which were significantly different (One-Way ANOVA, *p* value < 0.05). While the siRNA fraction recovered in the mannitol formulation was 28% only, 85% was recovered in the CSLA formulation. The siRNA in a single puff dose from the mannitol formulation was only 9.5 ng, while that for CSLA formulation was 26 ng. These results indicate that the strategy of encapsulating

siRNA-G4NH2 dendriplexes into CSLA microparticles using emulsification diffusion technique seems to have greater efficiency for delivering siRNA to the lungs.

The results from Table 5.2 were expressed as percentages, and are shown in Figure 5.9.

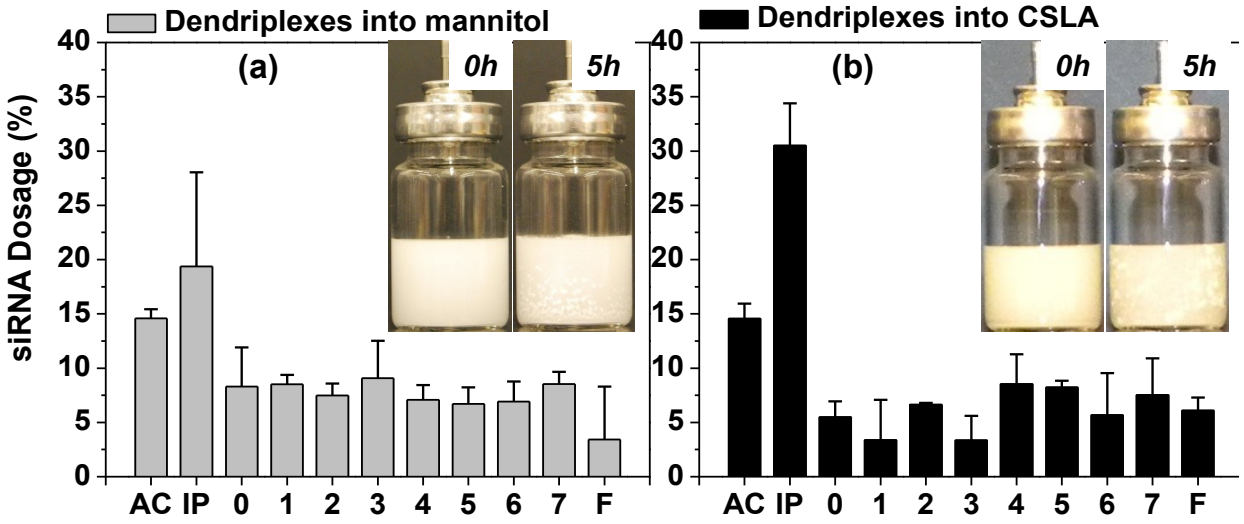

Figure 5.9. Aerosol properties of the pMDI formulations prepared with siRNA-G4NH2 dendriplexes at N/P 10 loaded into **(a)** mannitol and **(b)** CSLA microparticles. All formulations at 2 mg particles per 1 mL of HFA-227 at 25°C, and saturation pressure of the propellant. siRNA concentration of 290 - 550 ng.mL^{-1} for pMDI formulations prepared with mannitol loaded with dendriplexes, and 420 - 505 ng.mL^{-1} for those prepared CSLA loaded with dendriplexes. AC, IP, and F refer to actuator, induction port and filter, respectively. *Insets:* Physical stability of freshly prepared pMDI formulations.

Since there is no previous report in the literature discussing the formulation and aerosol characteristics of siRNA in pMDIs to date, the results shown here cannot be directly compared to other formulations, such as DPIs.[73, 78] Collectively, our results presented and discussed here indicate that pMDI formulations from both microparticle engineering strategies proposed generate aerosols conducive to deep deposition of the siRNA to the lungs. However, in terms of total siRNA recovered and the amount of siRNA actuated from the pMDI, the CSLA strategy showed a much greater efficiency.

5.4 Conclusions

This study demonstrated that siRNA-based dendriplexes can be successfully formulated in pMDIs. Dendriplexes were formed between siRNA and PAMAM G4NH2 dendrimer, and showed very high siRNA complexation efficiency, and efficient protection against RNase degradation. The *in vitro* release of siRNA from G4NH2 was found to be pH dependent, which can potentially help to keep the siRNA protected during intracellular traffic through endosomes and lysosomes, and facilitate its release in the cell cytosol. At concentrations used to measure the *in vitro* gene knockdown efficiency, both dendrimer and dendriplexes were found to be non-toxic to lung cells. siRNA-G4NH2 dendriplexes demonstrated good eGFP knockdown efficiency, and more importantly, this efficiency was kept even after transfecting siRNA stored directly in propellant HFA, strongly indicating that the biological activity of the siRNA was successfully preserved under commercial/end user conditions. Dendriplexes were loaded within non-active carriers – CSLA co-oligomer and mannitol sugar alcohol – and thus microparticles were formed with appropriate size for deep lung deposition when used in pMDIs. The size of the dendriplexes and the siRNA integrity were kept after the particle preparation processes. pMDI formulations prepared with CSLA and mannitol microparticles loaded with dendriplexes showed excellent physical stability and very good aerosol performance. Therefore, all these results are very promising, and strongly indicate that formulating siRNA-based dendriplexes into appropriate non-active microparticles has great potential to efficiently deliver siRNA to the lung tissue using portable and inexpensive pMDIs. Efforts to further optimize these proposed formulation strategies along with *in vivo* studies can help their development for knocking down

specific genes to treat medically relevant pulmonary diseases, including lung cancer, and cystic fibrosis, and asthma.

5.5 Acknowledgments

The authors would like to thank DuPont™ for the propellant HFA-227, 3M Drug Delivery Systems for the metering valves, and West Pharmaceutical Services for the canisters. At Wayne State University, we would like to thank Dr. Oupicky (for the access to the Synergy 2 Microplate Reader) and Dr. Merkel (for kindly providing the anti-eGFP and mismatch ds-DS-siRNA) at College of Pharmacy & Health Sciences; Dr. Chow (Chemistry), Dr. Mao and Dr. Matthew (Chemical Engineering and Materials Science) for access to LS and Spectra Max 250 UV plate reader; Dr. Pile (Biological Sciences) for access to the FOTO/Analyst® Investigator/Eclipse with UV Transilluminator Fotodyne; Dr. Jessica Back and Mr. Eric Van Buren (Microscopy, Imaging and Cytometry Resources Core) for the FACS analyses. The MICR Core is supported, in part, by NIH Center grant # P30CA022453 to The Karmanos Cancer Institute, and the Perinatology Research Branch of the National Institutes of Child Health and Development, both at Wayne State University.

This chapter is based on the manuscript: **Conti, D. S.**; Brewer, D.; Grashik, J.; Avasarala, S.; da Rocha, S. R. P. Dendrimer Nanocarriers and their Aerosol Formulations for siRNA Delivery to the Lung Epithelium. *To be submitted to Molecular Pharmaceutics*, **2013**.

5.6 References

1. Lam, J. K.-W.; Liang, W.; Chan, H.-K. Pulmonary delivery of therapeutic siRNA. *Adv. Drug Delivery Rev.* **2012,** *64*, (1), 1-15.
2. Pecot, C. V.; Calin, G. A.; Coleman, R. L.; Lopez-Berestein, G.; Sood, A. K. RNA interference in the clinic: Challenges and future directions. *Nat. Rev. Cancer* **2011,** *11*, (1), 59-67.
3. Siomi, H.; Siomi, M. C. On the road to reading the RNA-interference code. *Nature* **2009,** *457*, (7228), 396-404.
4. Arima, H.; Yoshimatsu, A.; Ikeda, H.; Ohyama, A.; Motoyama, K.; Higashi, T.; Tsuchiya, A.; Niidome, T.; Katayama, Y.; Hattori, K.; Takeuchi, T. Folate-PEG-appended dendrimer conjugate with α-cyclodextrin as a novel cancer cell-selective siRNA delivery carrier. *Mol. Pharmaceutics* **2012,** *9*, (9), 2591-2604.
5. Gao, K.; Huang, L. Nonviral methods for siRNA delivery. *Mol. Pharmaceutics* **2008,** *6*, (3), 651-658.
6. Taratula, O.; Garbuzenko, O. B.; Chen, A. M.; Minko, T. Innovative strategy for treatment of lung cancer: Targeted nanotechnology-based inhalation co-delivery of anticancer drugs and siRNA. *J. Drug Targeting* **2011,** *19*, (10), 900-914.
7. Singh, A.; Boldin-Adamsky, S.; Thimmulappa, R. K.; Rath, S. K.; Ashush, H.; Coulter, J.; Blackford, A.; Goodman, S. N.; Bunz, F.; Watson, W. H.; Gabrielson, E.; Feinstein, E.; Biswal, S. RNAi-mediated silencing of nuclear factor erythroid-2-related factor 2 gene expression in non-small cell lung cancer inhibits tumor growth and increases efficacy of chemotherapy. *Cancer Res.* **2008,** *68*, (19), 7975-7984.
8. Caci, E.; Melani, R.; Pedemonte, N.; Yueksekdag, G.; Ravazzolo, R.; Rosenecker, J.; Galietta, L. J.; Zegarra-Moran, O. Epithelial sodium channel inhibition in primary human bronchial epithelia by transfected siRNA. *Am. J. Respir. Cell Mol. Biol.* **2009,** *40*, (2), 211-6.
9. Li, T.; Koshy, S.; Folkesson, H. RNA interference for CFTR attenuates lung fluid absorption at birth in rats. *Respir. Res.* **2008,** *9*, (1), 55.
10. Séguin, R. M.; Ferrari, N. Emerging oligonucleotide therapies for asthma and chronic obstructive pulmonary disease. *Expert Opin. Invest. Drugs* **2009,** *18*, (10), 1505-1517.

11. Miyamoto, S.; Hattori, N.; Senoo, T.; Onari, Y.; Iwamoto, H.; Kanehara, M.; Ishikawa, N.; Fujitaka, K.; Haruta, Y.; Murai, H.; Yokoyama, A.; Kohno, N. Intra-airway administration of small interfering RNA targeting plasminogen activator inhibitor-1 attenuates allergic asthma in mice. *Am. J. Physiol.: Lung Cell. Mol. Physiol.* **2011,** *301*, (6), L908-L916.

12. Zamora, M. R.; Budev, M.; Rolfe, M.; Gottlieb, J.; Humar, A.; DeVincenzo, J.; Vaishnaw, A.; Cehelsky, J.; Albert, G.; Nochur, S.; Gollob, J. A.; Glanville, A. R. RNA interference therapy in lung transplant patients infected with respiratory syncytial virus. *Am. J. Respir. Crit. Care Med.* **2011,** *183*, (4), 531-538.

13. Li, B.-j.; Tang, Q.; Cheng, D.; Qin, C.; Xie, F. Y.; Wei, Q.; Xu, J.; Liu, Y.; Zheng, B.-j.; Woodle, M. C.; Zhong, N.; Lu, P. Y. Using siRNA in prophylactic and therapeutic regimens against SARS coronavirus in Rhesus macaque. *Nat. Med.* **2005,** *11*, (9), 944-951.

14. Fujita, Y.; Takeshita, F.; Kuwano, K.; Ochiya, T. RNAi therapeutic platforms for lung diseases. *Pharmaceuticals* **2013,** *6*, (2), 223-250.

15. Merkel, O. M.; Zheng, M.; Debus, H.; Kissel, T. Pulmonary gene delivery using polymeric nonviral vectors. *Bioconjugate Chem.* **2011**.

16. Paleos, C. M.; Tsiourvas, D.; Sideratou, Z. Molecular engineering of dendritic polymers and their application as drug and gene delivery systems. *Mol. Pharmaceutics* **2007,** *4*, (2), 169-188.

17. Heiden, T. C. K.; Dengler, E.; Kao, W. J.; Heideman, W.; Peterson, R. E. Developmental toxicity of low generation PAMAM dendrimers in zebrafish. *Toxicol. Appl. Pharmacol.* **2007,** *225*, (1), 70-79.

18. Kesharwani, P.; Gajbhiye, V.; Jain, N. K. A review of nanocarriers for the delivery of small interfering RNA. *Biomaterials* **2012,** *33*, (29), 7138-7150.

19. Zhou, J.; Wu, J.; Hafdi, N.; Behr, J.-P.; Erbacher, P.; Peng, L. PAMAM dendrimers for efficient siRNA delivery and potent gene silencing. *Chem. Commun.* **2006,** *2006*, (22), 2362.

20. Movassaghian, S.; Moghimi, H. R.; Shirazi, F. H.; Koshkaryev, A.; Trivedi, M. S.; Torchilin, V. P. Efficient down-regulation of PKC-α gene expression in A549 lung cancer cells mediated by antisense oligodeoxynucleotides in dendrosomes. *Int. J. Pharm.* **2013,** *441*, (1-2), 82-91.

21. Durcan, N.; Murphy, C.; Cryan, S.-A. Inhalable siRNA: Potential as a therapeutic agent in the lungs. *Mol. Pharmaceutics* **2008,** *5*, (4), 559-566.

22. Zhang, J.; Wu, L.; Chan, H.-K.; Watanabe, W. Formation, characterization, and fate of inhaled drug nanoparticles. *Adv. Drug Delivery Rev.* **2011,** *63*, (6), 441-455.

23. Merkel, O. M.; Beyerle, A.; Librizzi, D.; Pfestroff, A.; Behr, T. M.; Sproat, B.; Barth, P. J.; Kissel, T. Nonviral siRNA delivery to the lung: Investigation of PEG-PEI polyplexes and their *in vivo* performance. *Mol. Pharmaceutics* **2009,** *6*, (4), 1246-1260.

24. Yang, W.; Peters, J. I.; Williams III, R. O. Inhaled nanoparticles - A current review. *Int. J. Pharm.* **2008,** *356*, (1–2), 239-247.

25. Peguin, R. P. S.; Wu, L.; da Rocha, S. R. P. The ester group: How hydrofluoroalkane-philic is it? *Langmuir* **2007,** *23*, (16), 8291-8294.

26. Wu, L.; Bharatwaj, B.; Panyam, J.; da Rocha, S. Core-shell particles for the dispersion of small polar drugs and biomolecules in hydrofluoroalkane propellants. *Pharm. Res.* **2008,** *25*, (2), 289-301.

27. Bharatwaj, B.; Wu, L.; Whittum-Hudson, J. A.; Rocha, S. R. P. d. The potential for the noninvasive delivery of polymeric nanocarriers using propellant-based inhalers in the treatment of Chlamydial respiratory infections. *Biomaterials* **2010,** *31*, 7376-7385.

28. Wu, L.; Peguin, R. P. S.; da Rocha, S. R. P. Understanding solvation in hydrofluoroalkanes: *Ab Initio* calculations and chemical force microscopy. *J. Phys. Chem. B* **2007,** *111*, (28), 8096-8104.

29. Foster, K. A.; Oster, C. G.; Mayer, M. M.; Avery, M. L.; Audus, K. L. Characterization of the A549 cell line as a type II pulmonary epithelial cell model for drug metabolism. *Exp. Cell Res.* **1998,** *243*, (2), 359-366.

30. Tang, Y.; Li, Y.-B.; Wang, B.; Lin, R.-Y.; van Dongen, M.; Zurcher, D. M.; Gu, X.-Y.; Banaszak Holl, M. M.; Liu, G.; Qi, R. Efficient *in vitro* siRNA delivery and intramuscular gene silencing using PEG-modified PAMAM dendrimers. *Mol. Pharmaceutics* **2012,** *9*, (6), 1812-1821.

31. Mishra, M. K.; Gérard, H. C.; Whittum-Hudson, J. A.; Hudson, A. P.; Kannan, R. M. Dendrimer-enabled modulation of gene expression in *Chlamydia trachomatis*. *Mol. Pharmaceutics* **2012,** *9*, 413-421.

32. Molecular Probes - Invitrogen Detection Technologies, Quant-iT™ PicoGreen ® dsDNA Reagent and Kits. 2008; 'Vol.' MP 07581, pp 1-7.

33. Bedi, D.; Musacchio, T.; Fagbohun, O. A.; Gillespie, J. W.; Deinnocentes, P.; Bird, R. C.; Bookbinder, L.; Torchilin, V. P.; Petrenko, V. A. Delivery of siRNA into breast cancer cells via phage fusion protein-targeted liposomes. *Nanomed. Nanotech. Biol. Med.* **2011,** *7*, (3), 315-323.

34. Rasband, W. S. ImageJ, U. S. National Institutes of Health, Bethesda, Maryland, USA. *http://imagej.nih.gov/ij/* **1997-2012**.

35. Nomani, A.; Haririan, I.; Rahimnia, R.; Fouladdel, S.; Gazori, T.; Dinarvand, R.; Omidi, Y.; Azizi, E. Physicochemical and biological properties of self-assembled antisense/poly(amidoamine) dendrimer nanoparticles: The effect of dendrimer generation and charge ratio. *Int. J. Nanomed.* **2010,** *5*, 359.

36. Lavignac, N.; Nicholls, J. L.; Ferruti, P.; Duncan, R. Poly(amidoamine) conjugates containing doxorubicin bound via an acid-sensitive linker. *Macromol. Biosci.* **2009,** *9*, (5), 480-487.

37. Invitrogen by Life Technologies, Lipofectamine 2000. 2006; 'Vol.' 11668.2k.pps, pp 1-4.

38. Promega Corporation, CellTiter 96® aqueous non-radioactive cell proliferation assay. 2009; 'Vol.' Part# TB169, pp 1-16.

39. Promega Corporation, TransFast™ Transfection Reagent. 2009; 'Vol.' Part# TB260, pp 1-17.

40. Conti, D. S.; Bharatwaj, B.; Brewer, D.; da Rocha, S. R. P. Propellant-based inhalers for the non-invasive delivery of genes via oral inhalation. *J. Controlled Release* **2012,** *157*, (3), 406-417.

41. Lee, S. H.; Mok, H.; Lee, Y.; Park, T. G. Self-assembled siRNA-PLGA conjugate micelles for gene silencing. *J. Controlled Release* **2011,** *152*, (1), 152-158.

42. Lee, S. H.; Mok, H.; Jo, S.; Hong, C. A.; Park, T. G. Dual gene targeted multimeric siRNA for combinatorial gene silencing. *Biomaterials* **2011,** *32*, (9), 2359-2368.

43. Rogueda, P. G. A. HPFP, a model propellant for pMDIs. *Drug Dev. Ind. Pharm.* **2003,** *29*, (1), 39-49.

44. U.S. Department of Health and Human Services, Guidance for industry - metered dose inhaler (MDI) and dry powder inhaler (DPI) drug products - chemistry, manufacturing, and controls

documentation. Food and Drug Administration (FDA), Center for Drug Evaluation and Research (CDER): 1998; p 62.

45. Antipina, M. N.; Gainutdinov, R. V.; Rachnyanskaya, A. A.; Tolstikhina, A. L.; Yurova, T. V.; Khomutov, G. B. Studies of nanoscale structural ordering in planar DNA complexes with amphiphilic mono- and polycations. *Surf. Sci.* **2003,** *532-535*, (0), 1025-1033.

46. Jensen, L. B.; Pavan, G. M.; Kasimova, M. R.; Rutherford, S.; Danani, A.; Nielsen, H. M.; Foged, C. Elucidating the molecular mechanism of PAMAM-siRNA dendriplex self-assembly: Effect of dendrimer charge density. *Int. J. Pharm.* **2011,** *416*, (2), 410-418.

47. Biswas, S.; Deshpande, P. P.; Navarro, G.; Dodwadkar, N. S.; Torchilin, V. P. Lipid modified triblock PAMAM-based nanocarriers for siRNA drug co-delivery. *Biomaterials* **2013,** *34*, (4), 1289-1301.

48. Pavan, G. M.; Posocco, P.; Tagliabue, A.; Maly, M.; Malek, A.; Danani, A.; Ragg, E.; Catapano, C. V.; Pricl, S. PAMAM dendrimers for siRNA delivery: Computational and experimental insights. *Chem. Eur. J.* **2010,** *16*, (26), 7781-7795.

49. Juliano, R.; Bauman, J.; Kang, H.; Ming, X. Biological barriers to therapy with antisense and siRNA oligonucleotides. *Mol. Pharmaceutics* **2009,** *6*, (3), 686-695.

50. Perez, A. P.; Romero, E. L.; Morilla, M. J. Ethylendiamine core PAMAM dendrimers/siRNA complexes as *in vitro* silencing agents. *Int. J. Pharm.* **2009,** *380*, (1-2), 189-200.

51. Kang, H.; DeLong, R.; Fisher, M. H.; Juliano, R. L. TAT-conjugated PAMAM dendrimers as delivery agents for antisense and siRNA oligonucleotides. *Pharm. Res.* **2005,** *22*, (12), 2099-2106.

52. Mao, S.; Neu, M.; Germershaus, O.; Merkel, O.; Sitterberg, J.; Bakowsky, U.; Kissel, T. Influence of polyethylene glycol chain length on the physicochemical and biological properties of poly(ethylene imine)-*graft*-poly(ethylene glycol) block copolymer/siRNA polyplexes. *Bioconjugate Chem.* **2006,** *17*, (5), 1209-1218.

53. Liu, Y.; Bryantsev, V. S.; Diallo, M. S.; Goddard Iii, W. A. PAMAM dendrimers undergo pH responsive conformational changes without swelling. *J. Am. Chem. Soc.* **2009,** *131*, (8), 2798-2799.

54. De Rosa, G.; Quaglia, F.; Bochot, A.; Ungaro, F.; Fattal, E. Long-term release and improved intracellular penetration of oligonucleotide-polyethylenimine complexes entrapped in biodegradable microspheres. *Biomacromolecules* **2003,** *4*, (3), 529-536.

55. Jain, K.; Kesharwani, P.; Gupta, U.; Jain, N. K. Dendrimer toxicity: Let's meet the challenge. *Int. J. Pharm.* **2010,** *394*, (1–2), 122-142.

56. Jevprasesphant, R.; Penny, J.; Jalal, R.; Attwood, D.; McKeown, N. B.; D'Emanuele, A. The influence of surface modification on the cytotoxicity of PAMAM dendrimers. *Int. J. Pharm.* **2003,** *252*, (1-2), 263-266.

57. Li, C.; Liu, H.; Sun, Y.; Wang, H.; Guo, F.; Rao, S.; Deng, J.; Zhang, Y.; Miao, Y.; Guo, C.; Meng, J.; Chen, X.; Li, L.; Li, D.; Xu, H.; Wang, H.; Li, B.; Jiang, C. PAMAM nanoparticles promote acute lung injury by inducing autophagic cell death through the Akt-TSC2-mTOR signaling pathway. *J. Mol. Cell Biol.* **2009,** *1*, (1), 37-45.

58. Kannan, S.; Kolhe, P.; Raykova, V.; Glibatec, M.; Kannan, R. M.; Lieh-Lai, M.; Bassett, D. Dynamics of cellular entry and drug delivery by dendritic polymers into human lung epithelial carcinoma cells. *J. Biomater. Sci., Polym. Ed.* **2004,** *15*, 311-330.

59. Kim, Y.; Klutz, A. M.; Jacobson, K. A. Systematic investigation of polyamidoamine dendrimers surface-modified with poly(ethylene glycol) for drug delivery applications: Synthesis, characterization, and evaluation of cytotoxicity. *Bioconjugate Chem.* **2008,** *19*, (8), 1660-1672.

60. Wang, X.-L.; Xu, R.; Lu, Z.-R. A peptide-targeted delivery system with pH-sensitive amphiphilic cell membrane disruption for efficient receptor-mediated siRNA delivery. *J. Controlled Release* **2009,** *134*, (3), 207-213.

61. Merkel, O. M.; Mintzer, M. A.; Librizzi, D.; Samsonova, O.; Dicke, T.; Sproat, B.; Garn, H.; Barth, P. J.; Simanek, E. E.; Kissel, T. Triazine dendrimers as nonviral vectors for *in vitro* and *in vivo* RNAi: The effects of peripheral groups and core structure on biological activity. *Mol. Pharmaceutics* **2010,** *7*, (4), 969-983.

62. Zheng, M.; Librizzi, D.; Kılıç, A.; Liu, Y.; Renz, H.; Merkel, O. M.; Kissel, T. Enhancing *in vivo* circulation and siRNA delivery with biodegradable polyethylenimine-graft-polycaprolactone-block-poly(ethylene glycol) copolymers. *Biomaterials* **2012,** *33*, (27), 6551-6558.

63. Lin, S.-Y.; Zhao, W.-Y.; Tsai, H.-C.; Hsu, W.-H.; Lo, C.-L.; Hsiue, G.-H. Sterically polymer-based liposomal complexes with dual-shell structure for enhancing the siRNA delivery. *Biomacromolecules* **2012,** *13*, (3), 664-675.

64. Tschuch, C.; Schulz, A.; Pscherer, A.; Werft, W.; Benner, A.; Hotz-Wagenblatt, A.; Barrionuevo, L.; Lichter, P.; Mertens, D. Off-target effects of siRNA specific for GFP. *BMC Mol. Biol.* **2008,** *9*, (1), 60.

65. Naito, Y.; Yamada, T.; Matsumiya, T.; Ui-Tei, K.; Saigo, K.; Morishita, S. dsCheck: Highly sensitive off-target search software for double-stranded RNA-mediated RNA interference. *Nucleic Acids Res.* **2005,** *33*, (suppl 2), W589-W591.

66. Merkel, O. M.; Beyerle, A.; Beckmann, B. M.; Zheng, M.; Hartmann, R. K.; Stöger, T.; Kissel, T. H. Polymer-related off-target effects in non-viral siRNA delivery. *Biomaterials* **2011,** *32*, (9), 2388-2398.

67. Akhtar, S.; Benter, I. Toxicogenomics of non-viral drug delivery systems for RNAi: Potential impact on siRNA-mediated gene silencing activity and specificity. *Adv. Drug Delivery Rev.* **2007,** *59*, (2-3), 164-182.

68. Wanakule, P.; Liu, G. W.; Fleury, A. T.; Roy, K. Nano-inside-micro: Disease-responsive microgels with encapsulated nanoparticles for intracellular drug delivery to the deep lung. *J. Controlled Release* **2012,** *162*, (2), 429-437.

69. Patton, J. S.; Byron, P. R. Inhaling medicines: Delivering drugs to the body through the lungs. *Nat. Rev. Drug Discovery* **2007,** *6*, (1), 67-74.

70. Kho, K.; Hadinoto, K. Effects of excipient formulation on the morphology and aqueous re-dispersibility of dry-powder silica nano-aggregates. *Colloids Surf. A, Physicochem. Eng. Asp.* **2010,** *359*, (1–3), 71-81.

71. Young, P. M.; Adi, H.; Patel, T.; Law, K.; Rogueda, P.; Traini, D. The influence of micronised particulates on the aerosolisation properties of pressurised metered dose inhalers. *J. Aerosol Sci.* **2009,** *40*, (4), 324-337.

72. Son, Y.-J.; McConville, J. T. Advancements in dry powder delivery to the lung. *Drug Dev. Ind. Pharm.* **2008,** *34*, (9), 948-959.

73. Jensen, D. M. K.; Cun, D.; Maltesen, M. J.; Frokjaer, S.; Nielsen, H. M.; Foged, C. Spray drying of siRNA-containing PLGA nanoparticles intended for inhalation. *J. Controlled Release* **2010,** *142*, (1), 138-145.

74. Elversson, J.; Millqvist-Fureby, A. Particle size and density in spray drying - Effects of carbohydrate properties. *J. Pharm. Sci.* **2005,** *94*, (9), 2049-2060.

75. Mitchell, J. P.; Nagel, M. W.; Wiersema, K. J.; Doyle, C. C. Aerodynamic particle size analysis of aerosols from pressurized metered-dose inhalers: Comparison of Andersen 8-stage cascade impactor, next generation pharmaceutical impactor, and model 3321 aerodynamic particle sizer aerosol spectrometer. *AAPS PharmSciTech* **2003,** *4*, (4), 1-9.

76. McCabe, J. C.; Koppenhagen, F.; Blair, J.; Zeng, X.-M. ProAir® HFA delivers warmer, lower-impact, longer-duration plumes containing higher fine particle dose than Ventolin® HFA. *J. Aerosol Med. Pulm. Drug Delivery* **2012,** *25*, (2), 104-109.

77. LeBelle, M.; Pike, R. K.; Graham, S. J.; Ormsby, E. D.; Bogard, H. A. Metered-dose inhalers I: Drug content and particle size distribution of beclomethasone dipropionate. *J. Pharm. Biomed. Anal.* **1996,** *14*, (7), 793-800.

78. Jensen, D. K.; Jensen, L. B.; Koocheki, S.; Bengtson, L.; Cun, D.; Nielsen, H. M.; Foged, C. Design of an inhalable dry powder formulation of DOTAP-modified PLGA nanoparticles loaded with siRNA. *J. Controlled Release* **2012,** *157*, (1), 141-148.

CHAPTER 6

siRNA-Dendrimer Conjugates for the Lung Epithelium: Synthesis, Characterization, and Gene Silencing

6.1 Introduction

Since the discovery that RNA interference (RNAi) is operated by long double-stranded RNA (ds-RNA) in a nematode,[1] and that it can be mediated by small interfering RNA (siRNA) in mammalian cells,[2] RNAi has become a potent tool in biological research, and an important therapeutic approach to treat genetic disorders.[3] RNAi promotes silencing of gene expression in a post-transcriptional manner,[4] and its mechanism has been extensively discussed in the literature.[3, 5-7] Specificity, potency, and versatility are the major advantages of RNAi.[3] siRNAs are designed for high specific suppression of the target gene, and any type of gene can be targeted. The synthesis of siRNA is simple and very straightforward in contrast to therapeutic proteins, for instance. Compared to other types of gene therapies – e.g. DNA – siRNAs act in the cell cytoplasm thus avoiding an even greater barrier which is the nuclear envelope (in the case of DNA). siRNAs are robust, potent, have low risk of cytotoxic effects, and are catalytic in nature.[3] Therefore, RNAi offers great opportunity for the local and systemic treatment of gene-causing and gene-promoting diseases such as cancer,[8-14] diabetes,[8] and viral infections,[9, 10] in different types of tissues and organs, such as skin,[3, 15] lung,[4, 16-18] eye, nervous and digestive systems.[3]

However, the progress of siRNA delivery systems has been hampered largely by the lack of efficient nanocarriers capable to overcome the many extra and intracellular

barriers that siRNA faces to reach its target (the cytosol). Local extracellular barriers depend on the physiological structure of the target tissue.[19] Phagocytosis and interaction with bloodstream components, degradation by serum nucleases, extravasation (the transport from the intravascular space within blood vessels into the tissue interstitium), transport across the interstitial space to the target cells, and diffusion through the extracellular matrix[19, 20] are the extracellular barriers involved in systemic delivery of siRNA. Cellular internalization, endolysosomal escape, degradation by nucleases during the cytoplasmic trafficking, release from the carrier into the cell cytosol, and assembly into the RNA-induced silencing complex (RISC) are the major intracellular barriers.[21]

Since the administration of free siRNA usually fails to produce the desired therapeutic effect,[19, 22] current research has focused on natural or synthetic carriers (viruses, lipids, peptides, and polymers) engineered to pack, protect, and deliver the siRNA to the target cell.[22, 23] However, with regards to siRNA delivery systems based on the complexation with cationic polymers (polyplexes and dendriplexes, in the case of dendrimers) there are key disadvantages. The sizes vary widely from as low as 50 nm to ca. 750 nm – the process of particle formation cannot be controlled (entropically driven) and thus the particle size distribution has high polydispersity and variable shapes[24-26] which affect the cellular uptake.[27] Moreover, the highly positive charges from the complexes can be cytotoxic due to non-specific interactions with the cellular components,[28, 29] and moreover, cause aggregation in negatively charged fluids (e.g. serum, mucus, lung surfactant, and bronchoalveolar lavage – BAL).[24, 28, 29] The positively charged complexes can be entrapped by the negatively charged fluid

components, and thus have reduced transport and cellular uptake.[30] However, it has been demonstrated that charge is necessary, but not sufficient enough for cellular uptake.[31] Additionally, in order to compact the siRNA into nanoparticles (NPs), high amount of the cationic polymer is required (nitrogen/phosphate ratio – N/P – between 5 and 30) and due to this, the toxic effects may be significant.[9, 32]

In order to address the issues discussed above, the direct conjugation of molecules (e.g. antibodies, peptides, and polymers) to siRNA has been proposed as an alternative which can improve *in vivo* pharmacokinetic behavior of the siRNA, enhance its biological half-life, and increase the delivery efficiency to the target cell population, while maintaining the gene silencing activity.[33] Several reports have described the conjugation of siRNA with different compounds, e.g. HA,[34] PLGA,[35] PEG,[36-43] PLL-PEG-peptide,[44] gold (Au)[45, 46] and magnetic NPs,[47] QD,[48, 49] α-tocopherol,[50] poly(PEG acrylate),[51] amphipathic poly(vinyl ether),[52] and cell penetrating peptides.[53-55] Therefore, siRNA has a great versatility to be conjugated to several different molecules, and thus, the development of siRNA-based conjugates seems to be a viable strategy to overcome the extra and intracellular barriers present in the target tissue.

PAMAM dendrimers are highly branched polymers with low polydispersity, high functionality, and provide an ideal structure for construction of effective drug carriers, gene transfer vehicles, and imaging of biological systems.[56, 57] There has been a growing interest in the use of PAMAM with low generation (≤ G4) due to their low cytotoxicity at the needed concentrations in the delivery system.[58] In terms of conjugation, PAMAM dendrimers are very attractive as polymeric nanocarriers (PNCs) due to their very small size (c.a. 4.5 nm), molecular uniformity, and abundance of

functional groups that allow for chemical modification and linkage of different molecules.[9] Thus, PAMAM dendrimers are very promising PNCs for conjugation with siRNA. However, besides the great potential of PAMAM, their application to direct conjugation with siRNA in order to develop siRNA-delivery systems has not been explored in literature to date.

In this work we propose the use of generation-four amine-terminated PAMAM dendrimer (G4NH2) as PNC for conjugation with siRNA. We report here a strategy for the conjugation that facilitates cytosol delivery, the characterization of the conjugates, and their *in vitro* gene knockdown efficiency. G4NH2 and siRNA were conjugated via a reducible disulfide bond, and it is expected to be cleaved in the reductive cytosolic space, releasing the siRNA in the cytoplasm.[33] The ability of G4NH2-siRNA conjugates to deliver siRNA to the lung epithelium was tested using *in vitro* gene knockdown experiments in A549 cells stably expressing eGFP. This is the first report on siRNA-dendrimer conjugates, and such siRNA-delivery system has potential for conjugation with target ligands, pH- and reducible-trigged molecules, and thus, the cell specificity and gene silencing efficiency can be improved. Moreover, this work is relevant since it contributes for the development of siRNA-based therapies to treat medically relevant diseases.

6.2 Experimental Section

6.2.1 Materials

Generation-four amine-terminated poly(amidoamine) dendrimer (PAMAM G4NH2) with 64 NH2 surface groups and 14,215 $g.mol^{-1}$ (according to the supplier) was

purchased from Dendritech Inc. G4NH2 was received in methanol (15.35 w/w), which was removed by rotary evaporation (Buchi R-200) prior to use. *N*-succinimidyl 3-(2-pyridyldithio) propionate crosslinker (SPDP) was purchased from ProteoChem Inc. Double-stranded Dicer substrate siRNA (ds-DS-siRNA with 25/27 bp) targeting eGFP (sense: 5'- p ACC CUG AAG UUC AUC UGC ACC AC cg -3'; antisense: 5'- p CGG UGG UGC AGA UGA ACU UCA GGG UCA -3')[59] was purchased from Dharmacon Inc. (Thermo Fisher Scientific Biosciences). The 3'-end of the sense strand was modified with a thiol group (SH) and supplied in a protected form (SS) to prevent the formation of dimers.[60] Capital letters in the sequence above represent ribonucleotides, underlined bases depict 2′-O-methylribonucleotides, lower case letters represent 2′-deoxyribonucleotides, and "p" depicts an additional phosphate at the 5'-end. An irrelevant ds-siRNA (19/21 bp) not targeting eGFP and having a thiol modification in the 5'-end of the antisense strand was provided from Bioneer Inc. Deionized water (DI-water, resistivity of 18.2 MΩ.cm) was obtained from a NANOpure® DIamond™ UV ultrapure water system (Barnstead International), and treated with diethylpyricarbonate (DEPC, high purity grade) at 0.1% v/v overnight, following autoclaving. DEPC and EDTA (0.5 M sterile solution, pH 8, DEPC-treated) were purchased from Amresco. A549 cell line (human lung adenocarcinoma cells, an *in vitro* model of Type II alveolar epithelium)[61] was purchased from ATCC® (CCL-185™, passage 82). Gibco® Dulbecco's Modified Eagle Medium (DMEM, high glucose, GlutaMAX™, pyruvate), Gibco® Penicillin-Streptomycin Liquid (AB), and Lipofectamine® 2000 Transfection Reagent were purchased from Invitrogen™ Life Technologies Corporation. Fetal Bovine Serum Advantage (FBS, non-heat inactivated, S11050) was purchased from

Atlanta Biologicals Inc. Puromycin dihydrochloride (10 $mg.mL^{-1}$) was purchased from Toku-E. Trypsin EDTA 1X (0.25% trypsin, 2.21 mM EDTA in HBSS) Corning® Cellgro® was purchased from Mediatech Inc. TransFast™ Transfection Reagent was purchased from Promega Corporation. Cell culture flasks Cellstar® (75 cm^2) and 24-well Costar® cell culture microplates (flat bottom, tissue culture treated, polystyrene, sterile) were purchased from Corning® Inc. Dithiothreitol (DTT), fluorescein isothiocyanate (FITC), tris (2-carboxyethyl) phosphine hydrochloride solution (TCEP, Bond-Breaker®), sodium acetate anhydrous (99%), glacial acetic acid (100%), acetonitrile (HPLC grade, 99.9%), phosphate buffered saline (PBS 10X solution) were purchased from Thermo Fisher Scientific Inc. Amicon® Ultra-15 and Ultra-0.5 Centrifugal Filters (3K and 30K MWCO, respectively) were purchased from EMD Millipore Co. Dialysis membrane (1K MWCO Spectra/Por®) was purchased from Spectrum® Laboratories Inc. Ellman's Reagent – 5,5'-dithio-bis-(2-nitrobenzoic acid) – was purchased from Alfa Aesar. SaeKem® LE Agarose was purchased from Lonza. Ethidium bromide (98%, 10 $mg.mL^{-1}$) was purchased from IBI Scientific. Tris Base ultrapure bioreagent (99.5%) was purchased from J.T.Baker. Deuterium oxide (D_2O, 99.9%) was purchased from Cambridge Isotope Laboratories Inc. Monobasic sodium phosphate (monohydrate, 98-102%), dibasic sodium phosphate (anhydrous, 99%), and sodium chloride (99%) were purchased by EMD Chemicals Inc. Sodium azide SigmaUltra, 2,5-dihydroxybenzoic acid (DHB, 98%), p-toluenesulfonic acid monohydrate (p-TSA, 98.5%) were purchased from Sigma Aldrich. Dimethyl sulfoxide (DMSO, anhydrous, 99.7%, AcroSeal™) was purchased from Acros Organics. Ethanol (200 proof) was purchased from Decon Labs.

6.2.2 Synthesis and characterization of G4NH2-PDP conjugates

Figure 6.1(a) represents the reaction scheme between G4NH2 dendrimer and SPDP crosslinker.

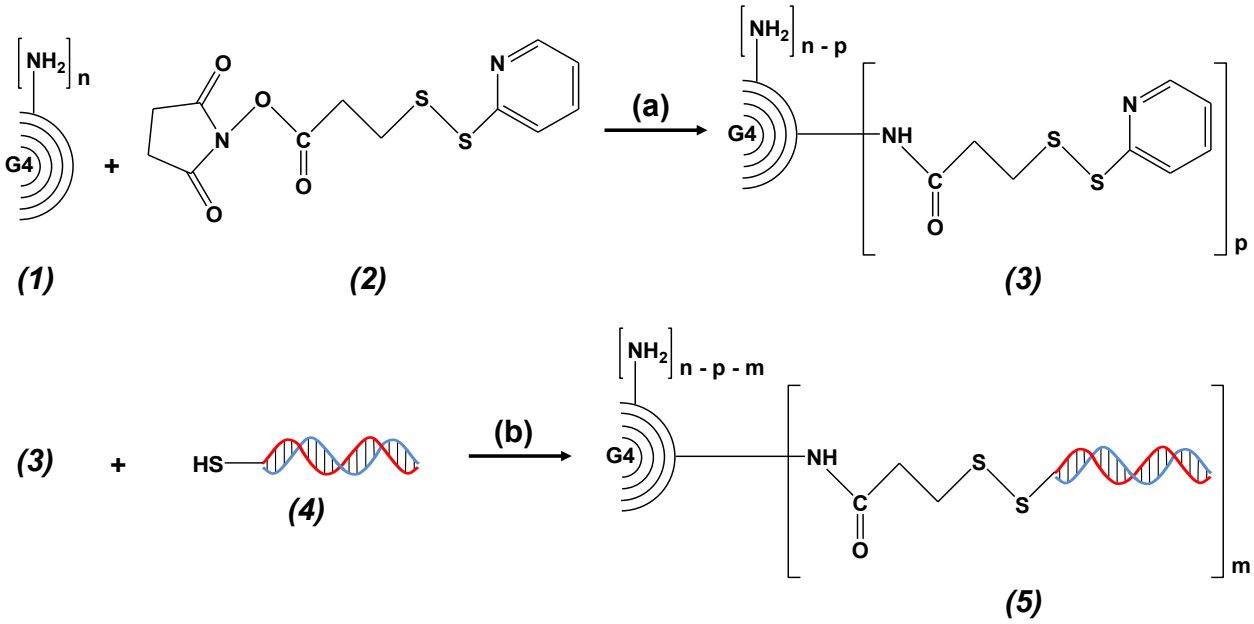

Figure 6.1. Schematic illustrating the two-step preparation of G4NH2-siRNA conjugate. **(a)** Synthesis of the G4NH2-PDP ***(3)*** via reaction between G4NH2 ***(1)*** and SPDP ***(2)*** crosslinker. **(b)** Synthesis of G4NH2-siRNA conjugate ***(5)*** via reaction between G4NH2-PDP ***(3)*** prepared in the first step and siRNA-SH immediately after thiol deprotection ***(4)***.

A known amount of G4NH2 ***(1)*** was dissolved in 6 mL PBS:EDTA (100 mM sodium phosphate, 150 mM NaCl, 1 mM EDTA, 0.02 % sodium azide, pH 7.5 buffer),[62] and a known amount of SPDP ***(2)*** was dissolved in 2 mL anhydrous DMSO. The G4NH2 solution was placed in ice-cold water, kept under agitation, and then the SPDP solution was added dropwise, and reacted for a total of 4 h. The reaction proceeded at room temperature and under agitation for further 24 h. The G4NH2-PDP conjugate ***(3)*** was concentrated using Amicon® Ultra-15 Centrifugal Filter (3K MWCO), followed by purification with RNase free DI-water to remove unreacted SPDP. The purified G4NH2-

PDP conjugate was frozen at -20°C overnight and lyophilized (Labconco Freeze Zone 1) at -47°C and 0.055 mbar for 48 h.

The final product (G4NH2-PDP conjugate) was stored at -20°C and characterized according to the Pyridine-2-Thione Assay[62] to determine the level of SPDP modification on the G4NH2. Briefly, the absorbance of the conjugate was measured in UV-Vis Spectrophotometer (JASCO V-630 with the SAH-769 One Drop Accessory) before and after reaction with DTT as reducing agent, which breaks the disulfide bond in the pyridyldithiol-activated dendrimer (G4NH2-PDP), and thus, enables the release of pyridine 2-thione, a molecule that is UV active at 343 nm.

The molecular weight (Mw) of the pure G4NH2 and G4NH2-PDP conjugate was evaluated by MALDI-TOF (Bruker Ultraflex). Briefly, the sample was dissolved in a mixture of DI-water and acetonitrile (50:50 v/v) and 1 µL was mixed with 1 µL of matrix solution (DHB, 30 $mg.mL^{-1}$) on the target plate (MTP 384, Bruker) and allowed to dry at room temperature prior to MALDI-TOF analysis. Proton Nuclear Magnetic Resonance (^{1}H-NMR, Varian Mercury 400, D_2O as solvent) was used to evaluate the chemical structure of the G4NH2 before and after conjugation of the SPDP crosslinker. Light Scattering (LS, Malvern ZetaSizer Nano ZS) was used to measure size and surface charge (zeta potential, ζ) of the pure G4NH2 and G4NH2-PDP conjugate. Samples were diluted to 1 mL using DI-water (5 - 50 µM) and measurements were performed at 25°C using refractive index, viscosity, and dielectric constant of DI-water. ζ calculations were performed according to Smoluchowski Model.

Fluorescent-labeled G4NH2-PDP conjugate was synthesized for the quantification of the number of siRNA molecules conjugated per dendrimer nanocarrier.

FITC was first conjugated to G4NH2, followed by the attachment of the SPDP on the dendrimer surface. Briefly, a known amount of G4NH2 was dissolved in 15 mL anhydrous DMSO, and kept under agitation at room temperature. A known amount of the catalist p-toluenesulfonic acid (p-TSA) was dissolved in 5 mL anhydrous DMSO, and added to the dendrimer solution. Next, FITC was dissolved in 5 mL anhydrous DMSO, and added to the dendrimer solution as well. The reaction proceeded under agitation, in the dark, and at room temperature for 48 h. The product was dialyzed against DI-water (1K MWCO Spectra/Por® dialysis membrane) for 4 days, concentrated using Amicon® Ultra-15 Centrifugal Filter (3K MWCO), and purified with PBS:EDTA pH 7.5 buffer[62] supplemented with 1M NaCl followed by RNase free DI-water in order to remove pTSA and unreacted FITC. The purified G4NH2-FITC conjugate was frozen at -20°C overnight, lyophilized (Labconco Freeze Zone 1) at -47°C and 0.055 mbar for 48 h, and characterized according to ^{1}H-NMR and MALDI-TOF, as described earlier in this section. Next, the G4NH2-FITC conjugate was reacted with SPDP according to the same methodology described earlier for pure G4NH2 and SPDP. The G4NH2-FITC-PDP conjugate was thus obtained, and characterized according to Pyridine-2-Thione Assay[62], ^{1}H-NMR, and LS, as detailed above.

6.2.3 Synthesis and characterization of G4NH2-siRNA conjugates

The reaction scheme for the conjugation of siRNA to the dendrimer nanocarrier is shown in Figure 6.1(b). The 2-pyridyldithio group in the PDP molecule attached on G4NH2 reacts optimally with sulfhydryl groups (SH) at pH 7 - 8.[62]

However, prior the synthesis of the G4NH2-siRNA conjugates, the integrity of the siRNA-SH under the reaction conditions was evaluated via gel electrophoresis. A known amount of the thiol-modified siRNA was deprotected according to protocol from the supplier,[60] and the siRNA-SH was dissolved in 0.5 mL PBS:EDTA pH 7.5 buffer supplemented with 1M NaCl,[62] kept under agitation and at room temperature for several days. The reaction conditions were thus reproduced, but without the presence of PDP-modified G4NH2 dendrimer. Aliquots were sampled out from this simulated reaction according to specific time points and stored at -20°C. The samples were then loaded into the slots of a 2% (w/v) non-denaturing agarose gel prepared with TAE 1X buffer and stained with 0.5 $\mu g.mL^{-1}$ of ethidium bromide. Untreated protected and deprotected siRNA were used as the controls. The electrophoresis was performed at 60 V (E0160-VWR Mini Gel Electrophoresis) for 40 min, and the siRNA-dye migration was observed under UV irradiation (FOTO/Analyst® Investigator/Eclipse with UV Transilluminator, Fotodyne Inc.). The images were recorded using the FOTO/Analyst® PC Image software (v.5).

The synthesis of G4NH2-siRNA conjugates was then performed according to reaction scheme in Figure 6.1(b). A known amount of G4NH2-PDP was dissolved in 0.5 mL PBS:EDTA 1M NaCl pH 7.5 buffer,[62] kept under agitation and room temperature for 30 min. Next, the air was purged from outside the flask using a light flow of nitrogen for 3 h. The flow of nitrogen was then stopped, and the G4NH2-PDP solution was kept under agitation at room temperature in a sealed environment. The thiol groups of a large excess of thiol-modified siRNA were deprotected according to the protocol.[60] Immediately after deprotection, the siRNA-SH ***(4)*** was dissolved in 0.5 mL PBS:EDTA

1M NaCl pH 7.5 buffer,[62] added to the G4NH2-PDP ***(3)*** in solution, and the reaction proceeded under agitation, at room temperature for 4 - 5 days. Prior the reaction, an aliquot of the siRNA-SH solution was used to quantify the amount of free sulfhydryl groups according to Ellman's Assay[63] to evaluate the thiol deprotection efficiency.[44, 64] The G4NH2-siRNA conjugate ***(5)*** was concentrated using Amicon® Ultra-0.5 Centrifugal Filter (30K MWCO), purified with several washes of PBS:EDTA 1M NaCl pH 7.5 buffer[62] and RNase free DI-water in order to remove unreacted siRNA-SH and G4NH2-PDP. The purified G4NH2-siRNA conjugates were stored at -20°C.

The siRNA content in the conjugate was quantified according to a UV linear calibration curve by measuring the siRNA absorbance at 260 nm. To confirm the cleavage of the reducible disulfide bond between G4NH2 and siRNA, a known amount of G4NH2-siRNA conjugate (equivalent to 300 ng siRNA) was reacted with DTT (reducing agent) in PBS:EDTA pH 8.3 buffer, under vortex at 1500 rpm, room temperature for 3 h. DTT was at the final concentration of 40 mM, which mimics the intracellular reducing environment[65]. After the DTT reaction, the sample was stored at -20°C overnight, and gel electrophoresis was performed as detailed earlier. Free untreated siRNA and G4NH2-siRNA conjugate without exposure to DTT were used as controls. The siRNA content conjugated on the G4NH2 was also quantified by densitometry using Image J 1.42q[66] based on the electrophoresis images.[35, 37, 67, 68]

The size and surface charge of the G4NH2-siRNA conjugates (equivalent to 1 - 5 μM siRNA) was evaluated by LS, as described in the previous section.

Fluorescent-labeled G4NH2-siRNA conjugates were synthesized for the quantification of the number of siRNA molecules per dendrimer nanocarrier. Briefly, the

G4NH2-FITC-PDP conjugate was reacted with siRNA-SH according to scheme shown in Figure 6.1(b), and thus the G4NH2-FITC-siRNA conjugates were prepared. The same methodology described earlier for the G4NH2-siRNA conjugates was used for reaction and characterization of the G4NH2-FITC-siRNA conjugates. In addition, the G4NH2 content was quantified based on a UV linear calibration curve of G4NH2-FITC-PDP by measuring the FITC absorbance at 502 nm, so that we could quantify the number of siRNA conjugated per dendrimer nanocarrier.

6.2.4 *In vitro* gene knockdown

In order to evaluate the gene knockdown efficiency *in vitro* of the G4NH2-siRNA conjugates, A549 cells stably expressing eGFP were developed as described in Appendix B. After establishing the eGFP A549 cell line, eGFP knockdown experiments were performed using G4NH2 conjugated to ds-DS-siRNA targeting eGFP – the positive sequence siRNA(+) – and G4NH2 conjugated to an irrelevant ds-siRNA that does not target eGFP, the siRNA(–). Thus, G4NH2-siRNA(+) and G4NH2-siRNA(–) conjugates were synthesized and characterized as described in the previous sections. Commercial transfection reagents (Lipofectamine® 2000 and TransFast™)[69, 70] were used as positive controls to deliver non-conjugated siRNA(+) and siRNA(–). Free siRNA (+ and –) were used as a negative controls. eGFP knockdown experiments were performed according to Lipofectamine® 2000 protocol.[69] Firstly, eGFP A549 cells were seeded onto 75 cm^2 cell culture flasks and subcultured until approximately 90% confluence. The culture medium (DMEM with 10% FBS v/v and 2.5 $\mu g.mL^{-1}$ puromycin selective antibiotic) was changed every two days. Then, eGFP expressing A549 cells

(passages 10 - 20 from the original passage provided by ATCC®) were seeded in a 24-well culture plate (60,000 cells per well) and cultured in 500 μL DMEM supplemented with 10% FBS (v/v, no antibiotics) for 24 h at 37°C and 5% CO_2 (Thermo Scientific Incubator, NAPCO 8000WJ). Cells were rinsed with PBS 1X buffer, and 250 μL transfection medium (DMEM containing siRNA (+ or –) equivalent to 20, 40, or 80 pmol per well – 80, 160, or 320 nM siRNA, respectively) was added to the wells, and the transfection proceeded for 6 h at 37°C and 5% CO_2. The transfection medium was then replaced by 500 μL culture medium (DMEM with 10% FBS only, no antibiotics) and the cells were returned to the incubator for 72 h at 37°C and 5% CO_2. Cells were dispersed in 1 mL PBS 1X buffer, and the median fluorescence intensity (MFI) was measured by flow cytometer (FACS, HWCRC 615 - BD LSR II Analyzer). Cellular debris due to dead or damaged dying cells was gated out during the FACS analyses to assure collection of data from 10,000 to 20,000 living cells. Untreated non-eGFP and eGFP A549 cells were used as controls. The level of eGFP expression in untreated eGFP expressing A549 cells was taken as 100% MFI. The % eGFP knockdown efficiency was calculated by correlating the eGFP expression of the untreated eGFP A549 cells with that from transfected cells. All transfection experiments were performed at a minimum of triplicates ($n \geq 3$).

6.3 Results and Discussion

6.3.1 Synthesis and characterization of G4NH2-PDP conjugates

G4NH2-PDP conjugates were prepared as shown in Figure 6.1(a). The level of SPDP modification on the G4NH2 surface was quantitatively determined according to

the Pyridine-2-Thione Assay,[62] and it was found to be ca. 15 PDP molecules per G4NH2. ^{1}H-NMR spectrum of the G4NH2-PDP conjugate (Figure 6.2b) indicated the presence of protons corresponding to the aromatic ring of the thiopyridyl group[71, 72] – 7.059 ppm (1H, Ar), 7.588 ppm (1H, Ar), and 8.166 ppm (2H, Ar) – which evidence the successful linkage of the SPDP crosslinker to G4NH2. Comparing the ^{1}H-NMR spectra of the pure G4NH2 (Figure 6.2a) and G4NH2-PDP (Figure 6.2b) conjugate at the region 6 - 9 ppm, the peaks assigned to PDP can be clearly observed. Calculations based on the ^{1}H-NMR spectrum of the G4NH2-PDP (Figure 6.2b) considering the integral intensities of the peaks at 8.166 ppm (2H from thiopyridyl group of the PDP) and 2.207 ppm (248H from methylene next to the carbonyl group of the PAMAM G4NH2)[73-76] indicated 14 PDP molecules per G4NH2. This result is in excellent agreement with that generated by UV-Vis spectroscopy method.

MALDI-TOF spectrum of G4NH2-PDP conjugate revealed the Mw ca. 17,817 g.mol^{-1} (*upper right inset* in Figure 6.2b) evidencing the conjugation of PDP when compared to the Mw of the pure G4NH2 (*upper right inset* in Figure 6.2a, Mw ca. 14,090 g.mol^{-1}). Considering that each PDP molecule attached to the dendrimer surface adds the Mw ca. 213.3 g.mol^{-1} (*upper left inset* in Figure 6.2b) the number of PDP molecules linked to G4NH2 could be estimated to be 17, which is very consistent with previous results obtained from ^{1}H-NMR and UV-Vis spectroscopy.

LS measurements revealed that the ζ of the pure G4NH2 was +30.6 ± 8.1 mV, which falls in the range of previous ζ published in literature for PAMAM G4NH2.[77, 78] After the SPDP modification, the ζ of the G4NH2-PDP conjugates was determined to be +27.8 ± 7 mV, indicating only a slight reduction in ζ. Thus, the loss of protonable

primary amine groups on the dendrimer surface that happens upon the attachment of PDP molecules was balanced by the presence of pyridine groups in the PDP molecules, which may also undergo protonation.[79-81] The hydrodynamic diameter of the pure G4NH2 was found to be 3.7 ± 0.3 nm (PDI = 0.3 ± 0.1), also in agreement with previously reported results,[77, 82, 83] and no significant increase in size was detected in the G4NH2-PDP conjugates.

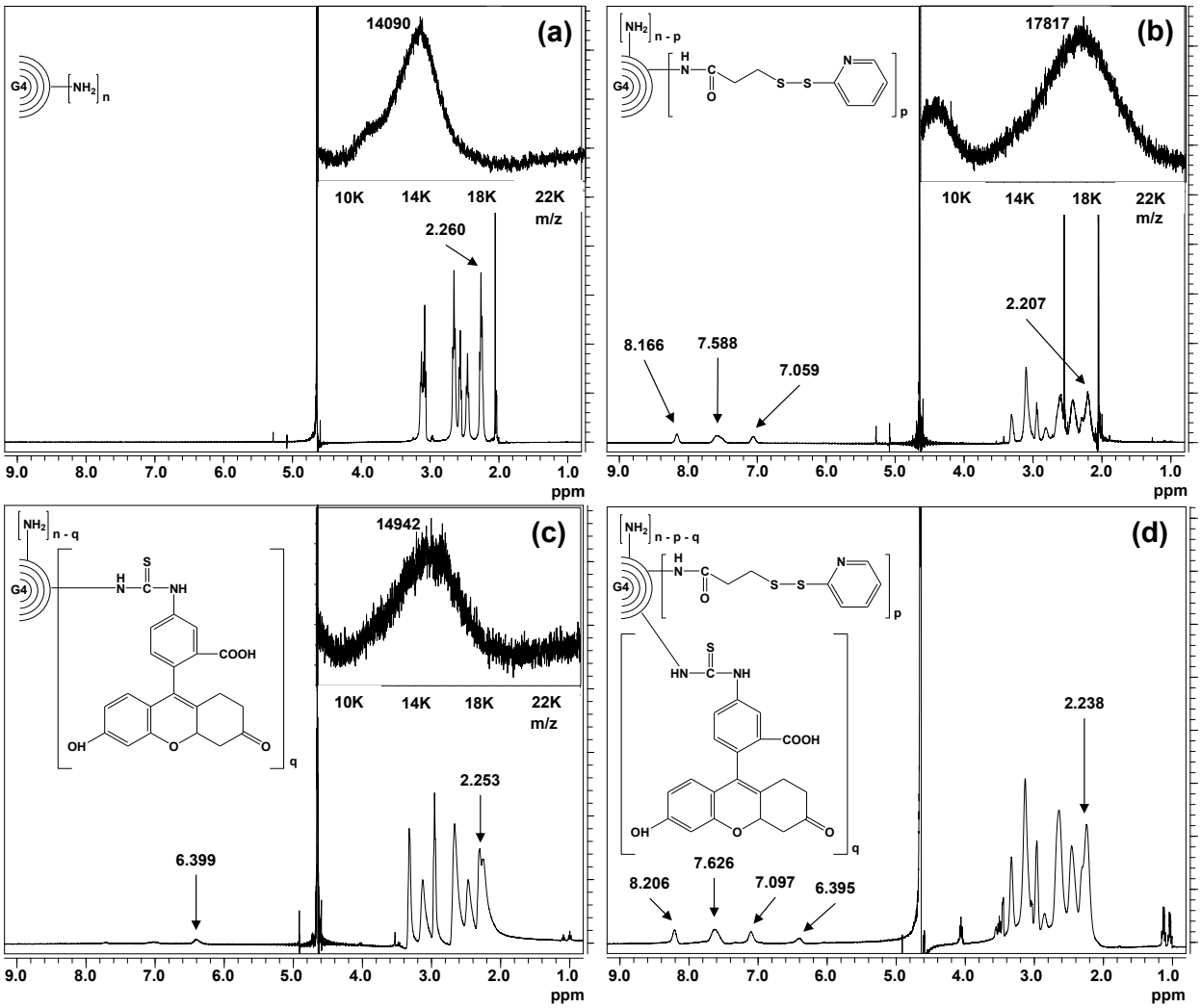

Figure 6.2. ^{1}H NMR characterization of **(a)** G4NH2, **(b)** G4NH2-PDP, **(c)** G4NH2-FITC, and **(d)** G4NH2-FITC-PDP conjugates. *Insets:* molecular structures (*upper left*) and MALDI-TOF spectra (*upper right*).

The G4NH2-FITC conjugate was prepared for further reaction with SPDP crosslinker, in order to estimate the number of siRNA molecules per G4NH2. FITC was conjugated to G4NH2 first, followed by the attachment of the SPDP crosslinker on the dendrimer surface. ^{1}H-NMR of the G4NH2-FITC conjugate (Figure 6.2c) showed the presence of protons corresponding to the aromatic rings of the FITC molecule[84] – 6.399 ppm (6H, Ar) – indicating the successful attachment of FITC on the G4NH2 surface. Comparing the ^{1}H-NMR spectra of the pure G4NH2 (Figure 6.2a) and G4NH2-FITC conjugate (Figure 6.2c) at the region 6 - 7 ppm, the peak assigned to FITC can be clearly observed. The Mw of the G4NH2-FITC conjugate was found to be ca. 14,942 g.mol^{-1} according to MALDI-TOF (*upper right inset* in Figure 6.2c), which evidences a slight increase compared to the Mw of the pure G4NH2 (*upper right inset* in Figure 6.2a, Mw ca. 14,090 g.mol^{-1}). These results indicate the conjugation of ca. 2 FITC molecules per G4NH2.

The G4NH2-FITC conjugate was reacted with SPDP crosslinker. Characterization according to ^{1}H NMR (Figure 6.2d) revealed protons that were assigned to the aromatic rings of the FITC molecule[84] – 6.395 ppm (6H, Ar) – and protons corresponding to the aromatic ring of the thiopyridyl group of the PDP molecule[71, 72] – 7.097 ppm (1H, Ar), 7.626 ppm (1H, Ar), and 8.206 ppm (2H, Ar). This result indicates the successful conjugation of the SPDP crosslinker on the G4NH2-FITC conjugate. Results from the Pyridine-2-Thione Assay[62] (the UV method) along with calculations based on the ^{1}H-NMR spectrum of the G4NH2-FITC-PDP conjugate (Figure 6.2d) indicated that such conjugate had similar number of PDP molecules linked on the dendrimer surface compared to the unlabeled previous one discussed above.

LS results revealed a ζ of +25.8 ± 1 mV for the G4NH2-FITC-PDP conjugates, which as expected, is very similar to the G4NH2-PDP conjugates.

6.3.2 Synthesis and characterization of G4NH2-siRNA conjugates

The integrity of the thiol deprotected siRNA-SH under reaction conditions (exposure to high salted buffer, stirring, and room temperature for several days) was qualitatively evaluated using gel electrophoresis. The results are seen in Figure 6.3, and show that the bands corresponding to the siRNA-SH kept under reaction conditions up to 14 days (*lanes 3 - 11*) are readily comparable to those from untreated siRNA (*lanes 1 - 2*). Since the reaction between siRNA-SH and G4NH2-PDP takes 4 - 5 days, these results indicate that the integrity of siRNA-SH after thiol deprotection is kept under the reaction conditions.

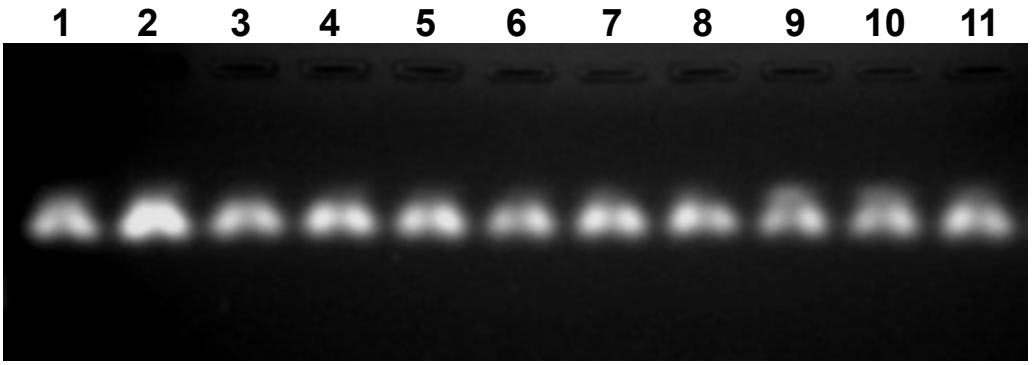

Figure 6.3. Non-denaturating agarose gel electrophoresis of siRNA-SH kept under reaction conditions (but no presence of PDP-modified G4NH2) for 6 h (*lane 3*), 1 day (*lane 4*), 4 days (*lane 5*), 5 days (*lane 6*), 7 days (*lane 7*), 8 days (*lane 8*), 12 days (*lane 9*), 13 days (*lane 10*), and 14 days (*lane 11*). Untreated siRNA before (*lane 1*) and immediately after (*lane 2*) thiol deprotection were used as controls. All lanes were loaded with ca. 300 ng siRNA.

G4NH2-siRNA conjugates were synthetized by the reaction between pyridyldithiol-activated dendrimer (G4NH2-PDP) and sulfhydryl-activated siRNA (siRNA-

SH). The result was the conjugation of siRNA onto G4NH2 via a crosslink containing a reducible disulfide bond, which may be cleaved in the cytosolic compartment (siRNA target site)[33] by reducing molecules such as glutathione (GSH).[85] The cytosol contains high concentration of GSH (2 - 10 mM) which can be 100 to 1000 times higher than that in the extracellular environment,[86] thus making this a highly desirable targeted delivery strategy for siRNA, whose target site is the cell cytosol. The cleavage happens via two thiol-disulfide exchange reactions. Actually, the disulfide bond is expected to be transferred from the G4NH2-siRNA conjugate to two GSH molecules in two steps:[87] *(i)* the thiolate ($-S^-$) of the GSH attacks the disulfide bond (-S-S-) (in this case from the G4NH2-siRNA conjugate), forming a mixed disulfide bond between the GSH and G4NH2 (or GSH and siRNA), which *(ii)* is attacked by another thiolate from the other GSH, releasing completely the G4NH2 and siRNA.

The thiol deprotection efficiency of the siRNA prior its reaction with G4NH2-PDP (or G4NH2-FITC-PDP) was > 90% as measured by Ellman's Assay.[63] The reaction between siRNA-SH and G4NH2-PDP (or G4NH2-FITC-PDP) was carried out in high salt concentrated buffer to minimize the complexation between the positively charged PDP-modified dendrimer and the negatively charged siRNA-SH, which can hinder the desired reaction. Purification of the G4NH2-siRNA and G4NH2-FITC-siRNA conjugates was performed using several washes of high salt concentrated buffer to remove all unreacted and complexed siRNA from the conjugates.[37, 44, 45, 49]

The cleavage of the reducible disulfide bond between G4NH2 and siRNA was confirmed via agarose gel electrophoresis after reacting DTT and G4NH2-siRNA conjugate. The results are shown in Figure 6.4, and indicated that the disulfide bond

between G4NH2 and siRNA can indeed be broken in a reducing environment similar to that of the cytosol.

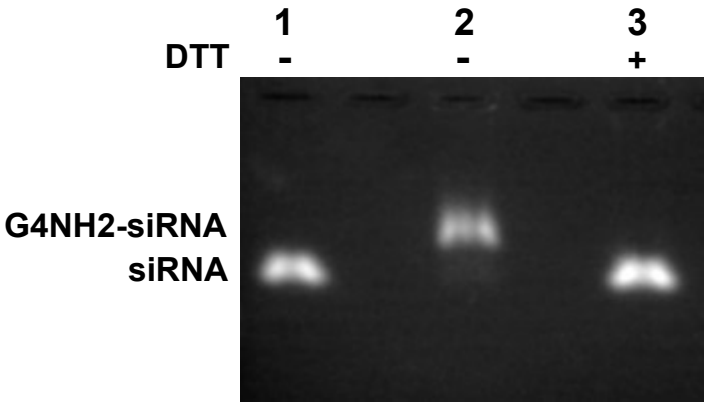

Figure 6.4. Non-denaturating agarose gel electrophoresis of G4NH2-siRNA conjugate without (*lane 2*) and with (*lane 3*) DTT treatment. Free and untreated siRNA control (300 ng) is shown in *lane 1*.

The siRNA from the conjugate free of DTT (–DTT) is visualized as an upper band (*lane 2*) compared to that siRNA from the conjugate after DTT reaction (+DTT) which appears as a lower band (*lane 3*), and at the same level of the untreated free siRNA (control, *lane 1*). The siRNA attached to the dendrimer travels at lower speed through the pores of the gel (*lane 2*) compared to the siRNA that was released from the dendrimer due to the cleavage of the disulfide bond by DTT (*lane 3*). Similar behavior has been observed in the gel electrophoresis of siRNA conjugated to quantum dots (QD),[48, 49] and can be attributed to the successful siRNA conjugation using a crosslink containing a reducible disulfide bond.

The siRNA loading efficiency was found to be on average 45% (three batches G4NH2-siRNA conjugates), as calculated using the results from UV-Vis spectroscopy and densitometry, which showed excellent agreement (> 90%). The characterization of G4NH2-FITC-siRNA conjugates indicated average loadings of 3 siRNA molecules

conjugated per G4NH2. This result shows a good agreement with literature which report ca. 2 - 3 siRNA molecules per QD.[48, 49] In contrast with siRNA delivery systems based on dendriplexes – nanoscale complexes formed between siRNA and dendrimers[88] – the siRNA loading result obtained with the conjugates reveals a great opportunity to deliver siRNA using small amounts of nanocarrier (in this case PAMAM G4NH2), and thus, with lesser potential toxic effects, besides the smaller and better controlled size, as discussed below. For example, siRNA-G4NH2 dendriplexes at N/P ratio of 10 – the typical N/P used in *in vitro* gene knockdown experiments[78, 89] – approximately 8 G4NH2 molecules are needed for each siRNA. Therefore, comparing both siRNA delivery strategies – dendriplexes *vs.* conjugation – the latter represents a 24-fold decrease in mass loading of the nanocarrier (PAMAM G4NH2) for the same amount of siRNA. This is an excellent result since the optimization of the G4NH2-siRNA conjugates was not even attempted yet.

Hydrodynamic diameter and ζ of G4NH2-siRNA conjugates were determined by LS, and found to be 10 ± 3 nm (PDI = 0.6 ± 0.2) and -16 ± 2 mV, respectively. These results are in sharp contrast with the much larger, highly heterogeneous and difficult to control and predict sizes of siRNA-based dendriplexes[83, 90] and polyplexes of ca. 50 - 750 nm.[91-93] The much smaller size of the G4NH2-siRNA conjugates reported here provides a great opportunity to modulate cellular responses,[29] uptake,[27, 94] intracellular trafficking,[94] and interaction with extracellular fluids,[30] since these properties are shown to be size-dependent on the nanocarriers, and thus, affect the gene suppression efficiency.[27] In addition, these conjugates, in spite of the overall negative surface charge, are expected to be able to adhere to the cellular membranes, as it has been

demonstrated to other negatively charged conjugates,[95] improve escape from macrophages, enhance blood circulation time, and accumulation in lung.[95] The ability of these conjugates to be internalized with the cell, trafficked and released onto the cytosol is discussed in the next section when their gene knockdown ability is evaluated.

It is worthwhile to mention here that the use of PAMAM dendrimers as nanocarriers for siRNA has unique advantages compared to other carrier systems such as dendriplexes and lipoplexes, as discussed earlier in the introduction. Their small size, molecular uniformity, and high functionality that will enable further optimization of the nanocarriers as for example through the conjugation of internalization ligands, reducible- and pH-trigged molecules, imaging agents, and combination of therapeutics (small molecule and siRNA).[9] Therefore, the use of PAMAM dendrimers offers a great potential for the development a “smart” siRNA delivery system.

6.3.3 *In vitro* gene knockdown

A549 cells stably expressing eGFP were used to investigate the gene silencing efficiency of G4NH2-siRNA conjugates. The commercial transfection reagents Lipofectamine® 2000 (LF) and TransFast™ (TF) were used as positive controls, and free siRNA was the negative control. siRNA concentrations in the conjugates were 80, 160, and 320 nM. The controls (free siRNA and siRNA complexed with LF and TF) were kept at 80 nM siRNA as base line, since LF and TF were very toxic and caused cell death during the experiments at higher siRNA concentrations. Transfection was performed with siRNA(+) and siRNA(–) conjugated to G4NH2, complexed with LF or TF, and delivered without any carrier (free), and the results are summarized in Figure 6.5.

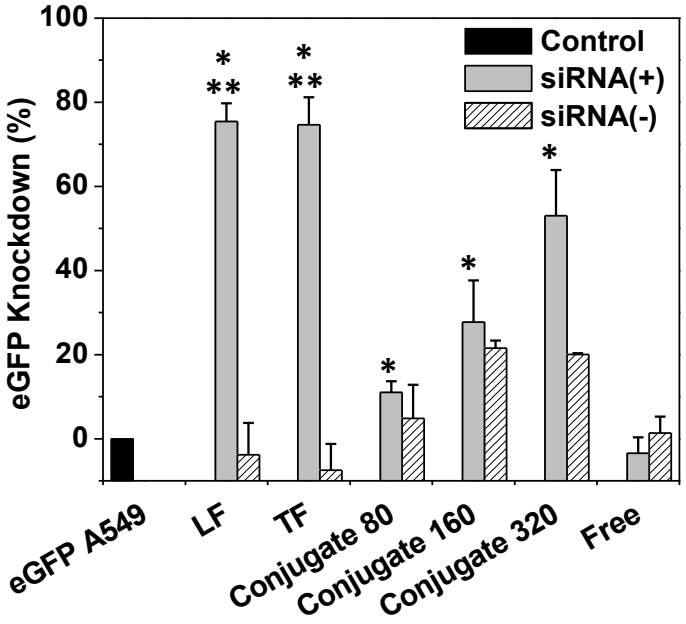

Figure 6.5. *In vitro* knockdown of eGFP expression in A549 cells stably expressing eGFP. G4NH2-siRNA conjugates were equivalent to 80, 160, and 320 nM siRNA, as indicated in the plot. Lipofectamine® 2000 (LF), TransFast™ (TF), and free siRNA were used as controls at 80 nM siRNA concentration. Knockdown with positive siRNA sequence (anti-eGFP) is compared with the irrelevant siRNA sequence (negative). G4NH2 concentration in the conjugate equivalent to 320 nM siRNA was 0.06 μM. ∗∗ = statistically different compared to untreated eGFP A549 cells control; ∗ = statistically different compared to eGFP A549 cells treated with free siRNA; *p* value < 0.05, One-Way ANOVA.

The silence of eGFP expression in A549 cells achieved by the G4NH2-siRNA(+) conjugates (11, 28, and 53% for 80, 160, and 320 nM siRNA, respectively) was found to be intermediate to LF and TF (both ca. 75%) and free siRNA (-3.5%). The nanocarriers provided a much higher and statistically significantly knockdown of eGFP compared to free siRNA(+) used as negative control (One-Way ANOVA, *p* value < 0.05). However, a reduction in eGFP expression was also observed when the irrelevant siRNA(–) was delivered using the conjugates (5, 21, and 20% for 80, 160, and 320 nM siRNA, respectively) and as free (1.5%).

This unwanted eGFP suppression is most likely due to off-target effects – the down regulation of specific genes caused by the siRNA(–) due to unintended interactions between silencing molecules and cellular components.[96] In RNAi, off-target

effects can be due to toxicity of the nanocarrier,[97] but also depend on the similarity between the nucleotide sequence from the siRNA and short motifs in the messenger RNA (mRNA) and other unrelated genes not targeted.[96, 98] It has been demonstrated that siRNAs can alter the mRNA levels of off-target genes in addition to the targeted gene.[99] Off-target effects in RNAi are quite common,[98] hard to avoid,[96] and still not well understood,[100] but important to address siRNA therapeutics moving into the clinic.

While no previous dendrimer-siRNA conjugates are available in the literature, the results obtained here can be contrasted with the reports on other siRNA conjugates. Disulfide-linked siRNA-QD conjugates (10 nM siRNA) were found to achieved 70% eGFP knockdown in HeLa cells when delivered together with Lipofectamine® 2000,[49] which is similar to the knockdown found here with Lipofectamine® 2000 and siRNA(+). In other works, disulfide-linked siRNA-QD conjugates (60 - 80 nM siRNA)[48] and siRNA-Au conjugates[45] (90 nM siRNA) were able to silence ca. 90% the luciferase expression in HeLa cells, but such conjugates were delivered directly to the cell cytosol via electroporation to avoid membrane interactions,[48] and via complexation with poly(β-amino ester),[45] respectively. siRNA-Au conjugates alone (100 nM siRNA) provided ca. 50% reduction in luciferase expression in HeLa cells.[46] This result is similar to the one achieved with our G4NH2-siRNA(+) conjugates at 320 nM siRNA. Nevertheless, it is worthwhile to mention that the cell line and experimental conditions, which were different in both systems, play a role in the gene knockdown process and thus, it is hard to establish a direct comparison.

It is interesting to observe the clear dose response in knockdown with the G4NH2-siRNA conjugates. As the siRNA concentration of the conjugates increased

(from 80 to 160 and 320 nM), the eGFP knockdown efficiency improved (from 11 to 28 and 53% with siRNA(+) in Figure 6.5). Typical siRNA concentrations applied in gene knockdown experiments using siRNA-carrier systems is usually around 80 - 100 nM,[45, 46, 48, 49] with the maximum concentration often limited due to the toxicity of the carrier/complexing agent, as is the case for TF and LF. In our work siRNA concentrations >> 100 nM could be applied because the high mass loading of siRNA conjugated onto the carrier, and the fact that the corresponding G4NH2 content in the conjugate during the transfection has been shown to be non-toxic to A549 cells (*in vitro* cytotoxicity results in the Chapter 5). The 320 nM siRNA was not limited due to toxicity of the conjugate but simply an arbitrary maximum concentration selected for this study. G4NH2-siRNA conjugates at the highest siRNA concentration of 320 nM during transfection is equivalent to 0.06 μM G4NH2, which falls within the range of G4NH2 concentration where the viability of the A549 cells was not statistically different from the untreated cells as control (*in vitro* cytotoxicity results in the Chapter 5). Based on cell viability studies and 3 siRNA molecules conjugated per dendrimer, we expect to be able to increase the concentration of siRNA up to 2.5 μM without sacrificing cell viability. Based on the linearity between siRNA concentration and knockdown response, this would correspond to a knockdown > 90%, i.e., which seems even better than the commercial transfection reagents.

The eGFP knockdown results obtained with G4NH2-siRNA conjugates are considerably better than those previously observed with siRNA-G4NH2(+) dendriplexes ca. 22 - 36%, as discussed in Chapter 5. It is worthwhile to mention that the delivery of higher siRNA content via dendriplexes was limited due to the toxicity of G4NH2 caused

by its higher amount needed to achieve the desired N/P ratio. Therefore, the results discussed here indicate that siRNA-delivery systems based on G4NH2-siRNA conjugates are very promising, and such systems can be optimized to increase the siRNA loading and via conjugation of other ligands (e.g. PEG and target ligands) in order to improve gene knockdown efficiency with less off-target effects. The poetical benefits of the conjugates in terms of size and ability to tailor their surface chemistry is expected to be even more evidenced when targeting tissues such as the upper airways where extracellular barriers (in that case mucus layer) represent a significant hindrance for the transport of encapsulated/complexed siRNA as they limit diffusion of larger particles and highly charged systems.[30, 101, 102] The conjugates-based nanocarriers, therefore, offer great opportunities in targeting mucus-dependent diseases, e.g. gastric and lung – such as asthma, cystic fibrosis, COPD, and others.[103, 104]

6.4 Conclusions

In this work we demonstrate the successful conjugation of siRNA on PAMAM G4NH2 dendrimer via a reducible disulfide crosslink which can be broke down in the cellular cytosol, the site of action for the therapeutic siRNA. G4NH2-siRNA conjugates were synthesized, characterized, and the disulfide bond between siRNA and G4NH2 was shown to be cleaved by a reducing agent at typical concentration found in the cell cytoplasm. The *in vitro* gene knockdown efficiency in A549 lung cell line stable expressing eGFP was found to be significantly improved relative to the free siRNA (negative control), and better when compared to siRNA-G4NH2 dendriplexes. In addition, and more importantly, the eGFP silencing effect of the G4NH2-siRNA

conjugates was found to be siRNA-concentration dependent, and very high concentration of the conjugates could be employed due to their high mass loading of siRNA and low toxicity, different from many other carrier systems and the positive controls used in this work. The G4NH2-siRNA conjugates proposed here provide a great potential for the development of an efficient and safe siRNA delivery platform, which can be further optimized via conjugation of specific ligands and therapeutics (e.g. small molecules) for targeting a wide range of local and systemic diseases.

6.5 Acknowledgments

The authors would like to thank Dr. Pile (Biological Sciences at Wayne State University) for access to FOTO/Analyst® Investigator/Eclipse with UV Transilluminator Fotodyne, Dr. Jessica Back and Mr. Eric Van Buren (Microscopy, Imaging and Cytometry Resources Core) for the flow cytometry. The MICR Core is supported, in part, by NIH Center grant # P30CA022453 to The Karmanos Cancer Institute, and the Perinatology Research Branch of the National Institutes of Child Health and Development, both at Wayne State University.

This chapter is based on the manuscript: **Conti, D. S.**; Zhong, Q.; Patel, A. M.; da Rocha, S. R. P. siRNA-Dendrimer Conjugates for the Lung Epithelium: Synthesis, Characterization, and Gene Silencing. *To be submitted to Journal of the American Chemical Society*, **2013**.

6.6 References

1. Fire, A.; Xu, S.; Montgomery, M. K.; Kostas, S. A.; Driver, S. E.; Mello, C. C. Potent and specific genetic interference by double-stranded RNA in Caenorhabditis elegans. *Nature* **1998,** *391*, (6669), 806-811.
2. Elbashir, S. M.; Harborth, J.; Lendeckel, W.; Yalcin, A.; Weber, K.; Tuschl, T. Duplexes of 21-nucleotide RNAs mediate RNA interference in cultured mammalian cells. *Nature* **2001,** *411*, (6836), 494-498.
3. Vicentini, F. M.; Borgheti-Cardoso, L. N.; Depieri, L. V.; Macedo Mano, D.; Abelha, T. F.; Petrilli, R.; Bentley, M. L. B. Delivery systems and local administration routes for therapeutic siRNA. *Pharm. Res.* **2013,** *30*, (4), 915-931.
4. Lam, J. K.-W.; Liang, W.; Chan, H.-K. Pulmonary delivery of therapeutic siRNA. *Adv. Drug Delivery Rev.* **2012,** *64*, (1), 1-15.
5. Pecot, C. V.; Calin, G. A.; Coleman, R. L.; Lopez-Berestein, G.; Sood, A. K. RNA interference in the clinic: Challenges and future directions. *Nat. Rev. Cancer* **2011,** *11*, (1), 59-67.
6. Siomi, H.; Siomi, M. C. On the road to reading the RNA-interference code. *Nature* **2009,** *457*, (7228), 396-404.
7. Shrey, K.; Suchit, A.; Nishant, M.; Vibha, R. RNA interference: Emerging diagnostics and therapeutics tool. *Biochem. Biophys. Res. Commun.* **2009,** *386*, (2), 273-277.
8. Yuan, X.; Naguib, S.; Wu, Z. Recent advances of siRNA delivery by nanoparticles. *Expert Opin. Drug Delivery* **2011,** *8*, (4), 521-536.
9. Singha, K.; Namgung, R.; Kim, W. J. Polymers in small-interfering RNA delivery. *Nucleic Acid Ther.* **2011,** *21*, (3), 133-147.
10. Burnett, J. C.; Rossi, J. J.; Tiemann, K. Current progress of siRNA/shRNA therapeutics in clinical trials. *Biotechnol. J.* **2011,** *6*, (9), 1130-1146.
11. Taratula, O.; Garbuzenko, O. B.; Chen, A. M.; Minko, T. Innovative strategy for treatment of lung cancer: Targeted nanotechnology-based inhalation co-delivery of anticancer drugs and siRNA. *J. Drug Targeting* **2011,** *19*, (10), 900-914.

12. Nakamura, K.; Abu Lila, A. S.; Matsunaga, M.; Doi, Y.; Ishida, T.; Kiwada, H. A double-modulation strategy in cancer treatment with a chemotherapeutic agent and siRNA. *Mol. Ther.* **2011**.

13. Bedi, D.; Musacchio, T.; Fagbohun, O. A.; Gillespie, J. W.; Deinnocentes, P.; Bird, R. C.; Bookbinder, L.; Torchilin, V. P.; Petrenko, V. A. Delivery of siRNA into breast cancer cells via phage fusion protein-targeted liposomes. *Nanomed. Nanotech. Biol. Med.* **2011,** *7*, (3), 315-323.

14. Ozpolat, B.; Sood, A. K.; Lopez-Berestein, G. Nanomedicine based approaches for the delivery of siRNA in cancer. *J. Intern. Med.* **2010,** *267*, (1), 44-53.

15. Gonzalez-Gonzalez, E.; Ra, H.; Hickerson, R.; Wang, Q.; Piyawattanametha, W.; Mandella, M.; Kino, G.; Leake, D.; Avilion, A.; Solgaard, O.; Doyle, T.; Contag, C.; Kaspar, R. siRNA silencing of keratinocyte-specific GFP expression in a transgenic mouse skin model. *Gene Ther.* **2009,** *16*, (8), 963-972.

16. Ramsey, J. M.; Hibbitts, A.; Barlow, J.; Kelly, C.; Sivadas, N.; Cryan, S.-A. 'Smart' non-viral delivery systems for targeted delivery of RNAi to the lungs. *Ther. Delivery* **2013,** *4*, (1), 59-76.

17. Fujita, Y.; Takeshita, F.; Kuwano, K.; Ochiya, T. RNAi therapeutic platforms for lung diseases. *Pharmaceuticals* **2013,** *6*, (2), 223-250.

18. Ballarín-González, B.; Thomsen, T. B.; Howard, K. A. Clinical translation of RNAi-based treatments for respiratory diseases. *Drug Delivery Transl. Res.* **2013,** *3*, (1), 84-99.

19. Wang, J.; Lu, Z.; Wientjes, M.; Au, J. Delivery of siRNA therapeutics: Barriers and carriers. *AAPS J.* **2010,** *12*, (4), 492-503.

20. Whitehead, K. A.; Langer, R.; Anderson, D. G. Knocking down barriers: Advances in siRNA delivery. *Nat. Rev. Drug Discovery* **2009,** *8*, (2), 129-138.

21. Zhu, Y.; Li, J.; Oupicky, D., Intracellular delivery considerations for RNAi therapeutics. In *RNA Interference from Biology to Therapeutics*, Howard, K. A., Ed. Springer US: 2013; pp 79-95.

22. Grigsby, C. L.; Leong, K. W. Balancing protection and release of DNA: Tools to address a bottleneck of non-viral gene delivery. *J. R. Soc. Interface* **2010,** *7*, (Suppl 1), S67-S82.

23. Gao, X.; Kim, K.-S.; Liu, D. Nonviral gene delivery: What we know and what is next. *AAPS J.* **2007,** *9*, (1), E92-E104.

24. Beyerle, A.; Braun, A.; Merkel, O.; Koch, F.; Kissel, T.; Stoeger, T. Comparative *in vivo* study of poly(ethylene imine)/siRNA complexes for pulmonary delivery in mice. *J. Controlled Release* **2011,** *151*, (1), 51-56.

25. Chou, L. Y. T.; Ming, K.; Chan, W. C. W. Strategies for the intracellular delivery of nanoparticles. *Chem. Soc. Rev.* **2011,** *40*, (1), 233-245.

26. Nafee, N.; Taetz, S.; Schneider, M.; Schaefer, U. F.; Lehr, C.-M. Chitosan-coated PLGA nanoparticles for DNA/RNA delivery: Effect of the formulation parameters on complexation and transfection of antisense oligonucleotides. *Nanomedicine* **2007,** *3*, (3), 173-183.

27. Rejman, J.; Oberle, V.; Zuhorn, I. S.; Hoekstra, D. Size-dependent internalization of particles via the pathways of clathrin- and caveolae-mediated endocytosis. *Biochem. J.* **2004,** *377*, (1), 159-169.

28. Remaut, K.; Sanders, N. N.; De Geest, B. G.; Braeckmans, K.; Demeester, J.; De Smedt, S. C. Nucleic acid delivery: Where material sciences and bio-sciences meet. *Mater. Sci. Eng., R* **2007,** *58*, (3-5), 117-161.

29. Sun, X.; Zhang, N. Cationic polymer optimization for efficient gene delivery. *Mini-Rev. Med. Chem.* **2010,** *10*, 108-125.

30. Sanders, N.; Rudolph, C.; Braeckmans, K.; De Smedt, S. C.; Demeester, J. Extracellular barriers in respiratory gene therapy. *Adv. Drug Delivery Rev.* **2009,** *61*, (2), 115-127.

31. Patil, M. L.; Zhang, M.; Betigeri, S.; Taratula, O.; He, H.; Minko, T. Surface-modified and internally cationic polyamidoamine dendrimers for efficient siRNA delivery. *Bioconjugate Chem.* **2008,** *19*, (7), 1396-1403.

32. Liu, X.; Howard, K. A.; Dong, M.; Andersen, M. Ø.; Rahbek, U. L.; Johnsen, M. G.; Hansen, O. C.; Besenbacher, F.; Kjems, J. The influence of polymeric properties on chitosan/siRNA nanoparticle formulation and gene silencing. *Biomaterials* **2007,** *28*, (6), 1280-1288.

33. Jeong, J. H.; Mok, H.; Oh, Y.-K.; Park, T. G. siRNA conjugate delivery systems. *Bioconjugate Chem.* **2009,** *20*, (1), 5-14.

34. Park, K.; Yang, J.-A.; Lee, M.-Y.; Lee, H.; Hahn, S. K. Reducible hyaluronic acid-siRNA conjugates for target specific gene silencing. *Bioconjugate Chem.* **2013,** *24*, (7), 1201-1209.

35. Lee, S. H.; Mok, H.; Lee, Y.; Park, T. G. Self-assembled siRNA-PLGA conjugate micelles for gene silencing. *J. Controlled Release* **2011,** *152*, (1), 152-158.

36. Jung, S.; Lee, S. H.; Mok, H.; Chung, H. J.; Park, T. G. Gene silencing efficiency of siRNA-PEG conjugates: Effect of PEGylation site and PEG molecular weight. *J. Controlled Release* **2010,** *144*, (3), 306-313.

37. Choi, S. W.; Lee, S. H.; Mok, H.; Park, T. G. Multifunctional siRNA delivery system: Polyelectrolyte complex micelles of six-arm PEG conjugate of siRNA and cell penetrating peptide with crosslinked fusogenic peptide. *Biotechnol. Prog.* **2009,** *26*, (1), 57-63.

38. Kim, S. H.; Jeong, J. H.; Lee, S. H.; Kim, S. W.; Park, T. G. Local and systemic delivery of VEGF siRNA using polyelectrolyte complex micelles for effective treatment of cancer. *J. Controlled Release* **2008,** *129*, (2), 107-116.

39. Kim, S. H.; Jeong, J. H.; Lee, S. H.; Kim, S. W.; Park, T. G. LHRH receptor-mediated delivery of siRNA using polyelectrolyte complex micelles self-assembled from siRNA-PEG-LHRH conjugate and PEI. *Bioconjugate Chem.* **2008,** *19*, (11), 2156-2162.

40. Lee, S. H.; Kim, S. H.; Park, T. G. Intracellular siRNA delivery system using polyelectrolyte complex micelles prepared from VEGF siRNA-PEG conjugate and cationic fusogenic peptide. *Biochem. Biophys. Res. Commun.* **2007,** *357*, (2), 511-516.

41. Kim, S. H.; Jeong, J. H.; Lee, S. H.; Kim, S. W.; Park, T. G. PEG conjugated VEGF siRNA for anti-angiogenic gene therapy. *J. Controlled Release* **2006,** *116*, (2), 123-129.

42. Oishi, M.; Nagasaki, Y.; Itaka, K.; Nishiyama, N.; Kataoka, K. Lactosylated poly(ethylene glycol)-siRNA conjugate through acid-labile β-thiopropionate linkage to construct pH-sensitive polyion complex micelles achieving enhanced gene silencing in hepatoma cells. *J. Am. Chem. Soc.* **2005,** *127*, (6), 1624-1625.

43. Oishi, M.; Sasaki, S.; Nagasaki, Y.; Kataoka, K. pH-responsive oligodeoxynucleotide (ODN)-poly(ethylene glycol) conjugate through acid-labile β-thiopropionate linkage: Preparation and polyion complex micelle formation. *Biomacromolecules* **2003,** *4*, (5), 1426-1432.

44. Meyer, M.; Dohmen, C.; Philipp, A.; Kiener, D.; Maiwald, G.; Scheu, C.; Ogris, M.; Wagner, E. Synthesis and biological evaluation of a bioresponsive and endosomolytic siRNA-polymer conjugate. *Mol. Pharmaceutics* **2009,** *6*, (3), 752-762.

45. Lee, J.-S.; Green, J. J.; Love, K. T.; Sunshine, J.; Langer, R.; Anderson, D. G. Gold, poly(β-amino ester) nanoparticles for small interfering RNA delivery. *Nano Lett.* **2009,** *9*, (6), 2402-2406.

46. Giljohann, D. A.; Seferos, D. S.; Prigodich, A. E.; Patel, P. C.; Mirkin, C. A. Gene regulation with polyvalent siRNA-nanoparticle conjugates. *J. Am. Chem. Soc.* **2009,** *131*, (6), 2072-2073.

47. Medarova, Z.; Pham, W.; Farrar, C.; Petkova, V.; Moore, A. *In vivo* imaging of siRNA delivery and silencing in tumors. *Nat. Med.* **2007,** *13*, (3), 372-377.

48. Singh, N.; Agrawal, A.; Leung, A. K. L.; Sharp, P. A.; Bhatia, S. N. Effect of nanoparticle conjugation on gene silencing by RNA interference. *J. Am. Chem. Soc.* **2010,** *132*, (24), 8241-8243.

49. Derfus, A. M.; Chen, A. A.; Min, D.-H.; Ruoslahti, E.; Bhatia, S. N. Targeted quantum dot conjugates for siRNA delivery. *Bioconjugate Chem.* **2007,** *18*, (5), 1391-1396.

50. Nishina, K.; Unno, T.; Uno, Y.; Kubodera, T.; Kanouchi, T.; Mizusawa, H.; Yokota, T. Efficient *in vivo* delivery of siRNA to the liver by conjugation of α-tocopherol. *Mol. Ther.* **2008,** *16*, (4), 734-740.

51. Heredia, K. L.; Nguyen, T. H.; Chang, C.-W.; Bulmus, V.; Davis, T. P.; Maynard, H. D. Reversible siRNA-polymer conjugates by RAFT polymerization. *Chem. Commun.* **2008**, (28), 3245-3247.

52. Rozema, D. B.; Lewis, D. L.; Wakefield, D. H.; Wong, S. C.; Klein, J. J.; Roesch, P. L.; Bertin, S. L.; Reppen, T. W.; Chu, Q.; Blokhin, A. V.; Hagstrom, J. E.; Wolff, J. A. Dynamic polyconjugates for targeted *in vivo* delivery of siRNA to hepatocytes. *Proc. Natl. Acad. Sci. U.S.A.* **2007,** *104*, (32), 12982-12987.

53. Moschos, S. A.; Jones, S. W.; Perry, M. M.; Williams, A. E.; Erjefalt, J. S.; Turner, J. J.; Barnes, P. J.; Sproat, B. S.; Gait, M. J.; Lindsay, M. A. Lung delivery studies using siRNA conjugated to TAT(48−60) and penetratin reveal peptide induced reduction in gene expression and induction of innate immunity. *Bioconjugate Chem.* **2007,** *18*, (5), 1450-1459.

54. Juliano, R. L. Intracellular delivery of oligonucleotide conjugates and dendrimer complexes. *Ann. N. Y. Acad. Sci.* **2006,** *1082*, (1), 18-26.

55. Muratovska, A.; Eccles, M. R. Conjugate for efficient delivery of short interfering RNA (siRNA) into mammalian cells. *FEBS Lett.* **2004,** *558*, (1-3), 63-68.

56. Heiden, T. C. K.; Dengler, E.; Kao, W. J.; Heideman, W.; Peterson, R. E. Developmental toxicity of low generation PAMAM dendrimers in zebrafish. *Toxicol. Appl. Pharmacol.* **2007,** *225*, (1), 70-79.

57. Ouyang, D.; Zhang, H.; Parekh, H. S.; Smith, S. C. The effect of pH on PAMAM dendrimer-siRNA complexation - Endosomal considerations as determined by molecular dynamics simulation. *Biophys. Chem.* **2011,** *158*, (2-3), 126-133.

58. Arima, H.; Motoyama, K.; Higashi, T. Potential use of polyamidoamine dendrimer conjugates with cyclodextrins as novel carriers for siRNA. *Pharmaceuticals* **2012,** *5*, (1), 61-78.

59. Raemdonck, K.; Naeye, B.; Høgset, A.; Demeester, J.; De Smedt, S. C. Prolonged gene silencing by combining siRNA nanogels and photochemical internalization. *J. Controlled Release* **2010,** *145*, (3), 281-288.

60. Thermo Scientific, TCEP reaction for thiol-modified siRNA/RNA oligonucleotides. Thermo Fisher Scientific Inc.: 2012; 'Vol.' 00159-07-H-02-U, p 1.

61. Foster, K. A.; Oster, C. G.; Mayer, M. M.; Avery, M. L.; Audus, K. L. Characterization of the A549 cell line as a type II pulmonary epithelial cell model for drug metabolism. *Exp. Cell Res.* **1998,** *243*, (2), 359-366.

62. Pierce Biotechnology, SPDP crosslinkers. Thermo Fisher Scientific Inc.: Rockford, IL, 2011; 'Vol.' 0279.4, pp 1-4.

63. Pierce Biotechnology, Ellman's reagent. Thermo Fisher Scientific Inc.: Rockford, IL, 2011; pp 1-4.

64. Meyer, M. Dynamic endosomolytic polymer conjugates for pDNA and siRNA delivery Dissertation, Ludwig-Maximilians-Universität München, 2008.

65. Lau, J. T. F.; Jiang, X.-J.; Ng, D. K. P.; Lo, P.-C. A disulfide-linked conjugate of ferrocenyl chalcone and silicon(iv) phthalocyanine as an activatable photosensitiser. *Chem. Commun.* **2013**.

66. Rasband, W. S. ImageJ, U. S. National Institutes of Health, Bethesda, Maryland, USA. http://imagej.nih.gov/ij/ **1997-2012**.

67. Lee, S. H.; Mok, H.; Jo, S.; Hong, C. A.; Park, T. G. Dual gene targeted multimeric siRNA for combinatorial gene silencing. *Biomaterials* **2011,** *32*, (9), 2359-2368.

68. Mao, S.; Neu, M.; Germershaus, O.; Merkel, O.; Sitterberg, J.; Bakowsky, U.; Kissel, T. Influence of polyethylene glycol chain length on the physicochemical and biological properties of poly(ethylene imine)-*graft*-poly(ethylene glycol) block copolymer/siRNA polyplexes. *Bioconjugate Chem.* **2006,** *17*, (5), 1209-1218.

69. Invitrogen by Life Technologies, Lipofectamine 2000. 2006; 'Vol.' 11668.2k.pps, pp 1-4.

70. Promega Corporation, TransFast™ Transfection Reagent. 2009; 'Vol.' Part# TB260, pp 1-17.

71. Navath, R. S.; Menjoge, A. R.; Dai, H.; Romero, R.; Kannan, S.; Kannan, R. M. Injectable PAMAM dendrimer-PEG hydrogels for the treatment of genital infections: Formulation and *in vitro* and *in vivo* evaluation. *Mol. Pharmaceutics* **2011,** *8*, (4), 1209-1223.

72. Talelli, M.; Rijcken, C. J. F.; Oliveira, S.; Meel, R. v. d.; Henegouwen, P. M. P. v. B. e.; Lammers, T.; Nostrum, C. F. v.; Storm, G.; Hennink, W. E. Nanobody - Shell functionalized thermosensitive core-crosslinked polymeric micelles for active drug targeting. *J. Controlled Release* **2011,** *151*, 183-192.

73. Zhu, S.; Hong, M.; Zhang, L.; Tang, G.; Jiang, Y.; Pei, Y. PEGylated PAMAM dendrimer-doxorubicin conjugates: *In vitro* evaluation and *in vivo* tumor accumulation. *Pharm. Res.* **2010,** *27*, (1), 161-174.

74. Hu, J.; Su, Y.; Zhang, H.; Xu, T.; Cheng, Y. Design of interior-functionalized fully acetylated dendrimers for anticancer drug delivery. *Biomaterials* **2011,** *32*, (36), 9950-9959.

75. Heldt, J.-M.; Fischer-Durand, N.; Salmain, M.; Vessières, A.; Jaouen, G. Preparation and characterization of poly(amidoamine) dendrimers functionalized with a rhenium carbonyl complex and PEG as new IR probes for carbonyl metallo immunoassay. *J. Organomet. Chem.* **2004,** *689*, (25), 4775-4782.

76. Fischer-Durand, N.; Salmain, M.; Rudolf, B.; Jugé, L.; Guérineau, V.; Laprévote, O.; Vessières, A.; Jaouen, G. Design of a new multifunctionalized PAMAM dendrimer with hydrazide-terminated

spacer arm suitable for metal-carbonyl multilabeling of aldehyde-containing molecules. *Macromolecules* **2007,** *40*, (24), 8568-8575.

77. Mishra, M. K.; Gérard, H. C.; Whittum-Hudson, J. A.; Hudson, A. P.; Kannan, R. M. Dendrimer-enabled modulation of gene expression in *Chlamydia trachomatis*. *Mol. Pharmaceutics* **2012,** *9*, 413-421.

78. Perez, A. P.; Romero, E. L.; Morilla, M. J. Ethylendiamine core PAMAM dendrimers/siRNA complexes as *in vitro* silencing agents. *Int. J. Pharm.* **2009,** *380*, (1-2), 189-200.

79. Walker, G. F.; Fella, C.; Pelisek, J.; Fahrmeir, J.; Boeckle, S.; Ogris, M.; Wagner, E. Toward synthetic viruses: Endosomal pH-triggered deshielding of targeted polyplexes greatly enhances gene transfer *in vitro* and *in vivo*. *Mol. Ther.* **2005,** *11*, (3), 418-425.

80. Yuan, Q.; Yeudall, W. A.; Yang, H. PEGylated polyamidoamine dendrimers with bis-aryl hydrazone linkages for enhanced gene delivery. *Biomacromolecules* **2010,** *11*, (8), 1940-1947.

81. Parra-Barraza, H.; Hernández-Montiel, D.; Lizardi, J.; Hernández, J.; Herrera Urbina, R.; Valdez, M. A. The zeta potential and surface properties of asphaltenes obtained with different crude oil/n-heptane proportions. *Fuel* **2003,** *82*, (8), 869-874.

82. Jasmine, M. J.; Prasad, E. Fractal growth of PAMAM dendrimer aggregates and its impact on the intrinsic emission properties. *J. Phys. Chem. B* **2010,** *114*, (23), 7735-7742.

83. Jensen, L. B.; Pavan, G. M.; Kasimova, M. R.; Rutherford, S.; Danani, A.; Nielsen, H. M.; Foged, C. Elucidating the molecular mechanism of PAMAM-siRNA dendriplex self-assembly: Effect of dendrimer charge density. *Int. J. Pharm.* **2011,** *416*, (2), 410-418.

84. Menjoge, A. R.; Navath, R. S.; Asad, A.; Kannan, S.; Kim, C. J.; Romero, R.; Kannan, R. M. Transport and biodistribution of dendrimers across human fetal membranes: Implications for intravaginal administration of dendrimer-drug conjugates. *Biomaterials* **2010,** *31*, 5007-5021.

85. Kim, T.-i.; Kim, S. W. Bioreducible polymers for gene delivery. *React. Funct. Polym.* **2011,** *71*, (3), 344-349.

86. Cheng, R.; Feng, F.; Meng, F.; Deng, C.; Feijen, J.; Zhong, Z. Glutathione-responsive nano-vehicles as a promising platform for targeted intracellular drug and gene delivery. *J. Controlled Release* **2011,** *152*, (1), 2-12.

87. Mamathambika, B. S.; Bardwell, J. C. Disulfide-linked protein folding pathways. *Annu. Rev. Cell Dev. Biol.* **2008,** *24*, 211-235.

88. Shcharbin, D.; Pedziwiatr, E.; Bryszewska, M. How to study dendriplexes I: Characterization. *J. Controlled Release* **2009,** *135*, (3), 186-197.

89. Biswas, S.; Deshpande, P. P.; Navarro, G.; Dodwadkar, N. S.; Torchilin, V. P. Lipid modified triblock PAMAM-based nanocarriers for siRNA drug co-delivery. *Biomaterials* **2013,** *34*, (4), 1289-1301.

90. Perez, A. P.; Cosaka, M. L.; Romero, E. L.; Morilla, M. J. Uptake and intracellular traffic of siRNA dendriplexes in glioblastoma cells and macrophages. *Int. J. Nanomed.* **2011,** *6*, 2715.

91. Arima, H.; Tsutsumi, T.; Yoshimatsu, A.; Ikeda, H.; Motoyama, K.; Higashi, T.; Hirayama, F.; Uekama, K. Inhibitory effect of siRNA complexes with polyamidoamine dendrimer/α-cyclodextrin conjugate (generation 3, G3) on endogenous gene expression. *Eur. J. Pharm. Sci.* **2011,** *44*, (3), 375-384.

92. Nielsen, E.; Nielsen, J.; Becker, D.; Karlas, A.; Prakash, H.; Glud, S.; Merrison, J.; Besenbacher, F.; Meyer, T.; Kjems, J.; Howard, K. Pulmonary gene silencing in transgenic EGFP mice using aerosolised chitosan/siRNA nanoparticles. *Pharm. Res.* **2010,** *27*, (12), 2520-2527.

93. Noh, S. M.; Park, M. O.; Shim, G.; Han, S. E.; Lee, H. Y.; Huh, J. H.; Kim, M. S.; Choi, J. J.; Kim, K.; Kwon, I. C.; Kim, J.-S.; Baek, K.-H.; Oh, Y.-K. Pegylated poly-l-arginine derivatives of chitosan for effective delivery of siRNA. *J. Controlled Release* **2010,** *145*, (2), 159-164.

94. Hillaireau, H.; Couvreur, P. Nanocarriers' entry into the cell: Relevance to drug delivery. *Cell. Mol. Life Sci.* **2009,** *66*, (17), 2873-2896.

95. He, C.; Hu, Y.; Yin, L.; Tang, C.; Yin, C. Effects of particle size and surface charge on cellular uptake and biodistribution of polymeric nanoparticles. *Biomaterials* **2010,** *31*, (13), 3657-3666.

96. Tschuch, C.; Schulz, A.; Pscherer, A.; Werft, W.; Benner, A.; Hotz-Wagenblatt, A.; Barrionuevo, L.; Lichter, P.; Mertens, D. Off-target effects of siRNA specific for GFP. *BMC Mol. Biol.* **2008,** *9*, (1), 60.

97. Merkel, O. M.; Mintzer, M. A.; Librizzi, D.; Samsonova, O.; Dicke, T.; Sproat, B.; Garn, H.; Barth, P. J.; Simanek, E. E.; Kissel, T. Triazine dendrimers as nonviral vectors for *in vitro* and *in vivo*

RNAi: The effects of peripheral groups and core structure on biological activity. *Mol. Pharmaceutics* **2010,** *7*, (4), 969-983.

98. Naito, Y.; Yamada, T.; Matsumiya, T.; Ui-Tei, K.; Saigo, K.; Morishita, S. dsCheck: Highly sensitive off-target search software for double-stranded RNA-mediated RNA interference. *Nucleic Acids Res.* **2005,** *33*, (suppl 2), W589-W591.

99. de Fougerolles, A.; Vornlocher, H.-P.; Maraganore, J.; Lieberman, J. Interfering with disease: A progress report on siRNA-based therapeutics. *Nat. Rev. Drug Discovery* **2007,** *6*, (6), 443-453.

100. Merkel, O. M.; Beyerle, A.; Beckmann, B. M.; Zheng, M.; Hartmann, R. K.; Stöger, T.; Kissel, T. H. Polymer-related off-target effects in non-viral siRNA delivery. *Biomaterials* **2011,** *32*, (9), 2388-2398.

101. Merkel, O. M.; Kissel, T. Nonviral pulmonary delivery of siRNA. *Acc. Chem. Res.* **2011,** *45(7)*, (7), 961-970.

102. Gottfried, L. F.; Dean, D. A., Extracellular and intracellular barriers to non-viral gene transfer. In *Novel Gene Therapy Approaches*, Licensee InTech: 2013; pp 75-88.

103. Suk, J. S.; Lai, S. K.; Wang, Y.-Y.; Ensign, L. M.; Zeitlin, P. L.; Boyle, M. P.; Hanes, J. The penetration of fresh undiluted sputum expectorated by cystic fibrosis patients by non-adhesive polymer nanoparticles. *Biomaterials* **2009,** *30*, (13), 2591-2597.

104. Lai, S. K.; Wang, Y.-Y.; Hanes, J. Mucus-penetrating nanoparticles for drug and gene delivery to mucosal tissues. *Adv. Drug Delivery Rev.* **2009,** *61*, (2), 158-171.

CHAPTER 7

Conclusions and Future Directions

Although widely recognized as a very promising non-invasive administration route of therapeutics *to* and *through* the lungs, oral inhalation (OI) has still not been extensively explored for the delivery of nucleic acids as therapeutics. Portable OI inhalers – such as pMDIs – are inexpensive, easy to use, and thus very popular to treat medically relevant pulmonary diseases, e.g. asthma and COPD, and have great potential for the treatment of other lung disorders, e.g. cystic fibrosis and lung cancer. However, due to the challenges in formulating therapeutics in HFA-based portable inhalers – *(i)* to achieve the appropriate aerodynamic size for deposition in the deep lungs, *(ii)* to find a suitable surface chemistry to be solvated by propellant HFA, and thus, generate stable and efficient dispersions, and *(iii)* lack of knowledge on the interactions between chemistries used in excipients (e.g. surfactants) in the HFA/co-solvent mixture – the use of pMDIs to deliver DNA and siRNA *locally to* the lungs is still in its infancy. Besides formulation challenges, the progress of OI for the delivery of DNA and siRNA *to* the lungs has been hampered largely by the lack of efficient nanocarriers capable of overcoming the lung structure, the extra and intracellular barriers present in the lung tissue to reach the site of action – the nucleus (DNA) and the cytoplasm (siRNA).

Polymeric nanocarriers (PNCs) have great potential to improve OI delivery of nucleic acids. However, most of the studies apply PNCs to form complexes with DNA or siRNA – polyplexes (cationic polymers in general) and dendriplexes (for dendrimers).

In spite of the advantages achieved by complexation, the disadvantages – the wide variation of the sizes, high polydispersity, variable shapes, possibility of interactions and entrapment in negatively charged extracellular fluids, and cytotoxicity issues – have suggested that alternative routes for DNA/siRNA delivery may be more appropriate, such as the conjugation of nucleic acids (instead of complexation) with nano-sized PNC using pH- and reducible-dependent crosslinks. The decoration of the PNC with target and internalization ligands, molecules to reduce toxicity and off-target effects, improve endolysosomal escape, and the release of the attached cargo in the targeted site of action, are the basic strategies to the development of "smart" nano-sized DNA- or siRNA-conjugates delivery systems, and more research in this area is needed to improve their design and application up to the level of clinical trials.

The main conclusions drawn from our studies and suggested future directions are discussed here:

(i) We were the first research group to evaluate quantitatively and systematically the enhancement in solvation capacity of propellant HFA upon addition of co-solvent ethanol. F_{ad} is widely recognized as a good predictor of solvation forces. CFM was the experimental approach used to determine the F_{ad} between surfaces containing the moieties of interest (alkyl, ether, and ester – all relevant to HFA-based pMDI formulations) in HPFP/ethanol liquid mixtures with varying volume fractions of ethanol. HPFP was the liquid at ambient conditions to mimic propallent HFA. CFM results indicated that ethanol is indeed capable of enhancing the solvation of all fragments, and that the solvation increases as the volume fraction of ethanol increases. However, for

the alkyl moiety, volume fractions of ethanol much larger than those typically employed in commercial MDI formulations (< 15%) are required to achieve a level of solvation comparable to that of the ether moiety in pure HPFP. The effect of ethanol in the solvation of the ether fragment is much more pronounced (same for the ester fragment), thus indicating the potential of ethanol to be applied in PEG-based pMDIs. The CFM experimental results were modeled using the JKR theory, which suggested a strong dispersive contribution of the alkyl tails to the solvation in HPFP/ethanol mixtures.

However, the reference state of ideal solvation – $F_{ad}/R \approx 0$ mN.m^{-1} – was not achieved for any system, and high volume fraction of ethanol in HPFP was needed to bring the $F_{ad}/R \approx 1$ mN.m^{-1} – the lowest value obtained – 90, 70, and 50% for alkyl, ether, and ester moieties, respectively. Since these ethanol contents are extremely elevated to be applied in commercial HFA-based formulations (10% approved by FDA via respiratory (inhalation), aerosol, metered dosage form) suggested future work is this area includes the application of CFM and molecular simulations to search other HFA-philic chemistries able to reach the ideal solvation state, but keeping the ethanol concentration within the range approved by FDA.

Hydrofluoroolefins (HFOs) have emerged as the non-ozone depleting and low global warming potential (GWP) alternatives to HFAs, and thus the transition from propellant HFAs to HFOs to be used in medical aerosols is not so far to start happening in the US market. Therefore, the use of CFM in combination with molecular simulations for the development of HFO-philic chemistries in presence/absence of co-solvent ethanol is of great relevance. In addition, the design and application of an apparatus

which makes able to measure F_{ad} under pressure – *in situ* – using HFA (or HFO) instead of other liquid mimicking the propellant, is also suggested as future work.

(ii) We were the first research group to develop formulations of DNA-based polyplexes and siRNA-based dendriplexes in HFA-based pMDIs to deliver nucleic acids to the lungs. CS-DNA polyplexes were prepared using low Mw CS, and high DNA complexation efficiency along with size < 200 nm were achieved. Emulsification diffusion was applied to load the CS-DNA polyplexes into a biodegradable, water soluble, HFA-philic co-oligomer. Thus, micron-sized core-shell particles (polyplexes as core, and co-oligomer as shell) were obtained and characterized as within the appropriate geometric diameter required for formulation in pMDIs. CS-DNA core-shell particles were then dispersed in propellant HFA, and such pMDI formulations showed excellent physical stability (no flocculation even after many hours stopped the mechanical energy input) and very good aerosol properties (MMAD ca. 2 μM and FPF ca. 63%). More importantly, CS-DNA polyplexes alone and formulated as core-shell particles (even after exposure to propellant HFA) were found to transfect and deliver DNA to alveolar lung epithelial cells *in vitro*. Collectively, all the results indicated that formulating polyplexes in core-shell particles is an efficient approach to deliver nucleic acids to the lungs using inexpensive and portable pMDIs with potential to treat medically relevant pulmonary diseases, including asthma, COPD, cystic fibrosis, and cancer.

Since RNAi-based therapies have been proposed for the treatment of several genetic, chronic, and infectious lung disorders, essentially due to the advantages of siRNA over DNA, dendriplexes formed between PAMAM G4NH2 dendrimer and siRNA

were evaluated. siRNA-G4NH2 dendriplexes showed high siRNA complexation efficiency, size ca. 250 nm, positive surface charge, efficient protection against RNase degradation. The *in vitro* release of siRNA from G4NH2 dendrimer was sustainable and pH-dependent. PAMAM dendrimers are very promising siRNA delivery vehicles, but their application to deliver siRNA to the lungs has not been well explored, and thus, we were the first group to demonstrate the use of siRNA-G4NH2 dendriplexes to knockdown gene expression in alveolar lung epithelial cells *in vitro*. More importantly, it was found that dendriplexes prepared with siRNA stored in propellant HFA were able to provide the same level of gene suppression than those formed with untreated siRNA.

The core-shell particles formulation strategy – successfully applied for CS-DNA polyplexes – was also employed for siRNA-G4NH2 dendriplexes. Since the method of loading NPs using spray drying is very common to prepare dry powders – but the application of such microparticles has not been explored in pMDIs – the encapsulation of siRNA-G4NH2 dendriplexes in spray-dried mannitol sugar alcohol particles was also evaluated. In conclusion, both strategies provided good siRNA loading, and particles in the appropriate size for deep lung deposition when applied in an aerosol. In addition, it was found that the particle engineering process (core-shell emulsification diffusion or mannitol spray drying) did not affect the integrity of DNA or siRNA, and gel electrophoresis showed that the nucleic acid is essentially the same before and after the load into micron-sized particles. pMDI formulations prepared using core-shell and mannitol particles loaded with siRNA-G4NH2 dendriplexes showed excellent physical stability and very good aerosol performance, which were equivalent to those from commercial pMDI formulations of therapeutic drugs.

Therefore, all these results are very promising, and strongly indicated that the formulation of DNA- and siRNA-delivery systems into appropriate non-active particles has great potential to deliver nucleic acids *locally to* the lung tissue using portable and inexpensive pMDIs.

Suggested future work is this area includes the optimization of siRNA-based dendriplexes to knock down the gene expression *in vitro* in airway lung epithelial cells, which are more difficult to transfect most likely due to the mucus layer. Colocalization studies using dendriplexes formed with fluorescent-labeled siRNA and dendrimer would be also relevant in order to explore the intracellular trafficking of the dendriplexes, free dendrimer and siRNA after its release from the PNC. *In vivo* studies would be also of great importance.

With regard to formulation strategies in portable OI devices, the use of porous particles for the delivery of siRNA-PNCs using pMDIs has the potential to be explored as future work. Initial studies could be based on blending (in HFA atmosphere) siRNA-PNCs with a porous non-active carrier (e.g. lactose or mannitol) as micron-sized particles. The presence of PEG conjugated to the PNC is expected to help the dispersion stability, since it has been shown that the ether moieties in the PEG display HFA-philicity. In addition, the formulation of siRNA-PNCs in DPIs is also very relevant as future work in this area.

(iii) We were the first research group to propose and evaluate PAMAM dendrimer as PNC for conjugation with siRNA. G4NH2-siRNA conjugates were designed to have a reducible disulfide crosslink, which cleaves in the cell cytoplasm by reducing agents

and releases the siRNA to its site of action. These conjugates were synthesized, characterized, and without any further optimization, they were able to knock down the expression of eGFP in alveolar lung epithelial cells *in vitro*. The eGFP knockdown efficiency was significantly different from that obtained with free siRNA treatment. More importantly, the eGFP silencing effect of the G4NH2-siRNA conjugates was found to be siRNA-concentration dependent, while keeping the G4NH2 content at low levels which are demonstrated to be not toxic to the cells. Therefore, siRNA-dendrimer conjugates are of great relevance in the development of safe and efficient siRNA-delivery systems, not only *locally to* the lungs, but they have potential to be expanded to other tissues and routes of administration.

Suggested future work is this area includes the optimization of G4NH2-siRNA conjugates via linkage of other molecules. *(i)* PEG, which has been shown to impart several advantageous traits to conjugates including faster diffusion and less aggregation in mucus and lung surfactant, improved aqueous solubility, decreased opsonization, and reduced cytotoxicity. *(ii)* Since PEGylation can prevent endolysosomal escape, the crosslink between G4NH2 and PEG could have a molecule capable of enhancing the buffering capacity, such as aryl hydrazone (AH). AH labile linker is hydrolyzed under acidic conditions (pH 5), and thus it is expected to release the PEG, exposing the amine groups from the dendrimer. *(iii)* In order to address the issue that PEG reduces cellular uptake, internalization ligands (such as folic acid and lauroyl) could potentially be conjugated to the end of the PEG chain, being thus more exposed to receptors on the cell surface. *(iv)* A fluorescent dye (such as Cyanine-3, Cy-3) should be linked to the G4NH2 surface, in order to facilitate the detection of the

conjugates in *in vitro* and *in vivo* experiments. This suggested optimization requires systematic studies with regard the density, Mw, and molar ratio among the molecules to be attached on the G4NH2-siRNA conjugates. Measures should include, but not limited to, *in vitro* and *in vivo* gene knockdown efficiency, cellular uptake, and colocalization experiments. The preparation of G4NH2-siRNA conjugates with fluorescent- or radio-labeled G4NH2 and siRNA would be thus important to elucidate cellular internalization mechanisms, intracellular trafficking pathways, and colocalization with cell organelles.

With regard to *in vivo* studies, pharmacokinetics, biodistribution, and toxicity would be the routine experiments. In addition, visualization in live animals or in isolated organs and tissues should also be considered in future work. The use of diseased animal models would be very relevant to evaluate the stability, safety, and efficiency of the siRNA-delivered systems proposed in this dissertation. For example, implantation of tumour cells into wild type or nude mice (xenograft) has been widely used as model for cancer in lung, breast, prostate, colon, ovarian, and liver. Genetically engineered mouse models (transgenic) have been proposed to study gene therapy in brain cancer and skin disorders, and thus should also be planned for future work.

Therefore, all the results discussed in this dissertation, along with the proposed future work, contribute significantly in the development of DNA- and siRNA-delivery systems and in their formulation in portable OI devices, with great potential to efficiently deliver nucleic acids *to* the lungs to treat medically relevant pulmonary disorders, such as COPD, asthma, virus infections, cystic fibrosis, and lung cancer.

APPENDIX A

Supporting Information for Chapter 4

A.1 Preparation of water soluble, low Mw CS

Low Mw CS was obtained according to a modified version of a method previously described literature.[1] Briefly, 4 g of CS (100 - 300 kDa, 80% DDA) were dissolved in 200 mL DI-water with 1 mL concentrated hydrochloric acid, under heating (65 - 70°C) and magnetic stirring (3 h). Hydrogen peroxide (5 mL) was added, and CS was depolymerized at 65 - 70°C for 12 h. At the end of the reaction, the solution was allowed to cool down, and the pH was adjusted to 8 with a 3 M sodium hydroxide solution. The water soluble, low Mw CS was separated by centrifugation (15 min at 5,000 rpm - 2,800 xg) since the low Mw CS remains in the supernatant, and the insoluble large Mw CS precipitates. The supernatant was diluted 1:1 (v/v) using DI-water, and it was nanoprecipitated (200 mL, slow drip, approximately one drop each 3 s) into a large volume of ethanol (900 mL) under stirring. The low Mw CS is water soluble but insoluble in the ethanol/water mixture. The final product was precipitated by centrifugation (5,000 rpm - 2,800 xg), washed repeatedly with ethanol and acetone, and dried in air at room temperature. The nanoprecipitation step is required as CS is not soluble in the grafting reaction medium (toluene), and a dispersion of uniform and small nanoparticles is expected to aid in the grafting reaction described below.

A.2 Synthesis of OLA-*g*-CS co-oligomer

It was performed according to a modified method described in the literature.[1] Briefly, 0.8 g of water soluble low Mw CS obtained as described earlier was dispersed in 50 mL of toluene with the help of a sonication bath (VWR, P250D, set to 180 W). Subsequently, 4.3 g of recrystallized LA was added in the CS dispersion, and the system was heated in an oil bath to 90 - 95°C under stirring. Nitrogen was purged for 30 min. Stannous octoate catalyst was added (40 mg in 5 mL toluene) and the reaction carried out at 90 - 95°C under nitrogen atmosphere for 24 h. The total mass of CS, LA and stannous octoate added to the system was calculated based on a 1:100:1/5 molar ratio, respectively. The product was precipitated by centrifugation (5,000 rpm - 2,800 xg) and washed with toluene. The precipitate was added to 50 mL toluene and the reaction repeated. An additional mass of 4.3 g of LA, and 40 mg of catalyst were added to the system, and the reaction continued at 90 - 95°C under nitrogen atmosphere for 50 - 60 h. The final product was separated in two fractions (precipitate and supernatant) by centrifugation (2,600 rpm - 760 xg, 5min). The OLA-*g*-CS in the supernatant (the final product) was then precipitated by centrifugation (10,000 rpm – 11,200 xg), repeatedly washed with toluene and acetone, and dried in air at room temperature overnight.

A.3 Characterization of low Mw CS and OLA-*g*-CS

The Mw of the CS and OLA-*g*-CS co-oligomers was evaluated by MALDI-TOF (Bruker Ultraflex).[2] A known amount of the sample (2 mg) was dissolved in 1 mL of 80:20 (v/v) DI-water:acetonitrile solution. The sample solution (1 µL) was mixed with

1 µL of matrix solution (DHB, 15 mg.mL^{-1}) on the target plate (MTP 384, Bruker), and allowed to dry at room temperature prior to MALDI-TOF analysis. Proton Nuclear Magnetic Resonance (^{1}H-NMR, Varian Mercury 400) and Fourier Transform Infrared Spectrometry (FTIR, Bruker Tensor 27) were used to obtain the chemical structure of the CS and OLA-*g*-CS co-oligomers.[1, 3] The sample (10 mg) was dissolved in 0.8 mL of DMSO-d6 for ^{1}H-NMR analyses, and for the FTIR, 5 mg was mixed with 200 - 500 mg of potassium bromide, and pressed to a pellet.

A.4 Characterization of low Mw CS and OLA-*g*-CS

Recrystallized LA was reacted with CS in toluene in the presence of stannous octoate catalyst as described above.[1, 3] Because the amine and hydroxyl groups of CS work as initiators during the reaction, the ring opening polymerization of LA results in grafts onto the CS backbone.[1] The chemical structure of the low Mw CS and OLA-*g*-CS co-oligomer were characterized by ^{1}H-NMR, FTIR and MALDI-TOF. The results are shown in Figure A1.

The ^{1}H-NMR spectrum of the CS (Figure A1a) indicates a singlet at 3.1 ppm (H-2), multiplets at 3.3 - 3.7 ppm (H-3, H-4, H-5, H-6), and a singlet at 4.3 ppm (H-1) corresponding to the ring methenyl protons.[3, 4] The singlet at 2.1 ppm is related to the methyl protons present in the N-acetyl-D-glucosamine units (-CH_3, H-7).[5] To verify whether the chemical structure of the low Mw CS changed due to potential deamination during the depolymerization process,[6] the degree of deacetylation (DDA) was calculated using the ^{1}H-NMR spectrum and the following equation below, where I_{CH3} refers to the integral intensity of the peak from the methyl group of the N-acetyl-D-glucosamine units

(H-7) and $I_{H2\text{-}H6}$ is the summation of integral intensities of the H2, H3, H4, H5 and H6 peaks.[7]

$$DDA = \{ [1 - [(1/3\ I_{CH3}) \div (1/6\ I_{H2\text{-}H6})] \} \times 100$$

The DDA of the CS was calculated to be 77% (ca. 1 acetyl and 5 amine units), suggesting that the molecular structure of the CS was not impacted due to deamination during depolymerization, given that the DDA before (80% reported by the supplier) and after were very similar.

The Mw of the water soluble CS was evaluated by MALDI-TOF, and the spectrum is shown in Figure A1c. Two predominant degrees of polymerization (DP) are clearly observed. The peak-to-peak mass difference is 162.1 $g.mol^{-1}$, in close agreement with the mass of one D-glucosamine unit (161.1 $g.mol^{-1}$).[8] Considering the DDA, the average molar mass between acetylated and deacetylated units, and the two dominant peaks, the spectrum in Figure A1c reveals that the CS is mainly composed of five and six repeat units (Mw 939 Da). Small deviations observed by comparing the measured and theoretical masses can be attributed to fragmentation, which corresponds to cleavage of bonds in oligosaccharides during the analysis,[8] despite the incorporation of a matrix.[9] However, such deviations did not have significant effect on the DP obtained. The MALDI-TOF spectrum of the OLA-*g*-CS co-oligomer shown in Figure A1c, indicates a larger molar mass compared to the CS, as expected. However, due to sample fragmentation,[8] especially because the easy degradation of the LA

chains,[10] ^{1}H-NMR is preferred for the characterization of the size and density of the LA grafts.[1, 3]

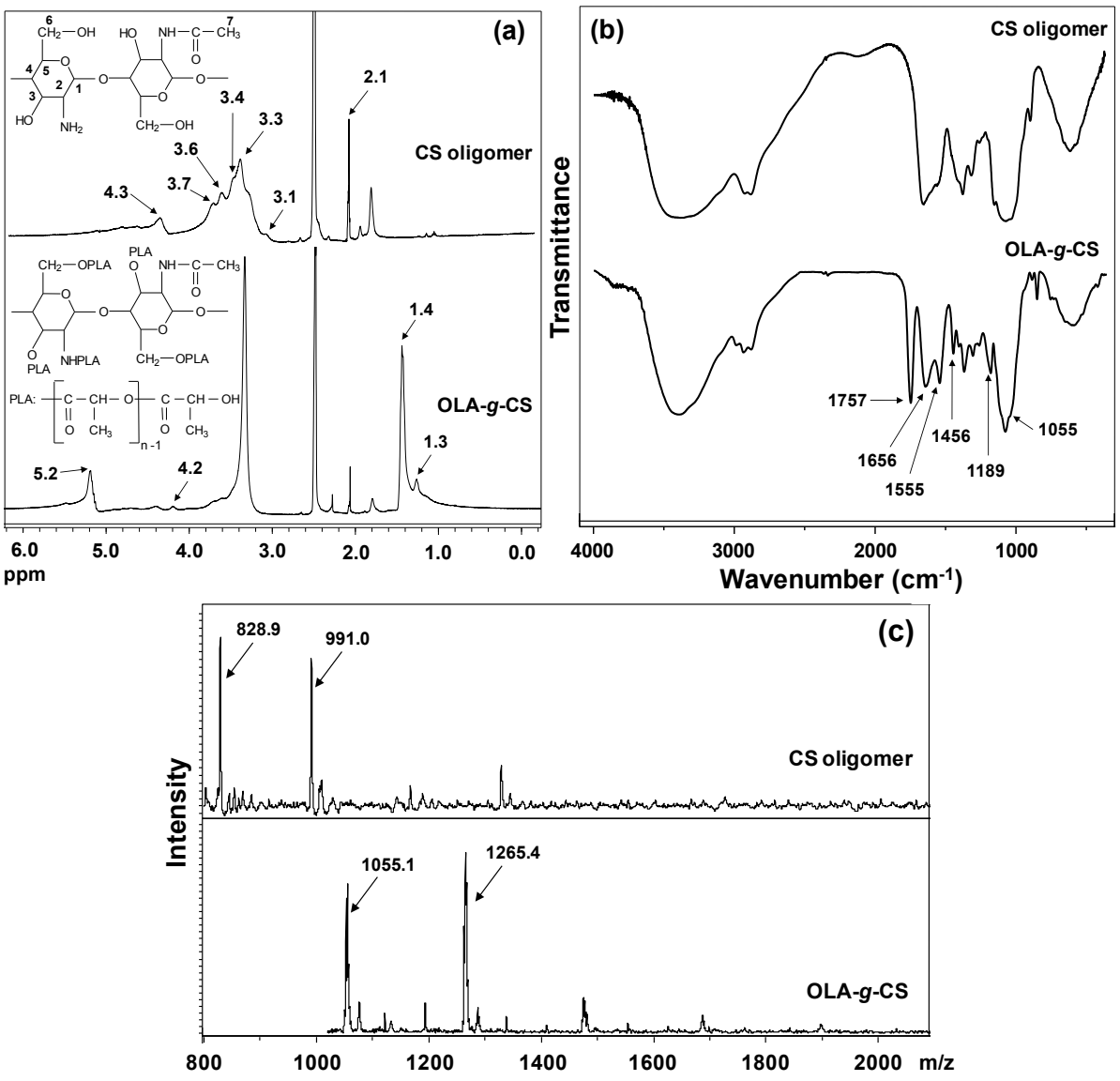

Figure A1. **(a)** ^{1}H-NMR; **(b)** FTIR; and **(c)** MALDI-TOF spectra for low Mw CS and OLA-*g*-CS.

Compared with the CS, the ^{1}H-NMR spectrum of the OLA-*g*-CS (Figure A1a) shows peaks at 4.2 and 5.2 ppm, which are assigned to the terminal methenyl protons of the oligo(LA), and its repeating units in the chain, respectively. The peaks at 1.3 and

1.4 ppm are attributed to the methyl protons of the oligo(LA) moiety located at the terminal groups and the backbone.[3] Structural changes in the low Mw CS brought by oligo(LA) grafting can be also seen in the FTIR spectra (Figure A1b). Compared to the FTIR spectrum of the CS, the OLA-*g*-CS has a new absorption peak at 1757 cm^{-1}, attributed to the carbonyl group of the LA repeat units.[1, 3] The methyl asymmetric deformation of oligo(LA) is found at 1456 cm^{-1}.[3] The peak at 1189 cm^{-1} is assigned to the symmetric C-O-C stretching modes of the ester group, and the C-CH_3 stretching vibrations appear at 1055 cm^{-1}.[3] The peaks at 1656 cm^{-1} and 1555 cm^{-1} can be attributed to C=O stretching vibrations (amide I) and N-H deformation coupled with C-N stretching vibrations (amide II) of the secondary amide[11] formed between CS and oligo(LA), respectively. Therefore, the results collectively indicate that oligo(LA) was successfully grafted onto the water soluble low Mw CS.

Calculations based on the ^{1}H-NMR spectrum of OLA-*g*-CS (Figure A1a), considering the integral intensities of the peaks at 4.3 ppm (from CS) and 5.2, 1.4, 1.3 ppm from oligo(LA),[1] indicated that there are ca. three oligo(LA) chains grafted on each CS backbone, and each oligo(LA) chain is composed of eight LA repeat units. Thus, the Mw of the OLA-*g*-CS co-oligomer was calculated to be 1729.6 $g.mol^{-1}$. Also using the ^{1}H-NMR spectrum of OLA-*g*-CS, the grafting percentage based on the number of reactive groups (amine and hydroxyl) was 21.4%. This result is in good agreement with the grafting percentage calculated by the gravimetric method,[3] (grafting % = [(mass of OLA-*g*-CS) – (mass of CS) / (mass of CS)] $\times$ 100), found to be 23.2%.

A.5 Characterization of the DDA of 31 kDa CS used in the preparation of the polyplexes

To evaluate whether the chemical structure of the 31 kDa Mw CS was altered due to potential deamination during the depolymerization process, ^{1}H-NMR was used to determine the DDA using the same methodology as detailed earlier. The DDA was calculated to be 77%. This result indicates that the molecular structure of CS was not changed due to deamination during depolymerization, based on the comparison with the DDA of CS as received (80% reported by the supplier).

A.6 Characterization of CS-DNA polyplexes during preliminary screening

In order to prepare CS-DNA polyplexes with small size (diameters around 200 nm or smaller), enhanced colloidal stability, and also good *in vitro* transfection efficiency in A549 cells, we performed a series of preliminary experiments that involved the preparation of polyplexes with varying CS Mw (80% DDA) and N/P ratio. The polyplexes were characterized according to DNA encapsulation efficiency (EE), size and polydispersity (PDI), zeta potential (ζ), and the ability of *in vitro* transfection (good/poor). The results are shown in Table A1.

Polyplexes containing Calf Thymus and gWIz-GPF DNA, prepared with CS 31 kDa and 80% DDA at N/P ratio of 6, showed high DNA EE (> 90%), similar size (ca. 180 nm) and ζ ca. + 21 mV, and thus were selected for further studies. Based on the results from this preliminary screening (Table A1), such improved properties were obtained through reduction in Mw of CS, and optimization of N/P ratio.

Table A1. Physicochemical properties of CS-DNA polyplexes according to Mw of CS (80% DDA) and nominal N/P ratio.

CS Mw (kDa)	Type of DNA	Nominal N/P ratio	DNA EE (%)	Particle Size (nm)	PDI of Size	Zeta Potential (ζ) (mV)	*In vitro* Transfection in A549 cells
310	Calf Thymus	6	88 ± 7	595 ± 85	0.3	-	N.A.
49	gWIz-GFP	6	95 ± 1	666 ± 21	0.6	+ 27 ± 1	Poor
31	Calf Thymus	6	90 ± 8	183 ± 51	0.4	+ 21 ± 4	N.A.
31	gWIz-GFP	2	97 ± 1	111 ± 71	0.9	+ 13 ± 1	Poor
31	gWIz-GFP	4	94 ± 2	167 ± 146	0.9	+ 16 ± 1	Poor
31	gWIz-GFP	5	95 ± 1	229 ± 93	0.8	+ 23 ± 1	Poor
31	gWIz-GFP	6	97 ± 5	268 ± 51	0.3	+ 31 ± 6	Good
31	gWIz-GFP	7	95 ± 3	181 ± 62	0.5	+ 22 ± 6	Good

N.A. = not applicable
PDI = polydispersity index

The Mw of CS has an effect on the size of polyplexes,[12, 13] and the size plays a role in the transfection process. It is expected that high Mw CS has enhanced binding affinity to DNA, and condenses the genetic material more efficiently than low Mw CS, producing polyplexes with smaller sizes.[12] However, several works[12-20] have reported the formation of CS-DNA polyplexes with small size using low Mw CS. This can be attributed to the higher solubility and flexibility of the short CS chains in solution, i.e., low Mw CS is more soluble than high Mw CS, and thus, low Mw CS becomes better hydrated by the aqueous solvent.[12, 15, 21, 22] During our preliminary screening, at N/P ratio of 6 and for both types of DNA, polyplexes with smaller sizes were prepared when the Mw of CS was reduced from 310 to 31kDa, as seen in Table A1.

The N/P ratio is another important property of the CS-DNA polyplexes which has effect on *in vitro* transfection efficiency.[14, 23, 24] At a low N/P ratio, physically unstable polyplexes were obtained, and that resulted in poor *in vitro* transfection. However,

stable complexes obtained at higher N/P ratio may also show reduced *in vitro* transfection,[14, 23, 24] probably due to the fact that highly positive charged polyplexes may be toxic to the cells and/or establish non-specific interactions with the cells.[25] In our preliminary screening, CS-DNA polyplexes exhibited poor *in vitro* transfection at N/P ratio of 2, 4, and 5, probably due to lower surface charge (ca. + 13 - 16 mV at N/P ratio of 2 and 4), or increased size of the NPs (large standard deviation and PDI at N/P ratio of 2, 4, and 5). The *in vitro* transfection was improved when the polyplexes were formulated at N/P ratio of 6 and 7. At these N/P ratios, CS-DNA polyplexes showed reduced size, and lower PDI.

Based on the results from our preliminary screening, which were in agreement with trends reported in the literature for CS-DNA polyplexes, there is an optimal range for the N/P ratio (which is specific to the type of CS used – Mw and DDA), that influences size and surface charge of the polyplexes, and *in vitro* transfection as well. We chose CS-DNA polyplexes which demonstrated appropriate size and transfection, and had similar properties (size and ζ) for both Calf Thymus DNA and pDNA.

A.7 References

1. Wu, L.; Bharatwaj, B.; Panyam, J.; da Rocha, S. Core-shell particles for the dispersion of small polar drugs and biomolecules in hydrofluoroalkane propellants. *Pharm. Res.* **2008,** *25*, (2), 289-301.

2. Cabrera, J. C.; Van Cutsem, P. Preparation of chitooligosaccharides with degree of polymerization higher than 6 by acid or enzymatic degradation of chitosan. *Biochem. Eng. J.* **2005,** *25*, (2), 165-172.

3. Luckachan, G. E.; Pillai, C. K. S. Chitosan/oligo L-lactide graft copolymers: Effect of hydrophobic side chains on the physico-chemical properties and biodegradability. *Carbohydr. Polym.* **2006,** *64*, (2), 254-266.

4. Wu, Y.; Zheng, Y.; Yang, W.; Wang, C.; Hu, J.; Fu, S. Synthesis and characterization of a novel amphiphilic chitosan-polylactide graft copolymer. *Carbohydr. Polym.* **2005,** *59*, (2), 165-171.

5. Tian, F.; Liu, Y.; Hu, K.; Zhao, B. Study of the depolymerization behavior of chitosan by hydrogen peroxide. *Carbohydr. Polym.* **2004,** *57*, (1), 31-37.

6. Qin, C. Q.; Du, Y. M.; Xiao, L. Effect of hydrogen peroxide treatment on the molecular weight and structure of chitosan. *Polym. Degrad. Stab.* **2002,** *76*, 211-218.

7. Tan, S. C.; Khor, E.; Tan, T. K.; Wong, S. M. The degree of deacetylation of chitosan: Advocating the first derivative UV-spectrophotometry method of determination. *Talanta* **1998,** *45*, (4), 713-719.

8. Trombotto, S.; Ladavière, C.; Delolme, F. d. r.; Domard, A. Chemical preparation and structural characterization of a homogeneous series of chitin/chitosan oligomers. *Biomacromolecules* **2008,** *9*, (7), 1731-1738.

9. Cohen, L. H.; Gusev, A. I. Small molecule analysis by MALDI mass spectrometry. *Anal. Bioanal. Chem.* **2002,** *373*, 571-586.

10. Lee, H.; Lee, W.; Chang, T.; Choi, S.; Lee, D.; Ji, H.; Nonidez, W. K.; Mays, J. W. Characterization of poly(ethyleneoxide)-*block*-poly(L-lactide) by HPLC and MALDI-TOF mass spectrometry. *Macromolecules* **1999,** *32*, 4143-4146.

11. Socrates, G., *Infrared and Raman characteristic group frequencies - Tables and charts*. 3rd ed.; John Wiley & Sons, LTD: Chichester, 2001; p 347p.

12. MacLaughlin, F. C.; Mumper, R. J.; Wang, J.; Tagliaferri, J. M.; Gill, I.; Hinchcliffe, M.; Rolland, A. P. Chitosan and depolymerized chitosan oligomers as condensing carriers for *in vivo* plasmid delivery. *J. Controlled Release* **1998,** *56*, (1-3), 259-272.

13. Huang, M.; Fong, C.-W.; Khor, E.; Lim, L.-Y. Transfection efficiency of chitosan vectors: Effect of polymer molecular weight and degree of deacetylation. *J. Controlled Release* **2005,** *106*, (3), 391-406.

14. Lavertu, M.; Méthot, S.; Tran-Khanh, N.; Buschmann, M. D. High efficiency gene transfer using chitosan/DNA nanoparticles with specific combinations of molecular weight and degree of deacetylation. *Biomaterials* **2006,** *27*, (27), 4815-4824.

15. Liu, W.; Sun, S.; Cao, Z.; Zhang, X.; Yao, K.; Lu, W. W.; Luk, K. D. K. An investigation on the physicochemical properties of chitosan/DNA polyelectrolyte complexes. *Biomaterials* **2005,** *26*, (15), 2705-2711.

16. Bozkir, A.; Saka, O. M. Chitosan nanoparticles for plasmid DNA delivery: Effect of chitosan molecular structure on formulation and release characteristics. *Drug Deliv.* **2004,** *11*, 107-112.

17. Köping-Höggard, M.; Varum, K. M.; Issa, M.; Danielsen, S.; Christensen, B. E.; Stokke, B. T.; Artursson, P. Improved chitosan-mediated gene delivery based on easily dissociated chitosan polyplexes of highly defined chitosan oligomers. *Gene Ther.* **2004,** *11*, (19), 1441-1452.

18. Gao, S.; Chen, J.; Xu, X.; Ding, Z.; Yang, Y.-H.; Hua, Z.; Zhang, J. Galactosylated low molecular weight chitosan as DNA carrier for hepatocyte-targeting. *Int. J. Pharm.* **2003,** *255*, (1-2), 57-68.

19. De Smedt, S. C.; Demeester, J.; Hennink, W. E. Cationic polymer based gene delivery systems. *Pharm. Res.* **2000,** *17*, (2), 113-126.

20. Strand, S. P.; Lelu, S.; Reitan, N. K.; de Lange Davies, C.; Artursson, P.; Vårum, K. M. Molecular design of chitosan gene delivery systems with an optimized balance between polyplex stability and polyplex unpacking. *Biomaterials* **2010,** *31*, (5), 975-987.

21. Wang, W.; McConaghy, A. M.; Tetley, L.; Uchegbu, I. F. Controls on polymer molecular weight may be used to control the size of palmitoyl glycol chitosan polymeric vesicles. *Langmuir* **2001,** *17*, (3), 631-636.

22. Mao, S.; Bakowsky, U.; Jintapattanakit, A.; Kissel, T. Self-assembled polyelectrolyte nanocomplexes between chitosan derivatives and insulin. *J. Pharm. Sci.* **2006,** *95*, (5), 1035-1048.

23. Kim, T.-H.; Jiang, H.-L.; Jere, D.; Park, I.-K.; Cho, M.-H.; Nah, J.-W.; Choi, Y.-J.; Akaike, T.; Cho, C.-S. Chemical modification of chitosan as a gene carrier *in vitro* and *in vivo*. *Prog. Polym. Sci.* **2007,** *32*, (7), 726-753.

24. Ishii, T.; Okahata, Y.; Sato, T. Mechanism of cell transfection with plasmid/chitosan complexes. *Biochim. Biophys. Acta* **2001,** *1514*, (1), 51-64.

25. Yoksan, R.; Akashi, M. Low molecular weight chitosan-*g*-L-phenylalanine: Preparation, characterization, and complex formation with DNA. *Carbohydr. Polym.* **2009,** *75*, (1), 95-103.

APPENDIX B

Supporting Information for Chapter 5

B.1 siRNA Degradation by RNase A

In order to determine the minimum RNase A concentration to degrade siRNA completely, siRNA (300 ng) was incubated with different amounts of RNase A in TE 1X pH 8 buffer (0.02, 0.07, 0.162, 0.348, 0.7, and 3.3 μg RNase A per 1 μg siRNA) for 45 min at 37°C, in presence or absence of RiboLock® RNase Inhibitor (RI, 1μL = 40U). The concentration of 0.35 μg RNase A per 1 μg siRNA has been reported in literature to be sufficient to degrade a large fraction of siRNA in polyplexes,[1, 2] and based on that, the amount of RNase A was varied in this experiment. Next, samples were frozen at -20°C overnight, and loaded in the slots of a casted non-denaturing agarose gel (1.5 % w/v in TAE 1X pH 8.2 buffer) stained with ethidium bromide (0.5 $\mu g.mL^{-1}$). The electrophoresis was performed at 60V (E0160-VWR Mini Gel Electrophoresis) for 40 min, and the siRNA-dye migration was visualized under UV irradiation (FOTO/Analyst® Investigator/Eclipse with UV Transilluminator Fotodyne Inc.) and the images were recorded using the FOTO/Analyst® PC Image software (v.5). The result is shown in Figure B1, and clearly indicates that free siRNA (not protected by RNase inhibitor) was completely degraded by RNAse A starting at concentration 0.162 μg RNase A per 1 μg siRNA, since no siRNA band was observed in *lane 6* compared to *lane 7* and *lane 1*.

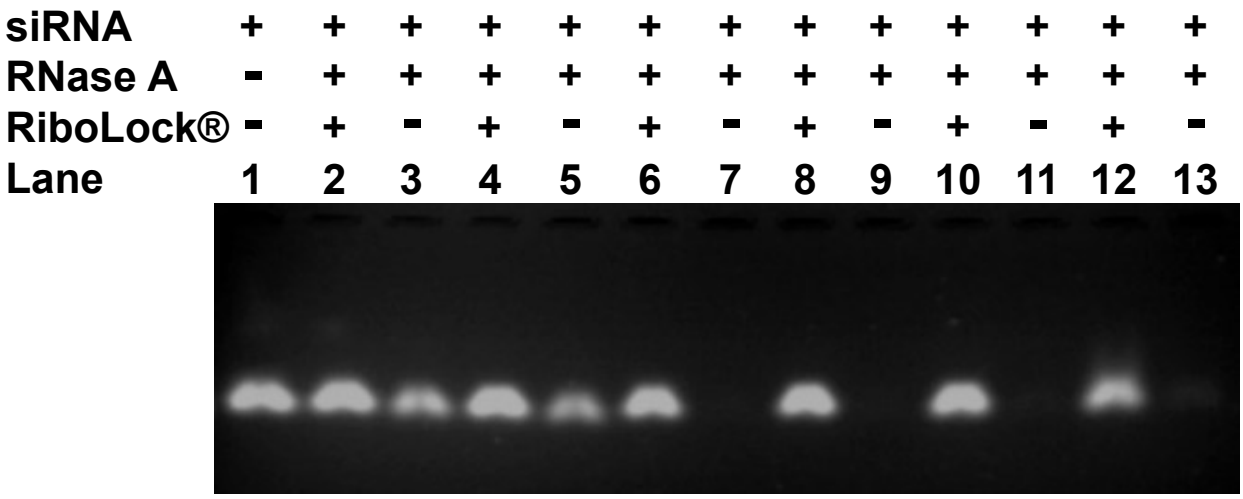

Figure B1. RNase degradation assay (non-denaturing agarose gel electrophoresis) of the free siRNA as a function of the RNase A concentration. siRNA (300 ng) was incubated with increased concentrations of RNase A (0.02, 0.07, 0.162, 0.348, 0.7, and 3.3 μg per 1 μg siRNA, in *lanes 2-3*, *4-5*, *6-7*, *8-9*, *10-11*, *12-13*, respectively) for 45 min at 37°C, in presence (+) or absence (-) of 1 μL (40 units) RiboLock® RNase inhibitor. Untreated siRNA control is in *lane 1*.

B.2 Heparin Decomplexation Assay

Heparin is known as a model polyanion competing agent with nucleic acids for electrostatic interactions with polycations,[3] and it has been used to dissociate siRNA from several polycationic carriers.[3-9] Thus, heparin was used in this work to dissociate siRNA from PAMAM G4NH2 dendrimer. In order to determine the most favorable condition of heparin treatment to release the highest siRNA content from the dendrimer, siRNA-G4NH2 at N/P 10 were formed in 10 mM Tris-HCl pH 7.4 buffer,[10] as described in the *Experimental Section of the Chapter 5*, incubated with heparin in TE 1X pH 8 buffer at 37°C for different time points, and frozen at -20°C overnight. The final heparin concentration was 5 $mg.mL^{-1}$ corresponding to 455 U per 1 μg siRNA calculated based on 1000 U per 1 mL.[4] The final siRNA concentration after dilution of the dendriplexes to 1 mL was 80 nM. siRNA-G4NH2 dendriplexes incubated in presence or absence of heparin (minimum of three independent batches, n = 3) were quantitatively analyzed

using PicoGreen® assay[11] in Synergy 2 Microplate Reader (BioTek, VT) for the siRNA content released, which was calculated using a linear calibration curve (siRNA concentration *vs.* fluorescent units). Thus, siRNA released from the dendriplexes due to heparin treatment was determined based on the difference between the siRNA content truly complexed with G4NH2 (siRNA CE was applied in the calculations) and the free siRNA released and remaining in the dendriplexes dispersion. Appropriate control (PAMAM G4NH2 in presence of heparin, but no siRNA) was used as blank. The results are shown in Figure B2, and indicate that the siRNA is released from G4NH2 dendrimer due to treatment of the dendriplexes with heparin. The incubation time of 30 min released the highest siRNA content – 80% on average, and narrower standard deviation – out of the total siRNA complexed with G4NH2, and thus, it was chosen as standard time for all further heparin decomplexation assay experiments.

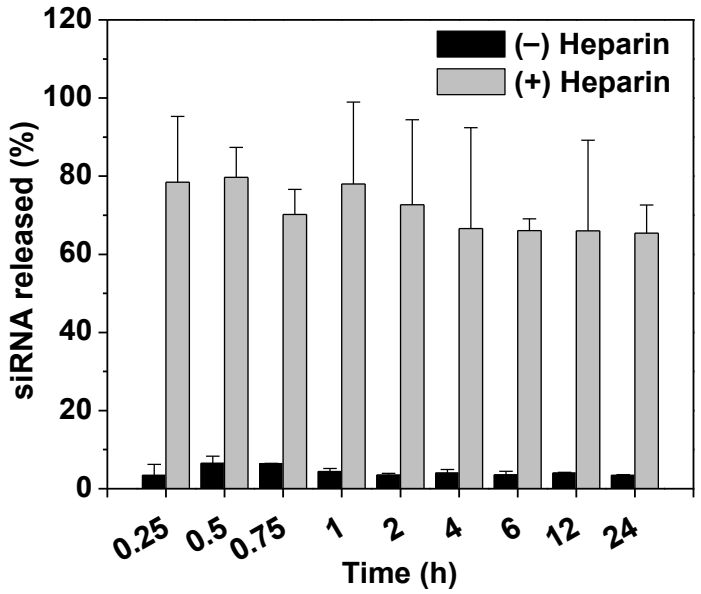

Figure B2. Heparin decomplexation assay of siRNA-G4NH2 dendriplexes at N/P 10. Dendriplexes were incubated with heparin (455 U per 1 μg siRNA) at 37°C for different time points, and the % siRNA released from PAMAM G4NH2 due to the heparin treatment was determined via PicoGreen® assay.

B.3 Development of eGFP Expressing A549 Cell Line

A549 cells were genetically modified to constitutively express eGFP (enhanced green fluorescence protein) according to GenTarget protocol.[12] Briefly, A549 cells (passage 5 from the original passage provided by ATCC®) were seeded in 24-well culture plate (25,000 cells per well) and cultured in 500 μL DMEM supplemented with 10% FBS and 1% AB (v/v) for 24 h at 37°C and 5% CO_2 (Thermo Scientific Incubator, NAPCO 8000WJ). Cells were rinsed with PBS 1X buffer, and fresh culture medium (DMEM with 10% FBS and 1% AB, v/v) was added to them, following 50 μL per well of eGFP lentiviral particles. Cells were kept in incubator for 72 h at 37°C and 5% CO_2, and after that, they were rinsed with PBS 1X buffer, and the selective medium was added to them (DMEM with 10% FBS and 2.5 $\mu g.mL^{-1}$ puromycin selective antibiotic, which concentration was previously determined by a kill curve). Cells were cultured under this selective condition for 4 weeks,[13] so that only eGFP positive transduced cells survived. Then, eGFP positive cells were sorted using flow cytometry (FACS, HWCRC 615 Cell Sorter) and visualized under inverted fluorescent microscope (Nikon Diaphot 300). Cells were cultured in DMEM with 10% FBS (v/v) and 2.5 $\mu g.mL^{-1}$ puromycin for 2 weeks at 37°C and 5% CO_2 before starting the *in vitro* gene knockdown experiments. The result is shown in Figure B3, and clearly demonstrates that the A549 cell line stably expressing eGFP was successfully established, since 99.7% of the transduced cells were found to express green fluorescence.

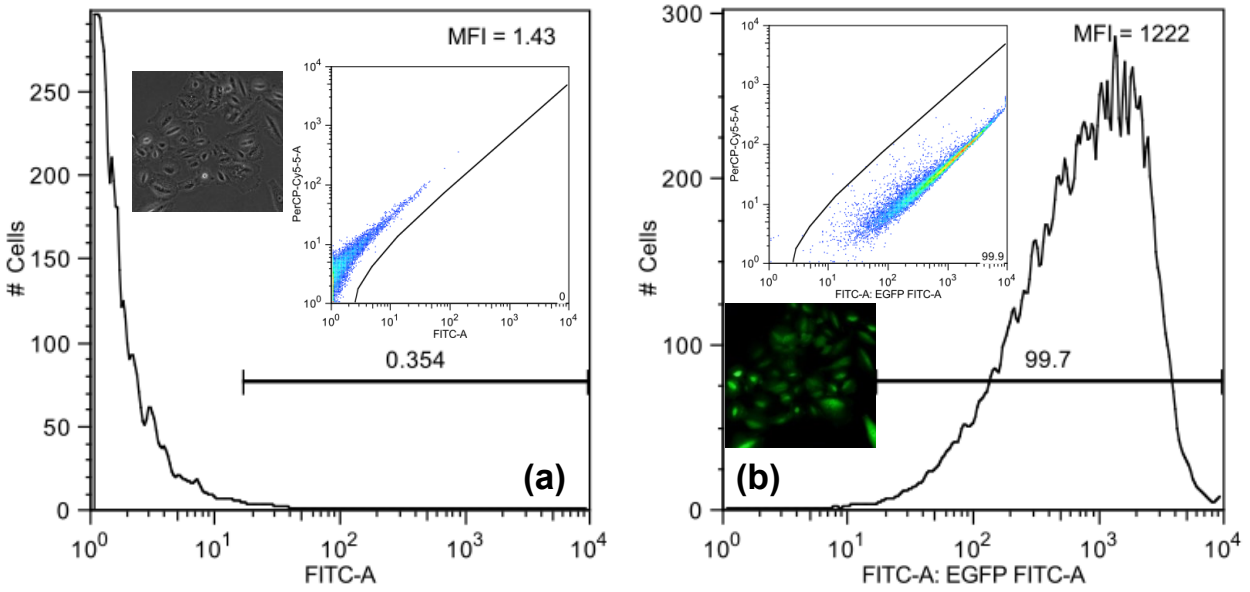

Figure B3. Histogram plots obtained from FACS of **(a)** A549 cells before and **(b)** after transduction using eGFP lentiviral particles. *Insets:* Dot plots from FACS, phase contrast and fluorescent images of A549 cells before and after eGFP transduction, respectively.

B.4 Characterization of CSLA Co-oligomer

Briefly, CSLA co-oligomer was synthesized by reacting low Mw CS (previously prepared by depolymerization of large Mw CS) with LA via ring opening polymerization.[14] See Appendix A for details about the methodologies. Thus, short lactide chains – oligo(LA) – were grafted onto CS backbone.[14] Proton Nuclear Magnetic Resonance (^{1}H-NMR, Varian Mercury 400) was used to obtain the chemical structure of the synthesized CSLA co-oligomer – density and length of the LA grafts, and Mw of the CSLA. Sample was prepared by dissolving 10 mg of CSLA in 0.8 mL of DMSO-d6. The ^{1}H-NMR spectrum of the CSLA co-oligomer (Figure B4) shows peaks at 4.061 and 5.186 ppm, which are assigned to the terminal methenyl protons of the oligo(LA), and its repeating units in the LA chain, respectively. The peaks at 1.3 and 1.442 ppm are attributed to the methyl protons of the oligo(LA) moiety located at the terminal groups and the chain.[15] Calculations based on the ^{1}H-NMR spectrum of CSLA (Figure B4),

considering the integral intensities of the peaks at 4.196 ppm (from CS backbone, correlated to 6.4H according to Mw determination via MALDI-TOF, Bruker Ultraflex) and 5.186, 1.442, 1.3 ppm from oligo(LA),[16] indicated that there were ca. 7.4 oligo(LA) chains grafted on each CS backbone, and each oligo(LA) chain was composed of ca. 5.1 LA repeat units. Thus, the Mw of the resulting CSLA co-oligomer was estimated to be ca. 3,650 $g.mol^{-1}$. Mw is a physical property which can be directly measured by MALDI-TOF.[17] However, due to sample fragmentation,[18] especially because the easy degradation of the LA segments of the CSLA,[19] ^{1}H-NMR is preferred for the characterization of the size and density of the LA grafts.[15, 16] The grafting percentage (% grafting) calculated via ^{1}H-NMR based on the total possible number of reactive groups (amine and hydroxyl) onto CS was 38.9%, and the one calculated via gravimetric method[15] – equation below – was found to be 25.3%.

$$\%\ grafting = \left(\frac{mass\ of\ CSLA - mass\ of\ CS}{mass\ of\ CS}\right) \times 100$$

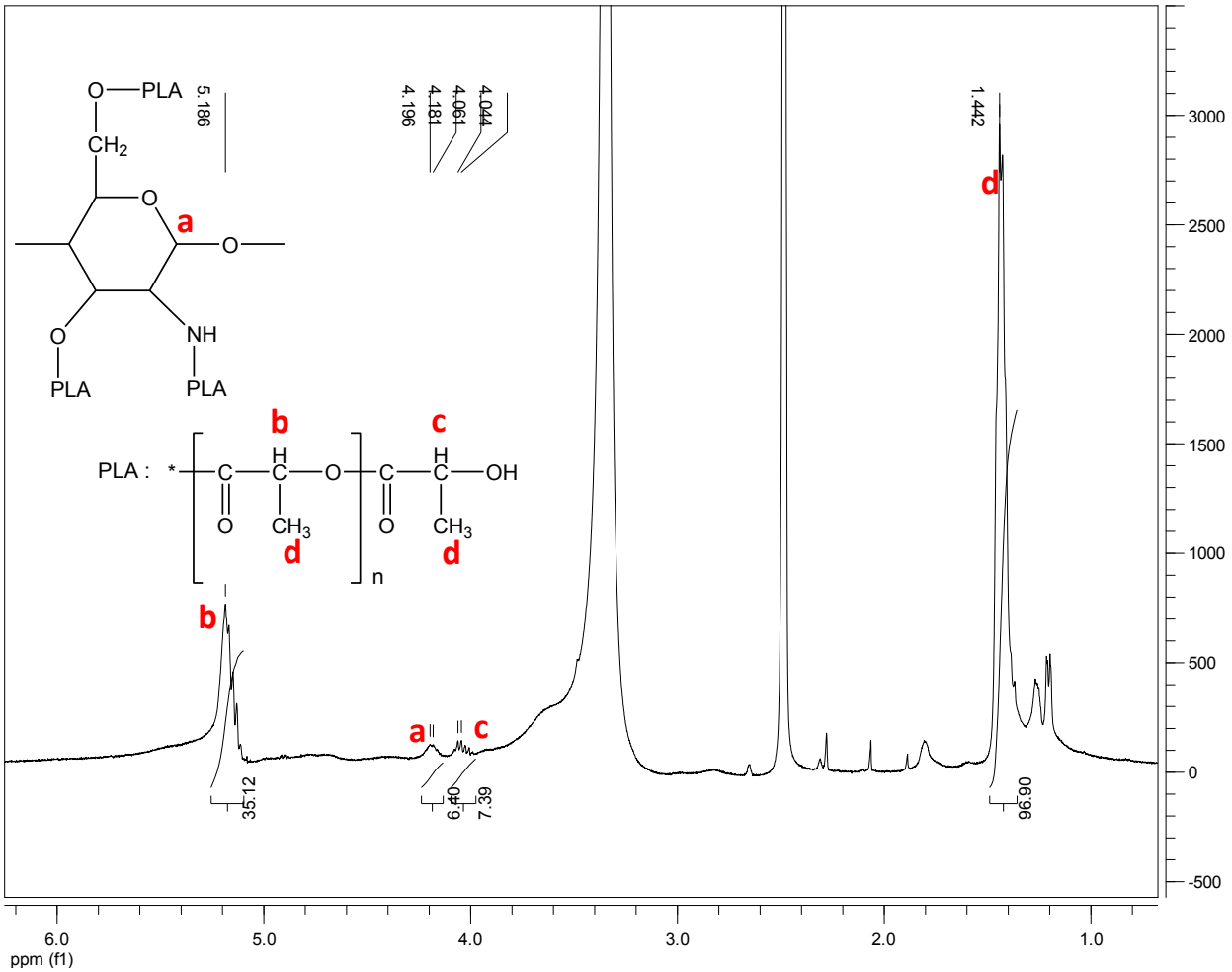

Figure B4. ^{1}H-NMR spectrum of CSLA co-oligomer.

B.5 pMDI Formulation of Free siRNA-G4NH2 Dendriplexes

Aiming to have a negative control for comparison of physical stability and aerosol performance, siRNA-G4NH2 dendriplexes alone were attempted to be formulated in pMDI. Dendriplexes at N/P 10 were prepared in RNase-free DI-water, the aqueous dispersion (siRNA and PAMAM G4NH2 at the same amount as loaded into CSLA and mannitol microparticles) was placed into the pressure proof glass vial, which was frozen at -20°C overnight and lyophilized. The canister was crimp sealed with a 63 μL metering valve, and a known volume of propellant HFA-227 was filled into it so that the

siRNA concentration was the same for pMDI formulations containing dendriplexes loaded into CSLA or mannitol microparticles.

Then, the pMDI formulation was placed into sonication bath (30 min at 15 - 20°C) to disperse the dendriplexes in the propellant. The result is shown in Figure B5. The dendriplexes were observed getting stuck on the wall of the glass vial, and even after sonication for a long time, they did not disperse in the propellant. Thus, it was not possible to have pMDI formulations of free siRNA-G4NH2 dendriplexes for further comparison with those prepared with CSLA and mannitol particles. Therefore, this result presents the difficulty of formulating siRNA-based dendriplexes alone in propellant HFA, and strongly suggests that an appropriate micro-carrier is needed for the job – such as CSLA and mannitol microparticles proposed in the *Chapter 5*.

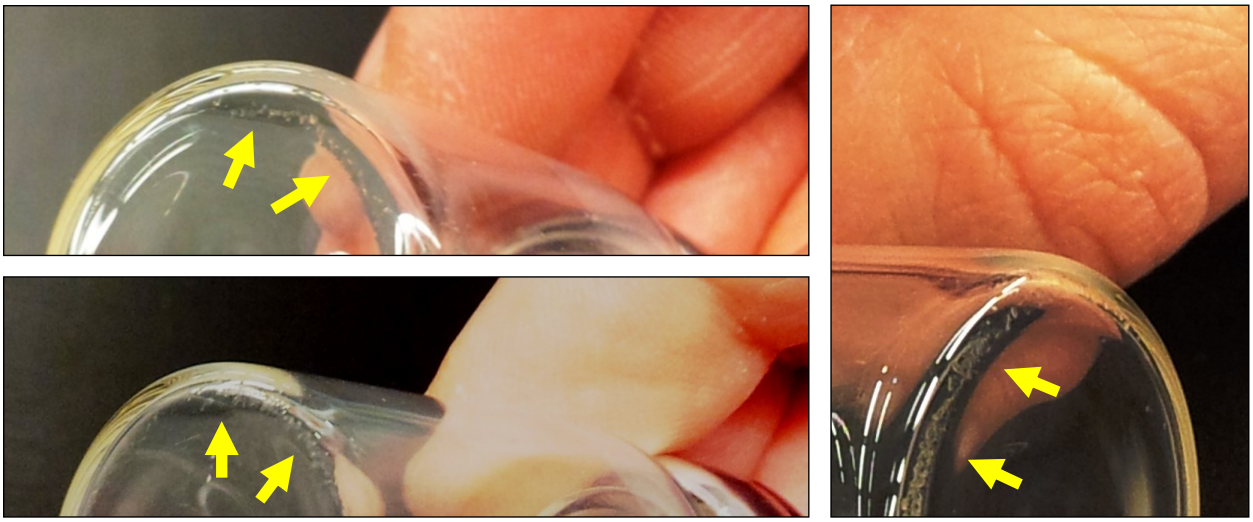

Figure B5. Free siRNA-G4NH2 dendriplexes at N/P 10 did not disperse in propellant HFA-227 and were observed to be stuck (yellow arrows) on the wall of the canister.

B.6 References

1. Sato, A.; Choi, S. W.; Hirai, M.; Yamayoshi, A.; Moriyama, R.; Yamano, T.; Takagi, M.; Kano, A.; Shimamoto, A.; Maruyama, A. Polymer brush-stabilized polyplex for a siRNA carrier with long circulatory half-life. *J. Controlled Release* **2007,** *122*, (3), 209-216.
2. Mao, S.; Neu, M.; Germershaus, O.; Merkel, O.; Sitterberg, J.; Bakowsky, U.; Kissel, T. Influence of polyethylene glycol chain length on the physicochemical and biological properties of poly(ethylene imine)-*graft*-poly(ethylene glycol) block copolymer/siRNA polyplexes. *Bioconjugate Chem.* **2006,** *17*, (5), 1209-1218.
3. Merkel, O. M.; Mintzer, M. A.; Librizzi, D.; Samsonova, O.; Dicke, T.; Sproat, B.; Garn, H.; Barth, P. J.; Simanek, E. E.; Kissel, T. Triazine dendrimers as nonviral vectors for *in vitro* and *in vivo* RNAi: The effects of peripheral groups and core structure on biological activity. *Mol. Pharmaceutics* **2010,** *7*, (4), 969-983.
4. Katas, H.; Alpar, H. O. Development and characterisation of chitosan nanoparticles for siRNA delivery. *J. Controlled Release* **2006,** *115*, (2), 216-225.
5. Weber, N.; Ortega, P.; Clemente, M. I.; Shcharbin, D.; Bryszewska, M.; de la Mata, F. J.; Gómez, R.; Muñoz-Fernández, M. A. Characterization of carbosilane dendrimers as effective carriers of siRNA to HIV-infected lymphocytes. *J. Controlled Release* **2008,** *132*, (1), 55-64.
6. Liu, G.; Xie, J.; Zhang, F.; Wang, Z.; Luo, K.; Zhu, L.; Quan, Q.; Niu, G.; Lee, S.; Ai, H.; Chen, X. N-alkyl-PEI-functionalized iron oxide nanoclusters for efficient siRNA delivery. *Small* **2011,** *7*, (19), 2742-2749.
7. Merkel, O. M.; Zheng, M. Y.; Mintzer, M. A.; Pavan, G. M.; Librizzi, D.; Maly, M.; Hoffken, H.; Danani, A.; Simanek, E. E.; Kissel, T. Molecular modeling and *in vivo* imaging can identify successful flexible triazine dendrimer-based siRNA delivery systems. *J. Controlled Release* **2011,** *153*, (1), 23-33.
8. Rodrigo, A. C.; Rivilla, I. n.; Pérez-Martínez, F. C.; Monteagudo, S.; Ocaña, V.; Guerra, J.; García-Martínez, J. n. C.; Merino, S.; Sánchez-Verdú, P.; Ceña, V. n.; Rodríguez-López, J. n. Efficient, non-toxic hybrid PPV-PAMAM dendrimer as a gene carrier for neuronal cells. *Biomacromolecules* **2011,** *12*, (4), 1205-1213.

9. Waite, C.; Sparks, S.; Uhrich, K.; Roth, C. Acetylation of PAMAM dendrimers for cellular delivery of siRNA. *BMC Biotechnol.* **2009,** *9*, (1), 38.

10. Tang, Y.; Li, Y.-B.; Wang, B.; Lin, R.-Y.; van Dongen, M.; Zurcher, D. M.; Gu, X.-Y.; Banaszak Holl, M. M.; Liu, G.; Qi, R. Efficient *in vitro* siRNA delivery and intramuscular gene silencing using PEG-modified PAMAM dendrimers. *Mol. Pharmaceutics* **2012,** *9*, (6), 1812-1821.

11. Molecular Probes - Invitrogen Detection Technologies, Quant-iT™ PicoGreen ® dsDNA Reagent and Kits. 2008; 'Vol.' MP 07581, pp 1-7.

12. GenTarget Inc., Pre-made lentiviral particles for fluorescent proteins. 2009; pp 1-6.

13. Christofk, H. R.; Heiden, M. G. V.; Harris, M. H.; Ramanathan, A.; Gerszten, R. E.; Wei, R.; Fleming, M. D.; Schreiber, S. L.; Cantley, L. C. The M2 splice isoform of pyruvate kinase is important for cancer metabolism and tumour growth. *Nature* **2008,** *452*, (7184), 230-233.

14. Conti, D. S.; Bharatwaj, B.; Brewer, D.; da Rocha, S. R. P. Propellant-based inhalers for the non-invasive delivery of genes via oral inhalation. *J. Controlled Release* **2012,** *157*, (3), 406-417.

15. Luckachan, G. E.; Pillai, C. K. S. Chitosan/oligo L-lactide graft copolymers: Effect of hydrophobic side chains on the physico-chemical properties and biodegradability. *Carbohydr. Polym.* **2006,** *64*, (2), 254-266.

16. Wu, L.; Bharatwaj, B.; Panyam, J.; da Rocha, S. Core-shell particles for the dispersion of small polar drugs and biomolecules in hydrofluoroalkane propellants. *Pharm. Res.* **2008,** *25*, (2), 289-301.

17. Chen, M.; Zhu, X.; Li, Z.; Guo, X.; Ling, P. Application of matrix-assisted laser desorption/ionization time-of-flight mass spectrometry (MALDI-TOF-MS) in preparation of chitosan oligosaccharides (COS) with degree of polymerization (DP) 5-12 containing well-distributed acetyl groups. *Int. J. Mass Spectrom.* **2010,** *290*, (2-3), 94-99.

18. Trombotto, S.; Ladavière, C.; Delolme, F. d. r.; Domard, A. Chemical preparation and structural characterization of a homogeneous series of chitin/chitosan oligomers. *Biomacromolecules* **2008,** *9*, (7), 1731-1738.

19. Lee, H.; Lee, W.; Chang, T.; Choi, S.; Lee, D.; Ji, H.; Nonidez, W. K.; Mays, J. W. Characterization of poly(ethyleneoxide)-*block*-poly(L-lactide) by HPLC and MALDI-TOF mass spectrometry. *Macromolecules* **1999,** *32*, 4143-4146.

APPENDIX C

Publication 1

JPP JOURNAL OF Pharmacy and Pharmacology

JPP
Journal of Pharmacy
And Pharmacology

Research Paper

Solvation in hydrofluoroalkanes: how can ethanol help?

Denise S. Conti, Jordan Grashik, Lin Yang, Libo Wu[1] and Sandro R. P. da Rocha

Department of Chemical Engineering and Materials Science, College of Engineering, Wayne State University, Detroit, MI, USA

Keywords
chemical force microscopy; ethanol; hydrofluoroalkanes; pressurized metered-dose inhalers; Johnson-Kendall-Roberts theory

Correspondence
Sandro R. P. da Rocha, Wayne State University, College of Engineering, Department of Chemical Engineering and Materials Science. 5050 Anthony Wayne Drive, Office 1133ENG, Detroit, MI, 48202, USA.
E-mail: sdr@eng.wayne.edu

Received August 9, 2011
Accepted October 11, 2011

doi: 10.1111/j.2042-7158.2011.01398.x

[1]Present address: MAP Pharmaceuticals, Mountain View, CA 94043, USA.

Abstract

Objectives The goal of this work was to evaluate the ability of ethanol mixed with hydrofluoroalkanes (HFAs) to improve solvation of moieties of relevance to pressurized metered-dose inhalers (pMDIs).

Methods Chemical force microscopy was used to measure the adhesion force (F_{ad}) between alkyl-based, ether-based and ester-based moieties (C8/C8, COC/COC and COOC/COOC interactions) in 2H,3H-perfluoropentane (HPFP)/ethanol mixtures. HPFP is a liquid that mimics propellant HFAs. The F_{ad} results are thus a measure of solvation in HFAs. Johnson–Kendall–Roberts (JKR) theory was used to model the results.

Key findings The F_{ad} normalized by the tip radius of curvature (F_{ad}/R) decreased upon the addition of ethanol, suggesting its ability to enhance the solvent environment. At 15% (v/v) ethanol, the F_{ad}/R was reduced 34% for the alkyl, 63% for the ether, and down 67% for the ester tails. Thus, the solvation could be ranked as: ester > ether > alkyl. JKR theory was a reasonable model for the F_{ad}/R.

Conclusions Ethanol, within the concentration range of interest in commercial pMDIs, provided limited enhancement in solvation of alkyl moieties. On the other hand, the cosolvent significantly enhanced solvation of ether-based and ester-based moieties, thus suggesting its potential for formulations containing amphiphiles with such groups.

Introduction

Pressurized metered-dose inhalers (pMDIs) are the most widely used portable oral inhalation devices,[1,2] and are usually associated with high compliance.[3,4] pMDIs also offer an efficacious and convenient way of delivering drugs to the lungs for cases where repeated administration is necessary,[5] and in disease states where moderate-to-high inspiratory flows cannot be achieved by the patient,[6] as the aerosol formation in pMDIs is independent of inhalation effort.[2] In a typical pMDI, the compressed liquid propellant, which is in equilibrium with its vapour, makes up 98% of the formulation. pMDI formulations contain drugs either in solution, where the therapeutic is dissolved in the liquid propellant, usually with the help of a cosolvent, or in suspension, where drug crystals or amorphous drug particles are dispersed in the liquid propellant, usually with the aid of excipients including surfactants and cosolvents.[2,7]

Hydrofluoroalkanes (HFAs) are fluorinated short-chain alkanes with a low degree of hydrogen substitution,[8] introduced as propellants in pMDIs in the late 1980s because of the phasing out of chlorofluorocarbons (CFCs).[9] HFAs are significantly less environmentally damaging than the fully halogenated CFCs.[10] HFA-227 (1,1,1,2,3,3,3-heptafluoropropane) and HFA-134a (1,1,1,2-tetrafluoroethane) are the two propellants currently used commercially in pMDIs.[8,11] They were selected on the basis of several criteria, including biological compatibility and inertness.[12] However, due to their unique chemistry,[10] HFAs have significantly different solvent properties compared with CFCs,[8] including larger dielectric constant and dipole moment.[13] HFAs have a dual character, being somewhat lipophobic, and at the same time hydrophobic.[11,14] Thus, most therapeutics of interest, and excipients used in previous CFC formulations, have very low solubility in HFAs.[10,12]

To overcome solubility limitations, the industry has resorted to a large extent to the use of cosolvents, especially ethanol,[12] not only as solubility enhancer for drugs in the development of solution formulations, but also as solubility enhancer for other excipients, for both solution and suspension formulations.[12,15] However, there are also many issues surrounding the use of ethanol.[1,7,12,15,16] In solution-based formulations, ethanol may reduce the chemical stability of the system and, depending on its concentration, the presence

APPENDIX D

Publication 2

GENE DELIVERY

Journal of Controlled Release 157 (2012) 406–417

Contents lists available at SciVerse ScienceDirect

Journal of Controlled Release

journal homepage: www.elsevier.com/locate/jconrel

Propellant-based inhalers for the non-invasive delivery of genes via oral inhalation

Denise S. Conti, Balaji Bharatwaj, Daniel Brewer, Sandro R.P. da Rocha *

Department of Chemical Engineering and Materials Science, College of Engineering, Wayne State University, Detroit, MI, 48202, USA

ARTICLE INFO

Article history:
Received 16 March 2011
Accepted 23 September 2011
Available online 1 October 2011

Keywords:
Pulmonary gene delivery
Pressurized-metered dose inhalers
Alveolar epithelium
CS–DNA polyplexes
Core–shell particles

ABSTRACT

In this work we describe the development of a propellant-based, portable oral inhalation platform for the pulmonary delivery of genes. A core–shell strategy is utilized to efficiently disperse cationic-polymer-DNA nanoparticles in hydrofluoroalkane propellants, and to generate aerosols from the corresponding pressurized metered-dose inhaler formulations (pMDIs) that have excellent aerosol characteristics, suitable for deep lung deposition. The engineered polyplexes and core–shell structures were fully characterized, and their ability to transfect model lung alveolar epithelium cells *in vitro* was demonstrated. We also show that the propellant does not affect the biological activity of the plasmid DNA, and that the core–shell formulations have no *in vitro* cytotoxicity. The relevance of this work stems from the fact that pMDIs are the least expensive and most widely used portable oral inhalation devices, and are thus promising platforms for targeting genes to the lungs for the treatment of medically relevant diseases including asthma, cystic fibrosis, chronic obstructive pulmonary disease, and lung cancer.

1. Introduction

There is tremendous potential in targeting genes to the lungs [1–3]. Asthma, cystic fibrosis, chronic obstructive pulmonary disease (COPD), emphysema, and lung cancer are just some of the many examples of pulmonary diseases that can be potentially treated by gene therapy [1,2,4–6]. However, there are several challenges associated with the formulation and regional delivery of genes via oral inhalation (OI) [1], the preferred mode of administration of therapeutics to the lungs.

The mucus layer in the airways and the lung surfactant in the alveolar region represent important extracellular barriers to the delivery of genes to the respiratory tract [7,8]. As transfection with free DNA is not efficient, the choice of the gene carrier system is also of great relevance [9]. For polymeric carriers, the polymer chemistry, and the physical properties of the polymer-DNA complexes (polyplexes), including their size, surface charge, and DNA loading greatly affect the transfection efficiency [10,11]. In addition, those parameters also influence the uptake and trafficking of the gene carriers and the release of DNA in the cellular environment, which are examples of intracellular barriers that need to be overcome [12]. The choice of the aerosolization technique is also expected to influence the transfection efficiency as the dose and location where the polyplexes will be delivered depend on device characteristics and particle engineering [5,13,14].

The ideal scenario in terms of gene delivery to the lungs would be for both patients and health care providers to be able to choose from a host of different delivery devices, as patient compliance and device suitability depends on the patient and disease state/condition. Nucleic acids can be potentially delivered to the lungs via nebulizers, dry powder inhalers (DPIs) or pressurized metered dose inhalers (pMDIs) [15]. Nebulization has many advantages [5,13,15,16], but it is less efficient and less convenient than portable devices [5]. Therapeutically active molecules can also be delivered to the lungs by DPIs. The delivery of such molecules using DPIs have several advantages, including the fact that DPIs are propellant-free, portable, simple use, have good shelf-life, and reduced time of administration [17]. Some studies have demonstrated the potential of liposomal gene powders [17], and also of gene powders prepared by supercritical CO_2 using chitosan (CS) as non-viral carriers for use in DPIs [18,19]. However, there are also some disadvantages associated with the delivery of genes with DPIs, as for example potential problems in dose uniformity, dependency on patient's inspiratory flow rate, and less protection from environmental effects [20].

Genes can also be delivered to the lungs using pMDIs. However, pMDIs have received considerably less attention than DPIs and nebulizers. The only work discussing gene delivery in hydrofluoroalkane (HFA)-based pMDIs consists in using surfactant-coated DNA particles prepared by reverse microemulsion [13]. However, liposomes were needed during transfection to improve the *in vitro* transfection efficiency of the particles used in the formulation. In spite of the limited amount of work on pMDIs, such devices offer a potentially more efficacious and convenient alternative than DPIs and nebulizers, especially for repeat administration [13], and serve as a complementary strategy to other devices. pMDIs are also simple to use, have high compliance, and are extensively used for drug delivery to the lungs [21,22]. Nevertheless, it has been shown to be difficult to stabilize

* Corresponding author at: Wayne State University, College of Engineering, Chemical Engineering and Materials Science Department, 5050 Anthony Wayne Drive, 1133ENG, Detroit, MI, 48202, USA. Tel.: +1 313 577 4669; fax: +1 313 578 5820.
E-mail address: sdr@eng.wayne.edu (S.R.P. da Rocha).

0168-3659/$ – see front matter © 2011 Elsevier B.V. All rights reserved.
doi:10.1016/j.jconrel.2011.09.089

ABSTRACT

POLYMERIC NANOCARRIERS AND THEIR ORAL INHALATION FORMULATIONS FOR THE REGIONAL DELIVERY OF NUCLEIC ACIDS TO THE LUNGS

by

DENISE SANTOS CONTI

December 2013

Advisor: Dr. Sandro R. P. da Rocha

Major: Chemical Engineering

Degree: Doctor of Philosophy

Gene therapy has attracted attention in the fields of medicine, pharmacy, and bionanotechnology due to the potential for treating a large number of medically relevant diseases. Oral inhalation (OI) is a promising route for the administration of therapeutics, including small molecules and biomacromolecules, such as nucleotides, peptides, and proteins, *to* (locally) and *through* (systemically) the lungs. The use of OI is especially attractive for the delivery of nucleic acids as it provides a direct and non-invasive route for targeting the lungs. Pressurized metered-dose inhalers (pMDIs), are the most commonly used OI in treatment of lung diseases and are thus promising OI devices to be used for the delivery of nucleic acids *to* the lungs. However, progress in the development of pMDI formulations for the delivery of DNA and siRNA *to* the lungs has been hampered largely by the lack of efficient nanocarriers capable of overcoming the lung structure, the extra and intracellular barriers present in the lung tissue, and formulation challenges – aerodynamic particle size, surface chemistry of the particles, and solvation forces in propellant/co-solvent mixture. In light of the challenges and opportunities described above, we propose in this work: *(i)* a quantitatively and

systematically evaluation of the enhancement in solvation capacity of propellant hydrofluoroalkane (HFA) upon addition of co-solvent ethanol; *(ii)* the development of efficient HFA-based pMDIs to deliver nucleic acids *to* the lungs; *(iii)* the design of siRNA-poly(amidoamine) (PAMAM) dendrimer conjugates. We demonstrate that both DNA and siRNA can be efficiently formulated in HFA-based pMDIs upon the development of novel particle engineering strategies to overcome issues associated with their size and physical stability in the propellant. We also demonstrate that the polymer-based nanocarriers are capable of enhancing gene expression (DNA) and knockdown (siRNA) in alveolar lung epithelial cells, and they do not lose their biological activity when formulated in the propellant HFA. In conclusion, the results reported in this dissertation contribute significantly in the development of DNA- and siRNA-delivery systems and in their formulation in portable OI devices, with great potential to efficiently deliver nucleic acids *to* the lungs to treat medically relevant pulmonary disorders, such as COPD, asthma, virus infections, cystic fibrosis, and lung cancer.

AUTOBIOGRAPHICAL STATEMENT

DENISE SANTOS CONTI

Denise Santos Conti received her B.Sc. in Chemical Engineering from Regional University of Blumenau (FURB, Brazil) in 2002, and M.Sc. in Materials Science and Engineering from Estadual University of Santa Catarina (UDESC, Brazil) in 2006. She worked as supervisor in polymer processing and quality control in various industries in Brazil from 1998 to 2004. She joined Wayne State University (Detroit, MI, USA) in the Fall 2008 to pursue her Ph.D. in Chemical Engineering. She worked under the guidance of Dr. Sandro da Rocha from Fall 2008 to Spring/Summer 2013 in the development of polymeric nanocarriers for the local delivery of nucleic acids to the lungs and strategies for their formulation in portable inhalers. She has authored and co-authored 6 publications in peer-reviewed journals, and has 5 more research papers under preparation (2 as first author). She has received several awards: *(i) Best student of the Department of Chemical Engineering at Regional University of Blumenau* (FURB, Brazil) awarded by Regional Council of Engineering, Architecture and Agronomy (CREA) and 13th Regional Council of Chemistry (CRQ) in 2003; *(ii) Best poster presentation* (Physical Sciences, Engineering and Mathematics category) at Wayne State University Graduate Exhibition (Detroit, MI, USA) in 2011; *(iii) Outstanding Teaching Assistant Service Award*, and *(iv) Ralph H. Kummler Award for Achievement in Graduate Student Research*, both from College of Engineering at Wayne State University (Detroit, MI, USA) in 2012. She has accepted a position at the Food and Drug Administration (FDA) to be part of a new Generic Inhalation Program starting on September 2013.